DEVELOPING FUNDAMENTAL UNDERSTANDING OF THERMAL PROCESSING OF (CATALYST) FORMULATIONS

By

Rebecca Louise Gibson

A thesis submitted to the School of Chemical Engineering at the University of Birmingham for the degree of

Doctor of Engineering (EngD)

School of Chemical Engineering
College of Engineering and Physical Sciences
University of Birmingham
B15 2TT

September 2021

```
IF(II.GT.1) Then
        IF (ABS(TOUT(II)-TOUT(II-1)).LE.ZERO) Then
                GOTO 150
        End if
End if
```

Abstract

Thermal processes are key steps in the manufacture of catalysts and functional materials. These large-scale processes are often scaled-up using empirically or experientially derived rules, which result in inefficiently sized assets and longer than necessary processing times. A model-based approach to interrogating thermal processes allows for safer, more informed scale up, resulting in optimised product quality.

A statistically rigorous modelling methodology based on the Sestak-Berggren equation has been developed to quantitatively interpret the results of thermal analysis experiments. This allows the kinetic modelling of multiple overlapped thermal events/reactions, without a priori peak deconvolution. Akaike weights, a statistical metric, allows the comparison of multiple potential models, allowing the optimal number of thermal events occurring during an experiment to be identified. Verification of the internal consistency of the method was completed using in silico (computer generated) data. The impact of experimental noise was also investigated, and it was concluded that this modelling technique could still extract meaningful physical parameters in the presence of up to 10% white noise, although additional experiments may be required if noise levels are this high.

This modelling methodology was applied to multiple experimental systems; temperature programmed reduction (TPR) of a Fischer-Tropsch (FT) catalyst, ammonia temperature programmed desorption (TPD) from SAPO-34, ammonia TPD from ZSM-5 and the temperature programmed decomposition (TPDecomp) of a zinc nitrate catalyst precursor and of calcium carbonate. All derived models were subject to

criticism, checking the plausibility of estimated mechanisms and parameters, and also checking for systematic error and overfit. The modified methodology produced good quality models for both the TPR and the ammonia TPD from SAPO-34 . However, fitting of data from both the ammonia TPD from ZSM-5 and the TPDecomp of the zinc nitrate catalyst precursor demonstrated systematic trends in residuals and implausible kinetic mechanisms. The study of calcium carbonate TPDecomp showed a dependence on weight hourly space velocity (WHSV). This raised issues with the data quality, implying transport limitations or reverse reactions could be present within some of the data.

These findings led to an investigation into the bulk heat and mass transport occurring within thermal analysis equipment. Pan-style and tubular reactors were compared using dimensionless analysis (Damköhler and Bodenstein numbers) based on the results of computational fluid dynamics (CFD) simulations. It was concluded that pan-style reactors are susceptible to heat and mass transport limitations and are not suitable for the collection of kinetic data. Tubular reactors of constant diameter are suitable for kinetic experimentation. However, not all thermal analysis experiments can be conducted in tubular equipment. Recommendations were made around conducting experiments to obtain data suitable for kinetic studies: where possible, tubular reactors with high carrier gas flow rates should be used.

Acknowledgements

Thank you to the EPSRC, Johnson Matthey and the University of Birmingham for the opportunity to complete this EngD. I have been well supported by my supervisors Professor Mark Simmons, Professor Thanos Tsolakis, Professor Hugh Stitt and Robert Gallen, alongside Dr Richard Greenwood as program director.

Mark and Hugh- thank you for your support throughout the past four years. Your advice has been vital in producing this thesis. Thank you for your technical input, emotional support and of course, those wonderful meals out.

Rob, I'm not sure I would have made it through these past four years without your help and support. At times that basket weaving course was looking tempting! Your technical input has raised the level of this work tremendously and I have learnt so much from you. Your faith in me has helped me build both personal and professional confidence. We've had so many laughs in these four years and I will treasure my Rob quotes for quite some time. Thank you so much, I hope you are as proud of this work as I am and thank you for turning me into the sceptic I am today.

Thank you to all the JM colleagues who reviewed reports, offered advice, and provided support over the last four years. Much appreciated expert technical support has been provided by John West, Stephen Schuyten and Lockhart Horsburgh. Specifically thank you to Li Liu for support with the CFD work in this thesis and to Carl Tipton, Robert Woodman and Lockhart Horsburgh for reviewing many drafts of this thesis and supplying their invaluable comments. Thank you to Michelle Gilhespy for advice on grammar and the wonderfully complex English language. A big thank you to Sarah Ridley, Deborah Dodds, and Michelle Gilhespy for all those much-needed tea breaks!

To my family and friends, without your support I would not have survived the last four years. Mum, Dad, Andrew, Hazel and Nick, thank you all for being there whenever I needed a rant, a hug, or a laugh.

Table of contents

List of figures

List of tables

List of abbreviations

AIC	Akaike information criteria
APIs	Active pharmaceutical ingredients
ARIMA	Autoregressive integrated moving average
Bo	Bodenstein number
BLC	Baseline correction
CA	Clean air
CFD	Computational fluid dynamics
CHA	Chabazite
CRTA	Constant rate thermal analysis
CSTR	Continuous stirred tank reactor
Da(R)	Damkholer number, reactor
Da(S)	Damkholer number, sample
DFT	Density functional theory
DoE	Design of experiments
DRM	Distributed reactivity model
DSC	Differential scanning calorimetry
DTG	Differential thermogravimetric
EGA	Evolved gas analysis
ENR	Efficient natural resources
FCC	Fast catalytic cracking
FT	Fischer-Tropsch
FTIR	Fourier transform infrared spectrometry
GC	Gas chromatography
GHG	Greenhouse gas
ICTAC	International confederation for thermal analysis and calorimetry
ID	Inner diameter
JM	Johnson Matthey
JMEAK	Johnson, Mehl, Avrami, Erofeev and Kholmogrov
JMTC	Johnson Matthey Technology Centre
KAS	Kissinger-Akahira-Sunose
KDA	Kinetic deconvolution analysis
MDA	Mathematical deconvolution analysis
MFI	Mobil five, a series of zeolite catalyst materials
MLM	Minimum likelihood method
MS	Mass spectrometry
MSE	Mean squared error
MTO	Methanol to olefins
m/z	Mass to charge ratio
NMR	Nuclear magnetic resonance
OFW	Ozawa-Flynn-Wall

PFR	Plug flow reactor
RSS	Residual sum of squares
RTD	Residence time distribution
SAR	Silica to alumina ratio
SCR	Selective catalytic reduction
TCD	Thermal conductivity detector
TEOM	Tapered oscillating microbalance
TG	Thermogravimetric
TGA	Thermogravimetric analysis
TIS	Tanks in series
TMA	Thermomechanical analysis
TPD	Temperature programmed desorption
TPDecomp	Temperature programmed decomposition
TPR	Temperature programmed reduction
WHSV	Weight hourly space velocity
XRD	X-ray diffraction

Nomenclature

Symbol	Definition	Units
Letters		
A_{ann}	Area of annulus	m^2
A_{eq}	Equivalent area	m^2
A_i	Pre-exponential factor	s^{-1}
A_{pan}	Area of pan	m^2
A_{sample}	Area of sample	m^2
AD	Anderson-Darling statistic	-
a_0	Fitting parameter for mathematical deconvolution analysis	-
a_1	Fitting parameter for mathematical deconvolution analysis	-
a_2	Fitting parameter for mathematical deconvolution analysis	-
a_3	Fitting parameter for mathematical deconvolution analysis	-
b	Point for Taylor series expansion	-
C	Intercept for baseline correction function	Varies
C_a	Concentration	$mol\ m^{-3}$
c_p	Heat capacity	$J\ kg^{-1}\ K^{-1}$
D^{eff}	Molecular diffusivity	$m^2\ s^{-1}$

Dh	Hydraulic diameter	m
d_i	Inner diameter	m
d_o	Outer diameter	m
d_p	Particle diameter	m
d_{pan}	Diameter of pan	m
d_{sample}	Diameter of sample	m
Ea_i	Activation energy	kJ mol^{-1}
Ed_i	Desorption energy	kJ mol^{-1}
e	Point source relationship	-
F	Force	N
$F_{v,i}$	Contribution factor	-
g	Acceleration due to gravity	N kg^{-1}
h	Specific enthalpy	J kg^{-1}
h_{bed}	Bed height	m
K	Permeability	-
k	Thermal conductivity	W m^{-1} K^{-1}
L	Length	m
l	Likelihood	-
M	Gradient for baseline correction function	Varies
Mr	Molar mass	g mol^{-1}
m_i	Exponent for Sestak-Berggren model	-
m_{mesh}	Mass of meshed pan lid/bottom	g

m_{pan}	Mass of pan	g
m_{sample}	Mass of sample	g
m_{wall}	Mass of pan wall	g
n_{asym}	Initial estimate for Sestak-Berggren model parameter n	-
n_{events}	Number of thermal events	-
n_i	Exponent for Sestak-Berggren model/ model fitting methods	-
n_m	Number of moles	mol
n_{tracer}	Number of moles of tracer	mol
$\dot{n_R}$	Reactor mass transfer rate	mol s^{-1}
$\dot{n_S}$	Sample mass transfer rate	mol s^{-1}
P	Pressure	Pa
p	Exponent for Sestak-Berggren model	-
Q	Flow rate	m^3 s^{-1}
Q_{ann}	Flow rate through annulus	m^3 s^{-1}
q	Temperature integral approximation	-
R	Universal gas constant	J mol^{-1} K^{-1}
r_k	Kinetic rate	mol s^{-1}
r_{ann}	Radius of annulus	m
r_{pan}	Radius of pan	m
r_{sample}	Radius of sample	m
s	Fitting parameter for distributed reactivity models	-

T	Temperature	K
T_b	Base temperature for thermal event	K
T_{high}	75 % maximum peak temperature	K
T_{low}	25 % maximum peak temperature	K
T_{max}	Maximum peak temperature	K
t	Time	s
t_{av}	Average time of experiment	s
t_m	Mean residence time, reactor	s
t_{mp}	Mean residence time, sample	s
u	Gas velocity	m s^{-1}
V_{bed}	Volume of sample	m^3
V_{wall}	Volume of pan wall	m^3
W_R	Ratio of measured curve width to that calculated from approximate value of A and Ea, derived from Kissinger equation	-
w	Akaike weight	-
w_T	Wall thickness	m
Y	Ordered datapoints	-
Greek Letters		
α	Extent of reaction	-
β	Temperature ramp rate	K s^{-1}
δ_T	Error tolerance on temperature	K
ε	Voidage	-

ε_{BL}	Baseline correction function	-
θ	Unknown parameter which requires estimation	Varies
κ	Fitting parameter for Weibull distribution	-
λ	Datapoint	-
μ	Viscosity of fluid	kg m^{-1} s^{-1}
ξ_i	Initial value	Varies
ξ_f	Final value	Varies
ρ	Density	kg m^{-3}
σ	Variance	s^2
τ	Number of isoconversion points	-
Φ	Temperature dependence	Varies
φ	Number of datapoints	-
ω	Number of parameters plus one	-

1. Introduction and business case

1.1. Project context

Energy consumption and greenhouse gas (GHG) emissions are a global concern. Whilst many catalysts and functional materials are developed to aid in the reduction of GHGs or aid in the development of cleaner energy systems, there is an energy consumption and release of GHG emissions associated with their manufacture.

The manufacturing routes for many heterogeneous catalysts and functional materials are similar and can be classified into three categories, shown in Figure 1.1.

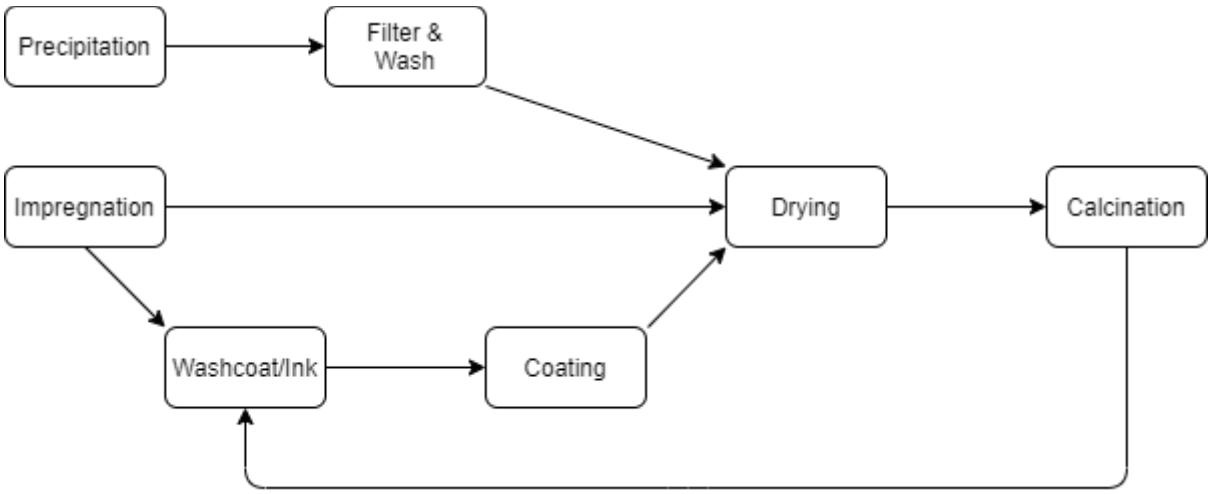

Figure 1.1: Schematic of common catalyst and functional materials manufacturing routes.

Precipitation is used for both single and multi-component catalysts and includes the mixing of aqueous phase metal salts with an alkali solution. The precipitation of an insoluble metal oxide, hydroxide or carbonate is induced by controlling temperature, pH and/or evaporation [1]. This process is commonly used for heterogeneous base metal catalysts, such as pre-reforming and methanol synthesis catalysts. Once

calcined, these materials would require forming into pellets, granules or extrudates depending on the required duty.

Impregnation involves the addition of a metal salt solution to a substrate, either in exact quantities for incipient wetness impregnation, or in excess for wet impregnation [1]. The solvent fills the pores of the chosen substrate. This method of catalyst preparation gives a smaller metal crystallite size compared to other preparation methods, (provided the adsorption chemistry has not been modified). Examples of catalysts commonly produced using this method include steam methane reforming, palladium on carbon and HTC™ nickel on alumina catalysts.

Washcoating and inking processes either involve the addition of a thin layer of liquid catalyst to a solid substrate/monolith or the mixing of support and active metal precursors together prior to formulation to the correct rheological properties. This method is used for preparation of automotive catalysts as well as for cathode materials in battery materials and fuel cells.

Thermal processing is required during the manufacturing process for many catalysts and functional materials, and it often consists of multiple steps. Thermal processes include:

- Drying: the removal of water from the formulation;
- Denitrification: the decomposition of nitrate precursors from the formulation;
- Calcination: a solid product is thermally decomposed (in a controlled manner), to convert the structure into that of the active material or to remove a precursor;
- Reduction: process of reducing the oxidation of state of a metal to an active state.

Historically, these thermal processes have been *empirically scaled-up*, rather than *designed*. This has resulted in inefficiently sized ovens/calciners and processing times and temperatures which may exceed requirements. Designing these thermal processes using reaction engineering approaches could greatly reduce the energy required and the GHG emissions produced.

Extracting process information from large-scale equipment is a complex and challenging problem. Transport limitations can be present which can make the data extracted equipment and product specific. Instead, small-scale, tightly controlled experiments can be used to extract fundamental data, which can then be related back to the large-scale through modelling techniques. This ensures the information extracted is scale independent and can be applied to different reactor designs and processing routes.

The class of small-scale experiments used to extract this fundamental data is called thermal analysis, and these lab-scale experiments are analogous to large-scale thermal processes. This field is broad and has been studied for decades [2]. Kinetic models for these small-scale processes are numerous, with wide ranging assumptions. Data from thermal analysis experiments are frequently used to identify suitable processing temperatures, however are underutilised for extracting information regarding suitable residence times or temperature ramp rates.

Thermal analysis experiments are also used as analytical techniques at Johnson Matthey (JM) to characterise catalyst samples, and kinetic modelling could allow for the extraction of thermodynamic information regarding active sites. This fundamental information could aid in the development of new catalyst formulations.

Extracting kinetic information, including a reaction mechanism, from this thermal analysis experimentation is a key step in the fundamental understanding of thermal processes. Multiple thermal events/processes can occur at similar temperatures, and these can manifest as overlapped peaks in thermal analysis data. Describing the correct number of overlapped thermal events with a suitable reaction mechanism and Arrhenius parameters can allow for the extraction of physically meaningful information. This work discusses the development of a modelling methodology designed to capture multiple overlapped thermal events/reactions, identify a statistically likely number of thermal events, and identify the reaction mechanism and Arrhenius parameters associated with each thermal event. To be appropriate for industrial use, this modelling methodology should be robust, which applies to all experiments in the broad class of thermal analysis. There are many existing models and deconvolution techniques within the literature (discussed in detail in Chapter 3). Deriving new models from first principles may not be necessary in this field, rather applying existing models in a statistically rigorous way.

This modelling methodology has been applied to a range of thermal analysis experiments. Temperature programmed reduction (TPR) (Chapters 4 and 5) and temperature programmed decomposition (TPDecomp) (Chapter 7) were selected to represent large-scale reductions and calcinations respectively. The methodology has also been applied to the results of ammonia temperature programmed desorption (TPD) (Chapter 6), for materials analysis. These experimental techniques will be covered in detail in Chapter 2.

Industrially relevant materials have been used throughout this work, to illustrate the power of this modelling methodology. These materials include a Fischer-Tropsch (FT)

catalyst, SAPO-34 which is used in the methanol-to olefins (MTO) process, ZSM-5 used for fast catalytic cracking (FCC), a zinc nitrate catalyst precursor and calcium carbonate. These materials represent a range of processing routes and end use.

Thermal analysis is carried out in a range of equipment available within JM. Broadly these reactors can be classified as pan-style or tubular. The choice of reactor is often dependent on the experiment, gas compositions and analysis method required. Thermal analysis equipment is discussed in detail in Chapter 2. The key assumption behind these small-scale experiments is that kinetically limited data are collected, hence transport limitations are not present within the sample or the reactor itself. Confirmation of this, through analysis of this equipment as a chemical reactor appears to be lacking in the literature. Understanding the transport phenomena occurring within these reactors is important for the interpretation of thermal analysis data and their use in process scale up. This work has developed a methodology to characterise the transport phenomena occurring within these thermal analysis reactors and compare different reactor configurations, discussed in Chapter 8. Recommendations regarding collection of intrinsic data are made.

The wider impact of this research has been demonstrated through the publication of journal papers and conference presentations (details given in Section 1.6).

1.2. Johnson Matthey plc

Johnson Matthey plc is a leading technology company in the FTSE100, employing around 15,350 people in 30 countries all around the world. In 2019/2020[1] JM had a

[1] 2019/2020 selected as the most representative data, due to COVID-19 pandemic occurring during 2020/2021.

revenue of £4.2 billion[2] and an underlying profit of £539 million[1] with £199 million invested in research and development in this period [3].

The company works towards its vision for “a world that’s cleaner and healthier today and for future generations” [3] through a range of technology sectors. These technology areas include emission control, precious metal refining, process catalysts and technology licensing, battery materials and pharmaceuticals. The business sectors of JM will be discussed briefly to give context to this work.

Clean Air (CA) is the largest sector in JM, accounting for 63 % of sales and 51 % of profits [3]. CA specialises in harmful gas abatement technologies for both vehicles and other (stationary) sources. It is estimated that one in three new cars carries a JM catalyst [4].

Efficient Natural Resources (ENR) is a diverse sector with JM, which aims to help customers achieve greater efficiency from natural resources [5] and accounts for 23 % of sales and 44 % of JM’s profits [3]. This sector covers a wide range of industries, including chemicals, oils and gas, food and beverage, agrochemicals and energy storage [5]. This sector includes:

- Catalyst technologies: supplies catalysts and technology licensing to a range of industries, including oil and gas, agrochemicals, and the food industry.
- Platinum group metals services: refining and recycling precious metal products.

[2] Excluding precious metals

The Health sector within JM is small and specialised, accounting for 5 % of profits and sales [3]. The health sector has two main focuses: the production of generic active pharmaceutical ingredients (APIs) and the development of innovative APIs. The health sector supplies directly into the pharmaceutical industry.

The New Markets sector encompasses the upcoming JM technologies, such as battery materials, fuel cells, life science technologies and medical device components. These growth areas in the business are focused on innovation [5].

The Technology Centre (JMTC) acts as a research and development group for the company and is involved in innovation for all the business sectors. This EngD project has been funded by JMTC.

1.3. Business case

As thermal processes are critical to producing the optimum catalysts and functional materials, these processes are of interest to most business sectors within JM.

Typically, these thermal processes are carried out at high temperatures (denitrification between 673 and 773 K, and calcination between 573 and 1673 K depending on the material), making them energy intensive. JM's global energy consumption was reported as ~4.8 million GJ (for 2019/2020) [3], and it is estimated that thermal processes account for 80 % of this consumption [6]. Previously many of these thermal process methodologies have been developed from batch laboratory protocols, which has resulted in processing and hold times which may exceed requirements. Having a model based approach to scale up of these thermal processes could reduce energy consumption and subsequent GHG emissions, through the identification of inefficiencies such as excessive hold times and temperatures.

Thermal processes such as calcination can result in the release of flammable and harmful gases. There have been several safety incidents within JM related to the unexpected or uncontrolled release of gases during calcination. Understanding what species are expected to form, at what temperature and rate is a key requirement for the safe scale up of such processes.

There are multiple potential benefits to a model based scale up of thermal processes. Designing large scale thermal processes in a similar way to a chemical reactor could result in capital cost savings (for new industrial units) and maximised productivity (for existing infrastructure) as well as energy/operational cost savings. Identifying potential hazards and the conditions these may occur, could also ensure a safe route for scale up. Generally, an increased understanding can unlock potential opportunities for innovation.

1.4. Thesis aim and objectives

The overall aim of this doctoral research project was to gain further understanding, quantification and modelling capability in selected JM-relevant thermal processes, for the development and manufacture of functional materials. This would allow for safe, optimised scale up of thermal processes and an improvement in product quality.

The work presented in this thesis addresses three specific objectives:

- Development of a unified approach for the kinetic modelling of all thermal analysis experiments.
    - This should include the ability to model multiple overlapped thermal events simultaneously, identify the most statistically likely number of thermal events

and predict a kinetic triplet (pre-exponential factor, activation energy and reaction mechanism) for each thermal event.

  - Thermal analysis data are often interpreted qualitatively within industry, this tool would allow quantitative analysis of the data which should lead to more consistency across the company.

- Application of this kinetic modelling methodology to a range of thermal analysis experiments and equipment types.
  - TPR and TPDecomp experiments conducted in both tubular and pan-style reactors were chosen to represent the large-scale industrial processes of catalyst reduction and calcination respectively.
  - Ammonia TPD in a tubular reactor, a common characterisation method, was selected to investigate how quantification of active site strengths could improve catalyst formulations.

- Characterisation of thermal analysis reactors using classic reaction engineering principles.
  - Use of computational fluid dynamics (CFD) to simulate simplified scenarios which relate to thermal analysis experiments.
  - Development of a methodology to calculate the mass and heat transfer rates occurring within different thermal analysis reactors.
  - Comparison of the transport phenomena occurring within the two broad classifications of thermal analysis reactors, tubular and pan-style.
  - Provision of recommendations for conducting thermal analysis experiments, based on the CFD simulations and equipment comparison.

1.5. Thesis structure

This thesis is comprised of eight chapters (plus conclusions). The contents of each chapter are briefly as follows:

Chapter 2 describes the thermal analysis methodologies and equipment used within this thesis. Key recommendations from literature are highlighted to describe the possible sources of error when conducting thermal analysis experiments.

Chapter 3 discusses the kinetic modelling techniques used in the literature. Recommendations for good practice and gaps in the current procedures are identified.

Chapter 4 outlines the modified Sestak-Berggren methodology [7], [8] developed to describe multiple overlapped thermal events without the need for prior peak deconvolution and the novel use of Akaike weights to identify the most likely reaction mechanism occurring during each thermal event. Also included in this chapter are an *in silico* (computer generated) verification and a TPR of an FT catalyst for experimental validation for this modelling methodology.

Chapter 5 extends the work on the TPR of an FT catalyst discussed in Chapter 4, exploring the use of constant rate thermal analysis (CRTA) to help in event identification. Linear temperature ramp rate experiments and CRTA experiments were regressed simultaneously for the first time, and it was found that CRTA provided a better constraint for the model compared to linear temperature ramp rate data alone and aided in event and solid-state mechanism identification.

Chapter 6 discusses the use of the modified Sestak-Berggren equation as a method of extracting information from ammonia TPD data. Extracting information regarding the active sites on a functional material or catalyst through thermal analysis could provide

an alternative to expensive and time consuming spectroscopic techniques. The power of this modelling methodology was demonstrated with a hydrothermal ageing study. Samples of SAPO-34 were aged for differing times (at constant temperature) and it was concluded that the energies associated with the active sites did not change due to ageing, rather just the number of acid sites.

Chapter 7 contains three experimental case studies to highlight the varying quality of fit obtained using the modified Sestak-Berggren modelling methodology. The ammonia TPD of ZSM-5 was monitored using a thermal conductivity detector (TCD) and was carried out in a tubular reactor. Implausible mechanisms were estimated for each thermal event and the activation energy estimates were lower than suggested in the literature. TPDecomp of a zinc nitrate catalyst precursor was conducted using a pan-style TGA reactor coupled with evolved gas analysis (EGA). Implausible high reaction order mechanisms and systematic residual trends were observed when the data were fitted using the modified Sestak-Berggren equation. Finally, the decomposition of calcium carbonate was studied using a pan-style TGA reactor and a design of experiments (DoE) approach. This DoE highlighted that the Sestak-Berggren model was unable to describe a range of weight hourly space velocities (WHSV), implying there were non-kinetic effects within the dataset. This chapter emphasises the need for model criticism, which is generally lacking in the literature, and that the poor data quality implies possible transport limitations or reversible reactions within the gathered data.

Chapter 8 investigates a possible source of the poor data quality encountered in Chapter 7 through a study using CFD. This innovative study compares different thermal analysis reactor styles (pan-style and tubular) and uses classic reaction

engineering principles such as residence time distributions and dimensionless analysis to compare the mass and heat transport within each reactor. It was found that pan-style reactors have significant heat and mass transport limitations and should not be used to gather kinetic data. Tubular reactors are suitable for kinetic experimentation provided expected reaction rates are in line with those used in this study. Recommendations for conducting kinetic experimentation are also outlined.

1.6. List of publications and conferences

1.6.1. Publications

- R. L. Gibson, M. J. H. Simmons, E. Hugh Stitt, J. West, S. K. Wilkinson, and R. W. Gallen, 'Kinetic modelling of thermal processes using a modified Sestak-Berggren equation', *Chem. Eng. J.*, vol. 408, 2021, doi: 10.1016/j.cej.2020.127318.
- R. L. Gibson, M. J. H. Simmons, E. H. Stitt, L. Liu, and R. W. Gallen, 'Non-kinetic phenomena in thermal analysis data; Computational fluid dynamics reactor studies', *Chem. Eng. J.*, vol. 426, p. 130774, Dec. 2021, doi: 10.1016/j.cej.2021.130774.
- R. L. Gibson, M. J. H. Simmons, E. H. Stitt, L. Horsburgh, and R. W. Gallen, 'Selection of formal baseline correction methods in thermal analysis', *Chem. Eng. Technol*., 2021, doi: 10.1002/ceat.202100120

1.6.2. Conference papers and presentations

- Gibson et al, 2019 'Kinetic Modelling of Ammonia Temperature Programmed Desorption using the Sestak Berggren Equation: An In-Silico Study', *North American Symposium on Chemical Reaction Engineering (NASCRE)*, Houston Texas, USA. Oral presentation.

- Gibson et al, 2019, ‘Modelling Thermokinetics Using the Sestak-Berggren Equation: A Calcium Carbonate Study’, *International Conference on Catalysis and Green Chemistry (IGC)*, Tokyo, Japan. Oral presentation.
- Gibson et al, 2019, ‘Kinetic Modelling of the Ammonia Temperature Programmed Desorption of ZSM-5’, *American Institute of Chemical Engineers Annual Meeting*, Orlando, USA. Poster presentation.
- Gibson et al, 2020, ‘Hydrothermal Ageing Mechanism of SAPO-34 Studied by Kinetic Analysis of Temperature Programmed Desorption Data’, *American Institute of Chemical Engineers Annual Meeting*, virtual meeting. Poster presentation.
- Gibson et al, 2021, ‘Kinetic Modelling of the Ammonia Temperature Programmed Desorption of ZSM-5’, *Chemical Engineering Day 2021, University of Bradford.* Poster presentation.
- Gibson et al, 2021, ‘Identification of transport derived errors in thermal analysis testing’, *17th International Congress on Thermal Analysis and Calorimetry (ICTAC 2020), Krakow, Poland.* Oral presentation.

1.7. References

[1] N. M. Deraz, ‘The comparative jurisprudence of catalysts preparation methods: I. Precipitation and impregnation methods.’, *Journal of Industrial and Environmental Chemistry*, vol. 1, no. 2, 2017, Accessed: May 26, 2021. [Online].

[2] T. Ozawa, ‘Thermal analysis review and prospect’, *Thermochimica Acta*, p. 8, 2000.

[3] Johnson Matthey plc, ‘2020 Annual Reports and Accounts’. Johnson Matthey plc, Jun. 24, 2020.

[4] ‘About us | Johnson Matthey’. https://matthey.com/about-us (accessed May 26, 2021).

[5] ‘Our sector structure | Johnson Matthey’. https://matthey.com/en/about-us/our-sector-structure (accessed May 26, 2021).

[6] S. Axon, ‘Internal discussion regarding sustainability of thermal processes with JM’, Jan. 29, 2018.

[7] J. Sestak and G. Berggren, ‘Study of the kinetics of the mechanism of solid-state reactions at increasing temperatures’, *Thermochimica Acta*, vol. 3, pp. 1–12, 1971.

[8] R. L. Gibson, M. J. H. Simmons, E. Hugh Stitt, J. West, S. K. Wilkinson, and R. W. Gallen, ‘Kinetic modelling of thermal processes using a modified Sestak-Berggren equation’, *Chemical Engineering Journal*, vol. 408, 2021, doi: 10.1016/j.cej.2020.127318.

2. Experimental methodologies

Summary

A review of commonly used measurement techniques in the thermal analysis field is presented. Techniques discussed include thermogravimetric analysis (TGA), differential scanning calorimetry (DSC) and thermomechanical analysis (TMA). Three common temperature programs are described, along with the associated benefits and potential drawbacks. The versatility of the two general classes of equipment, pan-style and tubular, are also discussed. These experimental techniques, temperature programs and equipment types can be used interchangeably to study a range of different chemical reactions. Kinetic modelling is sensitive to the quality of thermal analysis data, therefore possible sources of error are discussed, including the choice of temperature range, temperature program, carrier gas composition, carrier gas flow rate, sample mass and choice of sample pan.

2.1. Introduction

Thermal analysis is the study of how materials behave with temperature when heated or cooled in a controlled manner [1] – [3]. This field of study was introduced by Le Chatelier in 1887 and grew quickly due to automation in the 1960's [4].

Thermal processing is performed to obtain products which are more valuable than the reactants. Thermal analysis is used to obtain information about these products or processes, such as to establish the thermal stability of a material or obtain the crystal component which is formed into a product [5]. This class of experimental techniques have been applied to a range of fields as analytical tools, including minerals, inorganic substances, metals, ceramics, polymers, food products and biological systems [6].

In thermal analysis, kinetic data represent the change in a physical property as a function of time (*t*) [3]. This progress is typically defined as the dimensionless extent of reaction represented by α, shown in Equation 2.1.

$$\alpha = \frac{\xi_i - \xi}{\xi_i - \xi_f} \qquad \text{Eq. (2.1)}$$

Where ξ_i is the initial value and ξ_f is the final value of the measured variable. This means α has a value between 0 (no reaction has begun) and 1 (reaction is complete).

There are two types of signal which can be produced by thermal analysis experiments: integral and differential signals. An integral signal directly measures the change of a variable, such as mass loss for a thermogravimetric analysis (TGA) experiment. Differential signals are related to the rate of change of a variable, such as the rate of change of gas composition, when evolved gas analysis (EGA) is used to monitor an experiment.

There are four main properties which can be measured during a thermal analysis experiment:

- Mass
- Power consumption (which relates to enthalpy)
- Composition
- Shape

Each of these properties is measured using a different experimental technique (Section 2.2) but can apply to a wide range of reaction types through a range of temperature programs (Section 2.3). Thermal analysis is a complex field, and differing experimental techniques, temperature programs and reactions can be used interchangeably.

Details of all experiments included in this thesis are given in the chapters which discuss the relevant results. This chapter aims to outline the basic principles of each thermal analysis technique and give an overview of the equipment types and variables considered when collecting data for kinetic studies.

2.2. Experimental techniques

Schematics of equipment suitable for these techniques are discussed in Section 2.5.

2.2.1. Thermogravimetric analysis (TGA)

TGA continuously measures the mass of a sample during an experiment. This enables the detection of mass loss or gain as a function of the temperature program. Mass changes associated with temperatures can relate to physical processes such as evaporation/ desorption, transitions or chemical reactions [2]. An example of typical

TGA data is shown in Figure 2.2. Differential thermogravimetric (DTG) analysis indicates changes in $\frac{d\alpha}{dt}$.

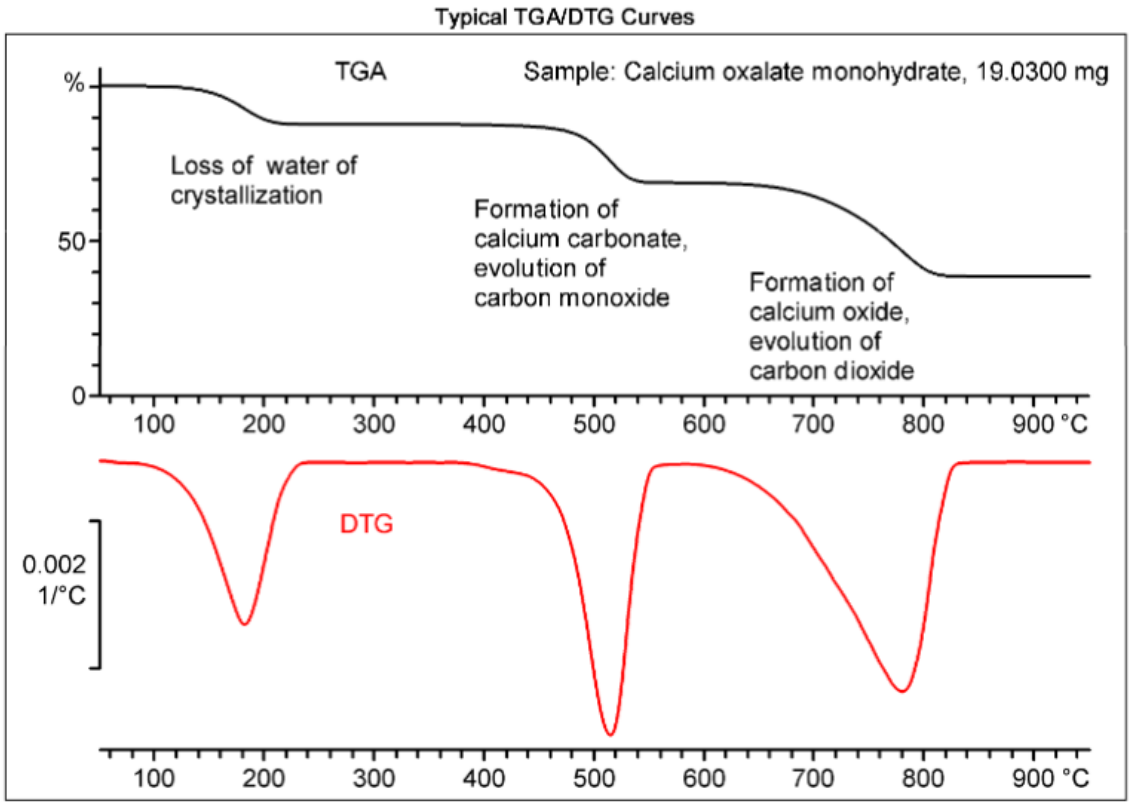

Figure 2.1: Example of typical TGA (and DTG) data, decomposition of calcium oxalate monohydrate, sample mass 19 mg, constant heating rate 30 K min^{-1}, under nitrogen atmosphere. [7].

Gas density is temperature dependent and can change an order of magnitude during a thermal analysis experiment [7]. This change would manifest as an increase in sample mass. To account for this buoyancy effect, a blank run (without sample) at the same conditions, (temperature program, gas flow rate, and sample pan) is subtracted from the experimental data [7]. In some instruments, this blank run is carried out at the same time as the measurement, through a reference pan. This correction is essential to capture mass changes accurately.

This analysis technique can only detect reactions with an associated weight change, such as decompositions. Transformations which result in the same product mass as reactant mass cannot be studied using this technique or using evolved gas analysis.

This technique is relatively cheap, fast and requires a small amount of sample, hence has become a widely available technique and is used to study a range of reactions in a range of application areas.

2.2.2. Differential scanning calorimetry (DSC)

During a DSC experiment, the heat balance on the sample and a reference is monitored as a function of temperature, while a temperature program is applied [2].

There are two main types of DSC, a heat flux and a power compensation DSC. A heat flux DSC uses a defined exchange of heat, with a measured temperature difference to determine intensity and therefore heat flow rate [8]. In power compensation DSC, two pans are used- with the power required to maintain the same temperature between the two pans used to calculate the heat flow rate [8].

The energy absorbed or released by the sample is the usual output for this experiment [2], a typical example is shown in Figure 2.2. This allows the measurement of specific heat capacity, heats of transitions and heats of reaction. This technique can be applied in isolation or combined with TGA, as discussed in Section 2.2.5.

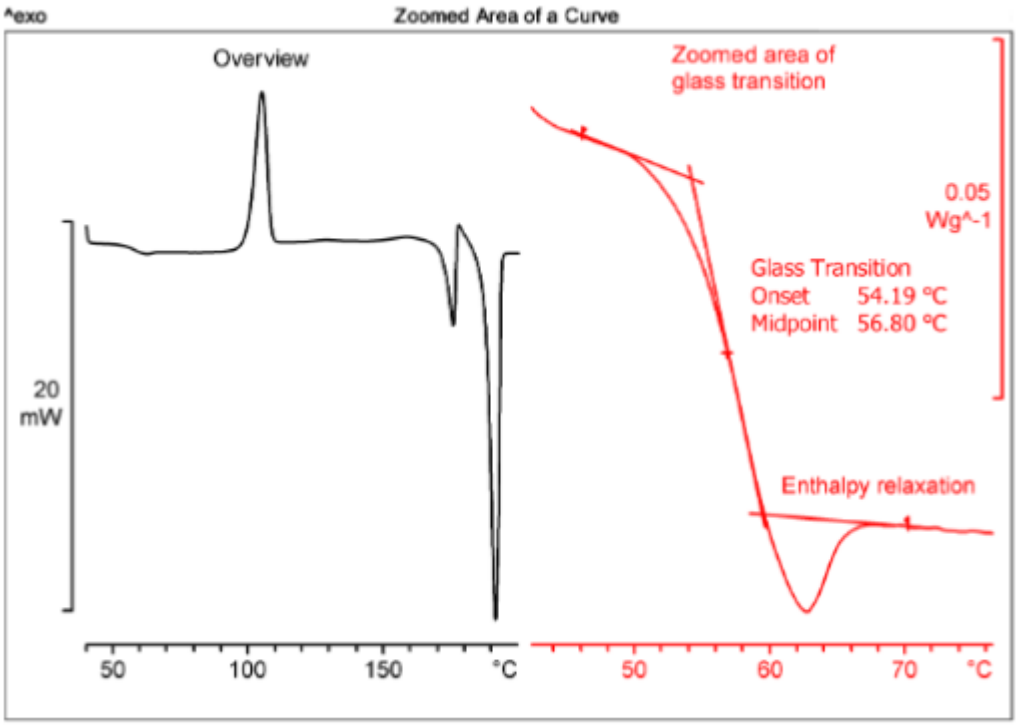

Figure 2.2: DSC results, organic substance. 8 mg sample, constant heating rate of 5 K min^{-1}.Exotherms shown in upwards direction. LEFT: shows overall curve, RIGHT: zoomed area of glass transition. [9].

DSC can be used to study reactions which do not result in a mass change, for example polymerization, rearrangements and curing [9].

For DSC, mass is not usually measured (except in combined techniques discussed in Section 2.2.5). However, the data processing often determines the energy change relative to the original sample mass (in J/g or similar). Thus, it's often common practice to analyse the sample in a sealed sample pan to ensure the sample mass does not change.

2.2.3. Evolved gas analysis (EGA)

EGA allows for the identification of the composition and/or quantity of gaseous species produced [2], [10]. Reactions which involve the carrier gas can be detected, as the carrier gas is also analysed.

These complementary techniques are key to identifying hazardous species and can supply additional information about the mechanism of reaction occurring [3]. Common techniques combined with thermal analysis include mass spectrometry (MS), Fourier transform infrared spectrometry (FTIR), and gas chromatography (GC) [10]. Combined techniques such as GC-MS are also used.

These techniques require calibration (Section 2.6.7) or internal standards to allow for quantification.

2.2.3.1. Mass spectrometry

MS is an online technique which can provide quantitative evaluation [10]. When coupled with a thermal analysis reactor (shown in Figure 2.3), such as a TG unit, the MS is connected using a heated capillary transfer line. As the MS is operated under vacuum, only ~1 % of the effluent gas is analysed [11]. As the absolute flow rate in the transfer line is limited by the capillary diameter, the absolute gas flow rate is constant. This means concentrations measured by MS are relative rather than absolute, for example if a large off-gassing event occurs, the apparent concentration of the carrier gas will decrease.

Once the effluent has entered the MS unit, the gas molecules are ionised, then separated by their mass-to-charge ratio (m/z) [11], [12]. This technique is better suited for detection of small molecules, as large ones can condense and block the capillary/transfer line, and/or are broken into smaller components making identification difficult [10]. There is a maximum mass of 300 amu [10].

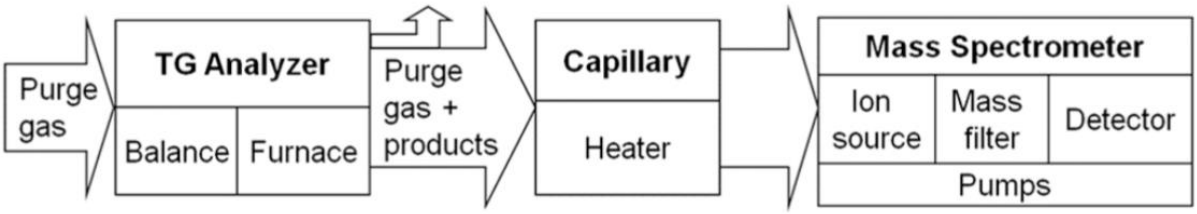

Figure 2.3: Schematic of a typical TGA/MS system [11].

Multiple ion fragments can have the same mass-to-charge ratio and care should be taken when interpreting results. For example, an m/z of 44 could relate to either CO_2^+ or N_2O^+ which could have resulted from CO_2 or N_2O respectively. These can be distinguished by interrogating the mass-to-charge ratio of broken-down species, for example for CO_2 a peak would also be expected at m/z 12.

This EGA technique is widely available, due to its range of application areas. Data collected for kinetic analysis in this thesis has used MS as the EGA technique.

2.2.3.2. Fourier transform infrared (FTIR) spectrometry

FTIR spectroscopy measures the interaction between infrared light and a chemical substance. Depending on the structure of the molecule, light will be absorbed at different frequencies, causing vibration of the molecule [13]. The absorbed frequencies are unique for a particular molecule/functional group, so can be used to identify a substance using libraries [13]. Some molecules (such as N_2, O_2, Cl_2) cannot be detected using this technique as vibration does not change the dipole moments [13].

Figure 2.4 shows a schematic for a typical TGA/FTIR system. The transfer line should be heated to prevent condensation. As the infrared light is low energy, no ionisation/fragmentation occurs (unlike MS), so further analysis with other techniques may be carried out [13].

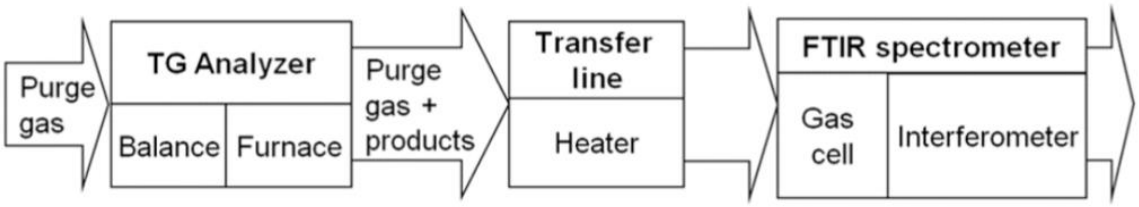

Figure 2.4: Schematic of a typical TGA/FTIR system [13].

2.2.3.3. Gas chromatography (GC)

This EGA technique is not commonly used online, instead gas samples are collected and analysed later, as the analysis takes a long time [14]. These GC units consist of a long, thin column, which the gas passes through; the time to pass through the loop depends on the size of the molecule. Different materials are used for the column, depending on the application studied. This is not an online technique and a maximum number of samples can be stored hence this could result in missing information during the thermal analysis experiment.

2.2.3.4. Combined EGA techniques

Combined techniques are possible, for example GC-MS. In this case, the GC would be used to separate species whilst the MS aids in species identification.

2.2.4. Thermomechanical analysis (TMA)

TMA is used to investigate the physical deformation of a material as a function of temperature, typical results are shown in Figure 2.5. A constant, increasing or modulated force is applied to the material which allows swelling, shrinkage etc and the temperatures at which these occur, to be identified [2]. A coefficient of thermal expansion can also be obtained from this experimentation.

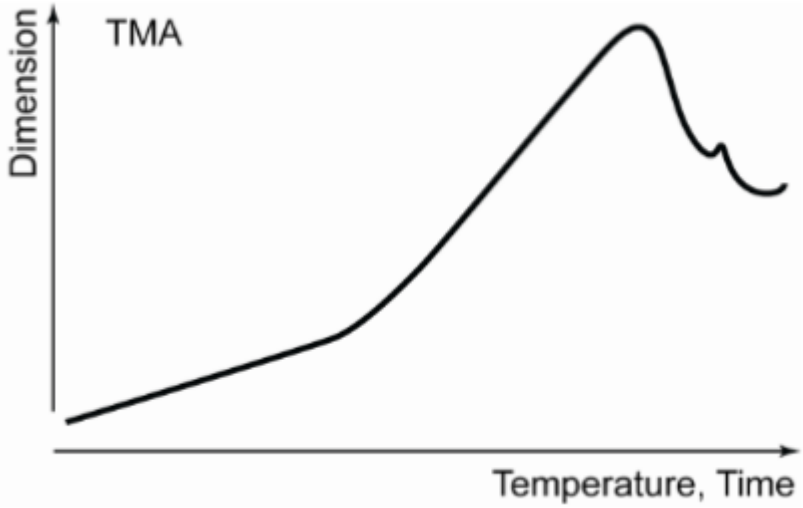

Figure 2.5: Typical TMA results, shows thickness of specimen with temperature [15].

2.2.5. Combined techniques

To maximise the information gained from a single experiment, often thermal analysis techniques are combined. For example, TGA combined with DSC would allow the mass changes to be related to the enthalpy changes. The addition of EGA would also allow the identification of product gases. Although these combined techniques have the clear benefit of additional insights, compromises are often required in data quality. For example, combined DSC/TGA would require a lid-less pan to allow the removal of evolved gases, however this reduces the accuracy of the DSC measurement.

2.3. Temperature program

There are many ways to control the temperature of a thermal analysis experiment. Three temperature control programs are considered in this thesis: isothermal, constant temperature ramp and constant reaction rate experiments.

Any temperature program discussed subsequently should start with an isothermal hold period, to allow a baseline to establish and initial weights to be taken (if applicable).

2.3.1. Isothermal

During an isothermal experiment a constant temperature is maintained, after an initial ramp period to achieve the desired temperature (example shown in Figure 2.6). However, the practical temperature range for these experiments is narrow. At lower temperatures, reactions progress slowly and long hold times are required to gather sufficient data to fully describe the process [16]. For higher temperatures the time to heat the sample may be similar to the time for the process, which could result in significant conversion occurring prior to the isothermal period being reached [7].

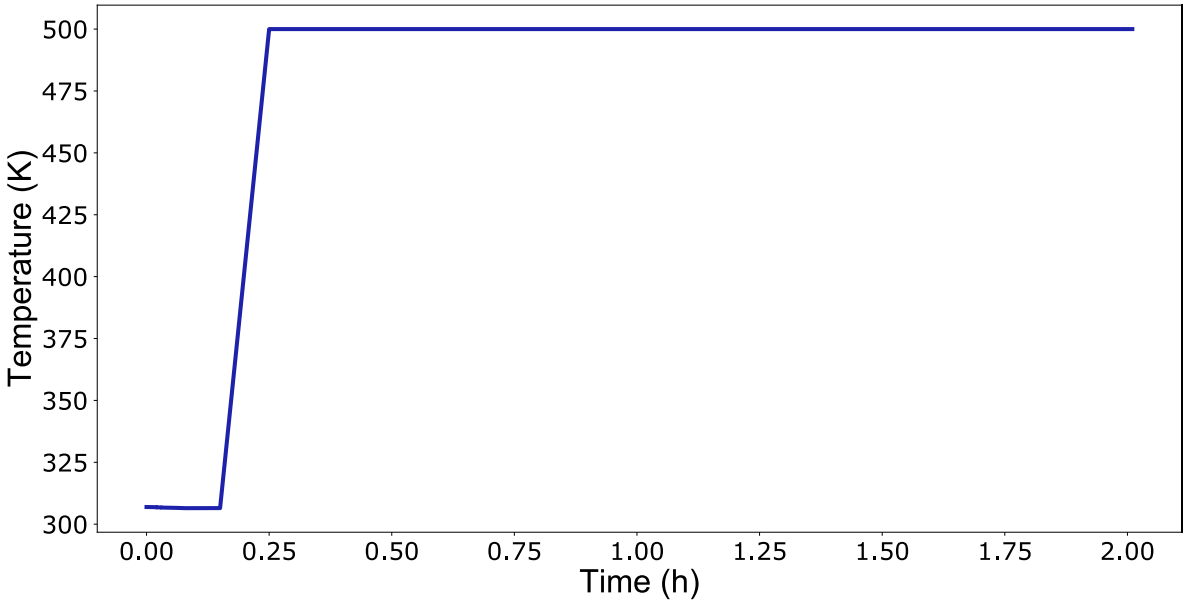

Figure 2.6: Example of isothermal temperature program, 500 K.

Stepwise isothermal experiments, which increase (or decrease) the temperature and maintain an isothermal hold for a fixed time, before repeating the process, can alleviate some of the disadvantages to this type of temperature program, however these experiments still take a long time to perform.

2.3.2 Constant temperature ramp rate

A non-isothermal temperature program using a constant / linear heating rate is often reported in the literature [5]. A common value used in JM is 10 K min^{-1}, an example is shown in Figure 2.7. One advantage of constant heating rate over isothermal experiments is that the full temperature range of interest can be observed in a single experiment [16].

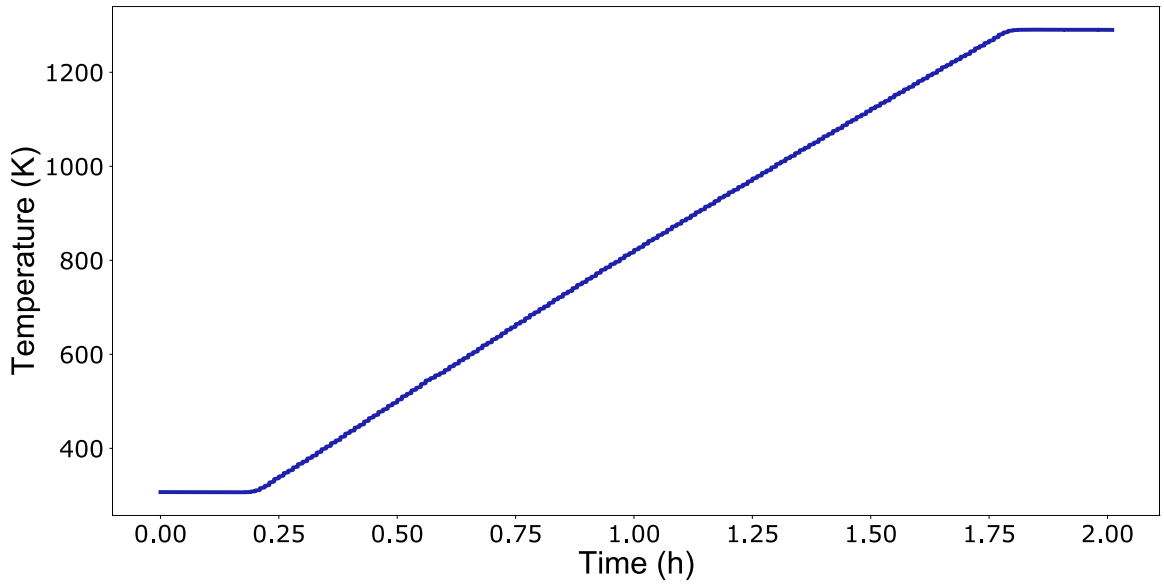

Figure 2.7: Example of linear temperature ramp program, 10 K min^{-1}.

Slower temperature ramp rates are used to separate overlapping thermal events. Care should be taken to avoid very fast temperature ramps (> 20 K min^{-1}) [3], as significant temperature gradients within the sample may occur. However this is system dependent and in some cases fast temperature ramp rate experiments may be appropriate.

2.3.3 Constant rate thermal analysis (CRTA)

Also known as sample controlled thermal analysis, this technique controls the temperature to achieve a constant rate of change in a measure property, for example

weight, using a feedback loop. An example of the temperature control for a CRTA experiment is shown in Figure 2.8.

A key advantage of CRTA is slower temperature increases are achievable when compared to linear temperature ramp rate experiments, this avoids potential transport issues within the sample. This slower temperature change means thermal events are separated further. Changes in mechanism may also be observed in the case of competing reactions [16].

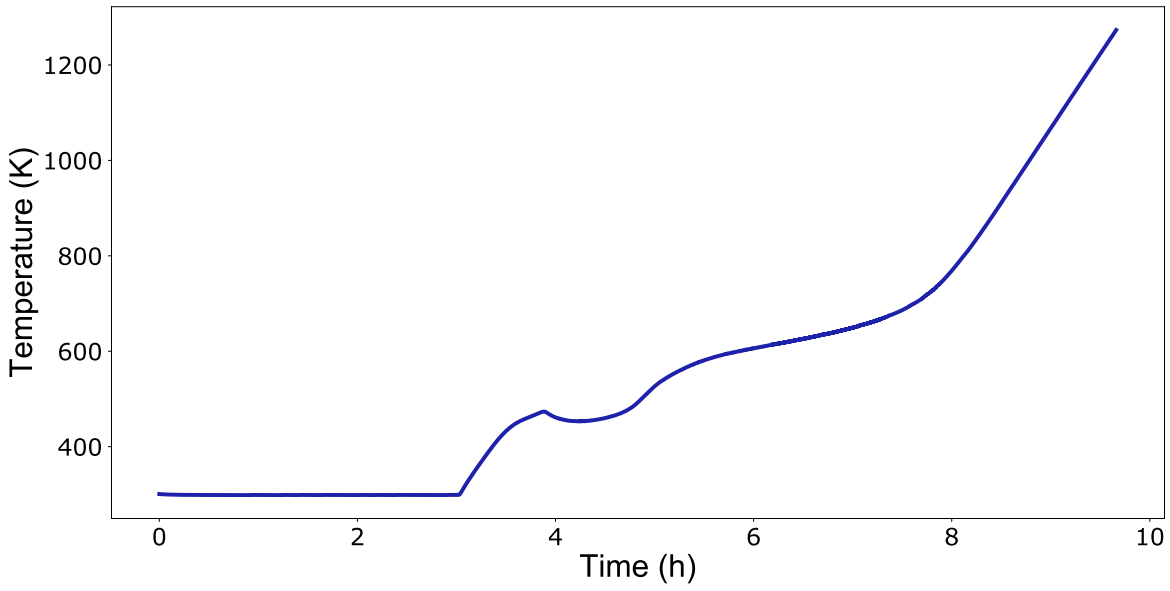

Figure 2.8: Example of CRTA temperature program, rate maintained at 1.7×10^{-3} min^{-1}.

Vyazovkin et al. [17] advocate using combined temperature control programs and suggest that at least one isothermal experiment should be present in all datasets, and that this could be used for model validation. Other combinations of temperature programs could aid in kinetic modelling and this will be discussed further in Chapter 5.

2.4 Reaction types

Using the experimental techniques discussed, it is possible to study a range of reactions.

2.4.1 Oxidation / reduction

An oxidation reaction is the increase in a metal's oxidation state (through the loss of electrons) whereas reduction is the decrease in a metal's oxidation state (increasing the number of electrons). Oxidising atmospheres include air/oxygen, and chlorine. Reducing atmospheres include hydrogen and carbon monoxide. The use of an oxidising or reducing atmosphere would allow for the investigation of such a reaction in a thermal analysis experiment such as TGA or DSC.

These reactions are of interest as these are analogous to those which occur during large-scale thermal processing. Oxidation can occur during calcination under an oxidising atmosphere (commonly air). Similarly, catalyst reduction is carried out to produce an oxidation state of metallic components lower than which exist in an air atmosphere [18], this can also be referred to as catalyst pre-reduction.

2.4.2 Desorption

Adsorption is the deposition of a chemical species to the surface of a solid. Desorption is the removal of the chemical species from the solid surface.

The desorption of a probe molecule can be used to investigate gas-solid interactions on the surface of a material and can provide insight into mechanisms of adsorption, reaction, and desorption [19]. The probe molecule will depend on the active site of interest. For example, ammonia (and to a lesser extent pyridine) temperature programmed desorption is a common analytical tool to evaluate acid sites on catalysts

and functional materials. The NOx storage capacity of a material can be determined via NO or NO_2 desorption [20].

During this experiment, a suitable probe molecule is first adsorbed onto the solid surface. A purge step is used to remove any unbound probe molecules from the surface. This is followed by the temperature programmed step, during which the desorption of the probe molecule is monitored. This reaction is associated with very small weight and energy changes and would not be detectable using TGA or DSC methods.

2.4.3 Decomposition

A thermal decomposition occurs when a single substance breaks down into smaller substances due to the application of heat. Decomposition can occur in an oxidising, reducing or inert atmosphere. The atmosphere can impact the desired products and by-products produced and/or the mechanism of reaction. A decomposition can be studied using TGA or DSC techniques, however, would benefit from the coupling of EGA to identify decomposition products.

This type of reaction relates to large-scale calcination, where precursors or templates are decomposed/reacted to leave the desired solid product.

2.5 Equipment

Generically, there are two classes of equipment design:

(i) Pan-style: where the sample is contained within a “pan”. This pan is connected to a sensitive balance which allows the mass or heat flow of the sample to be tracked during the experimental temperature program. The gas flow is around

rather than directed through the sample. The Netzsch “Jupiter” STA 449 F3 reactor (a TGA/DSC type reactor) and the TA Instruments Q500 reactor (a TGA type reactor) represent this design class, shown in Figure 2.9.

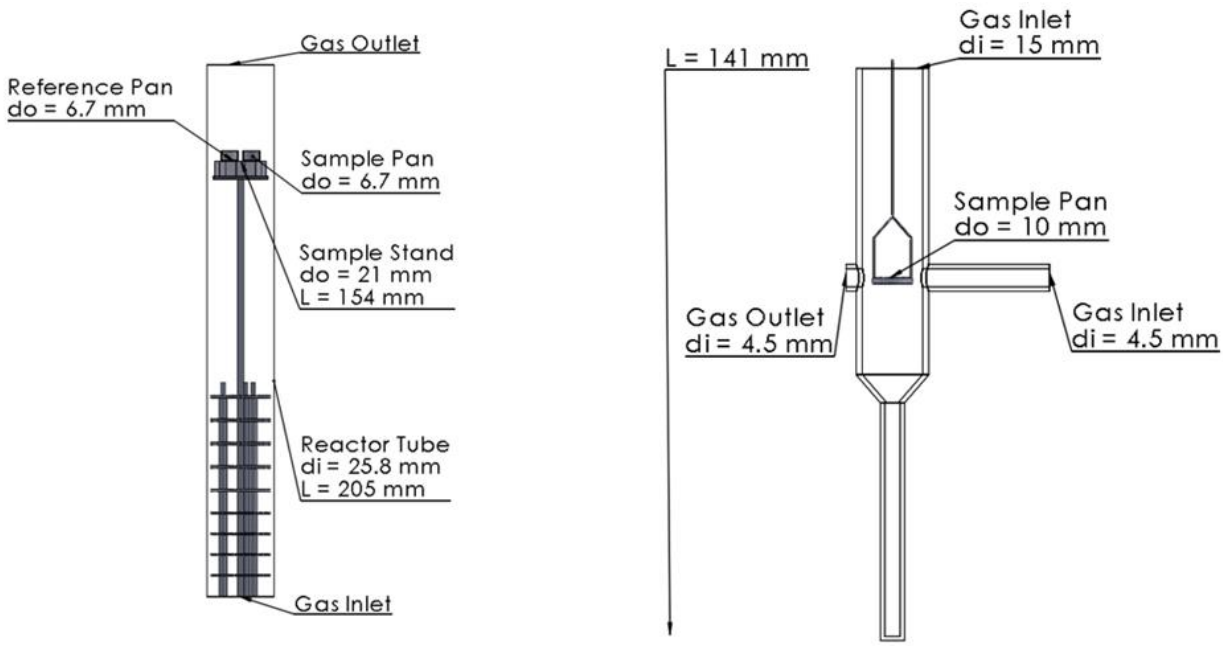

Figure 2.9: Sketch of the Netzsch “Jupiter” STA 449 F3 reactor (left), TA Instruments Q500 reactor (right), both pan-style reactors.

(ii) Tubular: where the sample is packed into a tube and supported using a plug of quartz wool, with the gas flow forced through the permeable powder sample. This class is not able to track the sample mass, eliminating the possibility of TGA experiments. Thermal conductivity detector (TCD) or MS are common ways to monitor the progress of a reaction. The Micromeritics 2920 reactor (a wide packed bed with a constriction downstream) and TA Instruments Altamira AMI 200 reactor (a narrow packed bed) represent this through-flow class, shown in Figure 2.10.

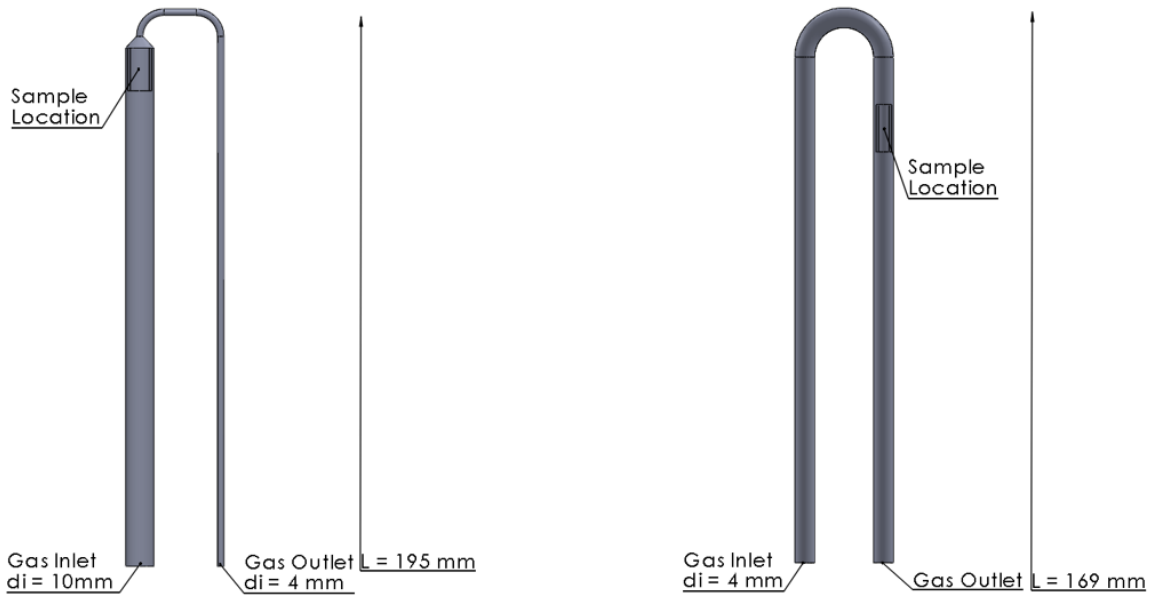

Figure 2.10: Sketch of tubular designs- Micromeritics 2920 reactor (left) and TA Instruments Altamira AMI 200 reactor (right).

Not all types of thermal analysis can be carried out in a single piece of equipment. This has led to varying equipment designs from different manufacturers. Table 2.1 shows the different techniques which can be applied in the different classes of thermal analysis reactor.

Table 2.1: Capabilities of thermal analysis equipment types.

Equipment type	TGA	DSC	Coupled with EGA
Pan-style	✓	✓	✓
Tubular	✗	✗	✓

2.6 Sources of error

The International Confederation for Thermal Analysis and Calorimetry (ICTAC) have a series of papers, which include a discussion on the collection of kinetic data [3]. This section will discuss their key recommendations. These recommendations have been followed when gathering the kinetic data presented in this thesis.

When conducting thermal analysis experiments, there are several parameters which can be changed: temperature range, temperature/temperature ramp rate, carrier gas composition, carrier gas flow rate, sample mass and choice of sample pan. Some of these variables are limited by the instrument chosen and the properties of the sample and the reaction of interest.

2.6.1 Sample

Sample mass and form should be selected to minimise potential temperature gradients inside the sample. Small mass values on the order of milligrams are conventionally used as these remove temperature and gas gradients [3]. The sample mass selected for a TGA experiment will influence the signal to noise ratio. Although small sample masses reduce gradients, this will create a smaller signal to noise ratio. There is a trade-off between the sample size and ensuring a detectable signal.

Vyazovkin et al. [3] recommend that for a series of kinetic experiments, the sample mass should be kept constant, as far as is reasonably practical (within measurement tolerances). However, if intrinsic data have been collected, the mass of the sample should not impact the results. Hence, varying the mass by small amounts can indicate whether a kinetic condition has been reached.

Many of the simple reaction models (discussed further in Chapter 3) are reliant on sample particles which are uniform in size and shape [21]. Using a specific sieve fraction can aid in ensuring the particle size is uniform.

Samples can either be a bulk or powder. For bulk samples, suitable segments must be cut (for example a thin cylindrical disk) [3]. If using a powder sample in a pan-style reactor, the sample should be spread evenly within the pan [3].

2.6.2 Sample pan

The pan material chosen should not react with the sample/catalyse the reaction and should be thermally stable for the temperature range studied. Aluminium pans are suitable up to 773 K, Al_2O_3, ZrO_2 and platinum up to 2023 K and tungsten and graphite up to 2673 K [3].

Pans are usually cylindrical with low height to diameter ratios to allow evolved gas to be removed. Pans with lids are also often used for DSC experiments [3], to ensure the sample mass remains constant, as evolved gases remain trapped in the pan.

2.6.3 Temperature range

The temperature range of an experiment should be based on the process of interest. An initial temperature ~50 K lower than the process start temperature allows acquisition of a reliable baseline and ending a thermal analysis experiment ~50 K after the process has ended allows comparison to the initial baseline [3]. Final isothermal hold periods can also be used to confirm all thermal events have completed and to establish a final baseline.

2.6.4 Temperature / temperature ramp rate

Most modern thermal analysis reactors measure the reference/reactor temperature and the sample temperature. For pan-style reactors the sample temperature can either be taken from the sample / reference pans (for a TGA/DSC type reactor, left Figure 2.9), or from a thermocouple in the gas above the sample (for a hanging pan-style reactor, right Figure 2.9). For tubular reactors, a thermocouple is commonly inserted into the sample bed. The sample temperature should always be used for the calculation of kinetic parameters [3].

It is preferable to maintain moderate reaction rates to avoid the influence of transport limitations. This is achieved by using low temperatures or low temperature ramp rates: temperature ramp rates of 1-20 K min^{-1} are common, but this is dependent on the capability of the equipment used.

The overarching conclusion from the ICTAC paper series was the inadequacy of a single heating rate experiment for kinetic modelling [5], [17], [22]–[26]. This issue had been identified as early as 1976 [27]. As the reaction mechanism is dependent on both the temperature and the reaction progress (extent of reaction) [5], interpreting a single non-isothermal experiment leaves the problem poorly-constrained. Hence, multiple distinct solid-state models can explain the same single heating rate experiment (by using different Arrhenius parameter values for each mechanism). If the range of heating rates is too low, a similar situation arises [24]. It is recommended to have multiple heating rates, which vary by a factor of 5-10 [25], to allow the identification of the reaction mechanism. Generally 3-4 measurements would be sufficient, but for more complex cases more data may be needed [25].

2.6.4.1 Temperature errors

The temperature required for kinetic analysis is that of the sample. Temperature is conventionally controlled using the furnace; however, the sample temperature can deviate from the set temperature due to the sample's thermal conductivity or the occurrence of an endo/exo-thermic reaction. Discrepancies can increase if large sample masses or fast heating rates are used. Vyazovkin et al. [17] recommend that scoping experiments of significantly different masses (under consistent temperature programs) are compared; if the results of the scoping experiments are the same within experimental error, the sample mass is appropriate for use in kinetic experimentation. These scoping experiments could be completed for any of the thermal analysis techniques, such as TGA or DSC. As the sample temperature is required, a thermocouple should be placed either within the sample bed, or as close as possible to the sample to ensure accurate measurements.

A constant systematic error in the temperature would have a small impact on the values of the pre-exponential factor and activation energy estimated using any kinetic modelling techniques [17]. A systematic error which is dependent on temperature ramp rate would cause a discrepancy in the values estimated for the pre-exponential factor and activation energy. This scenario could occur if the sample mass is too large and the sample and reference (furnace) temperature deviate with ramp rate [17]. Extrapolation from data affected by this type of temperature error could result in predictions which are grossly incorrect [17].

2.6.5 Carrier gas

The composition of the carrier gas is dependent on the reaction of interest. Common carrier gases include nitrogen, air, oxygen, argon and helium. When conducting

experiments under inert atmospheres, oxygen is removed prior to data collection via a system purge.

Ideally, evolved gases should be removed from the reactor immediately. The carrier gas flow rate should be constant and high enough to remove evolved gases. To allow the partial pressures of gases at the surface of the sample to be neglected when modelling, the carrier gas flow rate should be ~10 times higher than the rate of gas consumption/production [3]. Considerations should also be made regarding the signal-to-noise ratio, sample retention and buoyancy effects when selecting the carrier gas flow rate.

The direction of gas flow will be determined by the instrument. Vyazovkin et al. [3] reported that the most effective gas removal in TGA units is observed in the supported pan-style reactors in which the gas flows upwards around the sample (left in Figure 2.9), compared to horizontal flow arrangements.

2.6.6 Noise

Smoothing noisy experimental data using mathematical functions such as the Weibull function is possible [26], but should be done with caution as it can lead to the distortion of kinetic parameters and/or the masking of real reaction events [17].

2.6.7 Baseline

A baseline is the signal produced when no detectable thermal events are occurring. These baselines are used to identify the start and end of the thermal events occurring during an experiment. To extract meaningful kinetic parameters from these thermal analysis experiments, the data should be treated with a baseline correction method [28], which is a function subtracted from the data.

There are three groups of baseline correction methods; formal methods (these lack physical justification), methods based on physico-chemical assumptions and experimental methods. The choice of baseline correction method may impact the estimated kinetic parameters and it is recommended that the same correction method be used on a dataset of multiple temperature ramp rates [17].

During completion of this thesis, baseline correction methods have been investigated. Recommendations for choosing suitable correction methods are discussed in Appendix A.

2.6.8 Calibration

Calibration is a key step to achieve good quality kinetic data. All calibration runs are specific to gas flow rate, pan material and temperature ramp rate [3]. Multiple runs may be required for a kinetic study.

For DSC processes, the heat of reaction for known materials are used as a calibration, usually the melting of metals such as indium or zinc is used.

Some TG instruments require reference masses for calibration, others are self-calibrating for mass. To ensure the temperature is calibrated, ferromagnetic materials are heated whilst a magnet is placed above and below the sample. The temperature of the mass jump detected when the material transitions between ferromagnetic and paramagnetic is a well-known value, based on the Curie temperature of the material [3].

2.7 References

[1] M. E. Brown and P. K. Gallagher, ‘Introduction to Recent Advances, Techniques and Applications of Thermal Analysis and Calorimetry’, in *Handbook of Thermal Analysis and Calorimetry*, vol. 5, Elsevier, 2008, pp. 1–12. doi: 10.1016/S1573-4374(08)80004-0.

[2] M. Wagner, ‘1 - Introduction to Thermal Analysis’, in *Thermal Analysis in Practice*, M. Wagner, Ed. Hanser, 2018, pp. 10–15. doi: 10.3139/9781569906446.001.

[3] S. Vyazovkin *et al.*, ‘ICTAC Kinetics Committee recommendations for collecting experimental thermal analysis data for kinetic computations’, *Thermochim. Acta*, vol. 590, pp. 1–23, Aug. 2014, doi: 10.1016/j.tca.2014.05.036.

[4] *Characterization of Nanomaterials*. Elsevier, 2018. doi: 10.1016/C2016-0-01721-7.

[5] M. Maciejewski, ‘Computational aspects of kinetic analysis. Part B: The ICTAC Kinetics Project - the decomposition kinetics of calcium carbonate revisited, or some tips on survival in the kinetic minefield’, *Thermochim. Acta*, p. 10, 2000.

[6] T. Ozawa, ‘Thermal analysis review and prospect’, *Thermochim. Acta*, p. 8, 2000.

[7] M. Wagner, ‘Thermogravimetric Analysis’, *Fundam. Asp.*, p. 25.

[8] G. Höhne, W. F. Hemminger, and H.-J. Flammersheim, *Differential Scanning Calorimetry*. Springer Science & Business Media, 2013.

[9] M. Wagner, ‘7 - Differential Scanning Calorimetry’, in *Thermal Analysis in Practice*, M. Wagner, Ed. Hanser, 2018, pp. 66–143. doi: 10.3139/9781569906446.007.

[10] N. Fedelich, ‘1 - Introduction to Evolved Gas Analysis’, in *Evolved Gas Analysis*, N. Fedelich, Ed. Hanser, 2019, pp. 6–8. doi: 10.3139/9781569908105.001.

[11] N. Fedelich, ‘2 - TGA-MS’, in *Evolved Gas Analysis*, N. Fedelich, Ed. Hanser, 2019, pp. 9–17. doi: 10.3139/9781569908105.002.

[12] M. Wagner, ‘17 - Evolved Gas Analysis’, in *Thermal Analysis in Practice*, M. Wagner, Ed. Hanser, 2018, pp. 299–307. doi: 10.3139/9781569906446.017.

[13] N. Fedelich, ‘3 - TGA-FTIR’, in *Evolved Gas Analysis*, N. Fedelich, Ed. Hanser, 2019, pp. 18–30. doi: 10.3139/9781569908105.003.

[14] N. Fedelich, ‘4 - TGA-GC/MS’, in *Evolved Gas Analysis*, N. Fedelich, Ed. Hanser, 2019, pp. 31–39. doi: 10.3139/9781569908105.004.

[15] M. Wagner, ‘11 - Thermomechanical Analysis’, in *Thermal Analysis in Practice*, M. Wagner, Ed. Hanser, 2018, pp. 187–209. doi: 10.3139/9781569906446.011.

[16] T. Ozawa, ‘Temperature Control Modes in Thermal Analysis’, *J. Therm. Anal. Calorim.*, vol. 64, no. 1, pp. 109–126, Nov. 2004, doi: 10.1023/a:1011580811822.

[17] S. Vyazovkin, A. K. Burnham, J. M. Criado, L. A. Pérez-Maqueda, C. Popescu, and N. Sbirrazzuoli, ‘ICTAC Kinetics Committee recommendations for performing kinetic computations on thermal analysis data’, *Thermochim. Acta*, vol. 520, no. 1–2, pp. 1–19, Jun. 2011, doi: 10.1016/j.tca.2011.03.034.

[18] N. Pernicone and F. Traina, ‘Catalyst activation by reduction’, *Pure Appl. Chem.*, vol. 50, no. 9–10, pp. 1169–1191, Jan. 1978, doi: 10.1351/pac197850091169.

[19] T. Ishii and T. Kyotani, ‘Chapter 14 - Temperature Programmed Desorption’, in *Materials Science and Engineering of Carbon*, M. Inagaki and F. Kang, Eds. Butterworth-Heinemann, 2016, pp. 287–305. doi: 10.1016/B978-0-12-805256-3.00014-3.

[20] E. Fridell, M. Skoglundh, S. Johansson, B. Westerberg, A. Törncrona, and G. Smedler, ‘Investigations of NOx storage catalysts’, in *Studies in Surface Science*

and Catalysis, vol. 116, N. Kruse, A. Frennet, and J.-M. Bastin, Eds. Elsevier, 1998, pp. 537–547. doi: 10.1016/S0167-2991(98)80909-9.

[21] A. Khawam and D. R. Flanagan, 'Solid-State Kinetic Models: Basics and Mathematical Fundamentals', *J. Phys. Chem. B*, vol. 110, no. 35, pp. 17315–17328, Sep. 2006, doi: 10.1021/jp062746a.

[22] S. Vyazovkin, 'Computational aspects of kinetic analysis. Part C. The ICTAC Kinetics Project -the light at the end of the tunnel?', *Thermochim. Acta*, p. 9, 2000.

[23] A. K. Burnham, 'Computational aspects of kinetic analysis.: Part D: The ICTAC kinetics project — multi-thermal–history model-fitting methods and their relation to isoconversional methods', *Thermochim. Acta*, vol. 355, no. 1, pp. 165–170, Jul. 2000, doi: 10.1016/S0040-6031(00)00446-9.

[24] B. Roduit, 'Computational aspects of kinetic analysis.: Part E: The ICTAC Kinetics Project—numerical techniques and kinetics of solid state processes', *Thermochim. Acta*, vol. 355, no. 1, pp. 171–180, Jul. 2000, doi: 10.1016/S0040-6031(00)00447-0.

[25] J. Opfermann, 'Kinetic Analysis Using Multivariate Non-linear Regression. I. Basic concepts', *J. Therm. Anal. Calorim.*, vol. 60, no. 2, pp. 641–658, May 2000, doi: 10.1023/A:1010167626551.

[26] S. Vyazovkin *et al.*, 'ICTAC Kinetics Committee recommendations for analysis of multi-step kinetics', *Thermochim. Acta*, vol. 689, p. 178597, Jul. 2020, doi: 10.1016/j.tca.2020.178597.

[27] J.M. Criado, J. Morales, 'Defects of thermogravimetric analysis for discerning between first order reactions and those taking place through the Avrami-Erofeev's

mechanism', *Thermochim. Acta*, vol. 16, no. 3, pp. 382–387, Sep. 1976, doi: 10.1016/0040-6031(76)80031-7.

[28] W. F. Hemminger and S. M. Sarge, 'The baseline construction and its influence on the measurement of heat with differential scanning calorimeters', *J. Therm. Anal.*, vol. 37, no. 7, pp. 1455–1477, Jul. 1991, doi: 10.1007/BF01913481.

3 Modelling thermal analysis data: a critical review

Summary

Isoconversion and model fitting methods are discussed for the description of thermal analysis data. The assumptions behind the four most common isoconversion methods, Freidman, Vyazovkin, Kissinger-Akahira-Sunose (KAS) and Ozawa-Flynn-Wall (OFW) are discussed along with the limitations of these methods. These limitations include the occurrence of multiple thermal events, reverse reactions, transport limitations, reaction networks and reactions with opposing signs. Isoconversion methods can be used to interpolate single event data and the estimates for Arrhenius terms can be used as initial parameter estimates for model fitting methods. Model fitting methods, including deconvolution techniques are discussed and distributed reactivity models are discounted for use on crystalline solid-state reactions due to the discrete nature of the active sites. Common physico-geometric solid-state models are presented, along with their key assumptions. Identifying a suitable kinetic model is the main limitation of model fitting methods, and the use of the empirical Sestak-Berggren equation was suggested to reduce the number of these solid-state models which require model discrimination. Model fitting methods do suffer similar limitations to isoconversion models: reverse reactions, transport limitations, reaction networks. However, they can be used for overlapped thermal events (which are common) and can provide a physical insight into a process.

3.1 Introduction

Kinetic analysis of thermal analysis data reveals reaction complexities, identifies likely mechanisms, and describes the temperature dependence of the overall reaction rate [1]. Approaches for kinetic modelling can be grouped into either of two main classes, namely model fitting and isoconversion models [2], [3]. Both have proven useful in interpreting thermal analysis data [4] and are applicable to all types of thermal analysis experimental data including isothermal, non-isothermal and sample controlled thermal analysis. However, as with all modelling, the assumptions behind the models must be understood and respected, to ensure that any given model is applicable to the data at hand.

A thermally stimulated process can be described by Equation 3.1 and 3.2 [5]. The rate is dependent on temperature, extent of reaction and pressure.

$$\frac{d\alpha}{dt} = f(\alpha, T, \boldsymbol{P}) \qquad \text{Eq.(3.1)}$$

$$\frac{d\alpha}{dt} = k(T) \cdot f(\alpha) \cdot g(P) \qquad \text{Eq.(3.2)}$$

Equation 3.2 assumes that the kinetic mechanism is not dependent on the temperature. This assumption would not be valid when considering reversible reactions, inhibition terms or changing pathways. However this form is commonly used in thermal analysis literature, and is the basis for the following models.

The pressure dependence $g(P)$ is ignored for most computational kinetic analysis [5]. For reactions such as decompositions which produce significant gaseous products, the partial pressure of these products can influence the reaction rate, especially if the gaseous products are not removed from the reaction zone effectively [5]. In this case,

a reaction could become equilibrium limited, and the partial pressure of the product would be a key element to account for.

However the most common kinetic equation to describe a single thermal event is shown in Equation 3.3. [6], accounting for only the temperature and extent of reaction dependence.

$$\frac{d\alpha}{dt} = A \exp\left(-\frac{\mathrm{Ea}}{R.T}\right) f(\alpha) \qquad \text{Eq. (3.3)}$$

The applicability of the Arrhenius equation for solid-state reactions has been questioned. This derives from the Maxwell Boltzmann equation which does not account for the energy distribution of the immobilised components of a crystalline reactant [7]–[10]. Galwey and Brown [11] conclude that although the Arrhenius equation may not account for all components, no realistic alternative equation has gained acceptance within the literature.

The pre-exponential factor, activation energy and kinetic model $f(\alpha)$ make up a 'kinetic triplet' [1]. A system cannot be fully described without all three components, and no single parameter should be quoted alone [6] [12]. Equation 3.3 only considers the solid state present, hence does not consider the gas phase. This equation is used as a starting point for both model fitting and isoconversion models.

The kinetic triplet can either be viewed as:

- Physically meaningful and give an insight into solid-state mechanisms.
- Not physically meaningful but useful for predicting rates for conditions where data collection is impractical (for example high temperature ramp rates).

Maciejewski [6] suggests that the true meaning of the kinetic triplet lies somewhere between these two extreme opinions.

It is stressed that a reaction rate may be described adequately by a single thermal event, however this does not mean only a single reaction is occurring [5]. For multiple reactions which have a single rate determining step, Equation 3.3 can be a suitable description of the reaction rate.

Other systems may feature more than one thermal event, and these events can be overlapped [1]. For a system of multiple thermal events, with differing activation energies, the reaction rate will depend on both temperature and extent of reaction [2]. For these multistep reactions Equation 3.3 is modified to account for multiple kinetic triplets, as shown in Equations 3.4 and 3.5 [12]. This is achieved using $F_{v,i}$, the fractional contribution of each thermal event to the overall curve.

$$\frac{d\alpha}{dt} = \sum_i F_{v,i} \frac{d\alpha_i}{dt} \qquad \text{Eq.(3.4)}$$

$$\alpha = \sum_i F_{v,i} \ \alpha_i \qquad \text{Eq.(3.5)}$$

In systems containing multiple thermal events, these events can be either independent, consecutive, or competing. An independent reaction refers to multiple reactions which are not connected or dependent on each other [13]. The most common example would be a mixture of several materials.

$$A \rightarrow B$$

$$C \rightarrow D$$

A consecutive reaction contains an intermediate product which is required to form prior to reaction to the final product [13].

$$A \rightarrow B \rightarrow C$$

A competing reaction contains multiple routes to differing products [13].

$$A \rightarrow B$$

$$A \rightarrow C$$

These three reaction types are summarised in Figure 3.1.

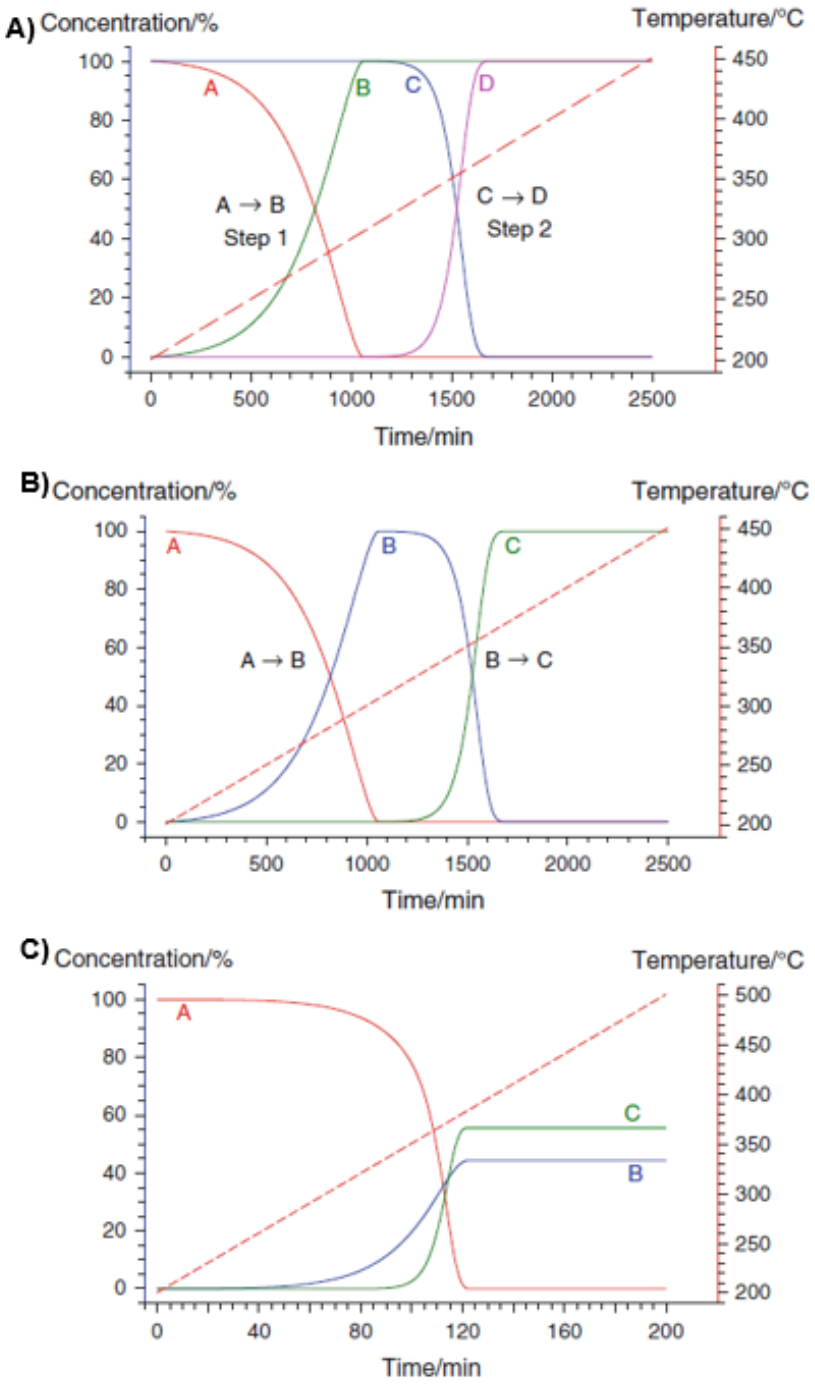

Figure 3.1: A) example of reaction scheme for independent reactions. B) example of reaction scheme for consecutive reactions. C) example of reaction scheme for competing reactions [13].

3.2 Statistical principles of model fitting

It has been said “all models are wrong, some are useful” [14], [15]. It follows that the pursuit of a perfect fit (measured with all metrics) to experimental data is not a sensible or desirable goal when dealing with the vagaries of real data. Instead, a ‘useful’ model which avoids excessive parameterisation should be the goal of modellers. To achieve this, the principles of ‘closeness of fit’, ‘quality of fit’ and parsimony/overfitting need to be understood and considered.

3.2.1 Closeness of fit

Closeness of fit (also commonly referred to as ‘goodness of fit’) evaluates how well the models describes the experimental data. There are many metrics to evaluate this, some of the most common include R^2 and residual sum of squares (RSS).

R^2 shows the dependence of the proposed linear model and the dependant variable. A value of zero implies none of the variance in the data is accounted for in the model, and a value of 1 shows that all the variance within the data is accounted for in the model. As some of the variance in a real dataset will be noise / experimental error, achieving $R^2 = 1$ implies overfit (discussed in Section 3.2.3).

A residual is the error between the experimental results and the model prediction. The smaller the residuals, the closer the model fits to the experimental data. RSS is often used as a metric to evaluate the closeness of fit, with smaller values reflecting a close fit.

A rigorous criticism of models and their fit is a recent development in the thermal analysis literature, despite being long standing practice in the statistical literature [14],

[15]. Vyazovkin et al. [12] express the need to evaluate the model fit using RSS and R^2 values.

Isoconversion models, due to the number of points of equal conversion used and the number of parameters fitted, very often show good closeness of fit. However, having a close fit may not reflect the quality of the model fit. Closeness of fit may be sufficient if interpolation of data is the goal, however, to predict or understand data, quality of fit is also needed.

3.2.2 Quality of fit

Quality of fit is evaluated using metrics such as confidence intervals and residual plots.

Confidence intervals should be tight, if this is not the case there is low confidence in the values of the parameters estimated. Vyazovkin et al. [12] fail to discuss the importance of confidence intervals as an indication of the quality of fit for a model.

Multipeak systems could have many local minima values for the RSS. Ensuring a global minimum has been achieved is vital when reporting parameter estimates.

Residuals should not only be small, but for a good quality model these should be distributed around zero. The distribution of residuals should be analysed, for signs of systematic trends. Systematic trends in residuals (for example with time or temperature) indicate that the model used does not fully describe the system. This could be the case for overlapped thermal events, as residuals would indicate the region of overlap.

Most of the literature for kinetic modelling of thermal analysis data does not include analysis of residual trends, and confidence intervals are rarely reported. This means possible trends within the residuals may exist, and the confidence in the model cannot be established. Although the closeness of fit for these models may be acceptable, the quality of fit has not been presented in the literature.

3.2.3 Parsimony/overfitting

An important part of model fitting/parameter estimation is the avoidance of overfit. Overfit is the inclusion of spurious, uncontrolled variables within a model, effectively experimental error. This is often a result of the addition of unnecessary parameters to achieve a closer 'fit' [16]; an example of this is shown in Figure 3.2. In extreme cases this can hide important systematic errors behind unreal confounding effects.

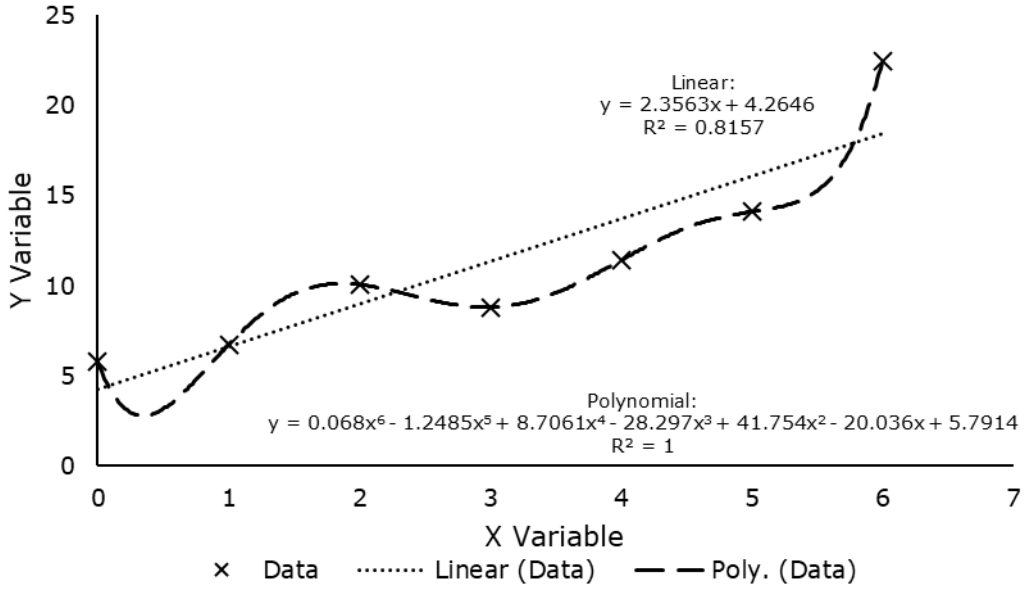

Figure 3.2: Example of overfit. Increasing the number of parameters, shown as polynomial (dashed line), increases R^2 value.

Overfit can cause a broadening of confidence intervals for estimated parameters [16]. As parameter estimation is a primary goal of kinetic modelling, high confidence in any

predicted parameters is desirable. As overfit would reduce confidence, this should be avoided. 95% confidence intervals are very rarely discussed in the thermokinetic modelling literature.

Vyazovkin et al. [12] refer to overfitting and stress that each step introduced in a model should have a mechanistic basis however the diagnosis of overfitting is not discussed.

Model criticism and consideration of overfitting applies to both model fitting and isoconversion methods.

3.3 Isoconversion methods

Isoconversion modelling is widely used within the literature [17]–[22] as it allows the estimation of kinetic parameters without the assumption of a specific kinetic model [2], [23]–[25]. This class of modelling has been referred to, erroneously, as ‘model free’ kinetic analysis [25].

Isoconversion methods estimate Arrhenius parameters for numerous points of equal conversion (i.e. isoconversion points). For example, multiple heating ramp rates are used, and the points for 5 % conversion, 6 % conversion (and so on), all the way to 100 % conversion will be used to estimate parameters. This means that many parameters (two per isoconversion point) are estimated for each method.

There are different methods used within the literature to carry out parameter estimation for isoconversion models. These methods can be classified into two types: differential and integral methods. An integral signal relates to the change of a variable, whereas differential signals are related to the rate of change of a variable, as discussed in Section 2.7. The most commonly employed methods in the literature are Friedman

[26], Vyazovkin [27], [28], Kissinger-Akahira-Sunose (KAS) [29] and Ozawa-Flynn-Wall (OFW) [30]–[32]. These will all be discussed in detail.

3.3.1 Friedman method

This isoconversion method is based on work by Friedman [26]. It is in a differential form, shown in Equation 3.6. Due to its differential form, this equation can only be used on integral data following numerical integration [1].

$$\ln\left(\left.\frac{d\alpha}{dt}\right|_{\alpha}\right) = -\frac{Ea_{\alpha}}{R.T|_{\alpha}} + \ln\left[A_{\alpha}.f(\alpha)\right] \qquad \text{Eq. (3.6)}$$

In this equation, the $\ln\left[A_{\alpha}.f(\alpha)\right]$ term becomes a constant at each isoconversion point, and this allows a linear ($y = m.x + c$) plot to be constructed. Hence a minimum of two temperature ramp rate experiments are required. For each datapoint, an activation energy is calculated from the gradient of this equation. The final estimate of activation energy is taken as an average of these values.

Within Equation 3.6, $f(\alpha)$ represents the kinetic function from Equation 3.3, however this function is not required to be in a conventional form (such as those described for solid-state kinetics in [33]) and cannot be extracted from this analysis as it is confounded with the pre-exponential factor to give the y-intercept value for Equation 3.3.

This isoconversion method has the fewest assumptions of those considered herein [2]. These are:

- There exists a function $f(\alpha)$ which gives a consistent value for a given observed α.
- Ea_{α} is consistent between ramp rates at a given conversion.

These result in the following implications:

- $f(\alpha)$ does not have to represent a plausible mechanism (and cannot be extracted from this 'model free' analysis as it is confounded with the pre-exponential factor).
- Although $f(\alpha)$ should be consistent between experiments at a given α, it does not have to be consistent between different isoconversion points within the same experiment.
- Ea_{α} does not have to be constant between different isoconversion points.
- A_{α} does not have to be constant between different isoconversion points

Thus, the value of Ea, the activation energy, can change over the course of the experiment (over the range of temperature ramp). This is in direct contravention of the thermodynamics underpinning the Arrhenius equation, which states that Ea should be constant for a given reaction (or mechanistic step). This variation might be acceptable if the variation is caused by condition-dependent experimental noise. This can be checked by treating deviations from the average value as a function of α as experimental noise and testing that its structure is normally distributed, as one expects for random error. The confirmation of this normal distribution of error is lacking in the Friedman analysis carried out in the literature [3], [17], [19].

Lumping the $\ln[A_{\alpha}.f(\alpha)]$ term together is only valid if the true behaviour for the process is a pure function, and hence gives the same answer for a given observed conversion, independent of temperature ramp rate. This is valid for a kinetically limited single event system with a constant mechanism. This assumption would be invalid for a process which has multiple thermal events, as the individual event conversions are not known, so the same observed α may represent different material states. It would

also be invalidated by the existence of non-kinetic effects, which would be temperature ramp rate dependent. These non-kinetic effects will be discussed further in Section 3.6.

Due to its differential form, this method has been criticised within the literature as it can be unstable and adversely affected by experimental noise [2], [24]. This impact of experimental noise is most likely a result of overfit, as parameters begin to include noise in the fitting. This model contains two parameters per isoconversion point, so for a system containing 50 isoconversion points, a total of 100 parameters are used to fit the Friedman model. Only half these parameters (the Ea values) have physical meaning which could be sense checked. This large number of parameters explains the tendency for this model to overfit. However, this form does mean that more features can often be observed [2]. To avoid issues with experimental noise, it has been suggested to smooth noisy data prior to processing using the Friedman model [2]. However, this can reduce the information provided and should be done with care. Alternatively, the autoregressive integrated moving average (ARIMA) class of modelling could be used to achieve this [34].

3.3.2 Integral methods

This class of isoconversion models rely on integrating the data from the start of each experiment to any given isoconversion point. This is solving Equation 3.7.

$$\int_0^t \frac{d\alpha}{dt}\,dt = A \cdot \int_0^t f(\alpha(t))\,dt \cdot \int_0^t \left(-\frac{Ea_\alpha}{RT(t)}\right) dt \qquad \text{Eq. (3.7)}$$

Assuming a given isoconversion end point, most terms of this equation become independent of temperature, and hence equal, with the significant exception of the

temperature integral. Different integral methods are built on different approaches to solving this temperature integral.

3.3.2.1 Vyazovkin method

Integral forms of isoconversion modelling reduce the impact of experimental noise compared to the Friedman method [24], as the experimental noise is averaged out overall.

Many advancements were made by Vyazovkin in the field of non-isothermal isoconversion modelling around the turn of the 21st century [1], [27], [28], [35]. His first key isoconversion method developed is shown in Equation 3.8-3.9 [28].

The integral of Equation 3.3 over the duration of the experiment gives the observed conversion, shown in Equation 3.8. Therefore, at isoconversion points, the ratio of the integrals for each temperature ramp rate should equal one. Minimising the sum of these ratios gives an objective function for estimating activation energy.

$$\Psi(Ea_\alpha) = \sum_{i=1}^{\tau} \sum_{j \neq \mathrm{i}}^{\tau} \frac{A \cdot \int_0^{t_i} f(\alpha(t_i))dt \cdot \int_0^{t_i} \left(-\frac{Ea_\alpha}{RT(t_i)}\right) dt}{\mathrm{A} \cdot \int_0^{t_j} f(\alpha(t_j))dt \cdot \int_0^{t_j} \left(-\frac{Ea_\alpha}{RT(t_j)}\right) dt} \qquad \text{Eq. (3.8)}$$

If one assumes that A is constant and $\int_0^{t_i} f(\alpha(t_i))\, dt$ is independent of temperature ramp rate, then this reduces to the form shown by Vyazovkin [28], in Equation 3.9.

$$\Psi(Ea_\alpha) = \sum_{i=1}^{\tau} \sum_{j \neq \mathrm{i}}^{\tau} \frac{J(Ea_\alpha, T_i(t_\alpha))}{J(Ea_\alpha, T_j(t_\alpha))} \qquad \text{Eq. (3.9)}$$

A value of Ea_α is found which minimises the value of $\Psi(Ea_\alpha)$, using Brent's algorithm of inverse quadratic interpolation [36]. This minimisation is repeated for every isoconversion data point. This isoconversion method uses numerical integration from

0 to t_α which results in the value for the activation energy being averaged over the whole reaction, hence smoothing the function, shown in Equation 3.10.

$$J(Ea_\alpha, T_\alpha) = \int_0^{T_\alpha} \exp\left(-\frac{Ea_\alpha}{RT}\right) dT \qquad \text{Eq. (3.10)}$$

For this method to be valid, the following assumptions are necessary:

- A is constant throughout the range of integration.
- $\int_0^t f(\alpha(t))\, dt$ is a single function which can describe the range of integration and is consistent between ramp rates.
- Ea_a should be a constant throughout the range of integration, even though it is estimated independently at each isoconversion point.

It follows that:

- $\int_0^t f(\alpha(t))\, dt$ does not have to represent a plausible mechanism.
- $f(\alpha)$ cannot be extracted from the analysis.
- If Ea_a is not consistent between isoconversion points then the method is invalid, because any given isoconversion data point has a different activation energy depending on the end point of integration.

It was found that features and sharp thermal events can be poorly-captured due to this smoothing of the function [27]. To avoid these effects, this method was modified to account for the 'variation in activation energy' using the following Equations 3.11 [27].

$$J[Ea_\alpha, T_i(t_\alpha)] \equiv \int_{t_\alpha - \Delta\alpha}^{t_\alpha} \exp\left[\frac{-Ea_\alpha}{RT_i(t)}\right] dt \qquad \text{Eq. (3.11)}$$

In this modification, integration is carried out over a small interval of time ($\Delta\alpha$). The trapezoid rule is used to find the value of *J*, and this is substituted into Equation 3.9 for

the minimisation to be carried out. The accuracy of the trapezoid rule is dependent on the size of the time interval selected, yet there is no discussion regarding the impact of this interval. Authors note that as a result of this modification, “the constancy of Ea_α is assumed for only a small segment $\Delta\alpha$” [27].

This modification does not directly change the assumptions associated with the model stated previously, however the range of integration is now small ($\Delta\alpha$) rather than over the full reaction.

The activation energy term in the Arrhenius equation is inherently constant for a given single reaction (or mechanistic step). It is therefore unclear why the authors considered modifying this almost axiomatic aspect of reaction kinetics. This shorter interval reduces the claimed benefit of averaging out experimental noise, and the method becomes no more robust than the Friedman method. In fact, this method is mathematically equivalent to using the Friedman method with a moving average of the data. This can be seen by considering the limit $\Delta\alpha \rightarrow 0$.

In this method the number of parameters equates to the number of isoconversion points used for the analysis. Due to the minimisation shown in Equation 3.9, only the Ea value is estimated for each isoconversion point. Although this approach halves the number of estimated parameters with respect to the other isoconversion methods, this is still a high number and risks overfit.

3.3.3 The ‘temperature integral’ methods

When the Arrhenius equation is integrated over a time dependant temperature range, the ‘temperature integral’ is obtained, where $x = \frac{Ea}{RT}$. This integral is shown in Equation 3.12 [30].

$$q(x) = \int_0^T A \exp\left(-\frac{Ea}{RT}\right) dT = [(-\exp x)/x] - \int_x^\infty \exp(-x)dx/\,x^2 \quad \text{Eq. (3.12)}$$

There are many methods to calculate this temperature integral, including a Schlömilch expansion, an expansion using a series of Bernoulli numbers, and other simpler approximations [30]. The accuracy of these approximations heavily impacts the activation energy parameter(s) obtained [30]. The KAS isoconversion method is based on a simple approximation of this integral, whereas the OFW method uses an empirical approximation. This appears to be a product of the age of these methods, which were developed when numerical integration was computationally expensive. This is no longer the case, so it is not clear why these approximations are still used.

Unlike the Friedman method, which allows the value of activation energy to vary at each datapoint, the KAS and OFW methods impose an invariant value for activation energy, which is consistent with the definition of the Arrhenius equation, for a single thermal event system.

The KAS and OFW methods both use this constant activation energy estimation to integrate from zero to a chosen extent of reaction (α) value; usually between 0.05 and 0.95 with a step of 0.05 [37]. No justification for the selected extent of reaction range is given. The gradient of these models allows the calculation of the activation energy. In Figure 3.3, the points represent the different temperature ramp rate experiments. The calculation of activation energy is repeated for many values of α, and these are averaged to give the final estimation. That is to say, although a constant activation energy is assumed for each integration, in reality a different value is assigned for each integration. Thus, at any given conversion the sample may be treated as having several different activation energies. This change makes these methods internally inconsistent.

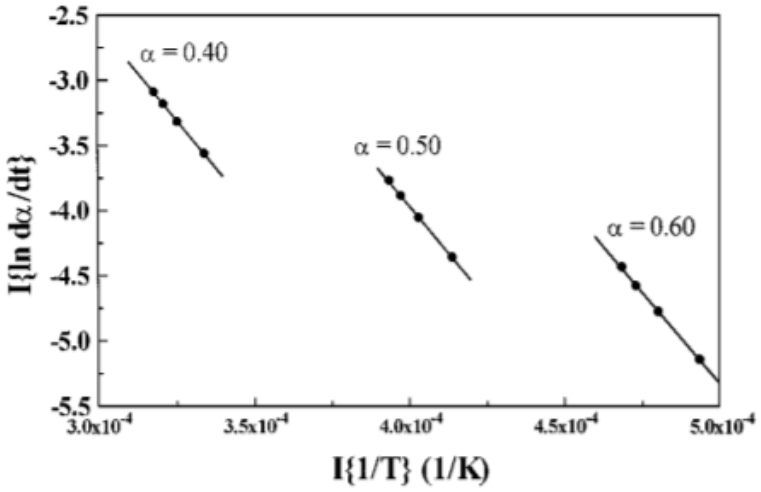

Figure 3.3: Example of graphical solution for Ea (slope of each curve) obtained by KAS or OFW methods, for different degrees of conversion (α = 0.4, 0.5, 0.6) [37].

The KAS and OFW methods both estimate two parameters per isoconversion point, and like the Freidman method, only the activation energy Ea will have physical meaning. This large number of parameters risks overfit, which reduces the confidence in any parameters estimated.

3.3.3.1 Kissinger-Akahira-Sunose (KAS)

The simple approximation for the temperature integral used for this method is given in Equation 3.13 [29].

$$q(x) \cong \exp(-x)/x^2 \ (20 < x < 50) \qquad \text{Eq. (3.13)}$$

The KAS method is known in the form shown in Equation 3.14. Where the $\ln\left(\left(\frac{Ea}{A\,R}\right)\int_0^\alpha \frac{d\alpha}{f(\alpha)}\right)$ term collapses to an estimated constant.

$$\ln\left(\frac{\beta}{{T_\alpha}^2}\right) \cong -\frac{Ea}{R}\left(\frac{1}{T_\alpha}\right) - \ln\left(\left(\frac{Ea}{A\,R}\right)\int_0^\alpha \frac{d\alpha}{f(\alpha)}\right) \qquad \text{Eq. (3.14)}$$

For this isoconversion method, the following assumptions are made:

- A is constant throughout the range of integration.
- $\int_0^\alpha \frac{d\alpha}{f(\alpha)}$ is a single function which can describe the range of integration and is consistent between temperature ramp rates.
- Ea_a should be a constant throughout the range of integration, even though it is estimated independently at each isoconversion point.
- The simple approximation for the temperature integral is accurate.

It follows that:

- $f(\alpha)$ cannot be extracted from analysis.
- $f(\alpha)$ does not have to represent a plausible mechanism.
- If the value of Ea_a is not consistent between isoconversion points then the method is invalid, and any given isoconversion data point is treated as having different activation energies, depending on the end point of integration.

To account for changing activation energy values (i.e. for multistep processes) Equation 3.14 requires modification to the form shown in Equation 3.15. This now gives a single value for the apparent activation energy and apparent pre-exponential factor ($\bar{E}_\alpha$ and $\bar{A}_\alpha$ respectively).

$$\ln\left(\frac{\beta}{{T_\alpha}^2}\right) \cong -\frac{\bar{E}a_\alpha}{R}\left(\frac{1}{T_\alpha}\right) - \ln\left(\left(\frac{\bar{E}a_\alpha}{\bar{A}_\alpha R}\right)\int_0^\alpha \frac{d\alpha}{f(\alpha)}\right) \qquad \text{Eq. (3.15)}$$

The derivation of Equation 3.15 follows the same method as Equation 3.14 (hence the same assumptions and implications apply). The Arrhenius terms are however now averaged values of those occurring from the beginning of the experiment. This would not give useful information about the processes occurring.

3.3.3.2 Ozawa-Flynn-Wall (OFW)

This isoconversion method uses an empirical approximation for the temperature integral, shown in Equation 3.16 [30]–[32].

$$q(x) \cong \exp(-1.052x - 5.33)\ (20 < x < 60) \qquad \text{Eq. (3.16)}$$

The empirical nature of this approximation results in the arbitrary constants in the temperature integral used in the OFW method. The known form of this method is shown in Equation 3.17.

$$\ln(\beta) \cong -1.052\frac{Ea}{R}\left(\frac{1}{T_\alpha}\right) - 5.33 - \ln\left(\left(\frac{R}{A\,Ea}\right)\int_0^\alpha \frac{d\alpha}{f(\alpha)}\right) \qquad \text{Eq. (3.17)}$$

Where the $\left(-5.33 - \ln\left(\left(\frac{R}{A\,Ea}\right)\int_0^\alpha \frac{d\alpha}{f(\alpha)}\right)\right)$ term collapses to a constant.

For this isoconversion method, the following assumptions are made:

- A is constant throughout the range of integration.
- $\int_0^\alpha \frac{d\alpha}{f(\alpha)}$ is a single function which can describe the range of integration and is consistent between temperature ramp rates.
- Ea_a should be a constant throughout the range of integration, even though it is estimated independently at each isoconversion point.
- The empirical approximation for the temperature integral is accurate.

It follows that:

- $f(\alpha)$ cannot be extracted from analysis.
- $f(\alpha)$ does not have to represent a plausible mechanism.
- If Ea_a is not consistent between isoconversion points, then the method is invalid.

Modification to account for multistep processes/numerous activation energy values is shown in Equation 3.18. This gives apparent values for the activation energy and pre-exponential factor ($\bar{E}a_\alpha$ and $\bar{A}_\alpha$ respectively).

$$\ln(\beta) \cong -1.052\frac{\bar{E}a_\alpha}{R}\left(\frac{1}{T_\alpha}\right) - 5.33 - \ln\left(\left(\frac{R}{\bar{A}_\alpha \bar{E}a_\alpha}\right)\int_0^\alpha \frac{d\alpha}{f(\alpha)}\right) \qquad \text{Eq. (3.18)}$$

The same comment applies to this expansion to multistep processes as was applied to the KAS method; the average Arrhenius values would not give valuable insight into the thermal events occurring during the experiments.

3.3.4 Method comparison

Li et al. [19] studied the thermal decomposition of zinc hydroxide carbonate using thermogravimetric analysis. The Friedman and OFW methods were used to estimate Arrhenius terms. Each method found differing activation energy values for each isoconversion point; this was attributed to a two stage mechanism. The authors found that the magnitudes of the activation energy estimated with each method were comparable, however the largest values occurred at different values of conversion. No comments were made to explain these differences, and the results from the OFW method were used as initial estimates in non-linear regression, without justification. The authors did acknowledge these isoconversion results “may contain systematic errors”.

Jankovic [17] compared all four methods discussed above for the decomposition of potassium metabisulfite, studied using thermogravimetric analysis. In general, the average values (for $0.05 < \alpha < 0.95$) for the activation energy estimated from the OFW and KAS methods were lower than those obtained from the Friedman and Vyazovkin

methods. The explanation given was that these differences arise due to the simplified estimation of the temperature integral, and that the OFW and KAS methods introduce error due to the assumption of constant apparent activation energy for each integration. This explanation regarding the source of error is equivocal. Assuming a constant activation energy is not itself a problem, rather taking an average of several of these values would introduce error. Estimated values from the Friedman and Vyazovkin methods were very close, and it was concluded that these models provided the best compromise between stability and accurate values of Arrhenius parameters. As this study uses experimental data (hence the actual value for the parameters are not known *a priori*) and this substance appears poorly investigated in the literature, the conclusion that the Freidman and Vyazovkin methods provide accurate Arrhenius parameters seems poorly justified.

Using *in silico* data for a three-event system, Burnham and Dinh [2] discussed differences in the Friedman, OFW and KAS modelling. The authors found the OFW method overestimated the activation energies used to generate the data (by ~ 13 %), hence under predicted the conversion substantially. This finding contradicts the study from Jankovic [17]. The OFW and KAS methods both estimate constant values for apparent activation energy and pre-exponential factors, features (peaks/troughs) are averaged/smoothed.

To study the thermal decomposition of coal, Jain et al. [3] compared the Friedman, OFW and KAS methods for isoconversion modelling. It was found that for conversions over $\alpha = 0.4$, these models were in good agreement, however below this value the Friedman model predicted substantially higher values for activation energy compared to the OFW and KAS models. The OFW method was deemed “the best fit among the

… methods” and this was taken further to provide initial estimates for model fitting methods. There was no discussion as to how this “best fit” was established, for example statistical goodness of fit tests.

There are many examples in the literature where one modelling method has been applied, however this model choice (and connecting assumptions) is rarely discussed [18], [21], [22].

As shown in this section, multiple authors in the literature have attempted to compare the results of these isoconversion methods. Differing estimates are obtained from each method in all cases. This is due to the underlying assumptions behind these methods. To date, it is believed that no author has dissected these assumptions in detail and the applicability of each method to case studies.

3.4 Model fitting

As model fitting methods inherently include all three components of the kinetic triplet, fewer assumptions are associated with these models than with isoconversion methods.

3.4.1 Deconvolution analysis

When multiple overlapped thermal events are present, deconvolution is required. Deconvolution of thermal events refers to the resolution of individual events, this can be achieved using either mathematical or kinetic deconvolution. Combining data from different experimental techniques is a powerful method to aid in deconvolution [12]. These deconvolution methods still require the statistical principles discussed in Section 3.2, especially degrees of freedom considerations.

3.4.1.1 Mathematical deconvolution analysis

Mathematical deconvolution analysis (MDA) uses individual mathematical functions to describe peak shapes and separate overlapped peaks/events. The common mathematical functions ($F(t)$) used for this deconvolution are shown in Table 3.1.

Table 3.1: Functions used in MDA [12].

Function	Equation
Gaussian	$F(t) = a_0\, exp\left(-\frac{(x-a_1)^2}{2a_2^2}\right)$
Weibull Mixture Model	$F(t) = a_0\left(\frac{a_3-1}{a_3}\right)^{\frac{1-a_3}{a_3}}\left(\frac{x-a_1}{a_2}+\left(\frac{a_3-1}{a_3}\right)^{\frac{1}{a_3}}\right)^{a_3-1} \cdot \exp\left[-\left(\frac{x-a_1}{a_2}+\left(\frac{a_3-1}{a_3}\right)^{\frac{1}{a_3}}\right)^{a_3}+\frac{a_3-1}{a_3}\right]$
Frazer-Suzuki	$F(t) = a_0 \exp\left[-ln2\left(\frac{\ln\left(1+2a_3\frac{x-a_1}{a_2}\right)}{a_3}\right)^2\right]$

The choice of function for MDA appears to be arbitrary in the literature. There are many examples of both the Weibull [38], [39] and Frazer-Suzuki [40]–[42] methods, as these can capture curve asymmetry. In MDA, the Weibull function used is the Weibull mixture model, as opposed to the Weibull distribution, discussed in Section 3.4.3.

As these mathematical functions are inherently independent, this method assumes the physical processes which describe the overall rate are also mutually independent. This method will only identify functions with a physico-geometric interpretation when the

events are independent, for systems with interaction between thermal events the indicated mechanisms may not have a physical interpretation.

Equation 3.19 shows the overall rate represented by the mathematical functions. This is not a kinetic equation, hence, to extract physically meaningful parameters kinetic models should be applied after MDA is completed [12].

$$\frac{d\alpha}{dt} = \sum_{i=1}^{n_{events}} F_{v,i}\,(t) \qquad \text{Eq.(3.19)}$$

The weightings for each thermal event may be known *a priori* from a reaction mechanism, or these can be estimated [12]. If weightings change between temperature programs, this can give an indication of competing reactions [12].

It is important that MDA is followed up by the fitting of either an isoconversion or mechanistic model [43]–[45]. Burnham [4] expressed that applying a purely mathematical function to data is not sufficient for kinetic analysis. For a mathematical function to be useful, transformation to a chemical rate law as a function of conversion must be possible. These mathematical functions do not provide parameter estimates with physical meaning, and would be better suited in data pre-processing, for noise removal or extrapolation of measured conversions to aid in isoconversion analysis [4], where the measured dataset ends before sample conversion is complete.

One danger, which appears undiscussed in the literature, is the idea of error propagation. This method of peak deconvolution requires the fitting of mathematical models, followed by the fitting of a physical model. Each modelling step will have an associated error of fitting. This error will be amplified by the fitting of another model, hence the error of the overall physical parameters estimated may be very high using

this method. Quantification of these errors does not appear standard practice in the literature.

Model criticism and evaluation must be completed on the original dataset to avoid overstating the confidence in a model, caused by possible data smoothing in the MDA step.

3.4.1.2 Kinetic deconvolution analysis

In kinetic deconvolution analysis (KDA) the parameters of Equation 3.3 are estimated directly from the original experimental curve, reducing the risk of error propagation. Wada et al. [46], [47] recommend the initial parameter values used to solve Equation 3.20 are determined first by MDA.

$$\frac{d\alpha}{dt} = \sum_{i=1}^{n_{events}} Fv_i \; A_i \exp\left(-\frac{Ea_i}{RT}\right) f_i(\alpha_i) \qquad \text{Eq.(3.20)}$$

This method can apply either a specific mechanistic model for each event $f(\alpha)$ (such as Avrami-Erofeev [46], [48]), or use an empirical general model such as the Sestak-Berggren model [12], [47], [49]–[51]. Although using the Sestak-Berggren method is empirical and requires re-fitting with the indicated mechanistic models, the issue of error propagation is still reduced as the mechanistic models are fitted to the original data, rather than the estimated Sestak-Berggren curve (as would be the case with the MDA method).

Kinetic deconvolution analysis (KDA) would estimate very similar kinetic parameters compared to those from the MDA method, provided the MDA assumptions apply to the system [12].

Deconvolution is a challenge due to the range of reaction types which can be occurring during thermal processes. When competing or consecutive reactions are present, both MDA and KDA become semi-empirical and may not have *true* physical meaning but could still supply an industrially relevant method for describing overlapped events (assuming similar temperature program conditions) [12].

When applying KDA, data with different temperature programs can either be modelled together or separately. If the data display a change in the extent of reaction curve based on the temperature program, then the data should be treated separately as this implies competing reactions [12].

If reactions with opposing signs i.e. endothermic and exothermic reactions are present within the same system, KDA can still be applied when combined with additional experimental techniques [12]. Muravyev et al. [52] used combined TGA-DSC data, on a system with opposing DSC signals. The weightings for each event were confirmed using a Freidman isoconversion analysis and the opposing DSC signals.

The literature examples on this topic appear limited to systems containing two thermal events [46]–[53], however the method could be applied to high numbers of overlapped thermal events.

3.4.2 Sestak-Berggren model

First identified in 1971 by J. Sestak and G. Berggren, the Sestak-Berggren model [54] is an empirical equation, designed to indicate which solid-state mechanism is occurring. The original form of the equation is shown in Equation 3.21.

$$\frac{d\alpha}{dt} = A \exp\left(-\frac{\mathrm{Ea}}{R.T}\right) \alpha^n (1-\alpha)^m \{-\log(1-\alpha)^p\} \qquad \text{Eq.(3.21)}$$

This form was found to contain an unnecessary degree of freedom [55] and has been reduced to what is often (incorrectly [56]) referred to as the 'truncated' form of the Sestak-Berggren, the Equation 3.22.

$$\frac{d\alpha}{dt} = A \exp\left(-\frac{Ea}{R.T}\right).\alpha^n(1-\alpha)^m \qquad \text{Eq.(3.22)}$$

The Sestak-Berggren equation is more flexible than other logistic (sigmoidal or S-shaped) models as it contains two parameters to describe the shape of the curve, *n* and *m*, rather than a single parameter τ [4]. The width of the curve is described by the *n* parameter and the curve asymmetry by the *m* parameter. This allows the Sestak-Berggren model to describe a range of solid-state reactions [12], [54], [56]–[58], including polymer and organic reactions [59]. The values of *n* and *m* which relate to these mechanisms are given in Table 3.2. Despite the wide range of reaction mechanisms which can be described using the Sestak-Berggren equation, there is still doubt to its applicability as a general model for all possible mechanisms [60].

Table 3.2: Exponent values relating to solid-state mechanisms.

Kinetic Model	*n*	*m*
R2	0.500	0
R3	0.666	0
F1	1.000	0
D2	0.441	-1.002
D3	0.933	-1.011
D4	0.590	-1.014
A2	0.807	0.515
A3	0.751	0.695
A4	0.725	0.787

The Sestak-Berggren equation contains mathematical singularities at both $\alpha = 0$ and $\alpha = 1$. Authors have had differing approaches to dealing with these singularities: the most common approach is to begin the integration from an arbitrary value of alpha [61] [45], an alternative method will be discussed in Chapter 4.

Burnham warned of overinterpreting the results of the 'qualitative' Sestak-Berggren analysis and recommended that the results be coupled with other complementary techniques [59]. The Sestak-Berggren model is empirical; hence the parameters do not have physical values. To obtain a physically meaningful kinetic triplet, the mechanism indicated by the Sestak-Berggren equation should be used to model the original data and obtain Arrhenius parameters.

Burnham [59] proposed a method for approximating initial parameter estimates for the Sestak-Berggren equation based on peak asymmetry, shown in Equations 3.24-3.25.

$$n_{asym} = \left(\frac{\frac{(T_{high} - Tmax)}{(Tmax - T_{low})}}{0.64} \right)^{0.78} \quad \text{Eq.(3.24)}$$

$$m = \frac{W_R^{1.92}}{n_{asym}} \quad \text{Eq.(3.25)}$$

Where T_{low} and T_{high} are the temperatures of the profile at 25 % and 75 % of the maximum reaction rate respectively.

The novelty of the Sestak-Berggren equation was questioned by Burnham in 2015 [4]. Burnham referred to the Sestak-Berggren equation as the 'extended Prout-Tomkins' model on several occasions [4], [59]. The Prout-Tompkins model is a nucleation and growth model and is discussed later in Section 3.4.4.2. In a retort to Burnham's apparent criticism of the Sestak-Berggren equation, Prof. Sestak [56] explained the

novelty of the Sestak-Berggren model was in the *arbitrary* exponents; other models had specified values for *n* and *m*. The Prout-Tomkins model is one such an example, with *n* = *m* = 1. Burnham in 2017 [62] claimed that for both Equations 3.21 and 3.22 in this chapter to be referred to as the Sestak-Berggren equation is illogical. Whilst this disagreement on the novelty and naming of these equations remains, the overwhelming number of citations for the Sestak-Berggren equation (over 785 in 2017 [56]) demonstrates its impact in the thermal analysis literature.

3.4.3 Distributed reactivity models (DRMs)

Multiple, independent reactions [63] can be modelled using distributed reactivity analysis. These models either describe a range of activation energies for one process, or a range of reactions occurring simultaneously, this makes them qualitative at best [12]. These models are based on Equation 3.26.

$$\frac{d\alpha}{dt} = \int_0^{\infty} A(Ea,T) \exp\left[-\int_0^t A(Ea,T)dt\right] D(Ea)\, dE_A \qquad \text{Eq.(3.26)}$$

The activation energy in these models has a distribution ($D(Ea)$). Common distributions used in literature are shown in Table 3.3.

Table 3.3:Distributions used in DRMs [12].

Distribution	Equation
Exponential	$D(Ea) = 1 - \exp(-\lambda t)$
Weibull	$D(Ea) = \frac{\kappa}{s}\left(\frac{Ea - Ea_o}{s}\right)^{\kappa-1} \exp\left(-\left(\frac{Ea - Ea_o}{s}\right)^{\kappa}\right)$
Gamma	$D(Ea) = \frac{\kappa^s}{\Gamma(s)}(Ea - Ea_o)^{s-1} \exp\left(-\kappa(Ea - Ea_o)\right)$
Gaussian	$D(Ea) = \frac{1}{s\sqrt{2\pi}} \exp\left(-0.5\left(\frac{Ea - Ea_o}{s}\right)^2\right)$
Symmetric logistic	$D(Ea) = \frac{\exp\left(-\frac{Ea - Ea_o}{s}\right)}{s\left(1 + \exp\left(-\frac{Ea - Ea_o}{s}\right)\right)^2}$
Asymmetric logistic	$D(Ea) = \frac{\exp\left(-\frac{Ea - Ea_o}{s}\right)}{s\left(1 + \kappa \exp\left(-\frac{Ea - Ea_o}{s}\right)\right)^{\frac{1}{\kappa}+1}}$

Both the Gaussian and symmetric logistic function have simple shapes, as they only have one additional fitting parameter (s) [12] when compared to a model which does not include a distribution. Conversely more complex curve shapes can be captured by the Weibull [64], [65] and asymmetric logistic functions due to the two additional parameters, which model curve width and asymmetry separately [12].

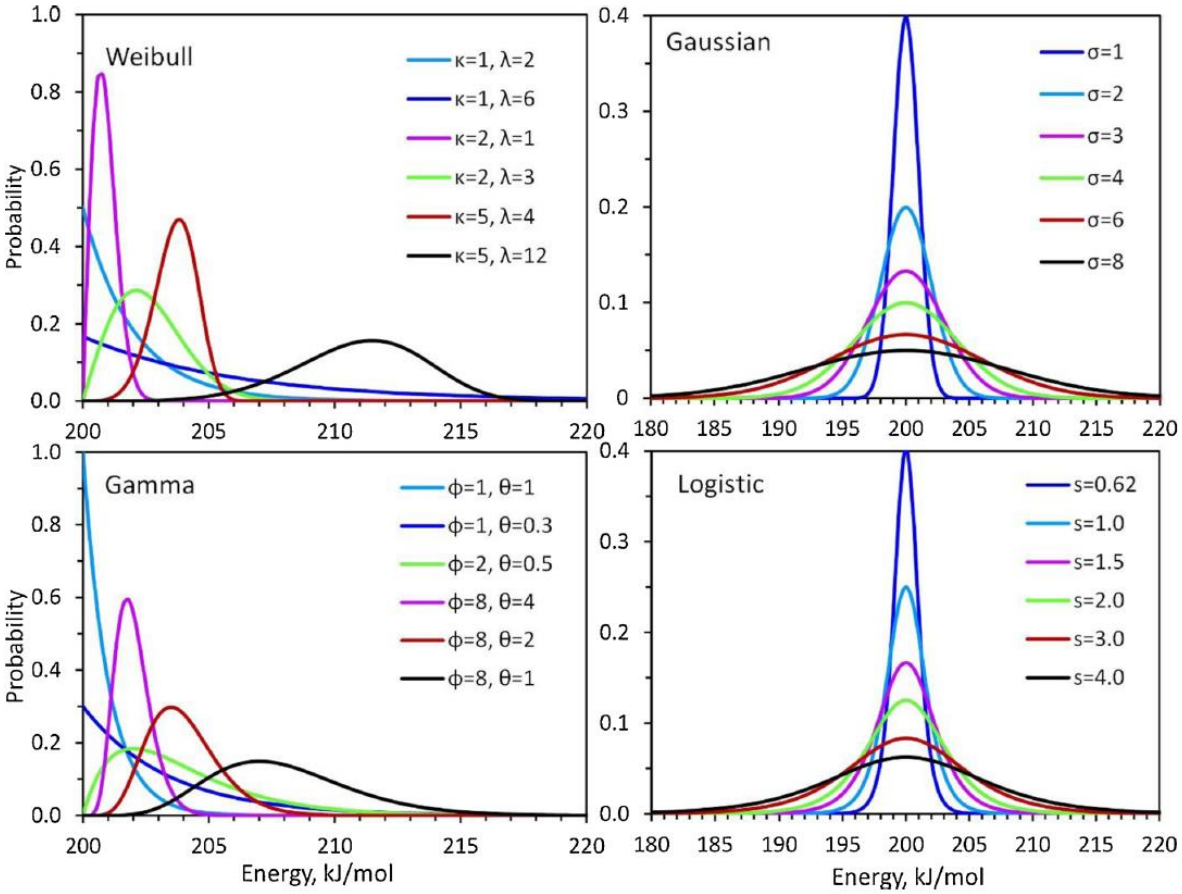

Figure 3.4: Examples of distribution shapes with varying parameter values [12].

Pyrolysis is a complex process, with many simultaneous reactions. DRMs have been successfully applied to the pyrolysis of coal [66] and biomass [67] [68]. Jankovic et al. [69] reported good agreement between Friedman isoconversion analysis and DRM using a single symmetric Gaussian for the decomposition of potassium metabisulfite.

Selection of a suitable distribution is not always justified within the literature [69] or is based on ‘previous success with the technique’ [68]. For a continuous distribution to apply, certain assumptions about the nature of the active sites are required to hold. However, the assumptions behind these distributions are not critically assessed within the literature.

Jain et al. [3] used error analysis (comparison of minimum, maximum and mean errors) to determine a Gaussian distribution was most suitable to describe the pyrolysis of coal. Jankovic [70] recommended that selection is based on the maximum likelihood method (MLM) Equation 3.27 [70], [71].

$$l(\theta) = \prod_i f(\lambda_i, \theta) \qquad \text{Eq.(3.27)}$$

Where l is the likelihood function to be maximised, f is the product densities of the datapoints λ_i, and θ is a constant to be estimated. This MLM method is applicable for models with the same number of parameters, however this is not the case for all the distribution functions shown in Table 3.2. Akaike weights [16] is an alternative method for model comparison, which accounts for the number of parameters.

The Anderson-Darling test [72] was also recommended [70] to test the goodness of fit of the distributions. This metric determines if the measured data obey a preselected distribution, which is deemed true if the value of AD^2 in Equation 3.28 is lower than the critical value [70]. However this requires the calculation of critical values for each distribution tested [73].

$$AD^2 = -\varphi - \left[\sum_{i=1}^{\varphi} \frac{(2i-1)}{\varphi}\left[lnF(Y_i) + \ln\left(1 - F\left(Y_{\varphi+1-i}\right)\right)\right]\right] \qquad \text{Eq.(3.28)}$$

Where F is the cumulative distribution of the selected function, Y_i are the ordered data, φ is the number of data points.

The Weibull distribution was indicated by the MLM and Anderson-Darling test to be the most suitable distribution, chosen from five possible distributions (exponential, logistic, Gaussian, gamma and Weibull) [70], for both the isothermal reduction of nickel oxide

under hydrogen and the isothermal degradation of bisphenol-A polycarbonate under nitrogen [70].

These DRMs are plausible for processes such as biomass pyrolysis which could have a range of active sites obeying such as a continuous distribution. However, they do not seem appropriate for crystalline materials which would have a small set of discrete active sites.

3.4.4 Solid-state reactions

The classes of solid-state mechanistic models are nucleation, geometric shape, diffusion, and reaction order [33]. The models used in these classifications are shown in Table 3.4, all of which can be described with different exponent parameters of the Sestak-Berggren equation (Section 3.4.2). The choice of suitable reaction mechanism should be supported by other techniques where possible [33].

Table 3.4: Mechanistic models for solid-state reactions.

Classification	Mechanism	Equation ($f(\alpha)$)
Geometric Shape	2D Interface Controlled	$2(1-\alpha)^{1/2}$
	3D Interphase Controlled	$3(1-\alpha)^{2/3}$
Nucleation	Avrami-Erofeev n=n	$n(1-\alpha)[-\ln(1-\alpha)]^{1-\frac{1}{n}}$
	Power Law	$n(\alpha)^{1-\frac{1}{n}}$
	Prout-Tompkins	$\alpha(1-\alpha)$
Diffusion	1D Diffusion	$\frac{1}{2\alpha}$
	2D Diffusion	$-[1/\ln(1-\alpha)]$
	3D Diffusion, Jander equation	$\frac{3(1-\alpha)^{\frac{2}{3}}}{2\left(1-(1-\alpha)^{\frac{1}{3}}\right)}$
	3D Diffusion, Ginstling Bronstein equation	$\frac{3}{2\left((1-\alpha)^{-\frac{1}{3}}-1\right)}$
Reaction Order	Zero Order	α
	First Order	$(1-\alpha)$
	n-th Order	$(1-\alpha)^n$

The models in Table 3.4 are in a dimensionless form, which means many contain singularities at either $\alpha = 0$ or $\alpha = 1$. The reason these solid-state mechanisms are in this dimensionless form is not discussed in the literature.

These models can also be described by the shape of the reaction profiles. There are broadly three classes: accelerating, decelerating and sigmoidal, shown in Figure 3.5.

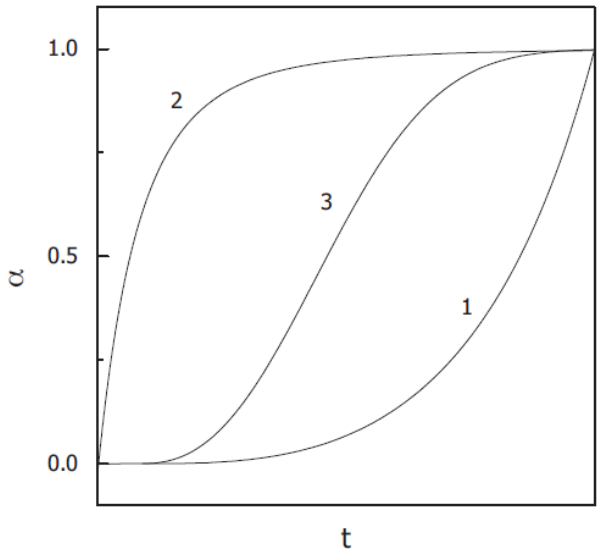

Figure 3.5: Reaction profiles, 1) accelerating 2) decelerating 3) sigmoidal curves [5].

For accelerating reaction profiles, the reaction rate increases continually with extent of reaction. Power law models produce acceleratory reaction profiles [5]. Reaction rates which decrease with extent of reaction are classed as decelerating reaction profiles and these are produced from reaction order or diffusion models [5]. Sigmoidal curves contain both accelerating and decelerating regions [5] and are described by Avrami-Erofeev or Prout-Tompkins models.

3.4.4.1 Geometric shape models

These models assume that the reaction occurs on the surface of a solid particle, and the rate is determined by the interface moving into the particle. The particle can be modelled as either a 2-dimensional cylinder or as a 3-dimensional sphere or cube (Figure 3.6).

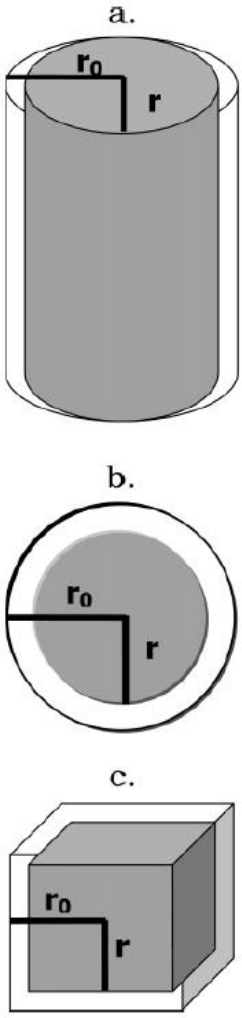

Figure 3.6: Interface model schematics. a) cylinder b) sphere c) cube [5].

The size of the particle is incorporated into the rate constant in these models, hence differing particle sizes within a sample could cause issues with model fitting. This can be avoided by using a specific sieve fraction for the sample.

3.4.4.2 Nucleation models

Imperfections on the solid surface cause a local decrease in activation energy and provide a site for the reaction nucleation [33]. The growth of a nucleus can be restricted by either ingestion or coalescence (Figure 3.7). Ingestion is the inclusion of a growth

nucleus within an existing nucleus. Coalescence occurs when two or more reaction nuclei merge/overlap.

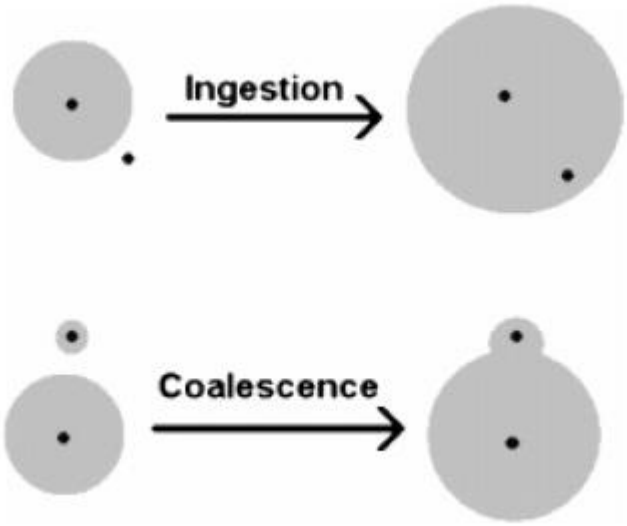

Figure 3.7: Nuclei restrictions. Black dots represent the nuclei, and the grey areas represent the growth regions [33].

The power law model can be used to model these processes if the nucleation rate follows a power law whilst the growth rate is assumed constant. Power law models do not account for growth restrictions; if these are significant the model fit for the decelerating area of the α-time curve may be poor [33].

The Avrami-Erofeev models [74] – [77], so called after the two researchers who independently identified the models, account for both ingestion and coalescence.

These models are sometimes referred to as JMAEK (Johnson, Mehl, Avrami, Erofeev and Kholmogrov) [33].

The Prout-Tompkins model is an autocatalytic model [78] – [80], originally developed for the decomposition of potassium permanganate. Autocatalytic refers to chemistries where the product catalyses the reaction, initially causing an acceleratory phase and

once the reactant is consumed, a termination phase occurs [33], giving similar mathematical properties for different physical reasons. Prout-Tomkins assumes the inflection point for the acceleration and deceleration is at $\alpha = 0.5$ [78]. It is worth noting that this model is integrated without limits (due to the singularity at $\alpha = 0$), resulting in the addition of an integration constant.

3.4.4.3 Diffusion models

Product formation is inhibited by the thickness of the product barrier layer formed; hence the reaction rate decelerates with time. In all these models both the diffusion coefficient and particle size are accounted for within the rate constant [33].

For a plane (1-dimensional surface) the model uses the parabolic law and assumes that the rate is directly proportional to the product layer thickness.

Jander and Anorg [81] used parabolic law to describe a 3-dimensional diffusion process, but this has been shown to be an oversimplification by Ginstling-Brounshtein [82]. Ginstling-Brounshtein used Fick's law for radial diffusion in a sphere to derive their model for 3-dimensional diffusion.

The common model reported in the literature [33] for 2-dimensional diffusion follows the derivation method of Ginstling-Brounshtein [82], assuming a cylinder rather than a sphere.

3.4.4.4 Reaction order models

These models are similar to those used in homogeneous kinetics and relate the reaction rate to the concentration of reactants remaining, to the exponent of the reaction order.

A zero-order reaction implies the rate is independent of the reactant concentrations, instead it could be related to transport phenomena such as mass transport. First order reaction models imply the rate is dependent on the concentration of a single reactant molecule. Whereas second order relates to two reactant molecules; these can either be the same reactant which is likely to be the case in thermal analysis, or two separate reactant species. Third order models relate to three reactant molecules, and so on for any integer value. The physical likelihood of the mechanism reduces with increasing reaction order, and either an alternative model should be considered or the influence of transport phenomena, as discussed in Chapter 7.

3.5 Number of thermal events

It is mathematically possible to assign any number of Gaussian curves to fit thermal analysis data [83], [84]. Fitting additional curves may improve a model's closeness of fit, however the parameter values extracted could cease to relate to physical parameters [83]. A kinetic model used to describe the system should have as few steps as possible to accurately describe the overall rate [12].

Vyazovkin et al. [12] recommend that events should be introduced into a multistep model based on either the visual evidence of peaks/events in the experimental data, or inconsistent values of activation energy estimated via isoconversion modelling. Basing the number of thermal events on a known or reported reaction mechanism is also common [46], [48].

The simplest method for identifying the number of thermal events occurring is visual inspection. Vyazovkin et al. [12] recommend this method as a basis for the *minimum* number of thermal events which should be accounted for during modelling. Whilst this

method is simple, there is a reliance on experience and this process can often be subjective. The absence of multiple visible thermal events does not ensure a single step kinetic process [12], multiple thermal events should still be considered. It is advised that this visual method should not be used in isolation [12].

More rigorous methods for determining the number of thermal events have been suggested. The use of the F-test to determine which model best describes the system was suggested by Opfermann [85] and was recommended by Vyazovkin et al. [12]. The F-test compares the significance of a proposed model compared to a model with no independent variables and can be used for model discrimination. Disproving this null hypothesis should be an essential statistical metric for a proposed kinetic model.

Roduit [86] recommended that overfitting be avoided by introducing a statistical metric which accounts for goodness of fit and the number of models/parameters, without suggesting a suitable metric to access this. Muravyev et al. [53] used Bayesian information criteria to preform model discrimination. This considered the reaction scheme: single or multistep reactions and the possible interactions between multiple reactions (parallel, consecutive, and independent).

3.6 Limitations

Burnham and Dinh [2] state that although isoconversion models are ‘model free’ they are not ‘assumption free’ and the assumptions and limitations associated with each method should be understood. Whilst model fitting methods have inherently fewer assumptions due to the explicit definition of a kinetic mechanism, these models still have limitations which should also be understood.

3.6.1 Imperfect experimental data

Firstly, there are a class of limitations which relate to imperfect experimental data. The collection of good quality thermal analysis data is a non-trivial task, with experienced experimenters encountering difficulties due to differing material properties and equipment designs. Transport limitations within thermal analysis equipment are investigated in Chapter 8.

All isoconversion methods assume the data are kinetically limited, hence free from transport effects (heat and/or mass transfer). If transport limitations are present, the observed α value is not equal to the actual α value in the solid sample. The isoconversion models would still allow calculation of activation energy, but due to the transport limitations, there would be a discrepancy in the temperature at which an event is (apparently) occurring, causing the estimated values to be inaccurate. In this case, these models would incorporate transport effects into the Arrhenius equation, which is inconsistent with the thermodynamics behind the equation. Should this incorporation of transport effects occur, it may be missed by even an experienced modeller - as the model closeness of fit (for all metrics, including R^2 and residual sum of squares) would be as good as with pure kinetic data.

An isoconversion model will always fit the data closely, making it impossible to investigate residual trends. Since the constant containing $f(\alpha)$ is not easily interpreted, even by those skilled in the field, it falls on the analyst to investigate for trends in activation energy. This is not the case for phemenologically based model fitting methods, which return poor closeness of fit when presented with transported limited data, discussed further in Chapters 7 and 8. Investigating the trends in the residuals of

the model can elucidate the problem. Hence when using model fitting methods, diagnosing imperfect experimental data is possible.

Another issue related to imperfect experimental data would be a data set with differing final points. For example, a thermogravimetric analysis (TGA) experiment with different temperature ramp rates which results in different final mass values. As both isoconversion and model fitting methods are based on an extent of reaction, which is calculated for each individual temperature ramp rate experiment, having differing final points would result in differing α curves. As with transport limitations, this would not cause issues with the closeness of isoconversion model fit but could be detected in the raw data by an experienced data analyst.

Both of these concerns can be investigated by using repeat data and repeating an experiment at different space velocities and linear velocities. Kinetically limited data should not be impacted by these experimental settings, however if differences are observed, this implies the presence of transport limitations.

3.6.2 Intrinsic experimental data

There are also limitations which apply, even to ‘perfect’ kinetically limited experimental data.

Many materials produce multiple thermal events which are detected by thermal analysis experiments. Vyazovkin [1] show that isoconversion models can be used to indicate a multiple step process through interrogation of the estimated activation energy values. When multiple events are overlapped however, which is common, the problem becomes ill-posed using isoconversion methods.

For multiple thermal events:

$$\frac{d\alpha}{dt} = \sum_{i=1}^{n_{events}} \left(\mathrm{F}_{v,i} \cdot \frac{d\alpha_i}{dt} \right), \sum_{i=1}^{n_{events}} F_{v,i} = 1 \qquad \text{Eq. (1.15)}$$

As these events overlap, α_i is only known for two points of isoconversion: when $\alpha = 0$ and $\alpha = 1$. Determining the extent of the individual reactions α_i is ill-posed using isoconversion methods, as there are infinite possibilities. To do this, pre-discretisation of the peaks would be needed (discussed in Section 3.4.1). There is little physical or mathematical basis for this, unless each thermal event can be monitored independently, which is uncommon without multiple signals. Modelling overlapping thermal events is possible using model fitting methods.

For multi-event systems studied using non-isothermal experiments, the value of α_i for each event encountered along the overall observed α curve would differ between temperature ramp rate experiments. For example, if the different events had a different sensitivity to temperature due to mechanism or activation energy; equal observed fractional conversion no longer guarantees a consistent material state. The value of $f(\alpha)$ could also be different for each thermal event. This means that the assumption that this is constant is no longer valid and isoconversion models are not appropriate for the extraction of kinetic parameters. This also applies if multiple peaks with opposing signals are overlapped, which is common in differential scanning calorimetry (DSC) data with observed endotherms and exotherms within the same experiment [23].

Similarly, the presence of a reverse reaction could mean that the α value can change depending on the temperature ramp rate used. It is also possible that the underlying assumption of isoconversion models, that full conversion is reached ($\alpha = 1$) would not be met [23]. This would mean that the use of isoconversion models would not be

suitable. The model fitting methods discussed in Section 3.4 assume an irreversible reaction, hence would require modification for use in systems with a reverse reaction.

The presence of reaction networks with multiple pathways would also make the use of these modelling methods inappropriate. Due to the selectivity of competing reaction pathways, this could mean that the extent of reaction may change with temperature ramp rate. Again, a pure function with a repeatable value of α is required for kinetic modelling and this would not be the case for reaction with different possible pathways. Fitting competing pathways is non-trivial.

The main limitation of model fitting methods is the selection of an appropriate kinetic model [5]. An inappropriate model would lead to physically meaningless parameters. Considerations of the reaction being studied and the morphology of the material should be made to inform this decision [5]. The reaction profiles can also be used to infer a suitable class of reaction mechanism. Vyazovkin et al. [12] recommend that a n-th order (Fn) reaction model should be used for events where no other information is present. Alternatively, a full model discrimination of possible solid-state mechanisms (discussed in Section 3.4.4) could be carried out, however this can be computationally expensive when considering multiple thermal events and all combinations of models. A comprehensive selection of models should be considered where possible. The use of the Sestak-Berggren model to identify likely mechanisms could reduce the number of mechanisms considered in a discrimination, this is explored in Chapter 4.

3.7 Applicability

Both isoconversion and model fitting methods have a place in thermal analysis, provided the previously discussed limitations are considered.

3.7.1 As initial estimates for model fitting methods

Isoconversion models can be used to postpone the fitting of a kinetic model and have frequently been used to identify sensible initial parameter estimates for non-linear regression model fits [2], [19], [24], [25]. These models do not replace the need for the identification of a suitable kinetic model, as this is an important part of the 'kinetic triplet' [6], [87]. Vyazovkin [1] show that these isoconversion methods can aid in mechanism identification.

3.7.2 As predictive models

The predictive nature of models has been addressed within the literature. Most often these are examples of interpolation; applying to a reaction rate within the range tested [18], [22], which is valid, for the same equipment and conditions. These interpolation studies are commonly performed on simple materials, such as calcium carbonate which only produce a single thermal event [1], [6]; this is valid.

Vyazovkin et al. [12] clearly state that extrapolation of kinetic models (both isoconversion and model fitting methods) outside of the tested experimental parameters should be done with care. When investigating the same reaction under considerably different temperature ramp rates, the mechanism has been known to change [12]. The occurrence of phase transitions or new/different chemical reactions would make model extrapolation inaccurate.

However, there are examples in the literature of extrapolation. Leroy et al. [20] extrapolate data, and use parameter estimates from non-isothermal experiments with temperature ramp rates of 5, 25, and 40 K min^{-1} to predict the rate of wildfires with a temperature ramp rate of 100 K min^{-1}. Validation of the model for this 100 K min^{-1}

temperature ramp rate is not possible with current thermal analysis experiments; the experiment would likely be heavily transport limited. This makes this extrapolation impossible to verify. Extrapolation without validation in general should be considered with extreme caution. Many authors warn of using these models predictively in this way [2], [23], [25], with Burnham and Dinh [2] using *in silico* data to show that isoconversion models poorly predict sharp changes in reaction rate which may occur outside of the data range tested. Extrapolating using isoconversion models should be avoided.

3.8 Conclusions

Kinetic modelling of thermal analysis data has been discussed. Both isoconversion modelling and model fitting methods have been analysed and the assumptions and limitations of each method highlighted.

Isoconversion methods have limited use in the modelling of thermal analysis data. For a kinetically limited single event system, use of the Friedman or Vyazovkin methods is appropriate however the impact of overfitting on parameter estimates should be recognised. The KAS and OFW methods should be avoided as the simplifications they use add significant error for marginal benefit.

There are limitations of the general isoconversion modelling method - situations which occur that invalidate the assumptions made to derive all of these models - such as competing reaction pathways, an extent of reaction which depends on the temperature ramp rate, the presence of transport effects, backwards reactions and overlapped events with or without opposing signs. Should any of these conditions occur, isoconversion modelling would not be suitable. However, these isoconversion techniques do have value and can be used as a first pass for the identification of kinetic

parameters. Parameters obtained by isoconversion methods should be used as initial estimates for more rigorous model fitting methods. These methods should not be used in isolation.

Both MDA and KDA methods are discussed for the separation of overlapped thermal events. Although common in the literature MDA methods risk overconfidence in estimated parameters and propagation of error and should be avoided.

DRMs have been discussed however it was concluded that the justification of the distribution for crystalline materials would be flawed, and that this methodology is best suited to biomass / pyrolysis type processes which have many components and the possibility of a continuous distribution of active sites on the solid material.

The empirical Sestak-Berggren equation was presented as a possible method for identifying suitable kinetic mechanisms and for reducing the number of model combinations required during model discrimination. The assumptions behind the physico-geometric solid-state reaction mechanisms indicated using the Sestak-Berggren equation were also presented.

The main limitation of model fitting methods is the selection of an appropriate kinetic mechanism. This can be done with either a full model discrimination or using the Sestak-Berggren equation. Selection of an inappropriate model would result in non-physical parameter estimates and reduce the models efficacy for gaining process information. A comprehensive set of models would be required for model discrimination. The mechanistic models discussed in this chapter provide a basis of common solid-state mechanisms and should provide sufficient options for practical application.

Model fitting methods also have limitations with competing reaction pathways, and an extent of reaction which depends on the temperature ramp rate. However, if transport limited data are used, the quality of model fit should indicate the inadequacy of the model. Overlapped events and events with opposing signs can be described using model fitting methods when suitable deconvolution is performed. The solid-state models discussed in this chapter are irreversible and would require modification if a reverse reaction was present.

Respecting the limitations discussed, both isoconversion and model fitting methods have a place in thermal analysis. Isoconversion models are simple and fast to calculate and can give an estimate for activation energy, provided the data used are intrinsic and the process is single step. Model fitting methods are more involved, and care should be taken to select the most appropriate kinetic mechanism, but these methods can give estimates for physical parameters and be used to gain process information.

3.9 References

[1] S. Vyazovkin, 'Computational aspects of kinetic analysis. Part C. The ICTAC Kinetics Project -the light at the end of the tunnel?', *Thermochim. Acta*, p. 9, 2000.

[2] A. K. Burnham and L. N. Dinh, 'A comparison of isoconversional and model-fitting approaches to kinetic parameter estimation and application predictions', *J. Therm. Anal. Calorim.*, vol. 89, no. 2, pp. 479–490, Aug. 2007, doi: 10.1007/s10973-006-8486-1.

[3] A. A. Jain, A. Mehra, and V. V. Ranade, 'Processing of TGA data: Analysis of isoconversional and model fitting methods', *Fuel*, vol. 165, pp. 490–498, Feb. 2016, doi: 10.1016/j.fuel.2015.10.042.

[4] A. K. Burnham, ‘Use and misuse of logistic equations for modeling chemical kinetics’, *J. Therm. Anal. Calorim.*, vol. 127, no. 1, pp. 1107–1116, 2015, doi: 10.1007/s10973-015-4879-3.

[5] S. Vyazovkin, A. K. Burnham, J. M. Criado, L. A. Pérez-Maqueda, C. Popescu, and N. Sbirrazzuoli, ‘ICTAC Kinetics Committee recommendations for performing kinetic computations on thermal analysis data’, *Thermochim. Acta*, vol. 520, no. 1–2, pp. 1–19, Jun. 2011, doi: 10.1016/j.tca.2011.03.034.

[6] M. Maciejewski, ‘Computational aspects of kinetic analysis. Part B: The ICTAC Kinetics Project - the decomposition kinetics of calcium carbonate revisited, or some tips on survival in the kinetic minefield’, *Thermochim. Acta*, p. 10, 2000.

[7] P. D. Garn, ‘An examination of the kinetic compensation effect’, *J. Therm. Anal.*, vol. 7, no. 2, pp. 475–478, Apr. 1975, doi: 10.1007/BF01911956.

[8] P. D. Garn, ‘The kinetic compensation effect’, *J. Therm. Anal.*, vol. 10, no. 1, pp. 99–102, Aug. 1976, doi: 10.1007/BF02179195.

[9] P. D. Garn, ‘Kinetics of decomposition of the solid state: Is there really a dichotomy?’, *Thermochim. Acta*, vol. 135, pp. 71–77, Oct. 1988, doi: 10.1016/0040-6031(88)87368-4.

[10] P. D. Garn, ‘Kinetics of thermal decomposition of the solid state: II. Delimiting the homogeneous-reaction model’, *Thermochim. Acta*, vol. 160, no. 2, pp. 135–145, Apr. 1990, doi: 10.1016/0040-6031(90)80254-V.

[11] A. K. Galwey and M. E. Brown, ‘Application of the Arrhenius equation to solid state kinetics: can this be justified?’, *Thermochim. Acta*, p. 8, 2002.

[12] S. Vyazovkin *et al.*, ‘ICTAC Kinetics Committee recommendations for analysis of multi-step kinetics’, *Thermochim. Acta*, vol. 689, p. 178597, Jul. 2020, doi: 10.1016/j.tca.2020.178597.

[13] E. Moukhina, ‘Determination of kinetic mechanisms for reactions measured with thermoanalytical instruments’, *J. Therm. Anal. Calorim.*, vol. 109, no. 3, pp. 1203–1214, Sep. 2012, doi: 10.1007/s10973-012-2406-3.

[14] G. E. P. Box, ‘Science and Statistics’, *J. Am. Stat. Assoc.*, vol. 71, no. 356, pp. 791–799, Dec. 1976.

[15] G. E. P. Box and N. R. Draper, *Empirical Model Building and Responce Surfaces*. New York: John Wiley & Sons, 1987.

[16] K. P. Burnham and D. R. Anderson, ‘Multimodel Inference: Understanding AIC and BIC in Model Selection’, *Sociol. Methods Res.*, vol. 33, no. 2, pp. 261–304, Nov. 2004, doi: 10.1177/0049124104268644.

[17] B. Jankovic, ‘Kinetic analysis of the nonisothermal decomposition of potassium metabisulfite using the model-fitting and isoconversional (model-free) methods’, *Chem. Eng. J.*, vol. 139, no. 1, pp. 128–135, May 2008, doi: 10.1016/j.cej.2007.07.085.

[18] V. J. Fernandes, A. S. Araújo, M. E. Madruga, and L. F. Nicolini, ‘Model-free kinetics applied to regeneration of coked alumina’, *Thermochim. Acta*, vol. 392–393, pp. 63–69, Sep. 2002, doi: 10.1016/S0040-6031(02)00073-4.

[19] Z. Li, X. Shen, X. Feng, P. Wang, and Z. Wu, ‘Non-isothermal kinetics studies on the thermal decomposition of zinc hydroxide carbonate’, *Thermochim. Acta*, vol. 438, no. 1–2, pp. 102–106, Nov. 2005, doi: 10.1016/j.tca.2005.08.026.

[20] V. Leroy, D. Cancellieri, E. Leoni, and J.-L. Rossi, ‘Kinetic study of forest fuels by TGA: Model-free kinetic approach for the prediction of phenomena’, *Thermochim. Acta*, vol. 497, no. 1–2, pp. 1–6, Jan. 2010, doi: 10.1016/j.tca.2009.08.001.

[21] I. Majchrzak-Kucęba and W. Nowak, ‘Application of model-free kinetics to the study of dehydration of fly ash-based zeolite’, *Thermochim. Acta*, vol. 413, no. 1–2, pp. 23–29, Apr. 2004, doi: 10.1016/j.tca.2003.10.021.

[22] B. Ramajo-Escalera, A. Espina, J. R. García, J. H. Sosa-Arnao, and S. A. Nebra, ‘Model-free kinetics applied to sugarcane bagasse combustion’, *Thermochim. Acta*, vol. 448, no. 2, pp. 111–116, Sep. 2006, doi: 10.1016/j.tca.2006.07.001.

[23] J. R. Opfermann, E. Kaisersberger, and H. J. Flammersheim, ‘Model-free analysis of thermoanalytical data-advantages and limitations’, *Thermochim. Acta*, vol. 391, no. 1–2, pp. 119–127, Aug. 2002, doi: 10.1016/S0040-6031(02)00169-7.

[24] P. Šimon, ‘Isoconversional methods’, *J. Therm. Anal. Calorim.*, vol. 76, no. 1, pp. 123–132, 2004, doi: 10.1023/B:JTAN.0000027811.80036.6c.

[25] J. D. Sewry and M. E. Brown, ‘“Model-free” kinetic analysis?’, *Thermochim. Acta*, vol. 390, no. 1–2, pp. 217–225, Jul. 2002, doi: 10.1016/S0040-6031(02)00083-7.

[26] H. L. Friedman, ‘Kinetics of thermal degradation of char-forming plastics from thermogravimetry. Application to a phenolic plastic’, *J. Polym. Sci. Part C Polym. Symp.*, vol. 6, no. 1, pp. 183–195, 1964, doi: 10.1002/polc.5070060121.

[27] S. Vyazovkin, ‘Modification of the integral isoconversional method to account for variation in the activation energy’, *J. Comput. Chem.*, vol. 22, no. 2, pp. 178–183, 2001, doi: 10.1002/1096-987X(20010130)22:2<178::AID-JCC5>3.0.CO;2-#.

[28] S. Vyazovkin, ‘Evalutation of activation energy of thermally stimulated solid-state’, *J. Comput. Chem.*, vol. 18, no. 3, pp. 393–402, 1997.

[29] T. Akahira and T. Sunose, *Res. Rep. Chiba Inst. Technol.*, vol. 16, no. 22.

[30] J. H. Flynn, ‘The “Temperature Integral” — Its use and abuse’, *Thermochim. Acta*, vol. 300, no. 1–2, pp. 83–92, Oct. 1997, doi: 10.1016/S0040-6031(97)00046-4.

[31] T. Ozawa, ‘Estimation of activation energy by isoconversion methods’, *Thermochim. Acta*, vol. 203, pp. 159–165, Jul. 1992, doi: 10.1016/0040-6031(92)85192-X.

[32] T. Ozawa, ‘Kinetic analysis of derivative curves in thermal analysis’, *J. Therm. Anal.*, vol. 2, no. 3, pp. 301–324, Sep. 1970, doi: 10.1007/BF01911411.

[33] A. Khawam and D. R. Flanagan, ‘Solid-State Kinetic Models: Basics and Mathematical Fundamentals’, *J. Phys. Chem. B*, vol. 110, no. 35, pp. 17315–17328, Sep. 2006, doi: 10.1021/jp062746a.

[34] G. E. P. Box and G. M. Jenkins, *Time series analysis: forecasting and control*, Rev. ed. San Francisco: Holden-Day, 1976.

[35] S. Vyazovkin and N. Sbirrazzuoli, ‘Mechanism and kinetics of epoxy-amine cure studied by differential scanning calorimetry’, *Macromolecules*, vol. 29, no. 6, pp. 1867–1873.

[36] R. P. Brent, *Algorithms for Minimization Without Derivatives*. Courier Corporation, 2013.

[37] C. Li and T. B. Tang, ‘Isoconversion method for kinetic analysis of solid-state reactions from dynamic thermoanalytical data’, *J. Mater. Sci.*, vol. 34, no. 14, pp. 3467–3470, 1999, doi: 10.1023/A:1004605820783.

[38] J. Cai and R. Liu, ‘Weibull Mixture Model for Modeling Nonisothermal Kinetics of Thermally Stimulated Solid-State Reactions: Application to Simulated and Real Kinetic Conversion Data’, *J. Phys. Chem. B*, vol. 111, no. 36, pp. 10681–10686, Sep. 2007, doi: 10.1021/jp0737092.

[39] J. Cai and S. Alimujiang, ‘Kinetic Analysis of Wheat Straw Oxidative Pyrolysis Using Thermogravimetric Analysis: Statistical Description and Isoconversional Kinetic Analysis’, *Ind. Eng. Chem. Res.*, vol. 48, no. 2, pp. 619–624, Jan. 2009, doi: 10.1021/ie801299z.

[40] R. Svoboda and J. Málek, ‘Applicability of Fraser–Suzuki function in kinetic analysis of complex crystallization processes’, *J. Therm. Anal. Calorim.*, vol. 111, no. 2, pp. 1045–1056, Feb. 2013, doi: 10.1007/s10973-012-2445-9.

[41] A. Perejón, P. E. Sánchez-Jiménez, J. M. Criado, and L. A. Pérez-Maqueda, ‘Kinetic Analysis of Complex Solid-State Reactions. A New Deconvolution Procedure’, *J. Phys. Chem. B*, vol. 115, no. 8, pp. 1780–1791, Mar. 2011, doi: 10.1021/jp110895z.

[42] A. Ambekar and J. J. Yoh, ‘Kinetics deconvolution study of multi-component pyrotechnics’, *Thermochim. Acta*, vol. 667, pp. 27–34, Sep. 2018, doi: 10.1016/j.tca.2018.07.007.

[43] N. Koga and Y. Yamane, ‘Effect of mechanical grinding on the reaction pathway and kinetics of the thermal decomposition of hydromagnesite’, *J. Therm. Anal.*

Calorim., vol. 93, no. 3, pp. 963–971, Sep. 2008, doi: 10.1007/s10973-007-8616-4.

[44] N. Koga, Y. Goshi, S. Yamada, and L. A. Pérez-Maqueda, 'Kinetic approach to partially overlapped thermal decomposition processes: Co-precipitated zinc carbonates', *J. Therm. Anal. Calorim.*, vol. 111, no. 2, pp. 1463–1474, Feb. 2013, doi: 10.1007/s10973-012-2500-6.

[45] Q.-L. Yan *et al.*, 'Decomposition kinetics and thermolysis products analyses of energetic diaminotriazole-substituted tetrazine structures', *Thermochim. Acta*, vol. 667, pp. 19–26, Sep. 2018, doi: 10.1016/j.tca.2018.04.010.

[46] T. Wada, M. Nakano, and N. Koga, 'Multistep Kinetic Behavior of the Thermal Decomposition of Granular Sodium Percarbonate: Hindrance Effect of the Outer Surface Layer', *J. Phys. Chem. A*, vol. 119, no. 38, pp. 9749–9760, Sep. 2015, doi: 10.1021/acs.jpca.5b07042.

[47] S. Iwasaki, S. Kodani, and N. Koga, 'Physico-Geometrical Kinetic Modeling of the Thermal Decomposition of Magnesium Hydroxide', *J. Phys. Chem. C*, vol. 124, no. 4, pp. 2458–2471, Jan. 2020, doi: 10.1021/acs.jpcc.9b09656.

[48] T. Wada and N. Koga, 'Kinetics and Mechanism of the Thermal Decomposition of Sodium Percarbonate: Role of the Surface Product Layer', *J. Phys. Chem. A*, vol. 117, no. 9, pp. 1880–1889, Mar. 2013, doi: 10.1021/jp3123924.

[49] N. Koga and S. Kodani, 'Thermally induced carbonation of $Ca(OH)_2$ in a CO_2 atmosphere: kinetic simulation of overlapping mass-loss and mass-gain processes in a solid–gas system', *Phys. Chem. Chem. Phys.*, vol. 20, no. 41, pp. 26173–26189, 2018, doi: 10.1039/C8CP05701J.

[50] Y. Noda and N. Koga, ‘Phenomenological Kinetics of the Carbonation Reaction of Lithium Hydroxide Monohydrate: Role of Surface Product Layer and Possible Existence of a Liquid Phase’, *J. Phys. Chem. C*, vol. 118, no. 10, pp. 5424–5436, Mar. 2014, doi: 10.1021/jp500322p.

[51] S. Kitabayashi and N. Koga, ‘Thermal Decomposition of Tin(II) Oxyhydroxide and Subsequent Oxidation in Air: Kinetic Deconvolution of Overlapping Heterogeneous Processes’, *J. Phys. Chem. C*, vol. 119, no. 28, pp. 16188–16199, Jul. 2015, doi: 10.1021/acs.jpcc.5b04975.

[52] N. V. Muravyev, N. Koga, D. B. Meerov, and A. N. Pivkina, ‘Kinetic analysis of overlapping multistep thermal decomposition comprising exothermic and endothermic processes: thermolysis of ammonium dinitramide’, *Phys. Chem. Chem. Phys.*, vol. 19, no. 4, pp. 3254–3264, 2017, doi: 10.1039/C6CP08218A.

[53] N. V. Muravyev, A. N. Pivkina, and N. Koga, ‘Critical Appraisal of Kinetic Calculation Methods Applied to Overlapping Multistep Reactions’, *Molecules*, vol. 24, no. 12, p. 2298, Jun. 2019, doi: 10.3390/molecules24122298.

[54] J. Sestak and G. Berggren, ‘Study of the kinetics of the mechanism of solid-state reactions at increasing temperatures’, *Thermochim. Acta*, vol. 3, pp. 1–12, 1971.

[55] V. M. Gorbachev, ‘Some aspects of Šestak’s generalized kinetic equation in thermal analysis’, *J. Therm. Anal.*, vol. 18, no. 1, pp. 193–197, Feb. 1980, doi: 10.1007/BF01909467.

[56] J. Šesták, ‘Šesták–Berggren equation: now questioned but formerly celebrated—what is right’, *J. Therm. Anal. Calorim.*, vol. 127, no. 1, pp. 1117–1123, Jan. 2017, doi: 10.1007/s10973-015-4998-x.

[57] L. A. Pérez-Maqueda, J. M. Criado, and P. E. Sánchez-Jiménez, ‘Combined Kinetic Analysis of Solid-State Reactions: A Powerful Tool for the Simultaneous Determination of Kinetic Parameters and the Kinetic Model without Previous Assumptions on the Reaction Mechanism’, *J. Phys. Chem. A*, vol. 110, no. 45, pp. 12456–12462, Nov. 2006, doi: 10.1021/jp064792g.

[58] P. E. Sánchez-Jiménez, L. A. Pérez-Maqueda, A. Perejón, and J. M. Criado, ‘Combined kinetic analysis of thermal degradation of polymeric materials under any thermal pathway’, *Polym. Degrad. Stab.*, vol. 94, no. 11, pp. 2079–2085, Nov. 2009, doi: 10.1016/j.polymdegradstab.2009.07.006.

[59] A. Burnham, ‘Application of the Šesták-Berggren Equation to Organic and Inorganic Materials of Practical Interest’, *J. Therm. Anal. Calorim.*, vol. 60, pp. 895–908, Jun. 2000, doi: 10.1023/A:1010163809501.

[60] J. Málek and J. M. Criado, ‘Is the šesták-berggren equation a general expression of kinetic models?’, *Thermochim. Acta*, vol. 175, no. 2, pp. 305–309, Mar. 1991, doi: 10.1016/0040-6031(91)80076-U.

[61] G. Munteanu and E. Segal, ‘Sestak–Berggren function in temperature-programmed reduction’, *J. Therm. Anal. Calorim.*, vol. 101, no. 1, pp. 89–95, Jul. 2010, doi: 10.1007/s10973-009-0435-3.

[62] A. K. Burnham, ‘Response to statements by Professor Šesták concerning logistic equations in kinetics’, *J. Therm. Anal. Calorim.*, vol. 127, no. 1, pp. 1127–1129, Jan. 2017, doi: 10.1007/s10973-015-5216-6.

[63] A. K. Burnham and R. L. Braun, ‘Global Kinetic Analysis of Complex Materials’, *Energy Fuels*, vol. 13, no. 1, pp. 1–22, Jan. 1999, doi: 10.1021/ef9800765.

[64] C. C. Lakshmanan and N. White, ‘A New Distributed Activation Energy Model Using Weibull Distribution for the Representation of Complex Kinetics’, p. 10.

[65] Lj. Kolar-Anić, S. Veljković, S. Kapor, and B. Dubljević, ‘Weibull distribution and kinetics of heterogeneous processes’, *J. Chem. Phys.*, vol. 63, no. 2, pp. 663–668, Jul. 1975, doi: 10.1063/1.431388.

[66] D. B. Anthony and J. B. Howard, ‘Coal devolatilization and hydrogastification’, *AIChE J.*, vol. 22, no. 4, pp. 625–656, Jul. 1976, doi: 10.1002/aic.690220403.

[67] B. Janković, N. Manić, D. Stojiljković, and V. Jovanović, ‘TSA-MS characterization and kinetic study of the pyrolysis process of various types of biomass based on the Gaussian multi-peak fitting and peak-to-peak approaches’, *Fuel*, vol. 234, pp. 447–463, Dec. 2018, doi: 10.1016/j.fuel.2018.07.051.

[68] G. Várhegyi, B. Bobály, E. Jakab, and H. Chen, ‘Thermogravimetric Study of Biomass Pyrolysis Kinetics. A Distributed Activation Energy Model with Prediction Tests’, *Energy Fuels*, vol. 25, no. 1, pp. 24–32, Jan. 2011, doi: 10.1021/ef101079r.

[69] B. Janković, S. Mentus, and M. Janković, ‘A kinetic study of the thermal decomposition process of potassium metabisulfite: Estimation of distributed reactivity model’, *J. Phys. Chem. Solids*, vol. 69, no. 8, pp. 1923–1933, Aug. 2008, doi: 10.1016/j.jpcs.2008.01.013.

[70] B. Janković, ‘Identification of the effective distribution function for determination of the distributed activation energy models using the maximum likelihood method: Isothermal thermogravimetric data’, *Int. J. Chem. Kinet.*, vol. 41, no. 1, pp. 27–44, Jan. 2009, doi: 10.1002/kin.20357.

[71] D. M. Bates and D. G. Watts, *Nonlinear regression analysis and its applications*. New York: Wiley, 1988.

[72] T. W. Anderson and D. A. Darling, ‘Asymptotic Theory of Certain “Goodness of Fit” Criteria Based on Stochastic Processes’, *Ann. Math. Stat.*, vol. 23, no. 2, pp. 193–212, Jun. 1952, doi: 10.1214/aoms/1177729437.

[73] M. A. Stephens, ‘EDF Statistics for Goodness of Fit and Some Comparisons’, *J. Am. Stat. Assoc.*, vol. 69, no. 347, pp. 730–737, Sep. 1974, doi: 10.1080/01621459.1974.10480196.

[74] M. Avrami, ‘Kinetics of phase change. I: General theory’, *J. Chem. Phys.*, vol. 7, no. 12, pp. 1103–1112, 1939, doi: 10.1063/1.1750380.

[75] M. Avrami, ‘Kinetics of phase change. II Transformation-time relations for random distribution of nuclei’, *J. Chem. Phys.*, vol. 8, no. 2, pp. 212–224, 1940, doi: 10.1063/1.1750631.

[76] M. Avrami, ‘Granulation, phase change, and microstructure kinetics of phase change. III’, *J. Chem. Phys.*, vol. 9, no. 2, pp. 177–184, 1941, doi: 10.1063/1.1750872.

[77] B. Erofeev, ‘Generalized equation of chemical kinetic and its application to reactions with hard substances participation’, *Dokl. SSSR*, vol. 52, p. 511, 1946.

[78] E. G. Prout and F. C. Tompkins, ‘The thermal decomposition of silver permanganate’, *Trans. Faraday Soc.*, vol. 42, no. 0, pp. 468–472, Jan. 1946, doi: 10.1039/TF9464200468.

[79] M. E. Brown, ‘The Prout-Tompkins rate equation in solid-state kinetics’, *Thermochim. Acta*, vol. 300, no. 1, pp. 93–106, Oct. 1997, doi: 10.1016/S0040-6031(96)03119-X.

[80] M. E. Brown and B. D. Glass, ‘Pharmaceutical applications of the Prout–Tompkins rate equation’, *Int. J. Pharm.*, vol. 190, no. 2, pp. 129–137, Nov. 1999, doi: 10.1016/S0378-5173(99)00292-6.

[81] W. Jander and Z. Anorg, ‘Kinetic Model for Solid-State Reactions’, *Z. Für Anorg. Allg. Chem.*, vol. 163, pp. 1–30.

[82] A. M. Ginstling and B. I. Brounshtein, ‘Concerning the diffusion kinetics of reaction in spherical particles’, *J Appl Chem USSR*, vol. 23, no. 12, pp. 1327–1338, 1950.

[83] S. Ashtekar, S. V. V. Chilukuri, and D. K. Chakrabarty, ‘Small-Pore Molecular Sieves SAPO-34 and SAPO-44 with Chabazite Structure: A Study of Silicon Incorporation’, *J. Phys. Chem.*, vol. 98, no. 18, pp. 4878–4883, May 1994, doi: 10.1021/j100069a018.

[84] F. Arena, R. D. Chio, and G. Trunfio, ‘An experimental assessment of the ammonia temperature programmed desorption method for probing the surface acidic properties of heterogeneous catalysts’, *Appl. Catal. Gen.*, vol. 503, pp. 227–236, Aug. 2015, doi: 10.1016/j.apcata.2015.05.035.

[85] J. Opfermann, ‘Kinetic Analysis Using Multivariate Non-linear Regression. I. Basic concepts’, *J. Therm. Anal. Calorim.*, vol. 60, no. 2, pp. 641–658, May 2000, doi: 10.1023/A:1010167626551.

[86] B. Roduit, ‘Computational aspects of kinetic analysis.: Part E: The ICTAC Kinetics Project—numerical techniques and kinetics of solid state processes’, *Thermochim. Acta*, vol. 355, no. 1, pp. 171–180, Jul. 2000, doi: 10.1016/S0040-6031(00)00447-0.

[87] M. Maciejewski and A. Reller, ‘How (UN)reliable are kinetic data of reversible solid-state decomposition processes?’, *Thermochim. Acta*, vol. 110, pp. 145–152, Feb. 1987, doi: 10.1016/0040-6031(87)88221-7.

4 Kinetic modelling of thermal processes using a modified Sestak-Berggren equation[3]

Summary

This chapter outlines the principles of modelling the kinetics of solid-state reactions through the simultaneous fitting of multiple peak curves using the modified Sestak-Berggren equation. This mathematical model gives an indication of the mechanism occurring and allows kinetic parameters, such as activation energy, to be estimated. This methodology is demonstrated using in silico thermal conductivity detector (TCD) data showing the internal consistency of the Sestak-Berggren modelling approach, its applicability to noisy data and its ability to predict mechanisms occurring during a thermally induced solid-state reaction. Using these in silico data it has been confirmed that this empirical model can separate overlapped peaks without a priori peak deconvolution. A rigorous statistical methodology based on the Akaike Information Criteria, is recommended to identify the optimum number of thermal events that should be applied to a system. This modified Sestak-Berggren model is then applied to an experimental dataset of temperature programmed reduction of a calcined cobalt on alumina catalyst precursor. This allows for the identification of a statistically adequate kinetic triplet for each thermal event. Recommendations on the treatment of datasets which contain "shoulders" and closely overlapped peaks are also given.

---

[3] This chapter has been published: R. L. Gibson, M. J. H. Simmons, E. Hugh Stitt, J. West, S. K. Wilkinson, and R. W. Gallen, 'Kinetic modelling of thermal processes using a modified Sestak-Berggren equation', *Chem. Eng. J.*, vol. 408, 2021, doi: 10.1016/j.cej.2020.127318.

4.1 Introduction

The characterisation of a functionalised material is an important step in understanding its performance, such as catalytic activity and selectivity. Extracting quantitative data from characterisation techniques could offer improved understanding and predictive modelling of industrial processes such as catalyst reduction. Columbo et al. [1] and Lietti et al. [2] have already demonstrated the advantages of applying the fundamental understanding gained from such techniques to a more complex system such as a selective catalytic reduction (SCR) monolith drive cycle model.

Solid-state reaction kinetics have been widely studied using thermal analysis methods, with major improvements in both experimental and computational techniques allowing more accurate kinetic parameters to be extracted [3]. However, the deconvolution of overlapped thermal events has historically relied on the expertise of experienced practitioners; with a judgement based on experience with equipment and the interpretation of the chemistry studied, impacting the assignment of the number of thermal events. A method to simultaneously deconvolute a statistically significant number of thermal events and extract kinetic information is outlined in this chapter.

It is common for thermal analysis results to feature more than one peak, which makes the resolution of these peaks an important part of the data processing. In the literature, thermal events (or peaks) are commonly deconvoluted first, before kinetic analysis can be carried out, as discussed in Chapter 3. Mathematical deconvolution analysis is most common, and involves fitting a mathematical function [4], but this process can introduce errors. To avoid these, the full curve would be better analysed simultaneously, via kinetic deconvolution analysis. It is mathematically possible to

assign any number of mathematical functions to fit the thermal analysis data [5], [6] and a focus of this study is to evaluate the optimum number of thermal events to assign to a system. Fitting additional curves may improve a model's closeness of fit, however the parameter values extracted could cease to relate to physical parameters [5].

However, the addition of curves may not improve quality of fit as this increases the risk of overfit. Overfit is the inclusion of spurious, uncontrolled variables within a model, effectively experimental error. In extreme cases this can hide important systematic errors behind unreal confounding effects [7]. Overfit causes a broadening of confidence intervals for estimated parameters giving low confidence in model predictions [8].

Overfitting would of course be unacceptable given the aim of the modelling work to extract physical parameters or produce a predictive model. This study thus evaluates a rigorous statistical method to determine the optimum number of thermal events, which would avoid this overfitting.

When extracting kinetic information, a system should be described using the "kinetic triplet" [8], [9], which comprises of the pre-exponential factor, activation energy and reaction mechanism. Solid-state reaction mechanisms capture the physico-geometrical aspects of these reactions and have been around for decades [10]. To discriminate between these kinetic models, multiple temperature ramp rate experiments are required [8], as multiple mechanisms may adequately fit a single temperature ramp rate by estimating different Arrhenius parameters but would fail to adequately fit a range of temperature ramp rates.

The final element of the kinetic triplet, the mechanism associated with the reaction, can have many forms. It is widely accepted that these forms can be split into the following categories: geometric shape, nucleation, diffusion, reaction order and empirical, as discussed in Chapter 3. These models are based on the dimensionless extent of reaction, α. The derivations of the models given in Table 4.1 are detailed in Garner [10] and also in Khawam & Flanagan [11].

Table 4.1: Kinetic models for solid-state reactions

Mechanism	Equation ($f(\alpha)$)	Singularities
2D Interface controlled	$2(1-\alpha)^{1/2}$	$\alpha = 1$
3D Interphase controlled	$3(1-\alpha)^{2/3}$	$\alpha = 1$
Avrami-Erofeev n=1	$(1-\alpha)$	
Avrami-Erofeev n=n	$n(1-\alpha)[-\ln(1-\alpha)]^{1-\frac{1}{n}}$	$\alpha = 0 \ and \ \alpha = 1$
Power law	$n(\alpha)^{1-\frac{1}{n}}$	$\left.\frac{d\alpha}{dt}\right\|_{\alpha=0} = 0$
2D Diffusion	$-[1/\ln(1-\alpha)]$	$\alpha = 0 \ and \ \alpha = 1$
3D Diffusion, Jander equation	$\frac{3(1-\alpha)^{\frac{2}{3}}}{2\left(1-(1-\alpha)^{\frac{1}{3}}\right)}$	$\alpha = 0 \ and \ \alpha = 1$
3D Diffusion, Ginstling Bronstein equation	$\frac{3}{2\left((1-\alpha)^{-\frac{1}{3}}-1\right)}$	$\alpha = 0 \ and \ \alpha = 1$
Random chain scission	$2(\alpha^{\frac{1}{2}}-\alpha)$	$\left.\frac{d\alpha}{dt}\right\|_{\alpha=0} = 0$

Since there are many of these kinetic models, and the mechanism of reaction could be different for each thermal event observed, there could be many model combinations which require investigation. The Sestak-Berggren equation is an empirical model which can be used to indicate which mechanism is present for a specific thermal event [12] through the estimated exponent parameters. These estimated parameters are compared to the values of *n* and *m* in Table 4.1, which allows the most likely mechanism to be determined. This reduces the number of model combinations that require testing.

The objective of this investigation is to validate the use of the Sestak-Berggren equation when multiple thermal event data have not been deconvoluted and to confirm its ability to predict mechanisms when presented with appropriate data. Initially this will be illustrated using an *in silico* dataset, generated using known parameter values. The impact of white noise on a dataset will also be investigated using these *in silico* data. This will then allow a strategy to be developed for potentially noisy experimental data. Finally, experimental validation will be carried out using a temperature programmed reduction (TPR) dataset for a calcined cobalt on alumina catalyst precursor.

4.2 Methodology

The measured variable in thermal analysis experiments can vary, but commonly a thermal conductivity detector (TCD) is used to monitor the release of gas from the sample. As a TCD signal is in the differential form (discussed in Chapter 2), the signal is integrated (using the trapezoid rule) and the signal is divided by this integral which renders it dimensionless, to give the extent of reaction (α).

In the approach used in this study, no assumptions are made about the peak shapes; rather the Sestak Berggren model is used to fit the data directly. The Sestak-Berggren model has been used in the reduced form (Equation 4.1), as the original contains an unnecessary additional degree of freedom [13] and modified to fit multi-peak data.

$$\frac{d\alpha}{dt} = \sum_{i=1}^{n_{events}} F_{v,i} \cdot A_i \cdot \exp\left(\frac{Ea_i}{R.T_{b,i}}\left(1 - \frac{T_{b,i}}{T}\right)\right) \cdot (1-\alpha_i)^{n_i} \alpha_i^{m_i}, \qquad \text{Eq. (4.1)}$$

where α is the extent of reaction (-), *A* is the pre-exponential factor (s^{-1}), *Ea* is the activation energy (kJ mol^{-1}), *R* is the universal gas constant (kJ mol^{-1} K^{-1}), T_b is the base temperature of the peak (K), *T* is the temperature (K) , *n* and *m* are fitted exponent parameters (-) and F_v is a contribution term (-).

The number of thermal events is specified as an input to the model and the parameters $A, E_a, n, m,$ and F_v are estimated for each thermal event.

As seen in Equation 4.1, the Arrhenius equation has been used in its reparameterised form to reduce cross correlation between parameters. For the parameter estimation, the activation energy is fitted using the dimensionless form $\frac{Ea_i}{R.T_{b,i}}$. However, the values reported in the results sections of this thesis have been converted to an energy value with the units of kJ mol^{-1}. Similarly, the pre-exponential factor was fitted in the form $A_i\ exp\left(-\frac{Ea_i}{R.T_{b,i}}\right)$ but is reported in the results in its conventional form. As the modified Sestak-Berggren equation is empirical, the activation energy estimated is not a "true" activation energy. To obtain a "true" activation energy a solid-state mechanism (identified using the modified Sestak-Berggren equation) should be used.

The contribution term indicates the fraction of the overall curve associated with the thermal event. The contribution for each peak must sum to one by definition, which gives Equation 4.2. The final thermal event contribution is calculated by the model from the estimated contributions of the other events.

$$F_{v,n_{events}} = 1 - \sum_{i=1}^{n_{events}-1} F_{v,i} \qquad \text{Eq. (4.2)}$$

This model is an empirical fit and the exponent parameters (*n* and *m*) indicate which kinetic mechanisms could be plausible for the system under investigation [12]. The parameter estimation results for the Sestak-Berggren model are analysed, from which candidate mechanistic models are identified. Mechanistic model discrimination can then be carried out, allowing the fitting of a statistically adequate kinetic triplet. The results of the Sestak-Berggren estimation give qualitative information about the rate-limiting step occurring during the process [11]; estimation with a mechanistic model resolves this quantitatively.

The kinetic mechanisms are based on the dimensionless extent of reaction, which, by definition, has a range between zero (no reaction) and one (complete reaction). Many of these mechanisms contain mathematical singularities, either at zero or one, which means that they are not valid for the entire range of operation.

Some of the kinetic models, such as random chain scission, have $\left.\frac{d\alpha}{dt}\right|_{\alpha=0} = 0$. Although this is not a singularity and is mathematically valid, this specific condition is not solvable with typical initial value problem numerical methods, such as the predictor-corrector solver used in this work. In terms of physical meaning, having a stationary point at zero conversion suggests that the reaction would never begin, and therefore occur. For a predictor-corrector solver, this means that the first step is $\alpha = 0$, leaving the

solver stuck at the start of the problem. Hence this stationary point also results in the invalidity of the model for the whole range of operation.

To circumvent the issues of singularity and enable modelling of the complete range between zero and one, these mechanisms have been linearised at a point close to these singularities, using a Taylor series expansion around a specific point, b. Table 4.1 indicates which of the kinetic models contain these singularities. In the case of Avrami-Erofeev *n* = *n* case: this singularity only occurs when values of *n* result in an exponent of $\frac{1}{1-n} < 0$.

For the Sestak-Berggren model singularities occur at both $\alpha = 0$ and $\alpha = 1$; hence two linearisations have been carried out. The results of these are shown in Equations 4.3 and 4.4.

For $0 \leq \alpha \leq 0.0005$:

$$\frac{d\alpha}{dt} = \sum_{i=1}^{n_{events}} F_{v,i} \cdot A_i \cdot \exp\left(\frac{Ea_i}{R.T_{b,i}}\left(1 - \frac{T_{b,i}}{T}\right)\right) \cdot (1-\alpha)^{n_i}.((1-b)^{m_i} + m_i.b^{m_i-1}.(\alpha - b)) \quad \text{Eq. (4.3)}$$

For $0.9995 \leq \alpha \leq 1.0$:

$$\frac{d\alpha}{dt} = \sum_{i=1}^{n_{events}} F_{v,i} \cdot A_i \cdot \exp\left(\frac{Ea_i}{R.T_{b,i}}\left(1 - \frac{T_{b,i}}{T}\right)\right).\alpha^{m_i}.(b^{n_i} + n_i.b^{n_i-1}.(\alpha - (1-b))) \quad \text{Eq. (4.4)}$$

Where $b = 5.0 \times 10^{-4}$.

A sensitivity analysis was carried out on the value of *b*, and it was found that values smaller than 5.0×10^{-3} had minimal impact on results. Hence a value of 5.0×10^{-4} was selected as it was within this range.

This modelling was carried out using Athena Visual Studio, (Athena Visual Inc. [14], version 14.2) using a non-linear least squares regression. Default tolerances for Athena Visual Studio have been used, details of which can be found in Stewart & Caracotsios [14]. The DDAPLUS predictor-corrector algorithm has been used to solve the differential equations, and the LSGREG non-linear least squares regression algorithm to carry out the parameter estimation, which is a 2nd order Newton solver constrained by trust regions [14]. The aim of the regression is to minimise the residual on $\frac{d\alpha}{dt}$. Quadratic splines have been used to incorporate the measured temperature ramp, as this allows the solver to interpolate a smooth function between discrete data points.

To evaluate the quality of fit 95% confidence intervals, along with the R^2 value and the residual sum of squares (RSS) have been used.

To determine the most statistically relevant number of thermal events for a system, Akaike weights is used [15]. This method is based on Akaike Information Criteria (AIC) [16] which is a measure of how much information is lost through modelling. The weighting method allows well-fitting models to be compared, with the most statistically significant model having the highest share of the weight (which is valid between 0 and 1).

From the original AIC values, the weights are calculated with Equations (4.5-4.7) below.

$$AIC = -\varphi \cdot ln\left(\frac{RSS}{\varphi}\right) + 2\omega + \frac{2\omega(\omega+1)}{\varphi-\omega-1} \quad \text{Eq. (4.5)}$$

$$\Delta_j = AIC_j - AIC_{min} \quad \text{Eq. (4.6)}$$

$$w_j = \frac{exp\left(-\frac{\Delta_j}{2}\right)}{\sum_{s=1}^{S} exp\left(-\frac{\Delta_s}{2}\right)} \quad \text{Eq. (4.7)}$$

Where φ is the number of data points, ω is the number of parameters plus one.

4.3 Experimental

4.3.1 *In silico* data generation

Data were generated using the relevant model pre-set input parameters. The exponents (*n* and *m*) were based on values from Table 4.1. As multiple temperature ramp rate experiments are required to discriminate between mechanisms [8], five dimensionless datasets were generated, using temperature ramp rates of 2, 4, 6, 8 and 10 K min^{-1}. The parameter values used for data generation are given in Table 4.2. The T_b values used to produce the low and high temperature peaks were 420 K and 700 K respectively. A 15 minute temperature hold was simulated; hence data begin after this time.

This “clean” data, with no noise applied, will be used to establish the feasibility of this methodology with an ideal dataset and will subsequently allow the investigation into the impact of noise.

Table 4.2: Parameter values for *in silico* data generation.

Peak	Parameter	Units	Expected value
Low temperature peak	A_1	s^{-1}	1.31×10^{6}
	Ea_1	kJ mol^{-1}	1.68×10^{1}
	n_1	-	1.00×10^{0}
	m_1	-	0.00×10^{0}
	Fv_1	-	6.00×10^{-1}
High temperature peak	A_2	s^{-1}	3.36×10^{11}
	Ea_2	kJ mol^{-1}	9.00×10^{2}
	n_2	-	8.07×10^{-1}
	m_2	-	5.15×10^{-1}
	Fv_2	-	4.00×10^{-1}

Figure 4.1 shows the data generated using the parameter values in Table 4.2.

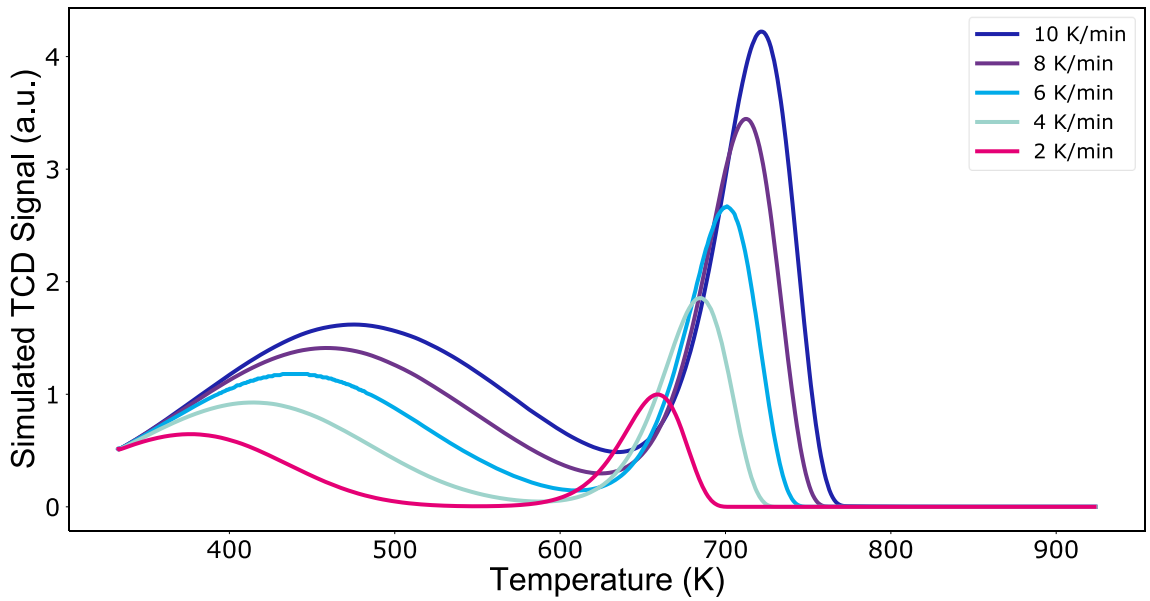

Figure 4.1: *In silico* data, showing five temperature ramp rates.

4.3.2 Temperature programmed reduction

TPR gives information on the surface chemistry of a catalyst and can be used to inform large-scale catalyst reduction. TPR was carried out on fresh samples of an FT catalyst, a 40 wt % cobalt oxide on alumina catalyst precursor using an Altamira AMI200. Catalysts samples of ~100 mg were loaded into a 4 mm ID tubular quartz reactor. The samples were then dried in Ar at 413 K for 1h prior to reduction. TPR was performed using 40 mL min^{-1} flow of 10 vol % H_2/Ar from 298 K to 1273 K. Five datasets were generated using temperature ramp rates of 2, 4, 6, 8 and 10K min^{-1}. Drierite desiccate removed the evolved water, and the hydrogen concentration was monitored using a TCD.

4.4 Results and discussion

4.4.1 *In silico* verification

4.4.1.1 Multiple peak modelling

Table 4.3 shows the fitting results for the system with two overlapping peaks. All five generated datasets have been treated with the Sestak-Berggren model simultaneously.

The T_b values of 420 K and 700 K were used for the low and high temperature peaks respectively. Selectivity analysis showed that providing T_b values fall within the thermal event temperature range, there is minimal impact on the final estimated parameters.

The estimated parameter values match those used in the initial data generation, within 95% confidence intervals. This parameter estimation resulted in an R^2 value of 1.00 and an RSS of 5.50×10^{-3}. The modelling results for the 10 K min^{-1} data are also

presented graphically in Figure 4.2. The data from the other temperature ramp rate "experiments" showed an equally good fit.

Table 4.3: Modified Sestak-Berggren model parameter estimation results, *in silico* data.

Parameter	Input value	Estimated value	95% confidence interval (±)
A_1 (s^{-1})	1.31×10^{6}	1.31×10^{6}	9.79×10^{-2}
Ea_1 (kJ mol^{-1})	1.68×10^{1}	1.68×10^{1}	4.91×10^{-7}
n_1(-)	1.00×10^{0}	1.00×10^{0}	4.79×10^{-8}
m_1(-)	0.00×10^{0}	0.00×10^{0}	4.87×10^{-8}
Fv_1 (-)	6.00×10^{-1}	6.00×10^{-1}	2.81×10^{-5}
A_2 (s^{-1})	3.36×10^{11}	3.36×10^{11}	5.26×10^{6}
Ea_2 (kJ mol^{-1})	9.00×10^{2}	9.00×10^{2}	6.37×10^{-4}
n_2(-)	8.07×10^{-1}	8.07×10^{-1}	9.56×10^{-5}
m_2(-)	5.15×10^{-1}	5.15×10^{-1}	1.87×10^{-6}
Fv_2 (-)	4.00×10^{-1}	4.00×10^{-1}	2.81×10^{-5}

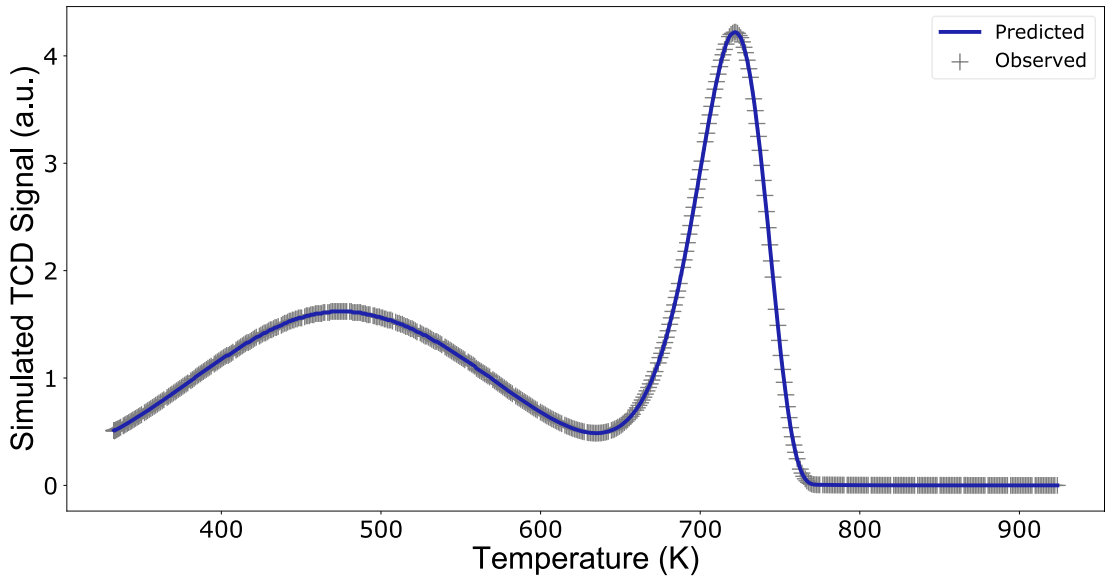

Figure 4.2: Modified Sestak-Berggren modelling results, *in silico* data, 10K min^{-1} peak.

This study on ideal data demonstrates that this approach to solving the inverse problem - the deconvolution of events - reaches a unique and (importantly) correct solution. This provides model verification and demonstrates that the Sestak-Berggren modelling can extract useful information about both known events and their contributions without the need for prior peak deconvolution. This provides proof of concept for the methodology on an idealised yet realistic dataset. This should reduce the possible errors introduced by separation of peaks prior to kinetic modelling.

4.4.1.2 Evaluation of the number of events (peaks)

Model discrimination techniques can be used to determine the most statistically plausible number of events without prior knowledge [17]. To demonstrate the statistical relevance of the number of peaks with this method, the parameter estimation methodology of the same *in silico* dataset was also carried out as a three-peak system. The confidence intervals for the predicted parameters were of a similar order of

magnitude to the two-peak system estimates shown in Table 4.3, hence this metric does not aid in model discrimination.

Table 4.4: Comparison between two and three peak fits, modified Sestak-Berggren model, *in silico* data.

Quality of fit metric	2 peak system	3 peak system
Number of parameters	9	14
R^2	1.00	1.00
RSS	5.49×10^{-3}	5.86×10^{-3}
AIC	-3.67×10^{4}	-9.05×10^{3}
Akaike weight	1.00	0.00

Table 4.4 shows the quality of fit metrics for each of these parameter estimation regressions. To compare the statistical relevance of these fits, the Akaike Information Criteria (AIC) [16] and Akaike weights [15] were used. It was found that the AIC for the two-peak system was significantly lower than the three-peak fitting, implying that the two-peak fitting is the most statistically relevant fit. Using this methodology avoids the addition of thermal events which have no statistical basis and may not have a physical basis.

This statistical analysis should be completed following regressions to identify the number of thermal events present, when this information is not previously known. Thermal analysis data can often contain “shoulders”, which may be separate thermal events or parts of a single kinetic mechanism. Discrimination between these cases should use this rigorous statistical method.

4.4.1.3 Predicting mechanisms

Using known mechanisms, a second *in silico* dataset was produced, again simulating temperature ramp rates of 2, 4, 6, 8 and 10 K min^{-1}. The low and high temperature peaks were modelled using Avrami-Erofeev (first order, n = 1) and 2D interphase-controlled mechanisms respectively. The Sestak-Berggren modelling was then carried out, the parameter estimation results shown in Table 4.5. The quality of fit metrics, R^2 and RSS are 1.00 and 1.59×10^{-4} respectively.

Table 4.5: Modified Sestak-Berggren model parameter estimation results for mechanistic data.

	Parameter	Input value	Estimated value	95% confidence interval (±)
Low temperature peak	A_1 (s^{-1})	1.31×10^{6}	1.31×10^{6}	6.48×10^{-1}
	Ea_1 (kJ mol^{-1})	1.68×10^{1}	1.68×10^{1}	1.01×10^{-5}
	n_1(-)	1.00×10^{0}	1.00×10^{0}	5.59×10^{-7}
	m_1(-)	0.00×10^{0}	0.00×10^{0}	2.63×10^{-7}
	Fv_1 (-)	6.00×10^{-1}	6.00×10^{-1}	4.94×10^{-6}
High temperature peak	A_2 (s^{-1})	4.45×10^{12}	4.45×10^{12}	9.86×10^{5}
	Ea_2 (kJ mol^{-1})	1.05×10^{2}	1.05×10^{2}	3.32×10^{-5}
	n_2(-)	5.00×10^{-1}	5.00×10^{-1}	3.67×10^{-7}
	m_2(-)	0.00×10^{0}	0.00×10^{0}	3.09×10^{-7}
	Fv_2 (-)	4.00×10^{-1}	4.00×10^{-1}	4.94×10^{-6}

The main purpose of the Sestak-Berggren model is to identify the solid-state mechanism occurring during a reaction. This is achieved through the values obtained for the *n* and *m* exponent parameters. The literature provide theoretical values for the *n* and *m* parameters for the Avrami-Erofeev (first order, *n* = 1) and 2D interphase-controlled models [10] and the estimates in Table 4.5 match these, within 95% confidence intervals. Hence, this allows the correct kinetic mechanism to be inferred from the Sestak-Berggren parameter estimation results.

As noted above, the Sestak-Berggren equation is an empirical model and, as a result the values for the Arrhenius terms are not representative of the physical values. The purpose of the Sestak-Berggren modelling is not to extract a statistically adequate kinetic triplet, but rather to allow a kinetic mechanism to be identified. Following the parameter estimation with the modified Sestak-Berggren equation, the identified solid-state mechanism should be used to extract Arrhenius terms, completing the kinetic triplet. The estimated values for the activation energy terms in Table 4.5 thus do not match the physical values used to produce the mechanistic *in silico* data. Given however that this is not an aim of this model, and since the discrepancies are in fact extremely small, these values are not a cause for concern.

An example of the "observed" (*in silico*) results and the predicted Sestak-Berggren modelling results are shown for a single temperature ramp rate experiment (10 K min^{-1}) in Figure 4.3. Similar fits were also observed for the other temperature ramp rate experiments.

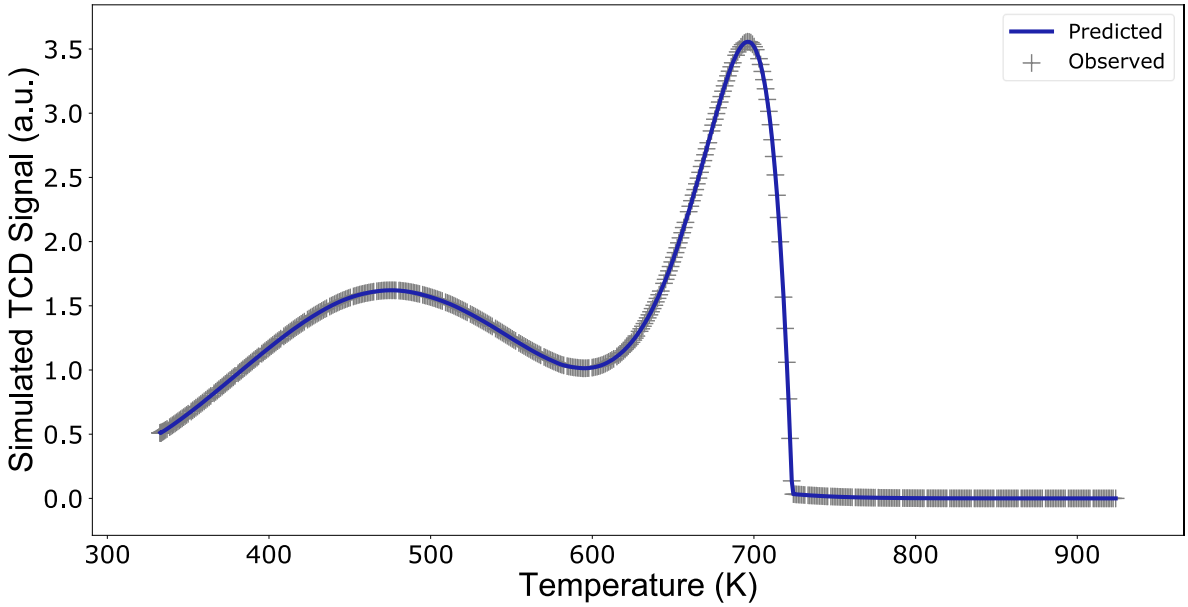

Figure 4.3: Modelling results of mechanistic data fitted with the Sestak-Berggren equation, 10 K min^{-1} example.

4.4.1.4 Noisy data

Experimental results obtained through, say, temperature programmed reduction can have experimental noise associated with them. This noise can vary between instruments, and the causes are not always clear. However, when fitting such systems, extracting accurate parameter estimates despite a noisy signal is imperative. In this section, the impact of white noise on the quality of fit obtained using the Sestak-Berggren equation is investigated.

White noise was added to the *in silico* mechanistic data discussed in the previous section. Standard deviations of 0.18 and 0.36 were used to generate white noise of 5% and 10% respectively, based on the maximum TCD signal. Figure 4.4 shows the original simulated data as used above, compared to the curve with random white noise added at 5%.

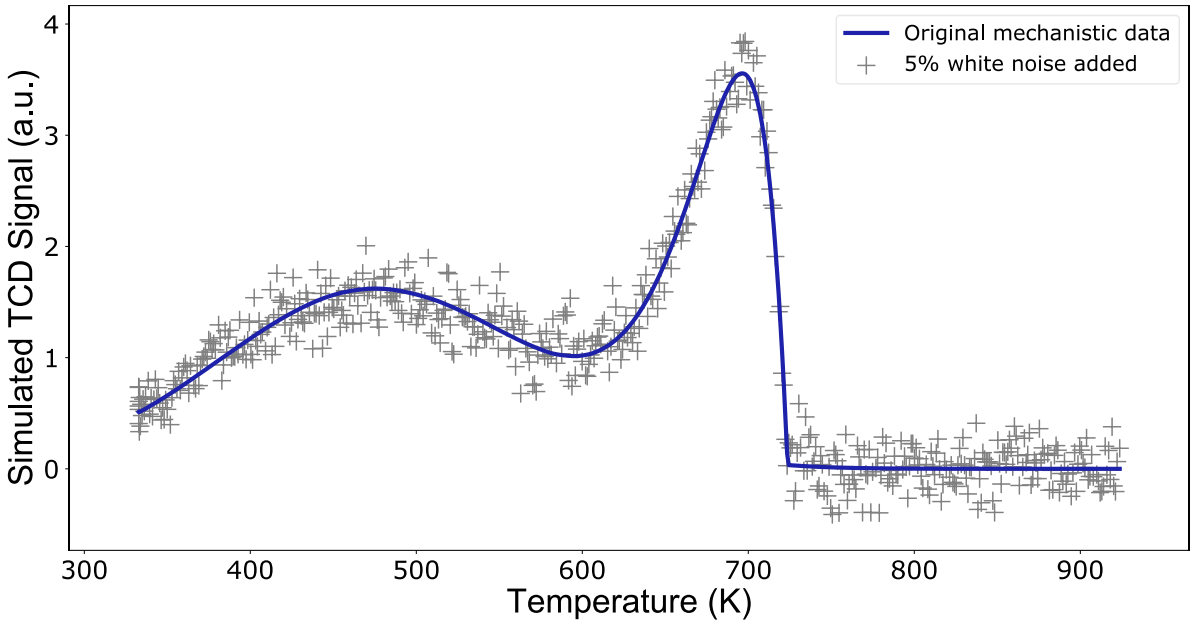

Figure 4.4: Comparison of original *in silico* data and 5% white noise added curves, 10 K min^{-1} example.

The Sestak-Berggren model fitting was carried out on these new noisy datasets. The parameter estimation results are shown in Table 4.6. A graphical representation of the 5% white noise added results are also shown in Figure 4.5. Similar fits were obtained for all five temperature ramp rates used.

The fitting metrics of R^2 and RSS significantly worsen with the white noise introduction. For the 5% addition, R^2 is 0.938 and RSS is 8.82×10^1. When 10% white noise is added, these worsen further to 0.790 and 3.51×10^2 respectively. This increase in the RSS value is expected since this model should not fit the random noise which has been added. As the residuals for the system are known, the lowest possible RSS value can be calculated; this was found to be 8.88×10^1 and 3.52×10^2 for 5% and 10% error respectively. As the RSS values from the regressions are lower than these calculated values, this implies some overfit has occurred. This emphasises that the Sestak-

Berggren model should only be used to identify the mechanism present for each thermal event, rather than be used to extract kinetic parameters.

Table 4.6: Modified Sestak-Berggren model parameter estimation results for noisy datasets.

Parameter	Input value	5% noise added		10% noise added	
		Estimated value	95% confidence interval (±)	Estimated value	95% confidence interval (±)
A_1 (s^{-1})	1.31×10^{6}	9.04×10^{5}	5.33×10^{3}	1.62×10^{6}	2.21×10^{4}
Ea_1 (kJ mol^{-1})	1.68×10^{1}	1.54×10^{1}	9.06×10^{-2}	1.75×10^{1}	3.38×10^{-1}
n_1(-)	1.00×10^{0}	9.80×10^{-1}	4.29×10^{-3}	1.02×10^{0}	1.12×10^{-3}
m_1(-)	0.00×10^{0}	3.00×10^{-2}	9.51×10^{-4}	-2.00×10^{-2}	2.01×10^{-3}
Fv_1 (-)	6.00×10^{-1}	6.00×10^{-1}	3.74×10^{-3}	6.00×10^{-1}	7.91×10^{-3}
A_2 (s^{-1})	4.25×10^{12}	5.69×10^{12}	5.54×10^{10}	7.74×10^{12}	4.97×10^{10}
Ea_2 (kJ mol^{-1})	1.05×10^{2}	1.06×10^{2}	3.15×10^{-1}	1.08×10^{2}	8.77×10^{-1}
n_2(-)	5.00×10^{-1}	5.00×10^{-1}	9.43×10^{-3}	4.80×10^{-1}	8.95×10^{-3}
m_2(-)	0.00×10^{0}	-1.00×10^{-2}	5.17×10^{-3}	-7.00×10^{-2}	5.68×10^{-3}
Fv_2 (-)	4.00×10^{-1}	4.00×10^{-1}	3.74×10^{-3}	4.00×10^{-1}	7.91×10^{-3}

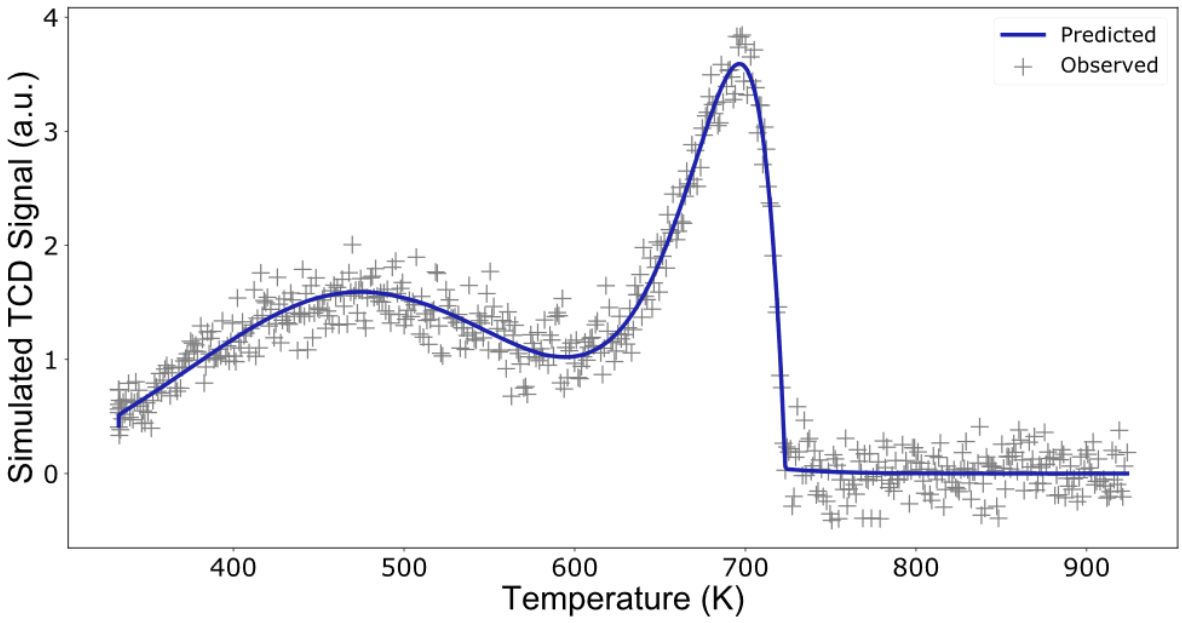

Figure 4.5: Example of modified Sestak-Berggren modelling results for 5% white noise dataset, 10 K min^{-1} example.

Although the estimates in Table 4.6 are close to the expected values, these are not within the confidence intervals estimated. In this case, the pre-exponential factor and activation energy values are not of concern as these are empirical values, unrelated to a physical mechanism and would be re-estimated after kinetic model discrimination. However, the purpose of this empirical equation is to indicate the mechanism occurring through the estimation of the *n* and *m* exponent values. Hence accurate prediction of these parameters even with the presence of noise is essential.

To improve the fit shown in Figure 4.5, there are two possible approaches. The first is to undertake repeat experiments of specific temperature ramp rates. The addition of repeats gives more information to the regression algorithm about the nature of the noise, as it is known that the noise is randomly distributed and is unique to each "experiment" (white noise). This should aid the model in determining the "true" signal from the white noise. This has been carried out for the 5% white noise dataset, by

adding three repeats of the central 6 K min^{-1} ramp rate, resulting in a dataset containing 8 “experiments” which were treated simultaneously. It was observed that this did not improve the model fit, in terms of R^2 value, RSS or confidence intervals.

In the second approach additional temperature ramp rate experiments can be added, increasing the number of “experiments” within the dataset to 6 or 7, which were treated simultaneously with the Sestak-Berggren model. For example, adding a 9 K min^{-1} “experiment” allowed the R^2 value to improve to 0.942. Although confidence intervals tighten, the known input value still does not fall within the range estimated. However, adding a further 7 K min^{-1} ramp rate allowed the exponent *n* and *m* parameters to be estimated within 95% confidence intervals, giving R^2 of 0.944 and RSS of 8.96×10^1.

Using the “clean” *in silico* data, Akaike weights have been shown to be useful in determining the number of thermal events. To understand the impact of noise on this statistic, the process of determining the number of thermal events was repeated for both the 5% and 10% white noise datasets, the results are shown in Table 4.7.

Table 4.7: Comparison of two and three peak fitting, white noise added data.

Dataset	Quality of fit metric	2 peak system	3 peak system
	Number of parameters	9	14
5% noise added	R^2	0.94	0.92
	RSS	8.81×10^1	10.8×10^2
	AIC	-9.64×10^{-3}	-9.04×10^{-3}
	Akaike weight	1.00	0.00
10% noise added	R^2	0.79	0.77
	RSS	3.50×10^2	3.80×10^2
	AIC	-5.78×10^{-3}	-5.54×10^{-3}
	Akaike weight	1.00	0.00

These results show that the Akaike weights can be used to identify the correct number of thermal events, even in the presence of 10% white noise. However, in cases of extreme noise, the Akaike weights may not show as much confidence towards a single model.

4.4.2 Experimental validation, TPR

Thermal events can often occur at similar temperatures, creating severely overlapped features. This case study aims to demonstrate the deconvolution of a “shoulder” (a severely overlapped feature). The raw experimental data are shown in Figure 4.6.

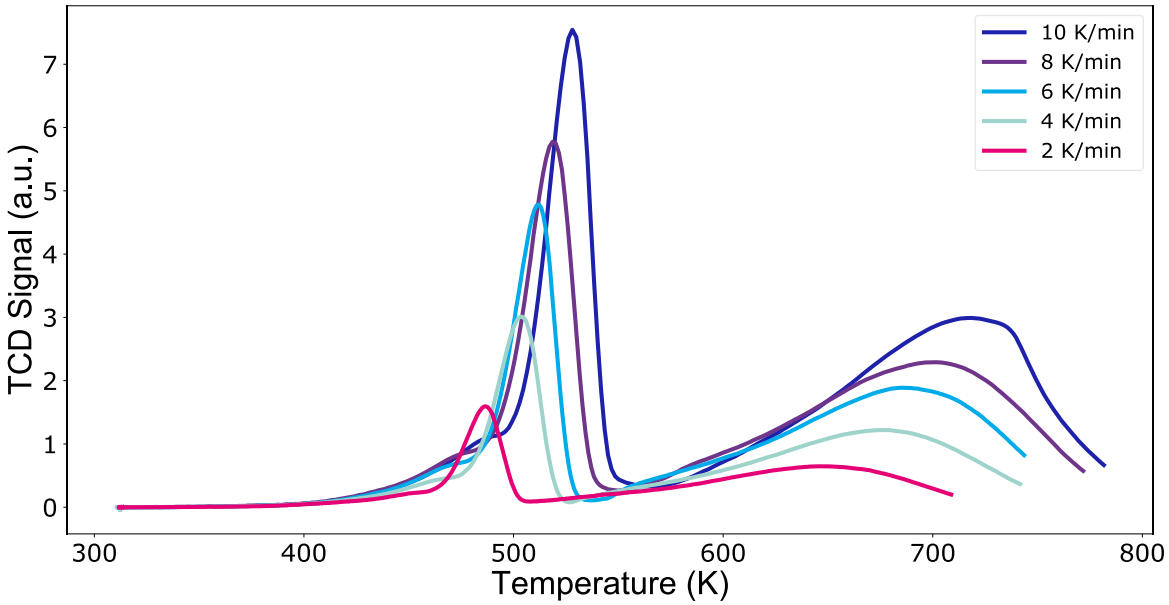

Figure 4.6: Raw TPR data for the cobalt oxide on alumina catalyst precursor, five temperature ramp rates

Based on literature recommendations [8], data were collected using five different temperature ramp rates. The white noise levels within this dataset were evaluated using a moving average model and were found to be on the order of 0.5-4%. Based on the *in silico* study at a slightly higher level of noise (5%), it would appear also that five ramp rate experiments should be sufficient to indicate a mechanism using the modified Sestak-Berggren equation.

The hydrogen consumption experimental data show two clear peaks at 520 K and 720 K. The results appear also to have a “shoulder” prior to the first clear peak (at ~480 K).

Attempts were made to fit both two and three thermal events to the hydrogen consumption dataset shown in Figure 4.6. The attempt to model the system using three peaks failed to estimate all the required parameters for the modified Sestak-Berggren equation. This implied the system is over specified using three peaks and, therefore,

that there is not enough information in the dataset to produce an adequately constrained three-peak model.

Parameter estimation results for the two-peak system are given in Table 4.8, with a graphical representation of the fit given in Figure 4.7 for the 2 K min^{-1} temperature ramp rate. This parameter estimation has an R^2 of 0.999 and an RSS of $1.58\ x\ 10^{-1}$.

Table 4.8: Modified Sestak-Berggren parameter estimation results for TPR experiments

Parameter	Estimated value	95% confidence interval (±)
A_1 (s^{-1})	2.18×10^{13}	6.88×10^{11}
Ea_1 (kJ mol^{-1})	8.08×10^{1}	1.29×10^{0}
n_1(-)	6.00×10^{-2}	4.00×10^{-2}
m_1(-)	-7.00×10^{-2}	2.00×10^{-2}
Fv_1 (-)	3.60×10^{-1}	1.82×10^{-3}
A_2 (s^{-1})	1.50×10^{11}	3.02×10^{9}
Ea_2 (kJ mol^{-1})	9.12×10^{1}	5.32×10^{-1}
n_2(-)	8.40×10^{-1}	1.35×10^{-1}
m_2(-)	-4.94×10^{-1}	1.95×10^{-2}
Fv_2 (-)	6.40×10^{-1}	1.82×10^{-3}

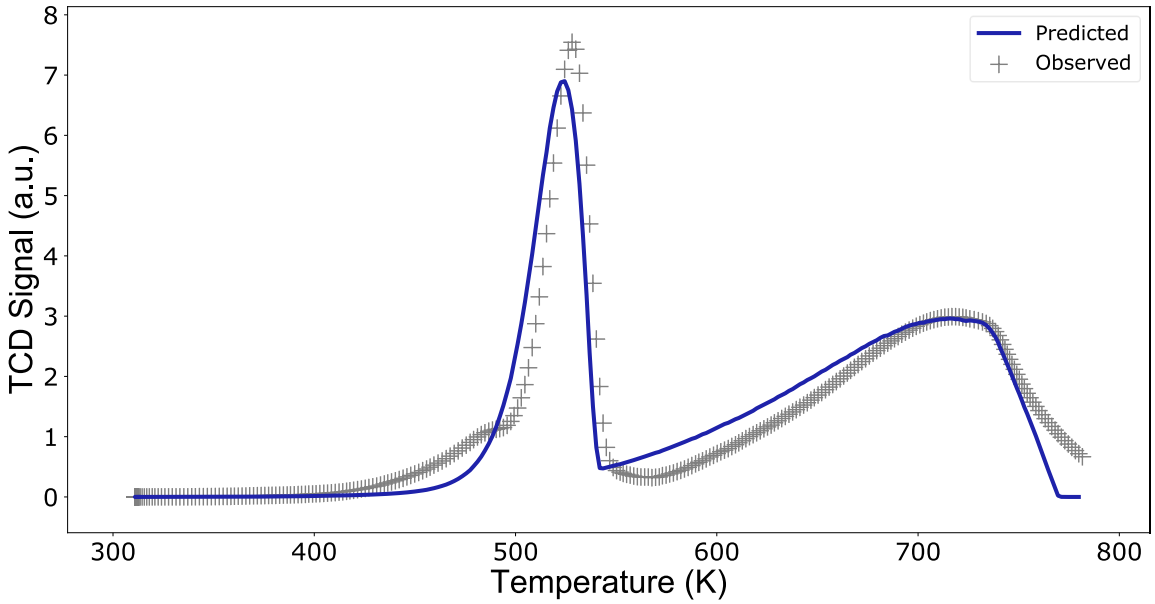

Figure 4.7: Graphical representation of modified Sestak-Berggren fit for TPR experimental data, 10 K min^{-1} experiment.

The mechanism predicted for peak one (520 K) is a zero order kinetically limited reaction, which could be interpreted as a film diffusion-controlled reaction. Exponent predictions for the second peak (720 K) do not exactly match a mechanism from Table 4.1 but indicate a diffusion type mechanism. This meant three mechanistic models from Table 4.1 were considered for a final model discrimination. It was found that a 3D diffusion (Jander equation) gave the best statistical fit and Akaike weight (of 1.0). The estimated Arrhenius parameters for these models are presented in Table 4.9, a graphical representation is given in Figure 4.8. When fitting these data with the mechanistic models indicated by the modified Sestak-Berggren equation, an R^2 of 0.999 and an RSS of $2.65\ x\ 10^{-1}$ were obtained.

Table 4.9: Parameter estimation results for mechanistic modelling, experimental TPR data

Parameter	Estimated value	95% confidence interval (±)
A_1 (s^{-1})	1.17×10^{13}	1.68×10^{11}
Ea_1 (kJ mol^{-1})	8.29×10^{1}	1.44×10^{0}
Fv_1 (-)	3.35×10^{-1}	2.18×10^{-3}
A_2 (s^{-1})	1.89×10^{12}	5.29×10^{10}
Ea_2 (kJ mol^{-1})	1.07×10^{2}	7.87×10^{-1}
Fv_2 (-)	6.65×10^{-1}	2.18×10^{-3}

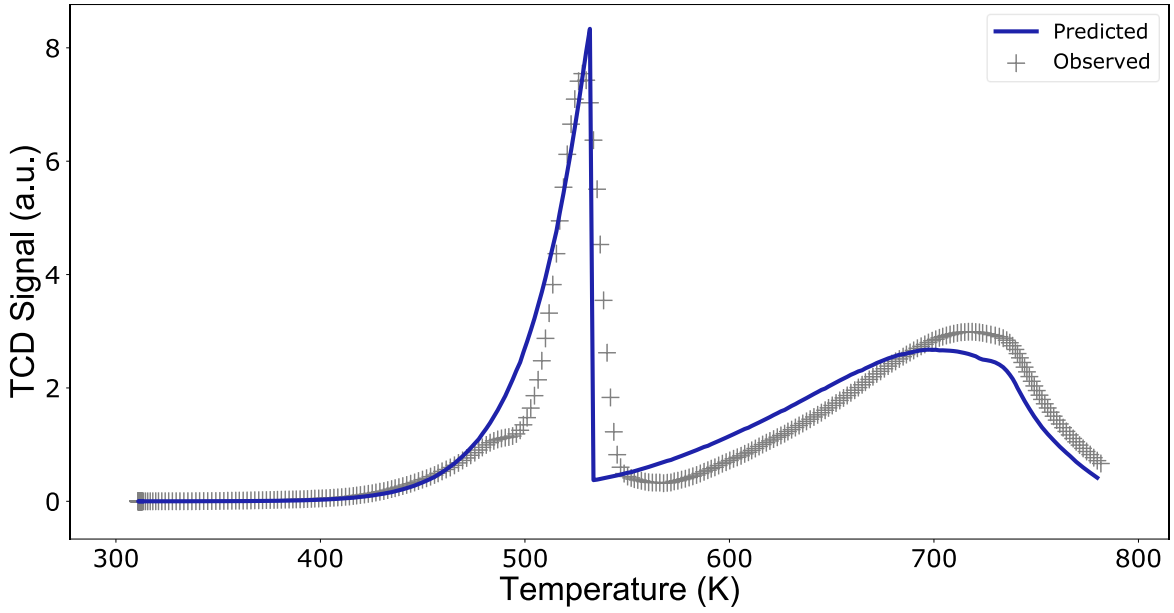

Figure 4.8: Graphical representation of mechanistic model fit for TPR experimental data, 10 K min^{-1} experiment.

This TPR experimental case study shows the modified Sestak-Berggren equation can be used on experimental data, without prior curve deconvolution. This allows for the

identification of a suitable mechanistic model, hence the prediction of a statistically adequate kinetic triplet. For this FT catalyst during reduction, the first peak has a zero-order model, with a pre-exponential factor of $1.17\,x\,10^{13} \pm 1.68\,x\,10^{11}\ s^{-1}$ and an activation energy of 82.9 ± 1.44 kJ mol^{-1}. The second, higher temperature peak has a 3D diffusion model (Jander equation, Table 4.1) with a pre-exponential factor of $1.89\,x\,10^{12} \pm 5.29\,x\,10^{10}\ s^{-1}$ and an activation energy of 107.0 ± 0.89 kJ mol^{-1}.

Whilst this two-peak model may be sufficient to describe these data and could be used for design of scale up processes, this may not be an accurate description of the system chemistry.

The two dominant peaks, which have been fitted using the modified Sestak-Berggren model, have been attributed to the reduction of the cobalt oxide in a two-step process: $Co_3O_4 \rightarrow CoO \rightarrow Co$ [18], [19]. Due to the low calcination temperature for this catalyst, it is expected that cobalt nitrate would still be present. The reduction of this nitrate could be appearing as the “shoulder” in these TPR results. These overlapped nitrate decomposition and $Co_3O_4 \rightarrow CoO$ thermal events have also been observed in the literature (e.g. Olusola and Sudip [18]).

With the standard set of temperature ramp rate experiments used in this paper, the “shoulder” (at ca. 480 K) does not separate from the adjacent larger peak (at 520K). This lack of separation prevents the statistically adequate fitting of a three-peak model.

Due to the rigorous nature of this modified Sestak-Berggren methodology, the inadequacy of studying this cobalt oxide reduction using temperature ramp rate experiments with only a thermal conductivity detector has been highlighted. As “shoulders” are a common feature of thermal analysis data, experimental methods to

separate these from more dominant thermal events are required. These methods may include evolved gas analysis (EGA) or constant rate thermal analysis (CRTA) [20].

4.5 Conclusions

This study has shown that the modified Sestak-Berggren equation can be used to describe simultaneously, multiple overlapped thermal events. When presented with appropriate thermomechanistic data, this empirical model can extract the required parameter estimates for mechanism identification. This allows subsequent kinetic modelling which can extract a statistically adequate kinetic triplet. This has been demonstrated with both *in silico* and experimental TPR data.

When the technique was applied to an *in silico* mechanistic system with white noise added, it was found that additional temperature ramp rate experiments were required to estimate the expected exponent values within 95% confidence intervals. The amount of additional information required depends on the level of noise within the system.

The TPR experimental validation highlighted that the use of constant temperature ramp rate experiments may restrict the separation of thermal events and result in “shoulders”. If “shoulders” do not separate from the more dominant thermal events within the range of temperature ramp rates used, as was shown in the cobalt nitrate reduction example, there may not be enough evidence to justify treating this feature as a thermal event in the modified Sestak-Berggren model. To ensure “shoulders” can be separated from dominant events, EGA or CRTA experiments could be used, this will be discussed further in Chapter 5.

4.6 References

[1] M. Colombo, G. Koltsakis, I. Nova, and E. Tronconi, ‘Modelling the ammonia adsorption–desorption process over an Fe–zeolite catalyst for SCR automotive applications’, *Catalysis Today*, vol. 188, no. 1, pp. 42–52, Jul. 2012, doi: 10.1016/j.cattod.2011.09.002.

[2] L. Lietti, I. Nova, S. Camurri, E. Tronconi, and P. Forzatti, ‘Dynamics of the SCR-DeNOx reaction by the transient-response method’, *AIChE Journal*, vol. 43, no. 10, pp. 2559–2570, Oct. 1997, doi: 10.1002/aic.690431017.

[3] M. E. Brown *et al.*, ‘Computational aspects of kinetic analysis Part A: The ICTAC kinetics project-data, methods and results’, *Thermochimica Acta*, p. 19, 2000.

[4] P. J. Barrie, ‘Analysis of temperature programmed desorption (TPD) data for the characterisation of catalysts containing a distribution of adsorption sites’, *Physical Chemistry Chemical Physics*, vol. 10, no. 12, p. 1688, 2008, doi: 10.1039/b717430f.

[5] S. Ashtekar, S. V. V. Chilukuri, and D. K. Chakrabarty, ‘Small-Pore Molecular Sieves SAPO-34 and SAPO-44 with Chabazite Structure: A Study of Silicon Incorporation’, *The Journal of Physical Chemistry*, vol. 98, no. 18, pp. 4878–4883, May 1994, doi: 10.1021/j100069a018.

[6] F. Arena, R. D. Chio, and G. Trunfio, ‘An experimental assessment of the ammonia temperature programmed desorption method for probing the surface acidic properties of heterogeneous catalysts’, *Applied Catalysis A: General*, vol. 503, pp. 227–236, Aug. 2015, doi: 10.1016/j.apcata.2015.05.035.

[7] A. K. Galwey and M. E. Brown, ‘Application of the Arrhenius equation to solid state kinetics: can this be justified?’, *Thermochimica Acta*, p. 8, 2002.

[8] M. Maciejewski, ‘Computational aspects of kinetic analysis. Part B: The ICTAC Kinetics Project - the decomposition kinetics of calcium carbonate revisited, or some tips on survival in the kinetic minefield’, *Thermochimica Acta*, p. 10, 2000.

[9] S. Vyazovkin, ‘Computational aspects of kinetic analysis. Part C. The ICTAC Kinetics Project -the light at the end of the tunnel?’, *Thermochimica Acta*, p. 9, 2000.

[10] W. E. Garner, *Chemistry of the Solid State*. Acedemic Press, 1955.

[11] A. Khawam and D. R. Flanagan, ‘Solid-State Kinetic Models: Basics and Mathematical Fundamentals’, *The Journal of Physical Chemistry B*, vol. 110, no. 35, pp. 17315–17328, Sep. 2006, doi: 10.1021/jp062746a.

[12] J. Sestak and G. Berggren, ‘Study of the kinetics of the mechanism of solid-state reactions at increasing temperatures’, *Thermochimica Acta*, vol. 3, pp. 1–12, 1971.

[13] V. M. Gorbachev, ‘Some aspects of Šestak’s generalized kinetic equation in thermal analysis’, *Journal of Thermal Analysis*, vol. 18, no. 1, pp. 193–197, Feb. 1980, doi: 10.1007/BF01909467.

[14] W. E. Stewart and M. Caracotsios, *Computer-aided modeling of reactive systems*. Hoboken, N.J: Wiley-Interscience : AIChE, 2008.

[15] K. P. Burnham and D. R. Anderson, ‘Multimodel Inference: Understanding AIC and BIC in Model Selection’, *Sociological Methods & Research*, vol. 33, no. 2, pp. 261–304, Nov. 2004, doi: 10.1177/0049124104268644.

[16] H. Akaike, ‘Information theory and an extension of the maximum likelihood principle.’, *In B. N. Petrov & F. Caski (Eds.),Proceedings of the Second International Symposium on Information Theory*, pp. 267–281, 1973.

[17] B. Janković, N. Manić, D. Stojiljković, and V. Jovanović, ‘TSA-MS characterization and kinetic study of the pyrolysis process of various types of biomass based on the Gaussian multi-peak fitting and peak-to-peak approaches’, *Fuel*, vol. 234, pp. 447–463, Dec. 2018, doi: 10.1016/j.fuel.2018.07.051.

[18] O. J. Olusola and M. Sudip, ‘Temperature programme reduction (TPR) studies of cobalt phases in -alumina supported cobalt catalysts’, *J. Pet. Technol. Altern. Fuels*, vol. 7, no. 1, pp. 1–12, Jan. 2016, doi: 10.5897/JPTAF2015.0122.

[19] G. Jacobs, Y. Ji, B. H. Davis, D. Cronauer, A. J. Kropf, and C. L. Marshall, ‘Fischer–Tropsch synthesis: Temperature programmed EXAFS/XANES investigation of the influence of support type, cobalt loading, and noble metal promoter addition to the reduction behavior of cobalt oxide particles’, *Applied Catalysis A: General*, vol. 333, no. 2, pp. 177–191, Dec. 2007, doi: 10.1016/j.apcata.2007.07.027.

[20] C. Ehrhardt, M. Gjikaj, and W. Brockner, ‘Thermal decomposition of cobalt nitrato compounds: Preparation of anhydrous cobalt(II)nitrate and its characterisation by Infrared and Raman spectra’, *Thermochimica Acta*, vol. 432, no. 1, pp. 36–40, Jul. 2005, doi: 10.1016/j.tca.2005.04.010.

5. Simultaneous kinetic modelling of data collected with different temperature programs

Summary

This chapter explores the use of the modified Sestak-Berggren equation for simultaneous regression of linear temperature programmed data and constant rate thermal analysis (CRTA) data. The addition of the CRTA temperature programmed method should allow the separation of thermal events which occur at similar temperatures. A case study of temperature programmed reduction on a calcined cobalt on alumina catalyst precursor has been used to demonstrate the ability to simultaneously regress the two signal types. Reduction mechanisms based on reaction stoichiometry constrain the event contributions used as well as the number of thermal events. Three datasets have been regressed: linear, CRTA and the combination of both linear and CRTA. Using Akaike weights for discrimination, it was found for all datasets that a mechanism which assumes no residual nitrate and three thermal events is the most likely to describe the system. With each of the three datasets, a successful kinetic triplet has been identified for each thermal event. For the combined dataset, mechanisms of first order, Avrami-Erofeev and first order were found for the three thermal events respectively. These kinetic triplets could be used for modelling large-scale reduction, after validation, but care is required for extrapolation.

5.1 Introduction

Chapter 4 outlined the experimental validation of the modified Sestak-Berggren model using a temperature programmed reduction (TPR) case study, which used a linear temperature ramp rate. The study concluded, that the system should be modelled as a two-event system, despite the appearance of a “shoulder” at around 480 K.

Constant rate thermal analysis (CRTA), as discussed in Chapter 2, can achieve higher resolution on sequential reactions or events which occur at similar temperatures as the temperature is controlled using a constant rate of change of a pre-selected sample property. This allows the temperature change to slow when reaction is occurring. It is proposed that CRTA could help distinguish the “shoulder” observed in the linear TPR data shown in Chapter 4, as a thermal event.

Sánchez-Jiménez et al. [1]–[5] claim that as a slower reaction rate can be predefined by the user, heat and mass transport effects are minimised therefore analysis via CRTA is more representative than via other methods. However, this technique can still suffer from pressure and temperature gradients, and according to Brown [6], this is especially likely during rapid/strong endothermic decompositions. Even when using CRTA, Koga and Criado [7] observed internal mass transport issues with sample masses over 10 mg. Hence care regarding sample size should still be taken. Although the apparent benefits are numerous, this temperature program is still not widely used within industry for materials analysis or the extraction of kinetic parameters due to the time consuming nature of the experiments [8] and the intricacies of tuning the control loop [9].

Criado and Pérez-Maqueda [10] discussed how multiple solid-state reaction mechanisms with differing Arrhenius parameters may give identical curves when studied under constant/linear heating rates. These authors discussed that when using CRTA, each reaction mechanism has differing shapes. This concept of differing curve shapes is widely accepted in the literature and is reflected in the use of ‘master plots’. Master plots are theoretical curves, dependent on the solid-state reaction mechanism occurring, but not the Arrhenius parameters of the reaction. The plots are used as a method of identifying which solid-state mechanism is occurring. Care should be taken when considering these theoretical curves, as many authors report differing axes [11].

Depending on the type of master plot used, some mechanisms can give very similar curves. Criado et al. [11] concluded that a master plot of the type shown in Figure 5.1 should be used, as this gives unique curves for each reaction mechanism. The y-axis on this master plot is based on Equation 5.1.

$$z(\alpha) = \frac{\left(\frac{d\alpha}{dt}\right)}{\beta}\pi(x)T \qquad \text{Eq. (5.1)}$$

Where $\pi(x)$ is the approximate temperature integral.

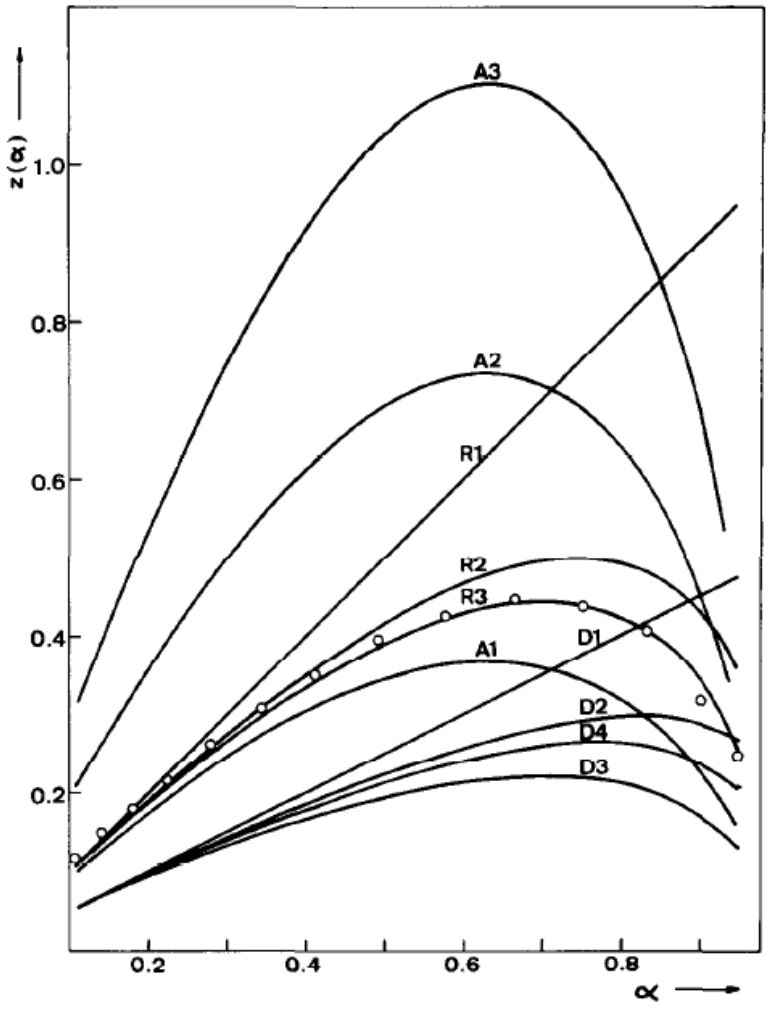

Figure 5.1: CRTA master curves based on $z(\alpha)$ [11].

An alternative to shape analysis of these master plots is the use of the Sestak-Berggren equation for mechanism discrimination [1]–[3], [12], [13].

Criado et al. [14] suggest that as $\ln \frac{1}{f(\alpha)}$ of the solid-state functions discussed in Chapter 3 are not linearly correlated, only a single CRTA curve is needed for kinetic mechanism discrimination. However, only the special case of a single thermal event system was considered. In contrast, Perez-Maqueda et al. [15] concluded that it is not possible to identify the activation energy and reaction order of an nth order model from a single

CRTA curve. In this study, a set of five rates has been used, to align with those used in the linear temperature ramp rate experiments.

Sánchez-Jiménez et al. [1] used the parameter estimates from linear temperature ramp rate experiments to predict a single CRTA curve. This predicted curve matched the experimental curve, and it was concluded that both the linear heating rate and CRTA experiments were free from transport phenomena. This methodology of using the kinetic triplet predicted from linear heating rate data to reproduce CRTA curves was also used in Sánchez-Jiménez et al. [13]. In this case, the nth order reaction model failed to capture the induction period of the CRTA experiment and it was concluded that this reaction mechanism was incorrect. The authors subsequently fitted a random chain scission model successfully.

The aim of this investigation is to use combined CRTA and linear temperature ramps to extract a kinetic triplet from TPR data. The simultaneous regression of CRTA and linear experiments should enable better resolution of ‘shoulders’ within the data. Evolved gas analysis (EGA) will be used to verify the results.

5.2 Evolved gas analysis (EGA)

The use of a thermal conductivity detector in isolation limits the information extracted about the composition of the evolved gas species, as only the conductivity influences the signal produced. The addition of EGA such as mass spectrometry (MS) would allow for the identification of these gaseous species and the temperature at which they are released (discussed in Chapter 2).

Figure 5.2 shows the qualitative MS results associated with the linear temperature programmed reduction experiments described in Chapter 4. This verifies that three

thermal events occur during this reduction, as Figure 5.2 shows a peak relating to NO^+ (mass to charge ratio of 30) at ~480 K, which corresponds to the 'shoulder' observed in the linear temperature ramp experiments.

Note that in Figure 5.2 the hydrogen (m/z 2) is consumed, whereas the NO^+ (m/z 30) is released.

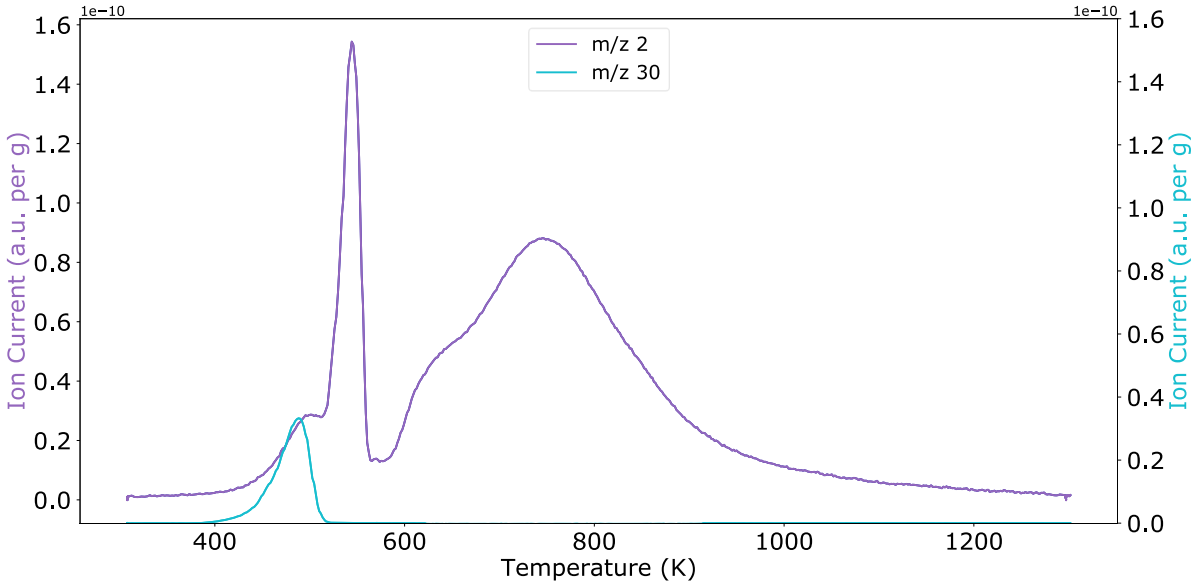

Figure 5.2: Mass spectrometry results, showing m/z 2 and m/z 30 traces. 10 K min^{-1}.

This raised concerns around the data quality of the experiments which were analysed in Chapter 4 and led to a review of the experimental procedure. It was identified that the use of drierite desiccate was insufficient to capture evolved water which could impact the TCD results. To better remove the evolved water from the carrier gas, a cold trap was installed onto the Altamira AMI200 unit. This led to the improved experimental method described in Section 5.3 and the re-collection of a set of linear temperature ramp rate experiments.

5.3 Experimental

5.3.1 Material

The material used in this study was a 40 wt% Co_3O_4 on alumina catalyst. This catalyst was prepared according to the methodology outlined in patent number WO 2010/049714 A1 [16].

5.3.2 Linear heating rate TPR

Reduction was conducted using an Altamira AMI200. A trap removed the evolved water, and the hydrogen concentration was monitored using a thermal-conductivity detector (TCD). Samples of ~100 mg were loaded into the 4 mm ID tubular quartz reactor. Samples were dried prior to reduction in flowing argon (40 mL min^{-1}) by heating at 10 K min^{-1} at 413 K then held for 1 hour. Reduction was carried out in an atmosphere of 10 vol% H_2 in Ar under a gas flow rate of 40 mL min^{-1}. Temperature ramp rates of 1, 2, 3, 4, 5, 6, 7, and 10 K min^{-1} were conducted in a random order, between temperatures of 298 K and 1273 K.

5.3.3 CRTA reduction

The experimental set up and conditions for the CTRA experiments were identical to the linear heating rate TPR case, except for the temperature program. In this case the temperature was controlled based on the rate of evolved gas, at rates of 1.7×10^{-3}, 1.4×10^{-3}, 1.1×10^{-3}, 8.0×10^{-4}, and 5.0×10^{-4} min^{-1}.

5.4 Modelling methodology

5.4.1 Reduction mechanisms

There are multiple possible routes for the reduction of cobalt on alumina. The following six models represent these chemical routes. The models in Table 5.1 assume there is no residual nitrate remaining in the material following calcination.

Table 5.1: Reduction mechanisms, no nitrates included.

Model number	Chemistry	Fv value
1	$Co_2O_3 + H_2 \rightarrow 2CoO + H_2O$	$1/3$
	$2CoO + 2H_2 \rightarrow 2Co + 2H_2O$	$2/3$
2	$3Co_2O_3 + H_2 \rightarrow 2Co_3O_4 + H_2O$	$1/9$
	$2Co_3O_4 + 2H_2 \rightarrow 6CoO + 2H_2O$	$2/9$
	$6CoO + 6H_2 \rightarrow 6Co + 6H_2O$	$6/9$
3	$Co_3O_4 + H_2 \rightarrow 3CoO + H_2O$	$1/4$
	$3CoO + 3H_2 \rightarrow 3Co + 3H_2O$	$3/4$

Due to the calcination conditions (523 – 923 K), it is possible that some of the cobalt remains as a nitrate species, which explains the presence of the NO^+ peak observed on the MS results in Figure 5.2. Models in Table 5.2 represent possible routes which include the decomposition of a nitrate.

Table 5.2: Reduction mechanisms, nitrates included.

Model number	Chemistry	Fv value
4	$2Co(NO_3)_3 + 9H_2 \rightarrow 6NO + Co_2O_3 + 9H_2O$	$9/12$
	$Co_2O_3 + H_2 \rightarrow 2CoO + H_2O$	$1/12$
	$2CoO + 2H_2 \rightarrow 2Co + 2H_2O$	$2/12$
5	$6Co(NO_3)_3 + 27H_2 \rightarrow 18NO + 3Co_2O_3 + 27H_2O$	$27/36$
	$3Co_2O_3 + H_2 \rightarrow 2Co_3O_4 + H_2O$	$1/36$
	$2Co_3O_4 + 2H_2 \rightarrow 6CoO + 2H_2O$	$2/36$
	$6CoO + 6H_2 \rightarrow 6Co + 6H_2O$	$6/36$
6	$3Co(NO_3)_3 + 14H_2 \rightarrow 9NO + Co_3O_4 + 14H_2O$	$14/18$
	$Co_3O_4 + H_2 \rightarrow 3CoO + H_2O$	$1/18$
	$3CoO + 3H_2 \rightarrow 3Co + 3H_2O$	$3/18$

These reduction mechanisms fix the value of Fv, the relative contribution of each thermal event to the overall curve, by reaction stoichiometry. Akaike weights, discussed in Chapter 4 will be used to determine the most statistically likely reduction model from Tables 5.1 and 5.2, using the following modelling method [17], [18].

All the models presented in Tables 5.1 and 5.2 are inherently consecutive mechanisms, which require event 1 to begin prior to event 2 and so on. Initially, although not strictly correct, these mechanisms will be modelled as individual events, prior to the development of sequential models.

5.4.2 Modified Sestak-Berggren methodology

The modified Sestak-Berggren methodology outlined in Chapter 4 (shown in Equation 5.1 as a duplicate of 4.1) will be used to model the thermal events as individual events.

$$\frac{d\alpha}{dt} = \sum_{i=1}^{n_{events}} F_{v,i} \cdot A_i \cdot \exp\left(\frac{Ea_i}{R.T_{b,i}}\left(1 - \frac{T_{b,i}}{T}\right)\right) \cdot (1-\alpha_i)^{n_i} \alpha_i^{m_i}, \qquad \text{Eq. (5.1)}$$

The parameter estimation results from the modified Sestak-Berggren equation will be used to indicate the likely solid-state mechanism occurring for each thermal event. A minimum of two standard sets of initial parameter values have been used for each regression, to ensure a global minimum is achieved.

In this work, different response models are required for the linear and CRTA datasets. CRTA data are in the integral form hence the response function is the same α vs *t* curve. The linear data are in the differential form, so the response function is the first differential with respect to time of the α vs *t* curve.

5.5 Results and discussion

5.5.1 Linear heating rate TPR

Figure 5.3 shows the raw results from the linear temperature ramp dataset. Noise analysis, using a moving average model was completed on this data, and it was found to have an average of 2.01 % noise, hence eight temperature ramp rates should be sufficient for the modified Sestak-Berggren model to discriminate solid-state mechanisms. No baseline correction was required for this dataset.

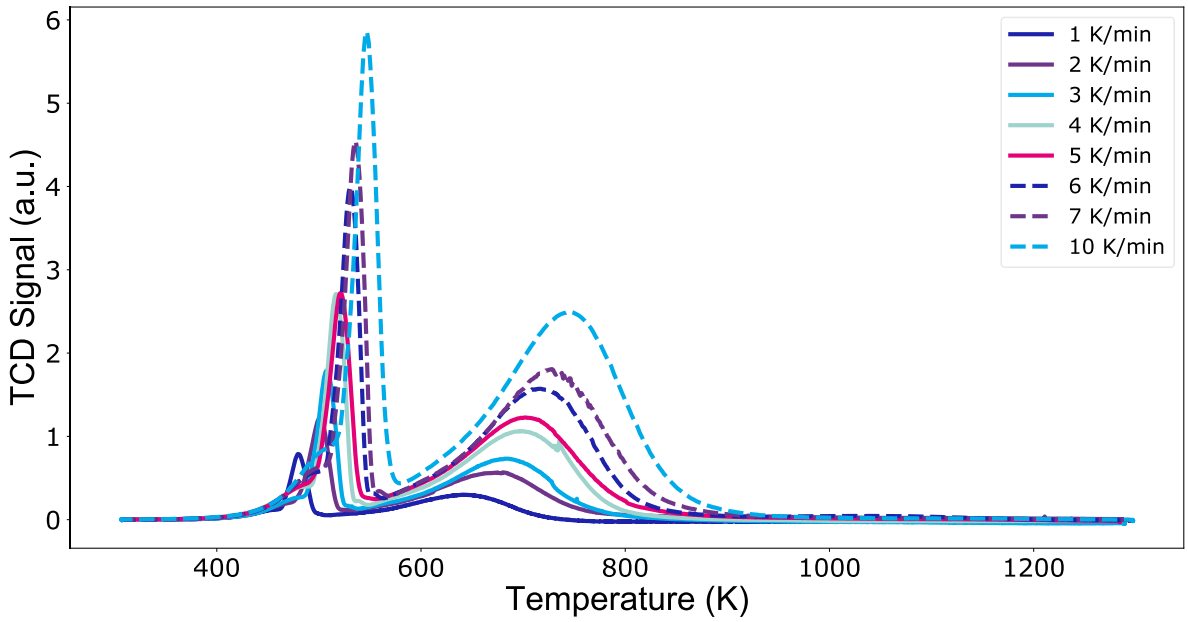

Figure 5.3: Raw dataset for linear experiments, eight temperature ramp rates.

5.5.1.1 Sestak-Berggren results

The six reduction mechanisms were trialled using the modified Sestak-Berggren model. Table 5.3 shows the results of these regressions, with Akaike weights used to indicate the most statistically likely reduction mechanism.

Table 5.3: Akaike weights discrimination of linear temperature programmed data, modified Sestak-Berggren model regressions.

Model	**1**	**2**	**3**
Number of parameters	8	12	8
R^2	0.958	0.989	0.970
RSS	3.56×10^3	8.88×10^2	2.52×10^3
AICc	-2.52×10^4	-4.81×10^4	-3.09×10^4
Akaike weight	0.0	**1.0**	0.0
Model	**4**	**5**	**6**
Number of parameters	12	16	12
R^2	0.862	0.746	0.807
RSS	1.17×10^4	2.15×10^4	1.63×10^4
AICc	-5.67×10^3	4.43×10^3	-1.33×10^2
Akaike weight	0.0	0.0	0.0

Table 5.3 shows that reduction mechanism 2, a three event model which does not include nitrates, was the most statistically likely mechanism for these linear TPR data.

The EGA in Figure 5.2 showed residual nitrates in the material after calcination, which are released during the reduction. The models in Table 5.2 which include the nitrate reduction assume all the material is in the nitrate form. This assumption is flawed for a pre-calcined material as some nitrates will have decomposed in the pre-calcination, meaning not all the material will remain in the nitrate form. However, determination of the amount of nitrate remaining after the pre-calcination would require another analytical method, such as quantitative EGA.

Although the nitrate form of the material is not accounted for in reduction mechanism 2, the fit and parameters obtained are sensible and could be used to describe this system. This implies the proportion of material in the nitrate phase at the start of the reduction is minimal and has little effect on the overall reduction profiles obtained.

5.5.1.2 Mechanistic results

The results of the modified Sestak-Berggren model were used to indicate which solid-state mechanisms are likely for each of the three thermal events. In this case, the first and second events have an Avrami-Erofeev mechanism (n = 2 and n = 3 respectively), and the final event is first order. Table 5.4 shows the results of the mechanistic modelling, with Figure 5.4 showing an example of the fit obtained.

Table 5.4: Parameter estimation results for linear temperature programmed data, mechanistic model regression.

Parameter	Estimated Value	95% Confidence Interval
A_1 (s^{-1})	7.66×10^{5}	2.09×10^{0}
Ea_1 (kJ mol^{-1})	1.62×10^{1}	5.63×10^{-5}
A_2 (s^{-1})	3.50×10^{11}	8.19×10^{5}
Ea_2 (kJ mol^{-1})	7.00×10^{1}	1.86×10^{-4}
A_3 (s^{-1})	6.58×10^{8}	9.13×10^{3}
Ea_3 (kJ mol^{-1})	6.20×10^{1}	9.67×10^{-4}

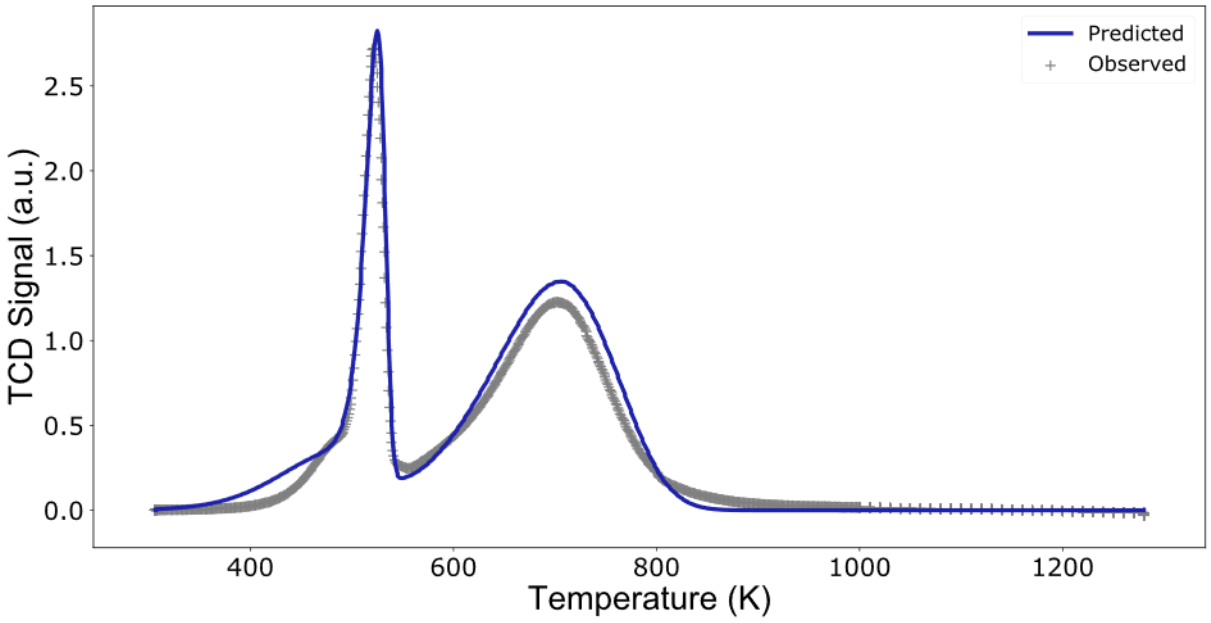

Figure 5.4: Results of mechanistic modelling, linear temperature ramp rate of 5 K min^{-1} example.

Chapter 4 discussed the issues with fitting a three event model to linear TPR data for the same material used in this study. The first event appeared as a shoulder and could not be separated sufficiently from event two to be modelled as an event in its own right.

However, the subsequent update to the experimental method has allowed a dataset to be gathered which is most likely to be described as a three event system, rather than the two events obtained previously. This emphasises that high quality kinetic data is required for detailed kinetic analysis such as interpretation with the modified Sestak-Berggren equation.

Although the ‘shoulder’ discussed in Chapter 4 has now been identified as a thermal event, the model’s closeness of fit for this event is still poor. This could indicate that the contribution term for this event is incorrect and could possibly be influenced by the small release of nitrates discussed previously.

5.5.2 CRTA TPR

Figure 5.5 shows the five rate dataset collected using CRTA TPR. A moving average model found that the average white noise in this dataset was 6.3 % however this average is increased substantially by the inclusion of the 5.0×10^{-4} min^{-1} rate, which has a white noise of 18.8 %.

This dataset has been baseline corrected. Each rate experiment, in its original differential form, was treated with a correction which was linear with time (discussed in Appendix A).

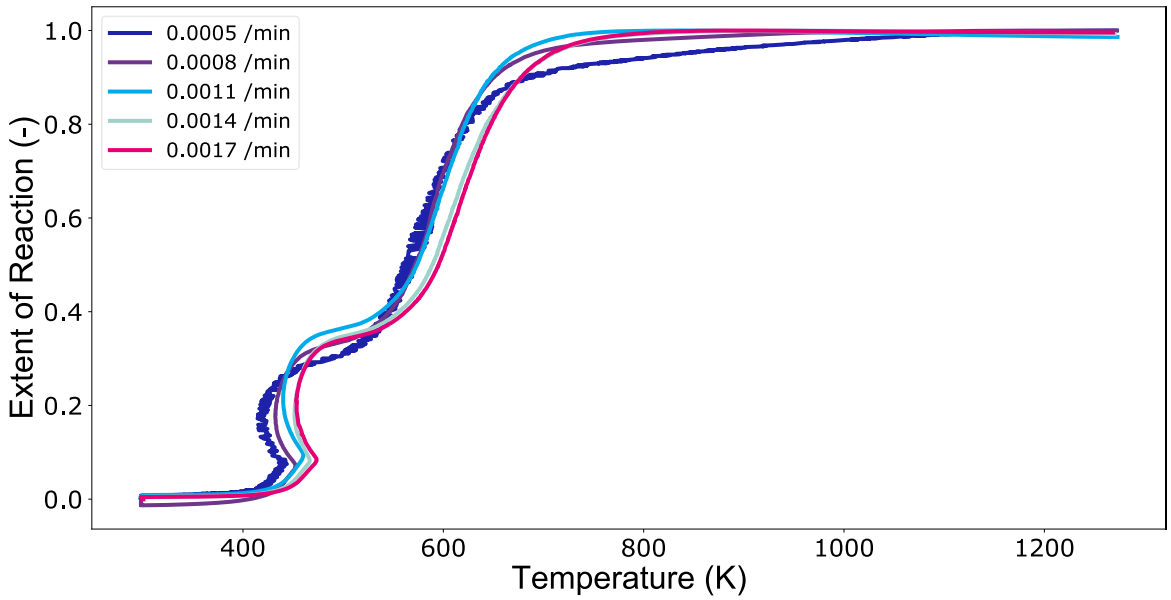

Figure 5.5: Raw dataset for CRTA experiments, five rates.

5.5.2.1 Sestak-Berggren results

As with the linear dataset, all six reduction mechanisms have been trialled using the modified Sestak-Berggren model. Table 5.5 shows the results of these regressions. For these data, only two mechanisms, numbers 1 and 2 converged to estimate all the required parameters. Hence only these mechanisms have been considered in the Akaike weights analysis in Table 5.5 [19].

Table 5.5: Akaike weights discrimination of CRTA data, modified Sestak-Berggren model regressions.

Model	1	2
Number of parameters	8	12
R^2	0.997	0.998
RSS	1.97×10^{0}	1.75×10^{0}
AIC	-3.92×10^{4}	-3.98×10^{4}
Akaike weight	0.0	1.0

The Akaike weights in Table 5.5 shows that mechanism 2, which is a three event model which assumes no nitrates are present, is the most likely to describe this constant rate system.

5.5.2.2 Mechanistic results

The results from the modified Sestak-Berggren modelling were used to identify the most likely solid-state mechanism for each thermal event. In this case, the Sestak-Berggren parameters do not clearly match solid-state mechanisms, hence various plausible mechanism combinations were trialled. Table 5.6 shows the Akaike weight comparison for these mechanistic fits.

Table 5.6: Akaike weights discrimination of mechanistic model combinations for CRTA dataset.

Model	Event 1 = A2 Event 2 = A3 Event 3 = 1st	Event 1 = 1st Event 2 = A3 Event 3 = 1st
Number of parameters	6	6
R^2	0.990	0.990
RSS	7.78×10^0	7.59×10^0
AIC	-3.23×10^4	-3.24×10^4
Akaike weight	0.0	1.0

The Akaike weight comparison in Table 5.6 indicates that the most likely solid-state mechanisms for the three events are first order, Avrami-Erofeev (n= 2) and first order respectively. Although the values for the AIC in Table 5.6 appear close, as there is a difference of > 10, there is no support for the higher value [18] (in this case the model which uses an A2 mechanism for the first thermal event).

Table 5.7 shows the results of the regression using these three solid-state mechanisms. Figure 5.6 shows an example of the closeness of fit obtained with the estimated model.

The 95 % confidence intervals obtained for this regression are poorer that those obtained for the linear data regression. This has been attributed to the higher level of white noise in the CRTA dataset.

Table 5.7: Parameter estimation results for CRTA mechanistic model regression.

Parameter	Estimated Value	95% Confidence Interval
A_1 (s^{-1})	2.15×10^{5}	1.26×10^{4}
Ea_1 (kJ mol^{-1})	4.54×10^{1}	2.05×10^{0}
A_2 (s^{-1})	4.81×10^{11}	6.29×10^{9}
Ea_2 (kJ mol^{-1})	1.02×10^{2}	2.88×10^{-1}
A_3 (s^{-1})	4.38×10^{6}	4.50×10^{4}
Ea_3 (kJ mol^{-1})	8.07×10^{1}	3.78×10^{-1}

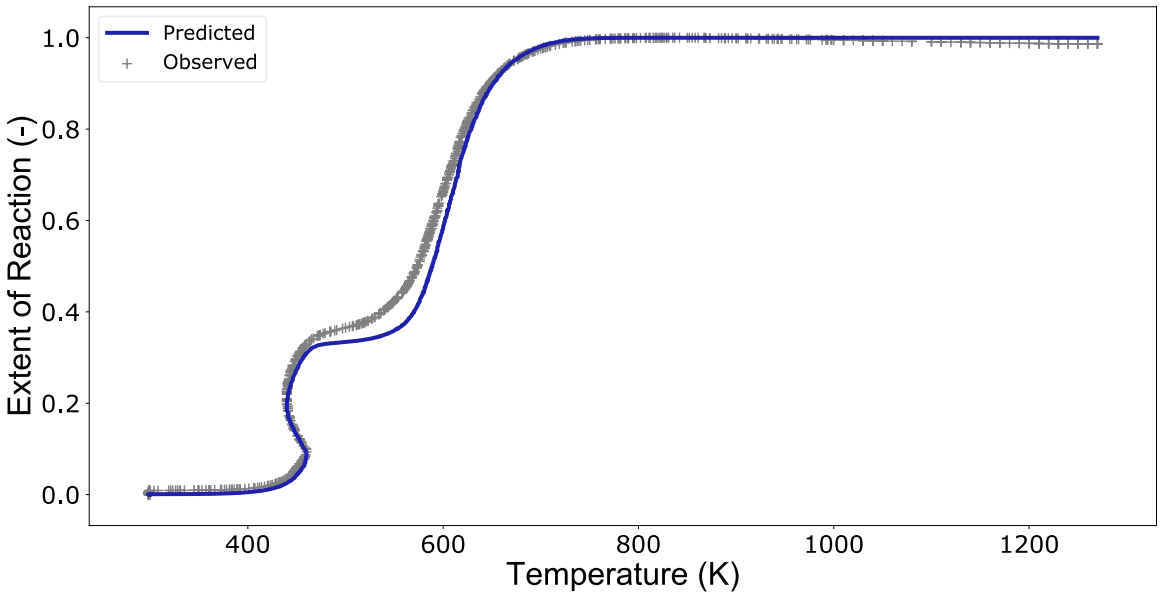

Figure 5.6: Results of mechanistic modelling, CRTA data, 1.1×10^{-3} min^{-1} rate example.

For the linear data, an Avrami-Erofeev (n = 2) mechanism was used to describe the first thermal event. Although this mechanism was considered for the CRTA dataset, Akaike weights indicated that a first order model is a more likely mechanism.

Higher values for the activation energies for each thermal event are estimated for the CRTA dataset compared to the linear dataset. This could indicate that internal transport limitations are present within the linear dataset, suppressing the activation energy estimates.

This small study shows that integral signals such as CRTA data can be analysed using the modified Sestak-Berggren equation. As this experimental technique is used to separate closely occurring thermal events, it could be useful for identifying whether ‘shoulders’ are either thermal events or artefacts in the data.

5.5.2.3 CRTA data using linear parameter estimates

Figure 5.7 shows the fit obtained using the estimated Sestak-Berggren parameters from the linear dataset regression, used to predict the CRTA data. The quality of fit improves with higher rates, reinforcing that the constant linear temperature ramp rate experiments relate to higher reaction rates than the CRTA data. The quality of fit for the first thermal event is extremely poor, again implying that the mechanism indicated in the linear data is not suitable for these slower reaction rates.

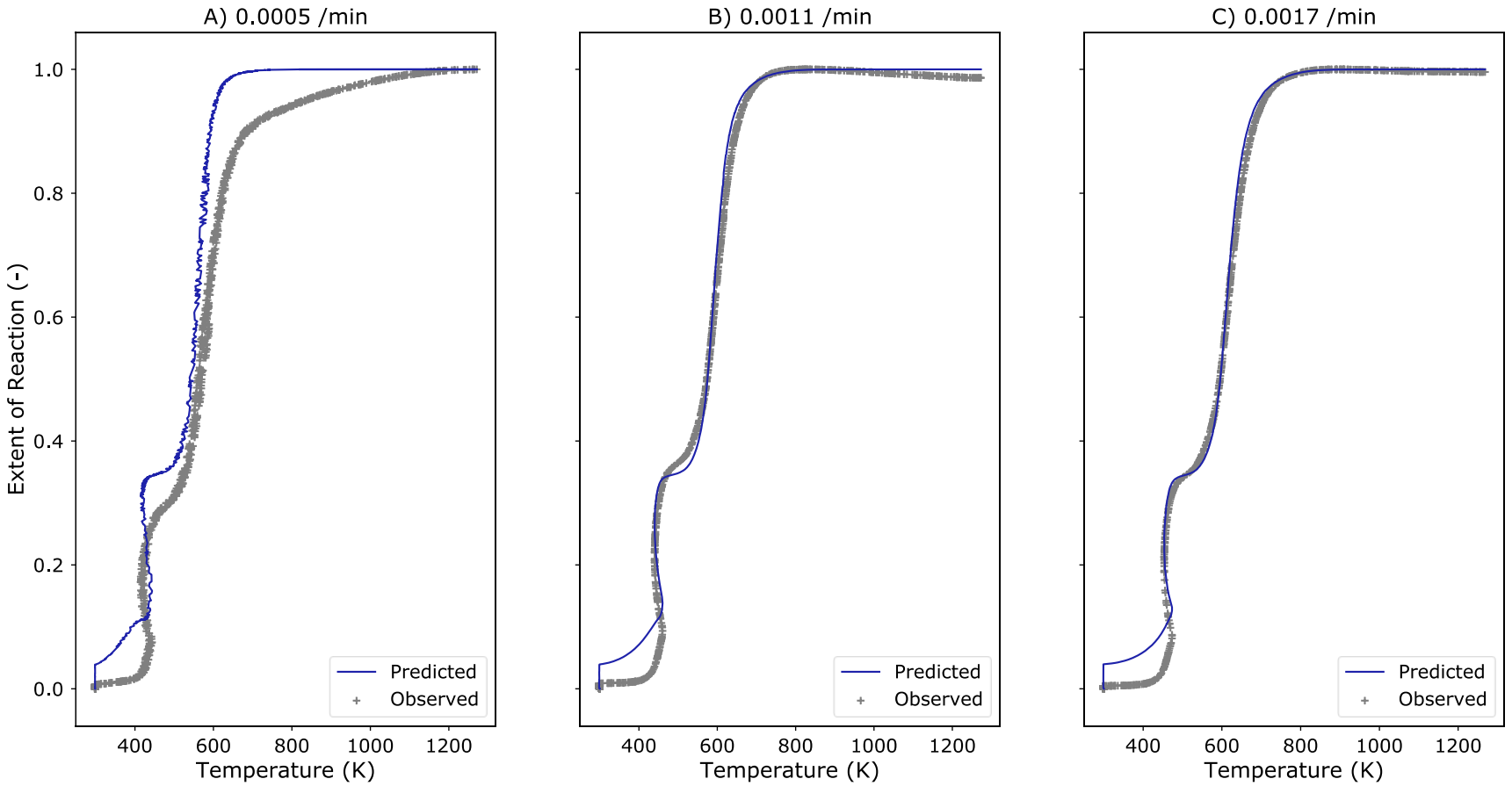

Figure 5.7: CRTA data fitted using the parameter estimates from the linear temperature ramp dataset.

5.5.3 Combined linear and CRTA TPR

This dataset has combined both the previous linear and CRTA datasets, and these two types of data/signal are regressed simultaneously, using the different response models discussed in Section 5.4.2. The number of data points in each experiment have been weighted to avoid bias.

5.5.3.1 Sestak-Berggren results

Table 5.8 shows the Akaike weight discrimination of the reduction models using the modified Sestak-Berggren equation, for the combined dataset.

Table 5.8: Akaike weights discrimination of combined linear and CRTA dataset, modified Sestak-Berggren model regressions.

Model	**1**	**2**	**3**
Number of parameters	8	12	8
R^2	0.968	0.991	0.974
RSS	3.73×10^3	1.11×10^3	3.05×10^3
AIC	-3.75×10^4	-6.35×10^4	-4.19×10^4
Akaike weight	0.0	1.0	0.0
Model	**4**	**5**	**6**
Number of parameters	12	16	12
R^2	0.883	0.784	0.828
RSS	1.37×10^4	2.54×10^4	2.02×10^4
AIC	-9.60×10^3	3.61×10^3	-1.26×10^3
Akaike weight	0.0	0.0	0.0

As with the individual datasets model 2, a three event mechanism which does not include nitrates, was the most statistically likely reduction mechanism.

5.5.3.2 Mechanistic results

As the estimated parameters for the modified Sestak-Berggren equation do not clearly indicate which solid-state mechanisms are suitable for these thermal events, multiple model combinations have been considered. Table 5.9 shows the Akaike weight discrimination for these model combinations.

Table 5.9: Akaike weights discrimination of mechanistic model combinations for combined linear and CRTA datasets.

Model	**Event 1 = A2** **Event 2 = A3** **Event 3 = 1st**	**Event 1 = 1st** **Event 2 = A3** **Event 3 = 1st**	**Event 1 = 1st** **Event 2 = A2** **Event 3 = 1st**
Number of parameters	6	6	6
R^2	0.982	0.983	0.968
RSS	2.12×10^3	1.98×10^3	3.72×10^3
AIC	-4.97×10^4	-5.12×10^4	-3.76×10^4
Akaike weight	0.0	1.0	0.0

The Akaike weight discrimination shows that a first order model is suitable for events one and three, with an Avrami-Erofeev (n = 3) model most likely for the second event. Table 5.10 shows the parameter estimation results obtained using these mechanistic models, with Figure 5.8 providing an example of the closeness of fit achieved.

The 95 % confidence intervals achieved for this regression of both data types are smaller than those achieved with only CRTA data. This is most likely due to the increased amount of data used, and that the introduction of linear temperature ramp data lowers the average white noise level.

Table 5.10: Parameter estimation results for combined linear and CRTA dataset mechanistic model regression.

Parameter	Estimated Value	95% Confidence Interval
A_1 (s^{-1})	4.72×10^{4}	1.75×10^{0}
Ea_1 (kJ mol^{-1})	3.69×10^{1}	8.28×10^{-4}
A_2 (s^{-1})	1.19×10^{8}	1.20×10^{3}
Ea_2 (kJ mol^{-1})	7.09×10^{1}	1.56×10^{-3}
A_3 (s^{-1})	3.97×10^{5}	3.19×10^{1}
Ea_3 (kJ mol^{-1})	6.66×10^{1}	4.12×10^{-3}

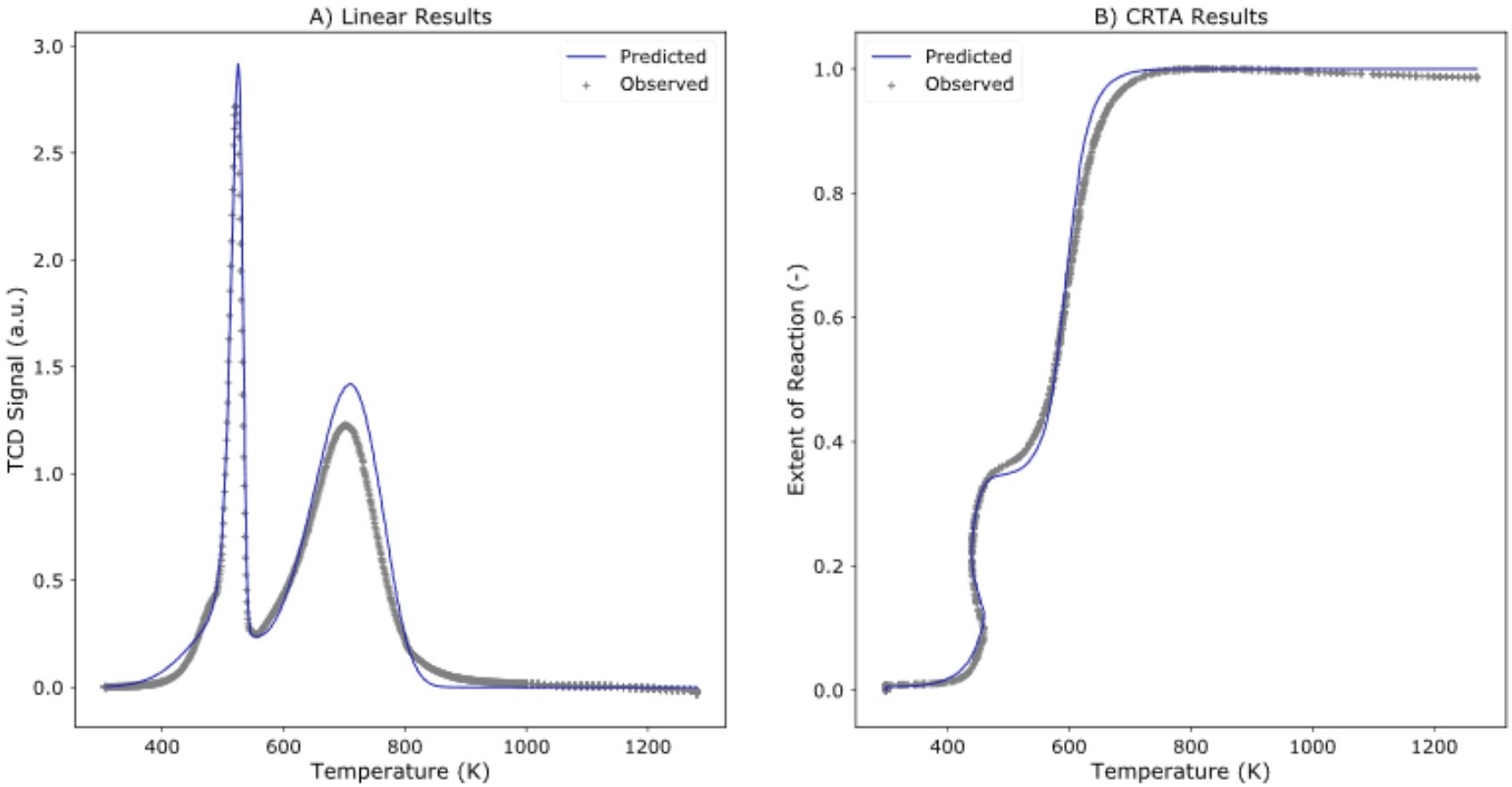

Figure 5.8: Results of mechanistic modelling. Left: linear heating rate example at 5 K min $^{-1}$. Right: CRTA example at 1.1×10^{-3} min^{-1}.

The closeness of fit achieved using the combined data appears to be improved compared to the linear dataset alone. Specifically, the first event is better described by the model. This implies that the CRTA data are a better constraint for the model than the linear data. It is possible that multiple combinations of solid-state mechanisms and Arrhenius parameters could adequately described the linear data, whereas only a single combination of mechanism and Arrhenius parameters are suitable for the CRTA data.

The reduction mechanisms presented in Tables 5.1 and 5.2 are sequential mechanisms, and strictly, modelling these reduction mechanisms as individual events is incorrect and not internally consistent. However, this combination of mechanistic models provides sensible estimates for Arrhenius parameters and good quality of fit, and closeness of fit for both types of signal. The estimated kinetic triplets could therefore be validated and used in a scale-up study. A suitable validation experiment could be a stepwise isothermal TPR, discussed in Chapter 2. The kinetic triplet estimated in this work should be able to adequately predict this alternative temperature program. In this case, this validation is key, as modelling this system as individual events may not be sufficient to describe the reduction outside of the experimental conditions tested. Although this case study has been modelled statistically adequately using individual thermal events, models which account for consecutive or competing events should also be explored.

This dataset has demonstrated that both integral and differential signals could be regressed simultaneously. This could aid in the separation of thermal events and could reduce the quantity of data required, with further investigation.

5.5.4 Comparison of modelling results

Table 5.11 compares the activation energy values estimated for each dataset. As mentioned previously, the linear temperature ramp rate data yielded lower values of activation energy compared to the CRTA data. The combined set appears to provide a compromise between the values, except for the first peak which closer reflects the value estimated with CRTA data alone. As this first thermal event relates to the ‘shoulder’ discussed in Chapter 4 (i.e. is severely overlapped with the second event), and that the quality of fit for the linear temperature ramp rate data is poor, this confirms that CRTA may a more suitable experiment for the separation of thermal events which occur at similar temperatures.

Table 5.11: Comparison of activation energy estimates for each dataset.

Parameter	Linear data		CRTA data		Combined data	
	Estimated Value	95% Confidence Interval	Estimated Value	95% Confidence Interval	Estimated Value	95% Confidence Interval
Ea_1 (kJ mol^{-1})	1.62×10^{1}	5.63×10^{-5}	4.54×10^{1}	2.05×10^{0}	3.69×10^{1}	8.28×10^{-4}
Ea_2 (kJ mol^{-1})	7.00×10^{1}	1.86×10^{-4}	1.02×10^{2}	2.88×10^{-1}	7.09×10^{1}	1.56×10^{-3}
Ea_3 (kJ mol^{-1})	6.20×10^{1}	9.67×10^{-4}	8.07×10^{1}	3.78×10^{-1}	6.66×10^{1}	4.12×10^{-3}

The first thermal event was described using the linear temperature ramp rate data as a first order reaction, which can also be viewed as a Avrami-Erofeev n = 1 mechanism. However, with the introduction of CRTA, this event was described as Avrami-Erofeev n = 2. Although these mechanisms are similar, the difference has been attributed to the better quality of fit obtained using the CRTA data, for the first thermal event.

As suggested in the literature, modelling of CRTA data has allowed for a better description (when the quality of fit is evaluated 'by eye') for severely overlapped thermal events, specifically thermal event one. This type of data could provide vital discrimination of 'shoulders' observed in thermal analysis data.

As the lower activation energy values estimated from the linear temperature ramp rate dataset imply transport limitations, as discussed previously, it may be prudent to use CRTA experiments were possible. This would increase the likelihood that the data gathered are intrinsic. However, CRTA experiments are time consuming and costly to perform. Hence a combination of CRTA and linear temperature ramp rate data could provide a reasonable compromise from an industrial perspective. Combining CRTA with linear temperature ramp rate data could also improve estimated confidence intervals in the most efficient manner- more linear data is faster and cheaper to gather, and should give more certainty to the parameter estimates, as shown in Table 5.11.

5.6 Conclusions

In this work, reduction mechanisms, based on possible reaction stoichiometry for reduction have been used to constrain the contributions of each thermal event. Six reduction mechanisms were trialled, three which did not include residual nitrate present after calcination, and three which do include the nitrate. These mechanisms also had

differing numbers of thermal events. For each dataset investigated, linear, CRTA and both linear and CRTA combined, it was concluded that a mechanism of three events, which did not include residual nitrate was the most likely to describe the system.

Although EGA showed the presence of residual nitrate, the quantity of this phase was unknown. As the reduction mechanism which was indicated using Akaike weights did not include residual nitrates, it was concluded that the amount of this phase present after calcination was minimal and had little impact on the overall consumption of hydrogen.

The impact of experimental method has been discussed and the need for high quality kinetic data emphasised by comparison of kinetic fits obtained using two different experimental methods. With the improved experimental method, three thermal events can be identified for this FT catalyst reduction, rather than the two shown in Chapter 4.

The key output of this work has been the simultaneous regression of two signal types, (differential, and integral). This demonstrates that data from any temperature program can be modelled using the modified Sestak-Berggren methodology, described in Chapter 4, to extract kinetic information.

CRTA has been shown to aid in the identification of thermal events which occur at similar temperatures. However, as the experiments are time consuming to perform, a combination of CRTA and linear temperature ramp rate data could provide a compromise from an industrial standpoint since the regression of both data types resulted in a statistically adequate kinetic triplet for each of the three thermal events identified, when treated as independent events.

5.7 Future Work

Currently the modified Sestak-Berggren methodology and the mechanistic models it represents, assume that the thermal events are independent from one another. As discussed in Chapter 3, it is possible for thermal events to be consecutive or competing. The current set of models should be adapted to allow for these other reaction routes in addition to the independent events.

In this work multiple CRTA rates have been used to ensure adequate constraints for the model, however it may be possible to use fewer rates, saving experimental time and costs. The minimum data required for multiple overlapped thermal events studied using CRTA requires further investigation.

This modelling has allowed the estimation of a statistically adequate kinetic triplet for each of the three thermal events occurring during the reduction of the cobalt on alumina catalyst. These kinetic triplets could be validated, then used to model large-scale reduction of this material, with care taken if extrapolation is required.

5.8 References

[1] P. E. Sánchez-Jiménez, A. Perejón, J. M. Criado, M. J. Diánez, and L. A. Pérez-Maqueda, ‘Kinetic model for thermal dehydrochlorination of poly(vinyl chloride)’, *Polymer*, vol. 51, no. 17, pp. 3998–4007, Aug. 2010, doi: 10.1016/j.polymer.2010.06.020.

[2] P. E. Sánchez-Jiménez, L. A. Pérez-Maqueda, A. Perejón, and J. M. Criado, ‘Generalized master plots as a straightforward approach for determining the kinetic model: The case of cellulose pyrolysis’, *Thermochim. Acta*, vol. 552, pp. 54–59, Jan. 2013, doi: 10.1016/j.tca.2012.11.003.

[3] P. E. Sánchez-Jiménez, L. A. Pérez-Maqueda, A. Perejón, and J. M. Criado, ‘Constant rate thermal analysis for thermal stability studies of polymers’, *Polym. Degrad. Stab.*, vol. 96, no. 5, pp. 974–981, May 2011, doi: 10.1016/j.polymdegradstab.2011.01.027.

[4] P. E. Sánchez-Jiménez, A. Perejón, J. M. Criado, M. J. Diánez, and L. A. Pérez-Maqueda, ‘Kinetic model for thermal dehydrochlorination of poly(vinyl chloride)’, *Polymer*, vol. 51, no. 17, pp. 3998–4007, Aug. 2010, doi: 10.1016/j.polymer.2010.06.020.

[5] J. M. Criado and A. Ortega, ‘A study of the influence of particle size on the thermal decomposition of $CaCO_3$ by means of constant rate thermal analysis’, *Thermochim. Acta*, vol. 195, pp. 163–167, Jan. 1992, doi: 10.1016/0040-6031(92)80059-6.

[6] M. E. Brown, *Introduction to Thermal Analysis: Techniques and Applications*. Springer Science & Business Media, 2001.

[7] N. Koga and J. M. Criado, ‘The influence of mass transfer phenomena on the kinetic analysis for the thermal decomposition of calcium carbonate by constant rate thermal analysis (CRTA) under vacuum’, *Int. J. Chem. Kinet.*, vol. 30, no. 10, pp. 737–744, 1998, doi: 10.1002/(SICI)1097-4601(1998)30:10<737::AID-KIN6>3.0.CO;2-W.

[8] J. Málek, J. šesták, F. Rouquerol, J. Rouquerol, J. M. Criado, and A. Ortega, ‘Possibilities of two non-isothermal procedures (temperature- or rate-controlled) for kinetical studies’, *J. Therm. Anal.*, vol. 38, no. 1, pp. 71–87, Jan. 1992, doi: 10.1007/BF02109109.

[9] T. Ozawa, ‘Thermal analysis review and prospect’, *Thermochim. Acta*, p. 8, 2000.

[10] J. M. Criado and L. A. Pérez-Maqueda, ‘Sample controlled thermal analysis and kinetics’, *J. Therm. Anal. Calorim.*, vol. 80, no. 1, pp. 27–33, Mar. 2005, doi: 10.1007/s10973-005-0609-6.

[11] J. M. Criado, J. Málek, and A. Ortega, ‘Applicability of the master plots in kinetic analysis of non-isothermal data’, *Thermochim. Acta*, vol. 147, no. 2, pp. 377–385, Jul. 1989, doi: 10.1016/0040-6031(89)85192-5.

[12] J. M. Criado, J. Málek, and F. J. Gotor, ‘The applicability of the Šesták-Berggren kinetic equation in constant rate thermal analysis (CRTA)’, *Thermochim. Acta*, vol. 158, no. 2, pp. 205–213, Mar. 1990, doi: 10.1016/0040-6031(90)80068-A.

[13] P. E. Sánchez-Jiménez, L. A. Pérez-Maqueda, A. Perejón, and J. M. Criado, ‘A new model for the kinetic analysis of thermal degradation of polymers driven by random scission’, *Polym. Degrad. Stab.*, vol. 95, no. 5, pp. 733–739, May 2010, doi: 10.1016/j.polymdegradstab.2010.02.017.

[14] J. M. Criado, F. J. Gotor, A. Ortega, and C. Real, ‘The new method of constant rate thermal analysis (CRTA): Application to discrimination of the kinetic model of solid state reactions and the synthesis of materials’, *Thermochim. Acta*, vol. 199, pp. 235–238, May 1992, doi: 10.1016/0040-6031(92)80267-Z.

[15] L. A. Pérez-Maqueda, A. Ortega, and J. M. Criado, ‘The use of master plots for discriminating the kinetic model of solid state reactions from a single constant-rate thermal analysis (CRTA) experiment’, *Thermochim. Acta*, vol. 277, pp. 165–173, May 1996, doi: 10.1016/0040-6031(95)02746-7.

[16] Hamera Abbas, Sharon Bale, Gordon James Kelly, and John West, ‘Cobalt catalysts’, WO 2010/049714 A1, May 06, 2010

[17] H. Akaike, ‘Information theory and an extension of the maximum likelihood principle.’, *B N Petrov F Caski EdsProceedings Second Int. Symp. Inf. Theory*, pp. 267–281, 1973.

[18] K. P. Burnham and D. R. Anderson, ‘Multimodel Inference: Understanding AIC and BIC in Model Selection’, *Sociol. Methods Res.*, vol. 33, no. 2, pp. 261–304, Nov. 2004, doi: 10.1177/0049124104268644.

[19] M. E. Brown *et al.*, ‘Computational aspects of kinetic analysis Part A: The ICTAC kinetics project-data, methods and results’, *Thermochim. Acta*, p. 19, 2000.

6. Characterising hydrothermal ageing of SAPO-34 using the modified Sestak-Berggren equation

Summary

This chapter discusses the use of the modified Sestak-Berggren modelling methodology for describing ammonia temperature programmed desorption (TPD) data, as an alternative characterisation method to expensive spectroscopic techniques. SAPO-34 was selected as an industrially relevant material, which is used in the methanol to olefins (MTO) process, and which has a lifetime on the order of months, due to the hydrothermal conditions experienced within the reactor and regenerator. To improve the long-term stability of the catalyst, the impact of this hydrothermal ageing on the chemical structure must be understood. Samples of SAPO-34 were hydrothermally aged at 923 K for different durations and then analysed by ammonia TPD. The low binding energy site strength was reduced by 0.037 kJ mol^{-1} h^{-1} of hydrothermal ageing. The strength of the high binding energy site remained constant. The primary deactivation of the SAPO-34 through hydrothermal ageing was instead associated with a reduction in the number of acid sites. The rate of reduction in the number of acid sites was comparable for both low and high binding energy sites.

6.1. Introduction

Lower olefins are important chemicals used to make a range of products, including plastics [1]. Conventionally these olefins are produced from crude oil, but with the move towards sustainable processing, these are increasingly produced from natural gas or syngas, through the methanol to olefins (MTO) process [1]–[4].

Zeolites and zeotypes are common catalysts used in the MTO reaction. Specifically, SAPO-34 has been identified [3] due to its high hydrothermal stability, moderate acidity and small 8-ring pore system [5], [6]. This small chabazite pore system enables good selectivity for the desired lower olefins as larger organics and aromatics which may be produced cannot leave the small cages within the catalyst [1].

There are two deactivation mechanisms which occur within MTO and associated processes. The first, short-term deactivation is related to the rapid coke formation during the MTO reaction. Coke is formed on the catalyst surface and within the pores [7], [8], eventually preventing the active acid sites from catalysing the reaction [9], [10]. The catalyst can be reactivated using either air combustion or steam gasification methods [4]. However, this cycle of reaction and regeneration introduces a long-term deactivation mechanism, due to the hydrothermal conditions experienced by the catalyst [11]. Although Barger and Lesch [12] reported some structural collapse of SAPO-34 when hydrothermally aged at 923 K, Changqin et al. [13] reported that the reduction in crystallinity observed (20 % reduction when steamed at 1073 K for 45 h) had little effect on catalytic activity. Conversely, Ying et al. [14] reported that the deactivation of SAPO-34 under hydrothermal conditions was due to a redistribution of

silicon atoms in the framework, rather than the collapse of the crystal structure. This redistribution or movement of silicon atoms has been confirmed using ^{29}Si NMR [15].

A study by Minova et al. [16] used samples from the same aged material as the work presented in this chapter. These were characterised by XRD, nitrogen sorption, and ^{29}Si MAS SS-NMR. The results showed that after 206 hours of steaming at 923 K there were no detectible changes in crystal phase by XRD and no loss in micropore volume. In contrast, the ^{29}Si NMR showed progressive loss of isolated $Si(OAl)_4$ at -94.5 ppm and emergence and growth of new peaks at -101, -107, -111, and -115 ppm which are indicative of $Si(OAl)_{4-k}(OSi)_k$ where k is 1 – 4, respectively, which is widely attributed to the formation of Si islands [16].

The strength of acid sites has been suggested to depend on the Si coordination, with strength increasing as k = 0, 1, 2, and 3 [17], [18]. Density functional theory (DFT) has been used to estimate the desorption energy of ammonia on SAPO- 34 in work by Suzuki et al. [19]. Isolated Si species have an estimated desorption energy of 100-117 kJ mol^{-1}. Whereas the desorption energy of acid sites based around the edge of an 8-Si island were estimated to be between 112 – 152 kJ mol^{-1} [19]. This implies that an increase in desorption energy should be observed with amount of Si islands, which are created with increased steaming time. It was hypothesised that it would be possible to calculate these changes using ammonia TPD combined with kinetic modelling.

Materials characterisation is a key area in catalyst development, and thermal analysis plays an important role in this suite of techniques. Ammonia TPD has been a widely used characterisation technique for investigating the acidity of materials for many years [20]. In many cases ammonia TPD is used qualitatively to compare materials or identify

the types of acid sites present [4]–[6], [21]. Gaining a quantitative insight from this experimentation would allow the extraction of kinetic parameters, making materials comparison more in-depth. This experimental technique is also quick to run and relatively cheap compared to spectroscopic techniques.

Many authors acknowledge that this class of experimentation can be impacted by diffusion within the solid and the readsorption of ammonia onto different/weaker acid sites [9]–[11], [22], [23]. There is disagreement about removing these effects through experimentation (under vacuum) [12]–[14], [24] or accounting for them during modelling [5], [15]– [17]. Even within these two broad techniques, there is no consensus on the correct model or even assumptions for the system [20]. In some cases the system is assumed to be irreversible, with a first order kinetic desorption often assumed [25] – [29]. When readsorption is included within models, often equilibrium is assumed [30] - [35]. A popular method for extracting site strengths from ammonia TPD data was developed by Katada [31] [32] and has been used in many studies [30], [33] - [35].

A choice must be made whether to assume the ammonia desorption is kinetically or equilibrium limited. In this work, we aim to use the irreversible, kinetically limited Sestak-Berggren equation to model the desorption of ammonia. This method may not extract physically meaningful parameters, but the aim is to allow quantitative comparison of these TPD profiles. This would establish the method as industrially relevant. There appears to be no papers within the literature to date which discuss the use of the Sestak-Berggren equation for modelling the TPD of ammonia.

The work presented in this chapter aims to determine the effect of hydrothermal ageing on the presence of acid sites in SAPO-34. This will be achieved through modelling of ammonia TPD data, using the modified Sestak-Berggren equation. In addition, this would demonstrate the applicability of the technique to provide a cheaper, faster alternative to XRD and ^{29}Si MAS SS-NMR to discriminate the surface acid site properties of materials, which enables its use as a primary screening tool, for example of selective catalytic reduction (SCR) catalysts.

6.2. Modelling methods

The kinetic modelling used in this work is based on the modified Sestak-Berggren model as discussed in Chapter 4 and shown in Equation 6.1 [36], [37]. In this case the activation energy (Ea) has been replaced with desorption energy (Ed) This methodology does not require *a priori* peak deconvolution. Non-linear regression has been used in Athena Visual Studio with default tolerances [38], with the aim of reducing the residual on $\frac{d\alpha}{dt}$.

$$\frac{d\alpha}{dt} = \sum_{i=1}^{n_{events}} F_{v,i} \cdot A_i \cdot \exp\left(\frac{Ed_i}{R.T_{b,i}}\left(1 - \frac{T_{b,i}}{T}\right)\right) \cdot (1-\alpha_i)^{n_i} \alpha_i^{m_i}, \qquad \text{Eq.(6.1)}$$

This empirical equation is used to identify the most likely kinetic mechanism through the values of the estimated *n* and *m* parameters and comparison to tabulated values [39].

6.3. Experimental

6.3.1. Materials

SAPO-34 is a chabazite (CHA) framework silicoaluminophosphate microporous material with eight-member ring windows with dimensions of 3.8 × 3.8 Å which partition elliptical 6.7 × 10 Å cages [40], [41]. For this work commercial SAPO-34 was obtained from Zeolyst International, product CP7129.

6.3.2. Hydrothermal ageing

Hydrothermal ageing was carried out in a fixed bed horizontal tubular reactor, with a 95% steam and 5% nitrogen atmosphere at ambient pressure. Temperature was held constant at 923 K, with variable steaming times resulting in 5 samples either receiving no treatment (fresh) or steam times of 20, 40, 110, and 206 h. Consistency of the hydrothermal treatment was verified with a second series of samples steamed for 110 and 206 h.

6.3.3. Ammonia TPD

The ammonia TPD experiments were carried out using a Micrometrics AutoChem 2920 unit. This experimental set up uses a quartz U-tube fixed bed reactor, with ~0.25 g of powder (particle size d(50) of approximately 3 μm) in a bed (settled by tapping) supported on a bed of quartz wool. The sample thermocouple is positioned just inside the bed.

Samples were pretreated in-situ at 923 K and cooled to 373 K in flowing He. Upon reaching 373 K the gas flow was switched to 0.5% NH_3 in He for 50 minutes to saturate the sample. Following saturation, the flow was changed back to He at a rate of

0.22 mol s^{-1} and held at 373 K for 30 minutes to purge the sample, then cooled to 333 K prior to the start of the temperature ramp.

For the fresh sample of SAPO-34, which had not undergone hydrothermal ageing, five temperature ramp rate experiments (2, 4, 6, 8 and 10 K min^{-1}) were completed. These varying temperature ramp rates were required to discriminate between kinetic mechanisms. These temperature ramp rate experiments (including pretreatment) were carried out on the same sample, in a random order, with a final repeat of the first experiment to confirm no zeolite damage was occurring due to the experimental procedure. For each of the hydrothermally aged samples, a single 10 K min^{-1} temperature ramp rate experiment was completed.

6.4. Results and discussion

6.4.1. Fresh SAPO-34

The raw experimental results for the ammonia TPD on the fresh SAPO-34 are shown in Figure 6.1.

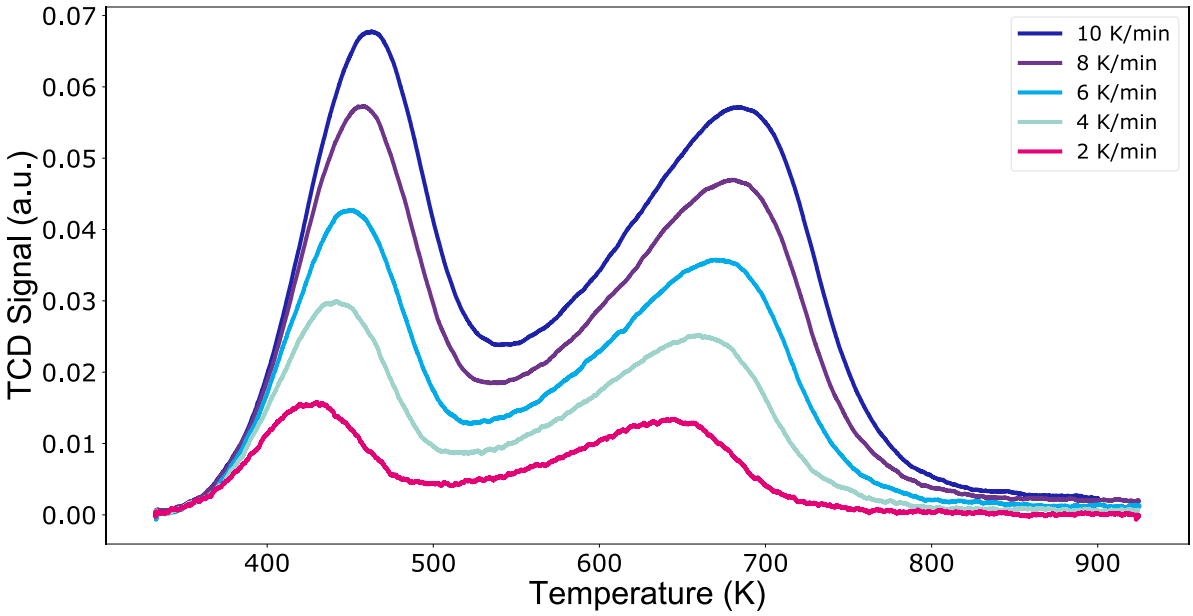

Figure 6.1: Raw experimental results, fresh SAPO-34 ammonia TPD, five temperature ramp rates.

The modified Sestak-Berggren methodology has been applied to this data. Table 6.1 shows the parameter estimates and 95% confidence intervals from this non-linear regression. For this data, no baseline correction was required (discussed in Appendix A [42]). Following the methodology outlined in Chapter 4 [36], models featuring two and three thermal events were considered. Akaike weights identified that the most statistically likely number of thermal events was two. The R-squared value for this regression was 0.98 and the mean squared error (MSE) was 7.24×10^{-3}.

Table 6.1: Parameter estimate results for modified Sestak-Berggren modelling of fresh SAPO-34.

Event	Parameter	Estimate	95% Confidence Interval
Low temperature event (event 1)	A_1 (s^{-1})	1.21×10^{12}	1.92×10^{3}
	Ed_1 (kJ mol^{-1})	6.51×10^{1}	6.84×10^{-8}
	n_1 (-)	1.27×10^{0}	2.39×10^{-9}
	m_1 (-)	-2.90×10^{-1}	8.67×10^{-10}
	Fv_1 (-)	3.80×10^{-1}	7.56×10^{-4}
High temperature event (event 2)	A_2 (s^{-1})	2.22×10^{11}	1.24×10^{3}
	Ed_2 (kJ mol^{-1})	9.31×10^{1}	2.22×10^{-7}
	n_2 (-)	1.10×10^{0}	4.83×10^{-9}
	m_2 (-)	-1.20×10^{0}	1.17×10^{-9}
	Fv_2 (-)	6.20×10^{-1}	7.56×10^{-4}

The hypothesis that Si species coordination environments change from isolated to islands does not imply a change in the ammonia desorption mechanism. Hence it has been assumed that the mechanism of desorption would not be impacted by the hydrothermal ageing of the samples, so the values for the *n* and *m* exponents in the modified Sestak-Berggren model have been fixed for the following modelling, based on the values shown in Table 6.1.

6.4.2. SAPO-34 Ageing Study

The raw ammonia TPD results for each of the hydrothermally aged samples is shown in Figure 6.2.

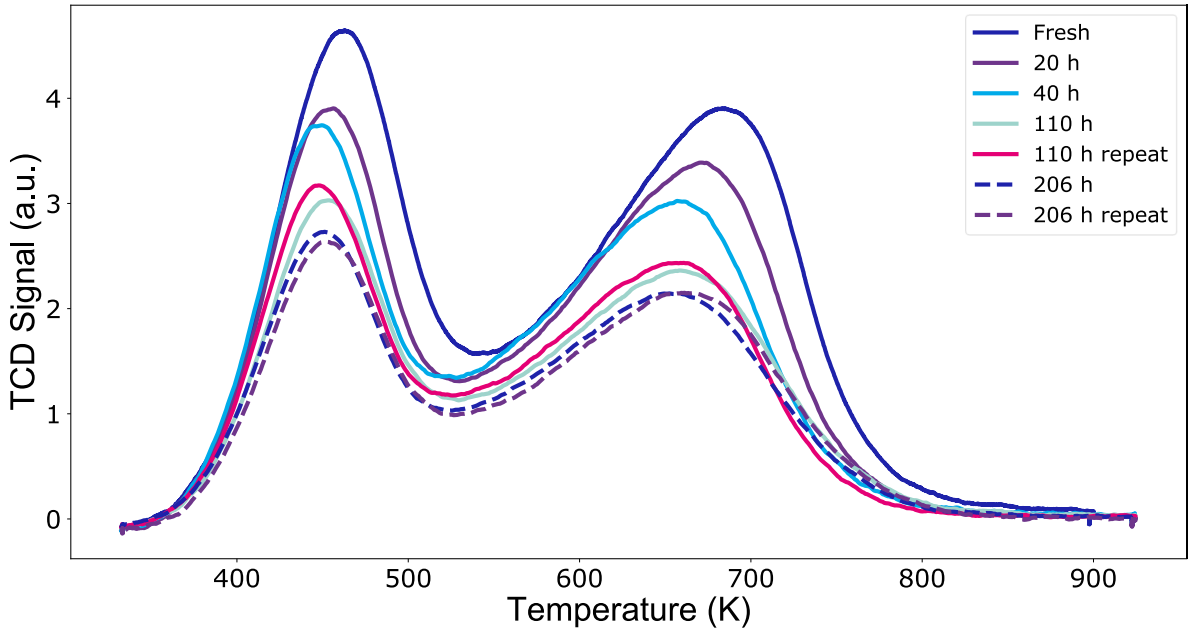

Figure 6.2: Raw experimental results, SAPO-34 ageing study, five differing ageing time.

The amount of ammonia desorbed from the zeotype surface has changed between experiments, due to the hydrothermal ageing of the samples, this is shown in Table 6.2. To treat these experiments as a single data set, would require the assumption of constant kinetics of desorption. Instead, as the aim of this investigation is to determine the impact of the hydrothermal ageing through the estimated Arrhenius values, these experiments have been modelled individually.

Table 6.2: Estimated ammonia desorbed, SAPO-34 ageing study data.

Sample	Desorbed ammonia (mmol g^{-1})
Fresh	1.49
20 h	1.21
40 h	1.12
110 h	0.94
110 h (repeat)	0.93
206 h	0.85
206 h (repeat)	0.87

As the desorption mechanism has been fixed, based on the modified Sestak-Berggren analysis of the fresh SAPO-34 ammonia TPD, the parameters estimated for these regressions were the pre-exponential factor, desorption energy and the contribution of the thermal events to the overall curve. Figure 6.3 shows a comparison of the observed and predicted curves for two of the aged samples. This is for clarity; similar fits were obtained across all aged samples.

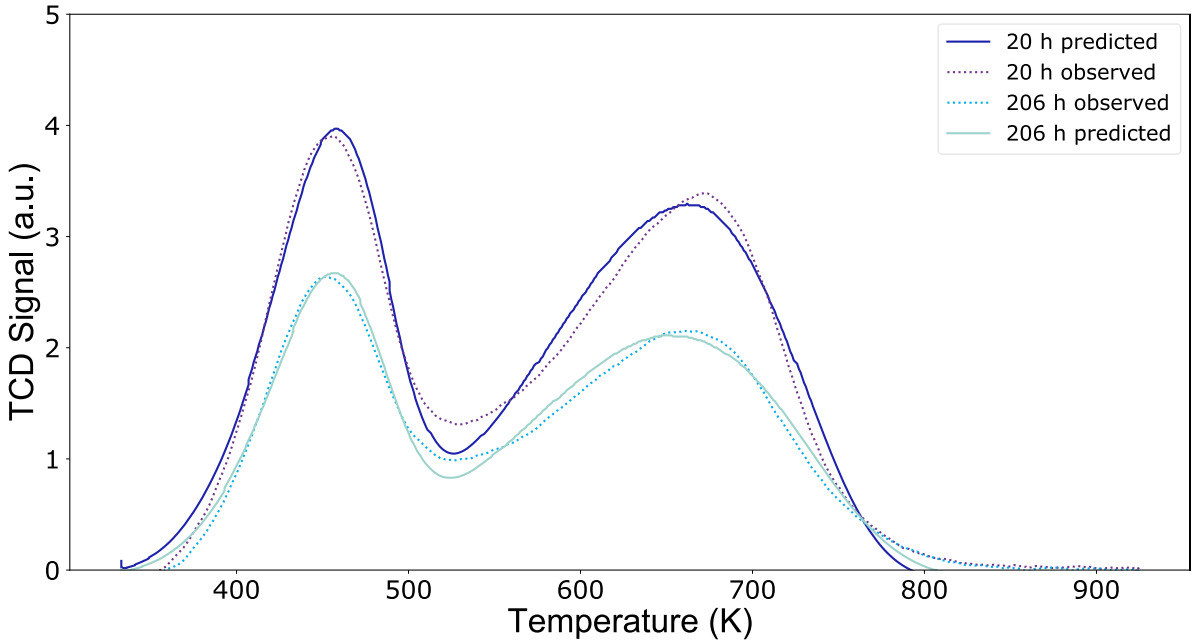

Figure 6.3: Comparison of experimental and predicted curves, modified Sestak-Berggren results, aged SAPO-34, example of 20 h and 206 h.

Figure 6.4 shows the estimated desorption energies for each thermal event, along with the contribution to the overall curve for the low temperature event. The remaining contribution term is calculated based on an overall sum of unity, rather than freely estimated in the modelling script, as was done in Chapter 4 [36].

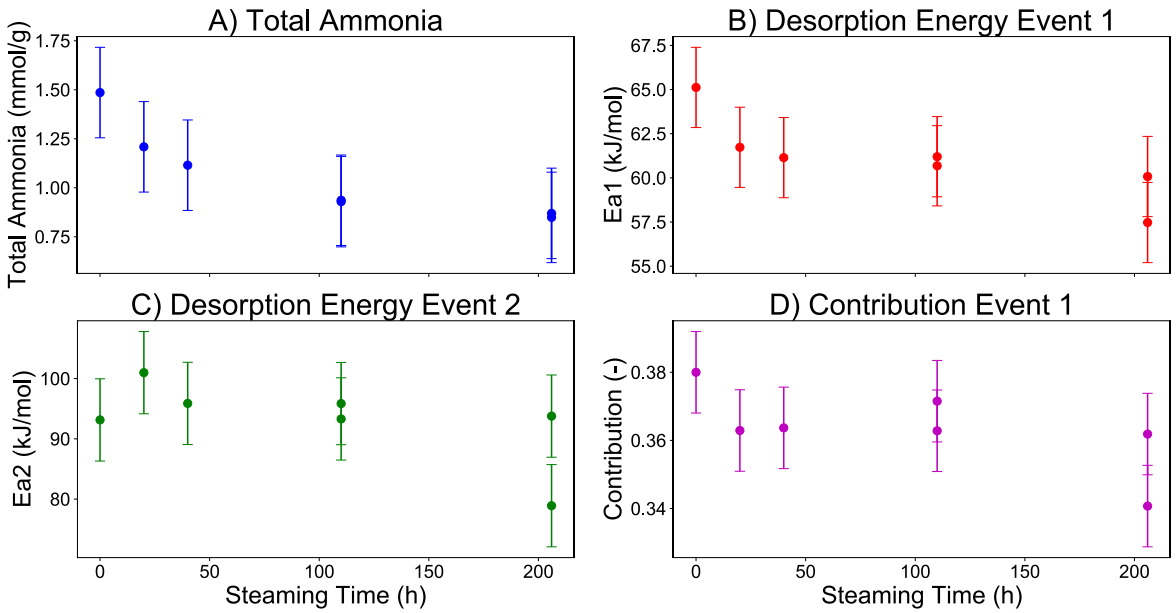

Figure 6.4: Comparison of estimated parameters values, aged SAPO-34.

The error bars shown on Figure 6.4 are based on a single standard deviation for the dataset. For each of the parameters shown in Figure 6.4, linear and non-linear regressions were performed. Using Akaike information criteria the fits were compared. For the total amount of ammonia an exponential function best described the system; whilst for the desorption energies and contribution, a linear function provided the best fit. Standardised residuals were analysed, and no outliers were identified.

It was established, through P values of 0.008 and 0.021 respectively, that the total amount of ammonia and the desorption energy for the first event, change significantly with steaming time. The total amount of ammonia reduces by 0.0031 mmol g^{-1} h^{-1} and the desorption energy for the first event by 0.037 kJ mol^{-1} h^{-1}. However, the desorption energy for the second event and the contribution of the first event to the overall curve do not change significantly with steaming time, this is reflected in P values of 0.126 and 0.112 respectively.

This work has found that the difference in ammonia TPD curves with steaming time is related to the amount of ammonia desorbed from the surface. This amount of desorbed ammonia decreases with ageing time, showing that the hydrothermal ageing reduces the number of acid sites.

The desorption energy estimated for the second thermal event, which relates to the high binding energy sites in the zeotype, in the fresh sample was comparable with that of the isolated Si species in Suzuki et al. [19]. However, this desorption energy (Ed_2) does not significantly change with steaming time, hence no increase is observed as would be expected in line with formation of Si island species. Although these Si islands have been shown to exist in these samples [16], the related change in energetics cannot be determined through ammonia TPD.

This comparison of parameter estimates to the binding energy values obtained thorough DFT modelling [19] allows the assumption that the system is kinetically limited to be scrutinised. As the parameter estimate values in this Sestak-Berggren work are similar to those from DFT, this implies the system is closer to fully 'irreversible'/kinetically limited, than equilibrium limited. Hence the assumption the system is kinetically limited is reasonable, and this analysis method is valid.

The ratio of low to high binding energy sites, reflected in the contribution term (Fv_1), does not change significantly. This implies that the reduction in the number of acid sites affects both the weak and strong sites at a comparable rate.

This case study has demonstrated the use of the modified Sestak-Berggren modelling methodology for ammonia TPD data. This could allow the extraction of kinetic parameters and information about ageing mechanism, as was shown with the

hydrothermal ageing study. This technique, although it may simplify the physical chemical processes, could give similar insight to the more expensive spectroscopic techniques, and should be considered as an alternative characterisation method. The Sestak-Berggren model provides a single, 'off-the-shelf' method, which does not require the specification of a kinetic. In an industrial setting this is advantageous over a micro-kinetic model approach which may require the inclusion of complex steps by an experienced practitioner.

6.5. Conclusions

The modified Sestak-Berggren model has been used to determine the source of the activity loss associated with the hydrothermal ageing of SAPO-34 samples. It was concluded that this activity loss is due to a decrease in the number of acid sites, rather than a significant increase in high binding energy site strength, even as Si species coordination environments change from isolated to Si islands. This is reflected in a decrease in the amount of ammonia desorbed from each sample, and the constant nature of the desorption energy estimated using the modified Sestak-Berggren equation for the high temperature event.

However, for the low binding energy sites, associated with the low temperature peak, there was a small decrease of 0.037 kJ mol^{-1} h^{-1} in the desorption energy. This decrease in acid site strength alone does not account for the reduction in adsorbed ammonia, because the ratio of ammonia adsorbed to low and high binding energy sites remains constant. This implies that an overall reduction in the number of sites must also be occurring.

This study has showed that the irreversible, kinetically limited Sestak-Berggren equation can give useful insight into the desorption of ammonia. This modelling technique coupled with the fast and cheap ammonia TPD experiments creates an improved characterisation technique for the comparison of catalyst formulations within industry.

6.6. References

[1] J. Goetze *et al.*, 'Insights into the Activity and Deactivation of the Methanol-to-Olefins Process over Different Small-Pore Zeolites As Studied with Operando UV-vis Spectroscopy.', *ACS Catal*, vol. 7, no. 6, pp. 4033–4046, May 2017, doi: 10.1021/acscatal.6b03677.

[2] D. Chen, K. Moljord, T. Fuglerud, and A. Holmen, 'The effect of crystal size of SAPO-34 on the selectivity and deactivation of the MTO reaction', *Microporous and Mesoporous Materials*, vol. 29, no. 1, pp. 191–203, Jun. 1999, doi: 10.1016/S1387-1811(98)00331-X.

[3] P. Tian, Y. Wei, M. Ye, and Z. Liu, 'Methanol to Olefins (MTO): From Fundamentals to Commercialization', *ACS Catal.*, vol. 5, no. 3, pp. 1922–1938, Mar. 2015, doi: 10.1021/acscatal.5b00007.

[4] J. Zhou *et al.*, 'Partial Regeneration of the Spent SAPO-34 Catalyst in the Methanol-to-Olefins Process via Steam Gasification', *Ind. Eng. Chem. Res.*, vol. 57, no. 51, pp. 17338–17347, Dec. 2018, doi: 10.1021/acs.iecr.8b04181.

[5] J. F. Haw, W. Song, D. M. Marcus, and J. B. Nicholas, 'The mechanism of methanol to hydrocarbon catalysis', *Accounts of Chemical Research*, vol. 36, no. 5, pp. 317–326, 2003, doi: 10.1021/ar020006o.

[6] U. Olsbye *et al.*, 'Conversion of Methanol to Hydrocarbons: How Zeolite Cavity and Pore Size Controls Product Selectivity', *Angewandte Chemie International Edition*, vol. 51, no. 24, pp. 5810–5831, 2012, doi: 10.1002/anie.201103657.

[7] J. W. Park, J. Y. Lee, K. S. Kim, S. B. Hong, and G. Seo, ‘Effects of cage shape and size of 8-membered ring molecular sieves on their deactivation in methanol-to-olefin (MTO) reactions’, *Applied Catalysis A: General*, vol. 339, no. 1, pp. 36–44, Apr. 2008, doi: 10.1016/j.apcata.2008.01.005.

[8] B. P. C. Hereijgers *et al.*, ‘Product shape selectivity dominates the Methanol-to-Olefins (MTO) reaction over H-SAPO-34 catalysts’, *Journal of Catalysis*, vol. 264, no. 1, pp. 77–87, May 2009, doi: 10.1016/j.jcat.2009.03.009.

[9] E. Epelde, M. Ibañez, A. T. Aguayo, A. G. Gayubo, J. Bilbao, and P. Castaño, ‘Differences among the deactivation pathway of HZSM-5 zeolite and SAPO-34 in the transformation of ethylene or 1-butene to propylene’, *Microporous and Mesoporous Materials*, vol. 195, pp. 284–293, Sep. 2014, doi: 10.1016/j.micromeso.2014.04.040.

[10] W. Dai, G. Wu, L. Li, N. Guan, and M. Hunger, ‘Mechanisms of the Deactivation of SAPO-34 Materials with Different Crystal Sizes Applied as MTO Catalysts’, *ACS Catal.*, vol. 3, no. 4, pp. 588–596, Apr. 2013, doi: 10.1021/cs400007v.

[11] B. Vora, J. Q. Chen, A. Bozzano, B. Glover, and P. Barger, ‘Various routes to methane utilization—SAPO-34 catalysis offers the best option’, *Catalysis Today*, vol. 141, no. 1, pp. 77–83, Mar. 2009, doi: 10.1016/j.cattod.2008.05.038.

[12] P. T. Barger and D. A. Lesch, ‘Hydrothermal stability of SAPO-34 in the methanol-to-olefins process’, *Arabian Journal for Science and Engineering*, vol. 21, no. 2, pp. 263–272, 1996.

[13] H. Changqin, L. Zhongmin, H. Xingyun, Y. Lixin, Y. Yue, and C. Guangyu, ‘Investigation on the stability of silicoaluminophosphate SAPO-34’, *Chinese Journal of Chemical Physics*, vol. 2, 1997.

[14] O. Ying, L. Yibin, and S. Xingtian, ‘Study on the deactivation of SAPO-34 under hydrothermal condition’, *Petroleum Processing and Petrochemicals*, vol. 04, 2009.

[15] B. Arstad *et al.*, ‘Structural changes in SAPO-34 due to hydrothermal treatment. A NMR, XRD, and DRIFTS study’, *Microporous and Mesoporous Materials*, vol. 225, pp. 421–431, May 2016, doi: 10.1016/j.micromeso.2016.01.024.

[16] I. Minova *et al.*, ‘Silicon Redistribution, Acid Site Loss and the Formation of a Core-Shell Texture upon Steaming SAPO-34 and their Impact on Catalytic Performance in the MTO Reaction’, *Journal of Catalysis*, vol. 395, pp. 425-444, March 2021, doi: 10.1016/j.jcat.2021.01.012.

[17] D. Barthomeuf, ‘Topological model for the compared acidity of SAPOs and SiAl zeolites’, *Zeolites*, vol. 14, no. 6, pp. 394–401, Jul. 1994, doi: 10.1016/0144-2449(94)90164-3.

[18] G. Sastre, D. W. Lewis, and C. R. A. Catlow, ‘Modeling of Silicon Substitution in SAPO-5 and SAPO-34 Molecular Sieves’, *J. Phys. Chem. B*, vol. 101, no. 27, pp. 5249–5262, Jul. 1997, doi: 10.1021/jp963736k.

[19] K. Suzuki, T. Nishio, N. Katada, G. Sastre, and M. Niwa, ‘Ammonia IRMS-TPD measurements on Brønsted acidity of proton-formed SAPO-34’, *Phys. Chem. Chem. Phys.*, vol. 13, no. 8, pp. 3311–3318, Feb. 2011, doi: 10.1039/C0CP00961J.

[20] W. E. Farneth and R. J. Gorte, ‘Methods for Characterizing Zeolite Acidity’, *Chemical Reviews*, vol. 95, no. 3, pp. 615–635, May 1995, doi: 10.1021/cr00035a007.

[21] K. Chao, B.-H. Chiou, C.-C. Cho, and S.-Y. Jeng, ‘Temperature-programmed desorption studies on ZSM—5 zeolites’, *Zeolites*, vol. 4, no. 1, pp. 2–4, Jan. 1984, doi: 10.1016/0144-2449(84)90063-0.

[22] D. J. Parrillo, C. Lee, and R. J. Gorte, ‘Heats of adsorption for ammonia and pyridine in H-ZSM-5: evidence for identical Brprnsted-acid sites’, p. 8, 1994.

[23] L. Rodríguez-González, F. Hermes, M. Bertmer, E. Rodríguez-Castellón, A. Jiménez-López, and U. Simon, ‘The acid properties of H-ZSM-5 as studied by NH3-TPD and 27Al-MAS-NMR spectroscopy’, *Applied Catalysis A: General*, vol. 328, no. 2, pp. 174–182, Sep. 2007, doi: 10.1016/j.apcata.2007.06.003.

[24] R. Barthos, F. Lónyi, Gy. Onyestyák, and J. Valyon, ‘An IR, FR, and TPD Study on the Acidity of H-ZSM-5, Sulfated Zirconia, and Sulfated Zirconia−Titania Using Ammonia as the Probe Molecule’, *J. Phys. Chem. B*, vol. 104, no. 31, pp. 7311–7319, Aug. 2000, doi: 10.1021/jp000937m.

[25] C. Costa, J. M. Lopes, F. Lemos, and F. R. Ribeiro, ‘Activity–acidity relationship in zeolite Y Part 2. Determination of the acid strength distribution by temperature programmed desorption of ammonia’, p. 11, 1999.

[26] E. Dima and L. V. C. Rees, ‘Temperature-programmed desorption of ammonia from Na- and H-Y zeolites: Desorption energies derived from analyses of t.p.d. profiles by two new methods’, *Zeolites*, vol. 10, no. 1, pp. 8–15, Jan. 1990, doi: 10.1016/0144-2449(90)90087-8.

[27] T. Masuda, Y. Fujikata, H. Ikeda, S. Matsushita, and K. Hashimoto, ‘A method for calculating the activation energy distribution for desorption of ammonia using a TPD spectrum obtained under desorption control conditions’, *Applied Catalysis A: General*, vol. 162, no. 1–2, pp. 29–40, Nov. 1997, doi: 10.1016/S0926-860X(97)00080-X.

[28] F. Arena, R. D. Chio, and G. Trunfio, ‘An experimental assessment of the ammonia temperature programmed desorption method for probing the surface acidic properties of heterogeneous catalysts’, *Applied Catalysis A: General*, vol. 503, pp. 227–236, Aug. 2015, doi: 10.1016/j.apcata.2015.05.035.

[29] H. G. Karge, V. Dondur, and J. Weitkamp, ‘Investigation of the distribution of acidity strength in zeolites by temperature-programmed desorption of probe molecules. 2. Dealuminated Y-type zeolites’, p. 6.

[30] S. Sharma, B. Meyers, D. Chen, J. Miller, and J. Dumesic, ‘Characterization of catalyst acidity by microcalorimetry and temperature-programmed desorption’, *Applied Catalysis A: General*, vol. 102, no. 2, pp. 253–265, Aug. 1993, doi: 10.1016/0926-860X(93)80232-F.

[31] N. Katada, H. Igi, and J.-H. Kim, ‘Determination of the Acidic Properties of Zeolite by Theoretical Analysis of Temperature-Programmed Desorption of Ammonia Based on Adsorption Equilibrium’, *The Journal of Physical Chemistry B*, vol. 101, no. 31, pp. 5969–5977, Jul. 1997, doi: 10.1021/jp9639152.

[32] N. Katada, T. Tsubaki, and M. Niwa, ‘Measurements of number and strength distribution of Brønsted and Lewis acid sites on sulfated zirconia by ammonia IRMS–TPD method’, *Applied Catalysis A: General*, vol. 340, no. 1, pp. 76–86, May 2008, doi: 10.1016/j.apcata.2008.01.033.

[33] M. Niwa and N. Katada, ‘New Method for the Temperature- Programmed Desorption (TPD) of Ammonia Experiment for Characterization of Zeolite Acidity: A Review: TPD of Ammonia for Characterization of Zeolite Acidity’, *The Chemical Record*, vol. 13, no. 5, pp. 432–455, Oct. 2013, doi: 10.1002/tcr.201300009.

[34] M. Niwa, K. Suzuki, N. Katada, T. Kanougi, and T. Atoguchi, ‘Ammonia IRMS-TPD Study on the Distribution of Acid Sites in Mordenite’, *J. Phys. Chem. B*, vol. 109, no. 40, pp. 18749–18757, Oct. 2005, doi: 10.1021/jp051304g.

[35] M. Niwa, N. Katada, M. Sawa, and Y. Murakami, ‘Temperature-Programmed Desorption of Ammonia with Readsorption Based on the Derived Theoretical Equation’, *The Journal of Physical Chemistry*, vol. 99, no. 21, pp. 8812–8816, May 1995, doi: 10.1021/j100021a056.

[36] R. L. Gibson, M. J. H. Simmons, E. Hugh Stitt, J. West, S. K. Wilkinson, and R. W. Gallen, ‘Kinetic modelling of thermal processes using a modified Sestak-Berggren equation’, *Chemical Engineering Journal*, vol. 408, 2021, doi: 10.1016/j.cej.2020.127318.

[37] J. Sestak and G. Berggren, ‘Study of the kinetics of the mechanism of solid-state reactions at increasing temperatures’, *Thermochimica Acta*, vol. 3, pp. 1–12, 1971.

[38] W. E. Stewart and M. Caracotsios, *Computer-aided modeling of reactive systems*. Hoboken, N.J: Wiley-Interscience : AIChE, 2008.

[39] A. Khawam and D. R. Flanagan, ‘Solid-State Kinetic Models: Basics and Mathematical Fundamentals’, *The Journal of Physical Chemistry B*, vol. 110, no. 35, pp. 17315–17328, Sep. 2006, doi: 10.1021/jp062746a.

[40] J. Denayer *et al.*, ‘Cage and Window Effects in the Adsorption of n-Alkanes on Chabazite and SAPO-34’, *Journal of Physical Chemistry C - J PHYS CHEM C*, vol. 112, Sep. 2008, doi: 10.1021/jp804349v.

[41] O. Yakubovich, W. Massa, P. Gavrilenko, and I. Pekov, ‘Crystal structure of chabazite K’, *Crystallography Reports*, vol. 50, pp. 544–553, Jul. 2005, doi: 10.1134/1.1996728.

[42] R. L. Gibson, M. J. H. Simmons, E. H. Stitt, L. Horsburgh, and R. W. Gallen, ‘Selection of Formal Baseline Correction Methods in Thermal Analysis’, *Chem. Eng. Technol*., 2021, doi: 10.1002/ceat.202100120

7. Non-kinetic phenomena in thermal analysis data: Experimental and kinetic modelling case studies[4]

Summary

Three experimental thermal analysis case studies are presented which are each modelled using the modified Sestak-Berggren equation. For the first case, an example of ammonia TPD on H-ZSM-5, an unlikely kinetic mechanism was estimated for each thermal event and the predicted acid site strength was considerably lower than reported in literature, implying the influence of mass transport. The second case, a thermal decomposition of a zinc nitrate catalyst precursor, studied using thermogravimetric analysis coupled with mass spectrometry (TGA-MS) resulted in the estimation of a high order (~7th order) kinetic mechanism for the high temperature event, which is not feasible. These high order mechanisms indicate non-kinetic phenomena occurring within the thermal analysis reactor. In the final case study, design of experiments was used to investigate the impact of weight hourly space velocity on the decomposition of calcium carbonate studied with TGA. It was found that the Sestak-Berggren could not estimate parameters when a dataset with varying space velocity was used. Using this modified Sestak-Berggren methodology, anomalous results have highlighted possible transport limitations occurring within thermal analysis reactors, which require more investigation.

---

[4] The zinc nitrate decomposition case study within this chapter has been published:R. L. Gibson, M. J. H. Simmons, E. H. Stitt, L. Liu, and R. W. Gallen, 'Non-kinetic phenomena in thermal analysis data; Computational fluid dynamics reactor studies', *Chem. Eng. J.*, vol. 426, p. 130774, Dec. 2021, doi: 10.1016/j.cej.2021.130774.

7.1. Introduction

Materials characterisation is key in catalyst development, and thermal analysis plays an important role in this suite of techniques. Chapter 4 [1] has established a modelling methodology to extract process insight from experimental temperature programmed reduction (TPR) data. The modified Sestak-Berggren methodology can be used to extract a kinetic mechanism for overlapped thermal events without the need for peak deconvolution *a priori* [1]. Due to the similarities in the experimentation, it is proposed that this method could also be used for thermal analysis experiments which are traditionally associated with materials characterisation, such as ammonia temperature programmed desorption (TPD) or thermogravimetric analysis.

Chapter 6 has highlighted the novel use of the modified Sestak-Berggren equation as a shorthand method to extract information from ammonia TPD. Although the use of the Sestak-Berggren equation is new for ammonia TPD, its use for extracting kinetic parameters from thermogravimetric analysis (TGA) data has been widely accepted within literature [2]– [5]. This technique is widely used to compare materials in development [6] and can also provide information useful for scale-up of thermal processes, such as calcination temperatures [7]– [9]. Along with weight monitoring, some TGA units are coupled with mass spectrometry to analyse the composition of gaseous products [10]. The modelling of reaction progress with this evolved gas analysis (EGA) technique has not been well studied in the literature and is one focus of this work.

This work aims to build upon the study of discussed in Chapters 4-6 [1], through three experimental case studies which use the modified Sestak-Berggren equation to extract

a statistically adequate kinetic triplet, with physically plausible parameters. The case studies include one example of ammonia TPD and two cases of thermal decomposition. This work will highlight some anomalies encountered when applying kinetic models to thermal analysis data.

7.2. Modelling methods

The kinetic modelling used in this work applies the method of the modified Sestak-Berggren equation (Equation 7.1, a duplicate of Equation 4.1) described in detail in Chapter 4 [1]. This methodology does not require *a priori* peak deconvolution. Non-linear regression has been used in Athena Visual Studio with default tolerances [1], with the aim of minimising the squares of the residuals between observation and model prediction, where the model prediction $\frac{d\alpha}{dt}$ is given by

$$\frac{d\alpha}{dt} = \sum_{i=1}^{n_{events}} F_{v,i} \cdot A_i \cdot \exp\left(\frac{Ea_i}{R.T_{b,i}}\left(1 - \frac{T_{b,i}}{T}\right)\right) \cdot (1-\alpha_i)^{n_i} \alpha_i^{m_i}, \qquad \text{Eq. (7.1)}$$

$$\text{Dimensionless observed signal} = \frac{\text{Observed Signal}|_t}{\int_{t_{start}}^{t_{end}} (\text{Observed Signal})\, dt} \qquad \text{Eq. (7.2)}$$

$$\text{Residual} = \text{Dimensionless observed signal} - \text{Model Prediction} \qquad \text{Eq. (7.3)}$$

This equation is used to identify the most likely kinetic mechanism for each thermal event, through the values of the estimated *n* and *m* parameters and comparison to tabulated values [11]. Once selected, the kinetic mechanism is used to model the system and extract a statistically adequate kinetic triplet.

7.3. Experimental

7.3.1. Materials

ZSM-5 is a medium pore MFI framework zeolite which has intersecting channels of 10-member rings with diameter ca. 5.5 Å [12]. This aluminosilicate is used in numerous applications such as a catalyst to improve propylene yield in fluid catalytic cracking (FCC) [13], xylene isomerization [14], and dewaxing [15]. The ZSM-5 sample was obtained from Zeolyst International (product CBV3024E).

The $Zn(NO_3)_2$/ Al_2O_3 catalyst precursor has been selected to represent catalysts prepared using incipient wetness impregnation. This precursor has a notional zinc loading of 10 %. Alumina (Sasol SCCA 100/100, 18.01 g) was combined with a solution of zinc nitrate hexahydrate (Alfa Aesar, 9.11 g) in water (6.0 mL). A Speedmixer (at 2000 rpm for 30 seconds) was used to combine these components. The material was dried in air at 378 K for 35 minutes.

High purity (99.0 %) calcium carbonate was obtained from Alfa Aesar with a batch number of I0BR021. Calcium carbonate is a well-studied mineral and is used in a variety of industries including the metallurgical industry, refractories and ceramics [16]. In its decomposed form CaO, it can also be used for carbon capture.

7.3.2. Ammonia TPD

Samples of ~0.25 g (particle size d(50) of approximately 3 μm) were tested in a Micromeritics AutoChem 2920 unit. This experimental setup uses a quartz U-tube fixed bed reactor, with a thermocouple positioned just inside the sample bed, which is supported by quartz wool.

Pretreatment of samples was carried out in-situ at 923 K. The sample was cooled to 373 K in a flow of He, at 373 K the gas was switched to 0.5% NH_3 in He for 50 minutes. This ensures the sample is saturated with ammonia. To remove excess ammonia, a flow of 0.22 mol s^{-1} He at 373 K was applied for 30 mins prior to the start of the temperature ramp. Five temperature ramp rates experiments (2, 4, 6, 8 and 10 K min^{-1}) were performed on the same sample, in a randomised order. A repeat of the initial temperature ramp rate confirmed no structural changes have occurred in the sample due to the experimental procedure.

7.3.3. TGA-MS

Zinc nitrate samples of 20.9 ± 0.5 mg were tested in a Netzsch *Jupiter* ™ STA 449 F3 TGA/DSC unit. This unit is coupled with a Netzsch *Aëolos* ™ QMS 403 D quadrupolar mass spectrometer, allowing both a weight loss profile and gas evolution profiles to be measured for each experiment. Signals for m/z 18 and m/z 30 have been considered as these represent water and nitric oxide respectively, which are the species of interest in this study.

Seven temperature ramp rate experiments were carried out for each sample: 8, 10, 12, 14, 16, 18, 20 K min^{-1}, between 313 K and 1273 K. These were carried out in a random order. A flow rate of 20 mL min^{-1} of air (under standard conditions) was used for each experiment. The temperature ramp rates and gas flow rates were selected to reduce the noise to signal ratio on the mass spectrometry data.

7.3.4. TGA

The decomposition of calcium carbonate was tested using a TA instruments Q500 TGA unit. The temperature ramp rates were carried out between 313 K and 1273 K. The

carrier gas used was air. The sample mass, carrier gas flow rate and temperature ramp rates were varied according to a 3-factor, 2-level design of experiments (DoE) approach, shown in Table 7.1. Two mid-point experiments were used to check for repeatability and two additional experiments were added to capture trends in weight hourly space velocity (WHSV). The experiments in Table 7.1 were carried out in a random order.

Table 7.1: Three factor, two level design of experiments for calcium carbonate decomposition.

Arrangement	Heating rate (K min^{-1})	Flow rate (mL min^{-1})	Mass (g)
HHH	30.0	240	0.030
LLL	1.0	10	0.002
MMM	15.5	125	0.016
MMM	15.5	125	0.016
LHL	1.0	240	0.002
LHH	1.0	240	0.030
HLH	30.0	10	0.030
HHL	30.0	240	0.002
LLH	1.0	10	0.030
HLL	30.0	10	0.002
EEE1	30.0	160	0.002
EEE2	30.0	160	0.004

7.4. Results and discussion

7.4.1. H-ZSM-5 ammonia TPD

7.4.1.1. Raw results

The raw experimental results for the ammonia TPD of H-ZSM-5 are shown in Figure 7.1.

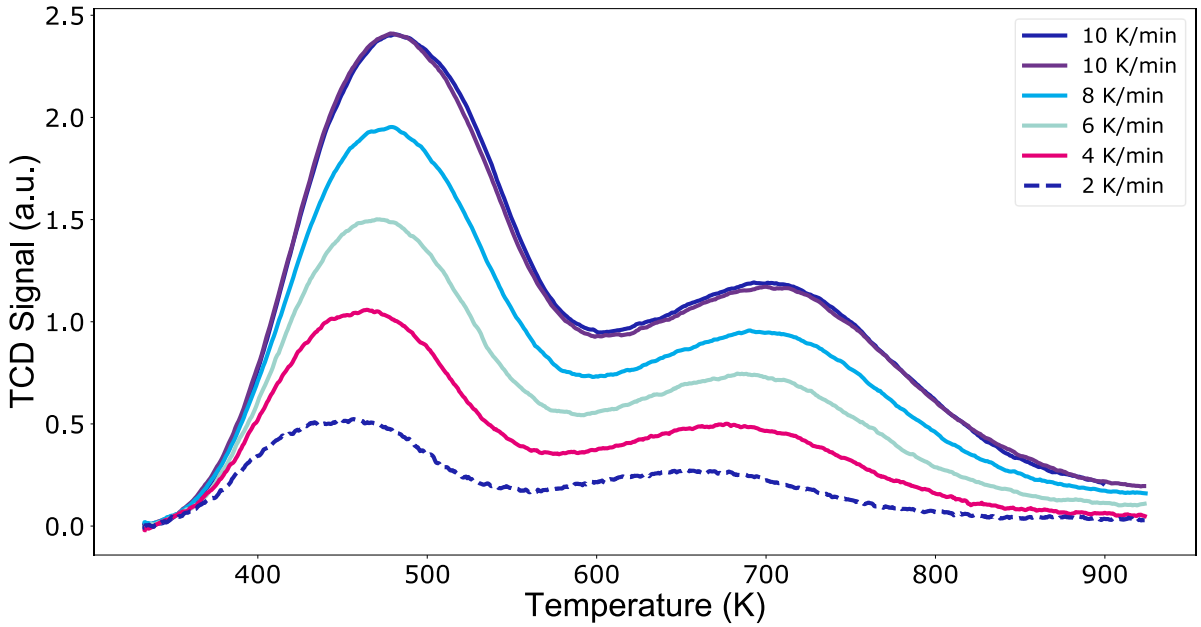

Figure 7.1: Raw experimental results, ammonia TPD on H-ZSM-5, five temperature ramp rate experiments.

The white noise in this dataset was estimated using a moving average model to be ~1.2 %, hence five temperature ramp rates are sufficient for analysis.

The repeat experimental run of 10 K min^{-1}, shows good agreement with the initial experiment, therefore it was concluded that no changes were made to the zeolite structure during the testing.

7.4.1.2. Event identification

Both two and three event models were considered to describe this system. The two event system was based on events occurring a T_b = 500 K and 650 K, with an additional event added at T_b = 750 K for the three peak system. The Akaike weights for each model are shown in Table 7.2.

Table 7.2: Event identification, modified Sestak-Berggren modelling of ammonia TPD of H-ZSM-5.

Quality of fit metric	2 events	3 events
Number of parameters	9	14
R^2	0.967	0.961
RSS	1.18×10^{-2}	1.31×10^{-2}
AICc	-4.22×10^{4}	-4.18×10^{4}
Akaike weight	1.00	0.00

With an Akaike weight of 1.00, the two event system is considered the most likely to best describe the system, hence the following parameter estimation is based on this two event model.

Table 7.3: Parameter estimation results, modified Sestak-Berggren modelling of ammonia TPD of H-ZSM-5.

Event	Parameter	Estimate	95% confidence interval
Low temperature event	A_1 (s^{-1})	6.50×10^{9}	7.04×10^{4}
	Ed_1 (kJ mol^{-1})	4.71×10^{1}	2.37×10^{-4}
	n_1 (-)	2.78×10^{0}	4.83×10^{-5}
	m_1 (-)	6.00×10^{-2}	4.83×10^{-5}
	Fv_1 (-)	7.00×10^{-1}	1.33×10^{-3}
High temperature event	A_2 (s^{-1})	4.90×10^{10}	1.82×10^{8}
	Ed_2 (kJ mol^{-1})	8.35×10^{1}	1.25×10^{-1}
	n_2 (-)	2.18×10^{0}	6.53×10^{-3}
	m_2 (-)	2.00×10^{-2}	9.57×10^{-4}
	Fv_2 (-)	3.00×10^{-1}	1.33×10^{-3}

The mechanism for both thermal events occurring in the ammonia TPD from H-ZSM-5 was identified as a 2.5 order kinetic mechanism, which could imply one of two scenarios. The first is that to adsorb onto the zeolite surface the ammonia molecules would form a transition state before interacting with the solid surface. Although this seems unlikely, it is difficult to discount entirely. While previous density functional theory (DFT) studies in the literature have also modelled this system as a single molecule of ammonia adsorbing to the surface, rather than a transition state [17] [18], this appears to be based on assumptions rather than through exploration of a network.

A second scenario could be that 2.5 molecules of ammonia adsorb onto the same acid site on the surface of the zeolite. This would mean that the calculated value for the

number of acid sites in the material based on ammonia TPD data would be 2.5 times the real value. In our case, the value calculated from TPD data was found to be $\approx 1.2 \times 10^{-3}$ mol g^{-1}. As the silicon-to-alumina ratio (SAR) of the material used is known, an estimate for the acidity can be made based on the aluminium content (as the aluminium creates the acid sites in the zeolite). Assuming the absence of extra-framework aluminium, a value of $\approx 1.05 \times 10^{-3}$ mol g^{-1} was calculated. As the estimates from the aluminium content and the TPD data are close to each other (and there is no clear factor of two difference), this implies that a single ammonia molecule adsorbs to a single acid site. Hence this scenario as a justification of a 2.5-order mechanism does not appear plausible.

The mechanism for ammonia desorption from ZSM-5 indicated from the model does not seem plausible based on the literature and technical knowledge of the material and system under investigation. It is reasonable to conclude that other mechanisms or processes not captured by the modified Sestak-Berggren model must be the cause. As an example, this empirical equation does not capture reversibility effects which may be occurring as the desorbed ammonia could re-adsorb onto another (now vacant) acid site. Another possibility could be the presence of transport limitations which are not captured using the modified Sestak-Berggren model, such as external transport limitations or diffusion through the pores of the zeolite.

The adsorption energy strengths estimated for the ammonia TPD from H-ZSM-5 are lower than others expressed in the literature. Despite the differences in the modelling approaches for ammonia TPD systems, for ZSM-5 the literature produce site strengths (for the high temperature peak) with a reasonable consensus, even while neglecting moderate differences in silicon-to-alumina ratio; 145 kJ mol^{-1} [19], 135-145 kJ mol^{-1}

[20], 145 kJ mol^{-1} [21], 90-110 kJ mol^{-1} [22] and 130 kJ mol^{-1} [23]. Microcalorimetry has also been used to reinforce these findings from ammonia TPD [19] [23] [24]. In this work a value of ~88 kJ mol^{-1} has been estimated using mechanistic modelling, this lower than expected value could imply that transport effects may be suppressing the true energy value. This suppression of activation energy implies internal diffusion limitations may be present.

7.4.2 $Zn(NO_3)_2/Al_2O_3$ decomposition

7.4.2.1 Raw results

The raw TGA data are shown in Figure 7.2. Figures 7.3 and 7.4 show the mass spectrometry data with respect to m/z 18 and m/z 30 respectively.

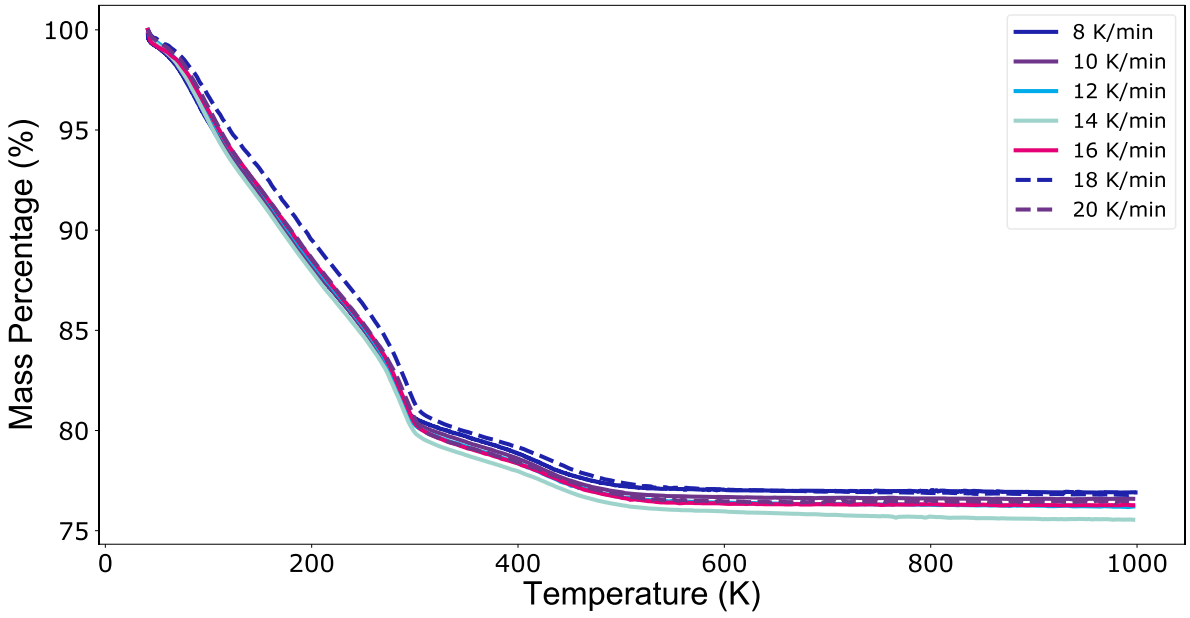

Figure 7.2: Raw experimental results, TGA data, $Zn(NO_3)_2/Al_2O_3$ catalyst, seven temperature ramp rate experiments.

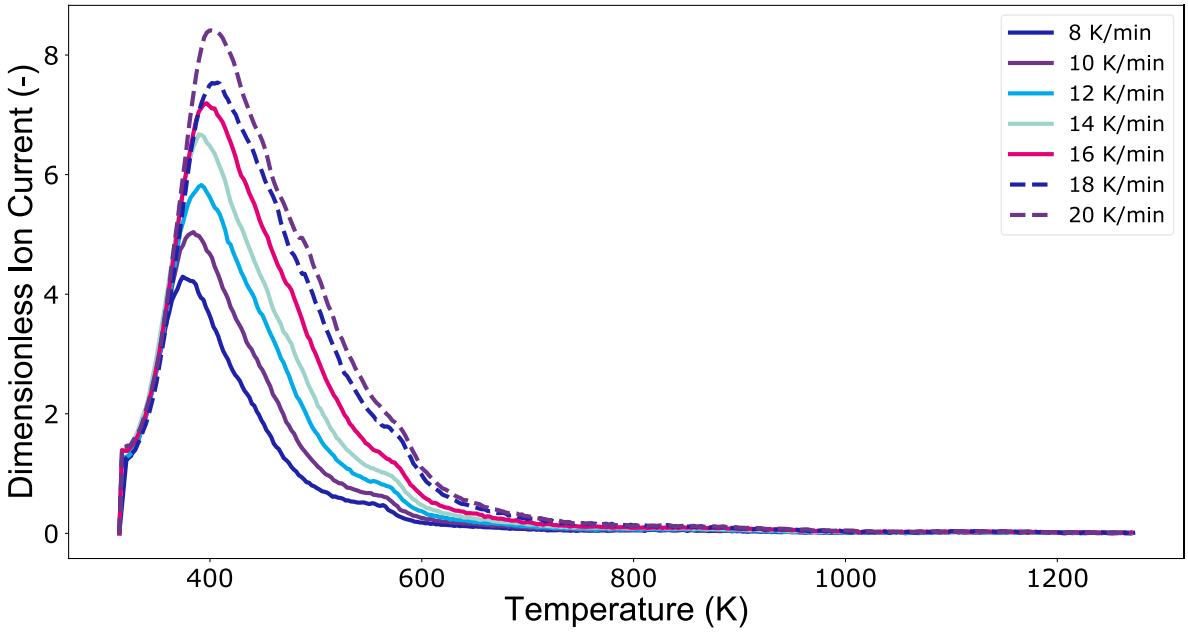

Figure 7.3: Mass spectrometry data for m/z 18, $Zn(NO_3)_2/Al_2O_3$ catalyst seven temperature ramp rate experiments.

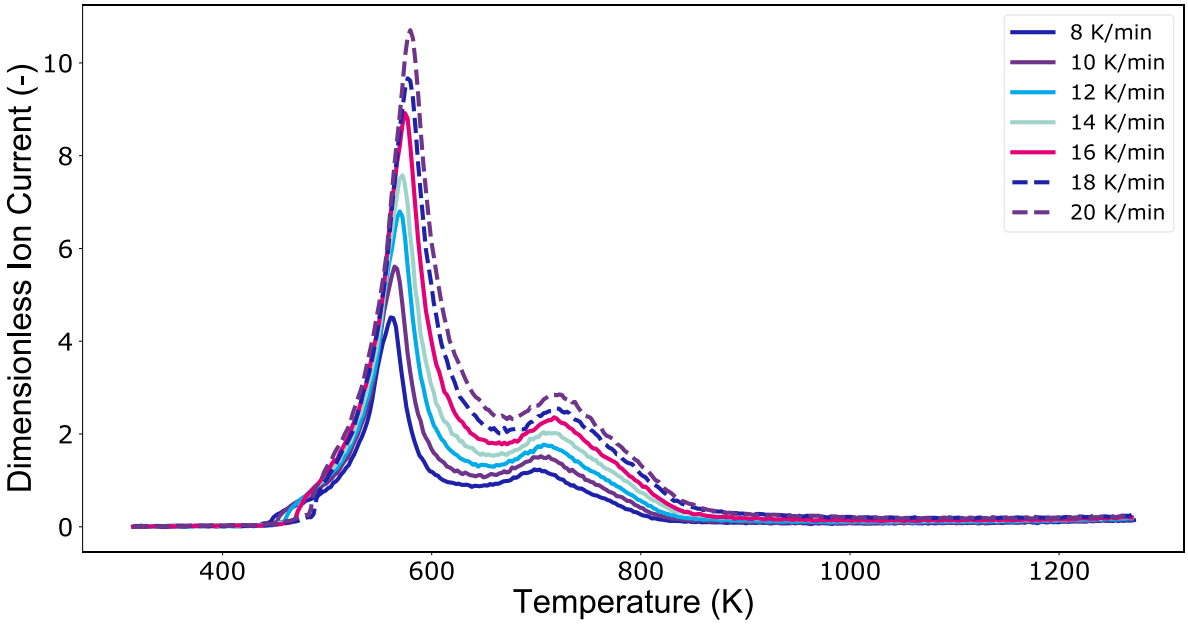

Figure 7.4: Mass spectrometry data for m/z 30, $Zn(NO_3)_2/Al_2O_3$ catalyst, seven temperature ramp rate experiments.

The white noise for these datasets has been estimated using a moving average model. The TGA data has an average white noise value of 1%, whilst the m/z 18 and m/z 30 datasets have 2.2% and 3% average white noise respectively. Hence the seven

temperature ramp rates should be sufficient for mechanism identification for each dataset.

7.4.2.2 Event identification

Three models, with two, three and four thermal events, were considered for the decomposition reaction measured via TGA. The four thermal events model failed to estimate all required parameters, hence was discounted. Table 7.4 shows the quality of fit metrics associated with the two and three event systems. It was concluded based on Akaike weights that the three-event model was most likely.

Table 7.4: Event identification, TGA data modelled using modified Sestak-Berggren equation.

Quality of fit metric	2 events	3 events
Number of parameters	9	14
R^2	0.999	0.999
RSS	3.92×10^{-3}	1.57×10^{-3}
AICc	-3.60×10^{4}	-3.84×10^{4}
Akaike weight	0.00	1.00

For m/z 18, three models were considered: one, two and three thermal events. Using Akaike weights [25], shown in Table 7.5, it was found that the most statistically likely model contained two thermal events.

Table 7.5: Event identification, m/z 18 data modelled using modified Sestak-Berggren equation.

Quality of fit metric	1 event	2 events	3 events
Number of parameters	4	9	14
R^2	0.994	0.995	0.995
RSS	5.32×10^1	4.35×10^1	4.36×10^1
AICc	-9.92×10^3	-1.04×10^4	-1.04×10^4
Akaike weight	0.00	1.00	0.00

For m/z 30, models for two, three and four thermal events were considered. The four event model failed to estimate all the parameters for the modified Sestak-Berggren model, implying there was insufficient information to constrain this number of thermal events, hence this option was discounted. Using Akaike weights, shown in Table 7.6, it was concluded that the most statistically significant model included three thermal events.

Table 7.6: Event identification, m/z 30 data modelled using modified Sestak-Berggren equation.

Quality of fit metric	2 events	3 events
Number of parameters	11	16
R^2	0.982	0.994
RSS	1.08×10^2	2.44×10^1
AICc	-8.58×10^3	-1.26×10^4
Akaike weight	0.00	1.00

The following parameter estimation results are based on a two event system for the m/z 18 data and a three event system for the m/z 30 data.

7.4.2.3 Mechanism identification

The parameter estimates for the modified Sestak-Berggren equation are shown for each of the three datasets in Table 7.7. It should be noted that blank table entries relate to parameters which were not required.

For the TGA and m/z 18 data no baseline correction was required [26], however the m/z 30 data required baseline correction. Using Akaike weights, no baseline, linear with time, linear with temperature and linear with extent of reaction correction methods were considered. It was found that a baseline correction method based on temperature was the most appropriate [26] (Appendix A).

Table 7.7: Parameter estimation results of modified Sestak-Berggren model, TGA, m/z 18 and m/z 30 datasets.

Parameter	TGA dataset		m/z 18 dataset		m/z 30 dataset	
	Estimate	95% confidence interval	Estimate	95% confidence interval	Estimate	95% confidence interval
A_1 (s^{-1})	1.72×10^{15}	2.32×10^{14}	4.21×10^{10}	1.04×10^{7}	1.67×10^{13}	1.37×10^{11}
Ea_1 ($kJmol^{-1}$)	6.79×10^{1}	5.44×10^{1}	4.32×10^{1}	4.52×10^{-3}	8.47×10^{1}	3.61×10^{-1}
n_1 (-)	3.89×10^{1}	5.38×10^{-1}	3.62×10^{0}	1.05×10^{-2}	9.80×10^{-1}	1.45×10^{-2}
m_1 (-)	2.31×10^{-1}	7.73×10^{-2}	-1.00×10^{-2}	6.09×10^{-5}	-2.00×10^{-2}	3.30×10^{-3}
Fv_1 (-)	2.95×10^{-1}	2.59×10^{-2}	9.60×10^{-1}	2.68×10^{-3}	2.20×10^{-1}	2.23×10^{-3}
A_2 (s^{-1})	2.38×10^{24}	3.12×10^{23}	2.19×10^{7}	3.75×10^{3}	1.42×10^{15}	2.63×10^{13}
Ea_2 ($kJmol^{-1}$)	1.87×10^{2}	1.38×10^{1}	3.03×10^{1}	1.05×10^{-3}	1.05×10^{2}	6.89×10^{-1}
n_2 (-)	6.59×10^{-1}	5.66×10^{-2}	2.00×10^{-1}	2.04×10^{-2}	7.75×10^{0}	8.21×10^{-2}
m_2 (-)	-2.29×10^{-1}	1.24×10^{-1}	-3.80×10^{-1}	1.53×10^{-5}	6.60×10^{-1}	3.33×10^{-3}
Fv_2 (-)	1.19×10^{-1}	4.63×10^{-3}			5.90×10^{-1}	4.76×10^{-3}
A_3 (s^{-1})	9.13×10^{12}	8.87×10^{11}			1.39×10^{16}	7.01×10^{14}
Ea_3 ($kJmol^{-1}$)	8.02×10^{1}	2.87×10^{0}			1.56×10^{2}	4.34×10^{0}
n_3 (-)	3.49×10^{0}	9.06×10^{-2}			1.71×10^{0}	6.06×10^{-2}
m_3 (-)	-1.77×10^{0}	1.60×10^{-1}			-3.00×10^{-1}	4.06×10^{-2}
BL Grad					4.00×10^{-2}	9.49×10^{-3}
BL Intercept					2.00×10^{-2}	7.57×10^{-3}

The statistical evaluation of these regressions, in terms of R^2 and mean squared residual are shown in Table 7.8.

Table 7.8: Quality of fit statistics, MS data.

Regression	TGA	m/z 18	m/z 30
R^2	0.99999	0.99488	0.99433
MSE	5.89×10^{-7}	1.70×10^{-2}	9.16×10^{-3}

This good statistical fit implies the mass spectrometry data can be successfully modelled when used to monitor the progress of a thermal analysis experiment.

However, despite this good statistical fit, the *n* and *m* parameters estimated do not clearly indicate a mechanism from literature; the high order indicated (nearly 8th order, shown in red text in Table 7.7) is generally implausible. Therefore, no mechanistic fit was attempted.

As these high order mechanisms are implausible for the system under investigation (and in general) this implies that the kinetic modelling is not capturing all effects within the data.

Figure 7.5 shows the effect of a higher order (value of *n*) on the predicted mass spectrometry curve, including an example of a 7th order reaction mechanism. To produce the curves in Figure 7.5, the modified Sestak-Berggren equation was used, with values of $5.22 \times 10^{+10}\ s^{-1}$ and $35.17\ kJ\ mol^{-1}$ used for the pre-exponential factor and activation energy, respectively. Exponent values of 1, 3 and 7 were used for *n*, whilst the exponent *m* was consistently set to 0.

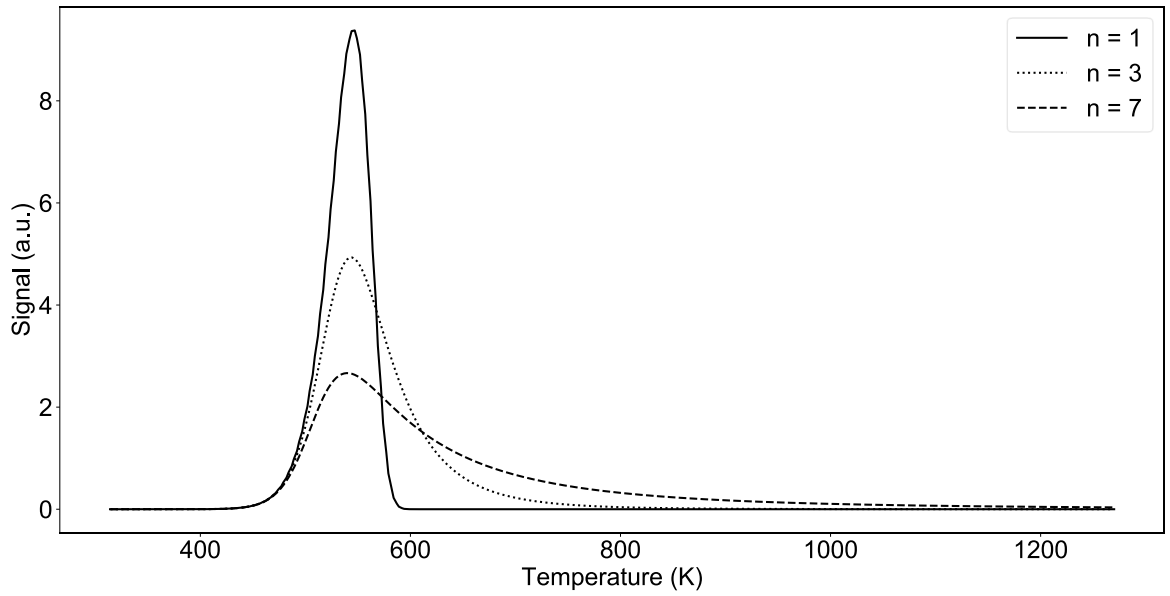

Figure 7.5: Example of high (7th) order kinetically limited curve.

A high *n* value gives the mechanism a ‘long tail’. This could be caused by gas being detected a long time after initial release/ the start of the detected thermal event. This would imply that there are transport issues within the thermal analysis reactor; this requires further investigation.

An alternative explanation for the apparent ‘long tail’ is a distribution of site energetics in the material. Such variation can be captured in two main ways; through the addition of thermal events or the description of an acid site with a range of strength values. The addition of thermal events to capture this material inhomogeneity has been trailed as discussed previously, with Akaike weights used to identify the most statistically likely number of thermal events as discussed in Chapter 4 [1]. To introduce a distribution of site strengths requires significant justification. This adds at least an additional parameter per thermal event (such as standard deviation in the case of Gaussian distribution) to the modified Sestak-Berggren model, which increases the likelihood of overfitting. The selection of the distribution is also problematic, as discussed in Chapter

3, Section 3.4.3. In this case, a three-parameter asymmetric distribution would be required, and as there is no strong evidence for a distribution of site strengths and there is no theoretical basis for such an asymmetric distribution, this approach has been discounted.

7.4.2.4 Analysis of residuals

Figure 7.6 shows the mean residual with temperature ramp rate, for each of the zinc nitrate datasets.

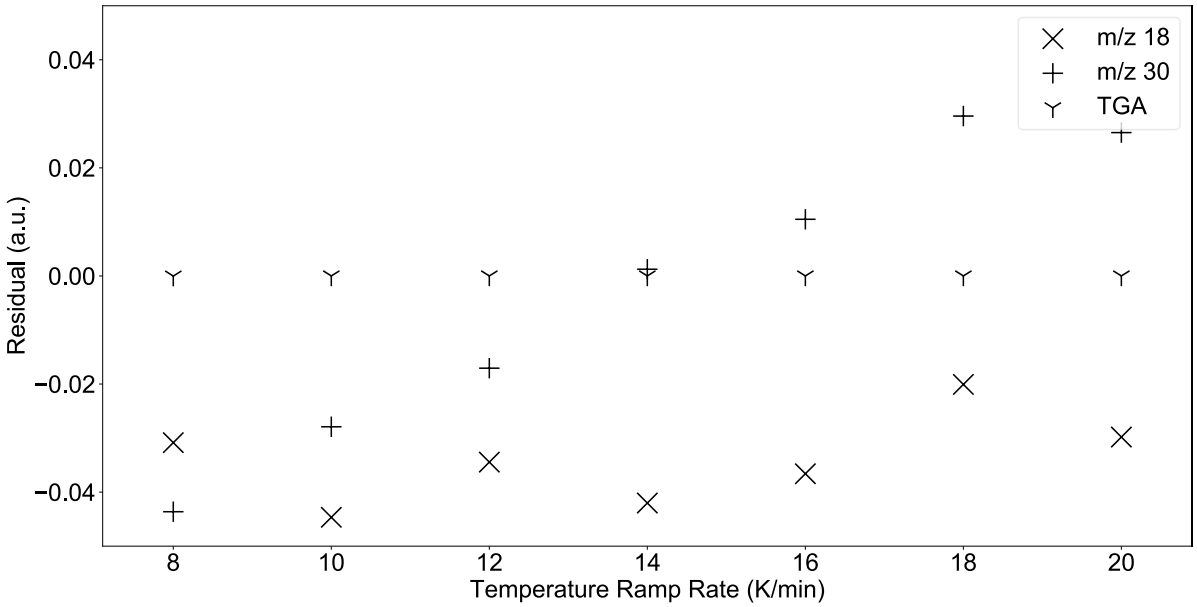

Figure 7.6: Residual trends, TGA, m/z18 and m/z 30 data.

Figure 7.6 shows the very small residuals obtained for the modified Sestak-Berggren model fit for the TGA data. These residuals range ~1.0×10^{-5} and show no significant trend (P value = 0.15).

A P value of 0.28 implies the linear trend between mean residual and temperature ramp rate is not significant for the m/z 18 dataset. The fluctuations observed in Figure 7.6 are most likely due to variations in lab humidity when the experiments were

conducted, but only represents a mean residual range of ~0.025. This lack of residual trend gives confidence in the modified Sestak-Berggren fit for this data.

Figure 7.6 shows a clear trend between mean residual and temperature ramp rate for the m/z 30 dataset, which is reflected in a P value of <0.001. The range for the mean residuals is ~0.07, which is larger than in any other case study discussed in this chapter.

7.4.3 Calcium carbonate decomposition

7.4.3.1 Raw results

The raw results of the full experimental design are captured in Figure 7.7. Good agreement is shown between the mid-point repeats, implying these results are repeatable.

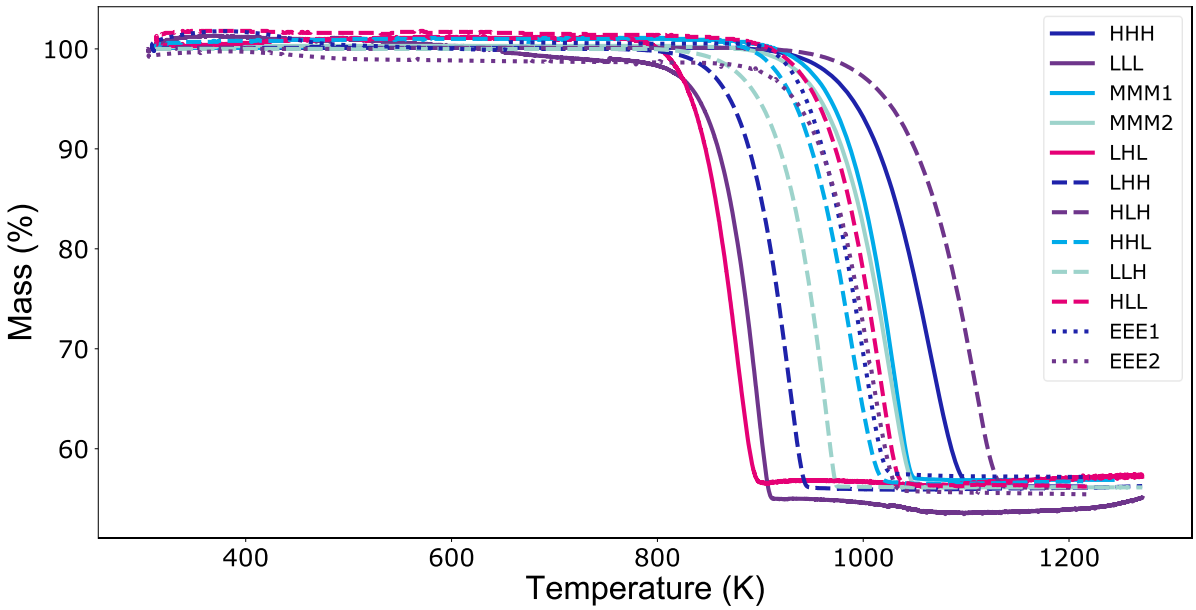

Figure 7.7: Raw TGA results for the full experimental design, decomposition of calcium carbonate.

7.4.3.2 Full DoE

As calcium carbonate is a well-studied material [2], it is known that a single event should be used to describe the decomposition data. The parameter estimation results for the full experimental design, modelled using the modified Sestak-Berggren equation are presented in Table 7.9.

Table 7.9: Parameter estimation results for the modified Sestak-Berggren equation, for full DoE.

Parameter	Estimate	95% confidence interval
A_1 (s^{-1})	1.08×10^{13}	2.42×10^{12}
Ea_1 (kJ mol^{-1})	1.12×10^{2}	9.52×10^{0}
n_1 (-)	Indeterminate	
m_1 (-)	Indeterminate	

Indeterminate parameters indicate the model has failed to capture the data adequately and shows this is the wrong model for these data. As the decomposition of calcium carbonate is reversible, it is possible that the irreversible Sestak-Berggren model does not capture the impact of the reverse reaction.

The model proposed by Lietti et al. [27], which assumes the reaction is adsorption controlled, was rederived for a continuous stirred tank reactor and used to model the full experimental design. Indeterminate parameters were also found in this model; hence it was concluded that adsorption is not the dominating process.

7.4.3.3 Analysis of residuals

Figure 7.8 shows the mean residual with WHSV for the full experimental design when modelled using the modified Sestak-Berggren equation.

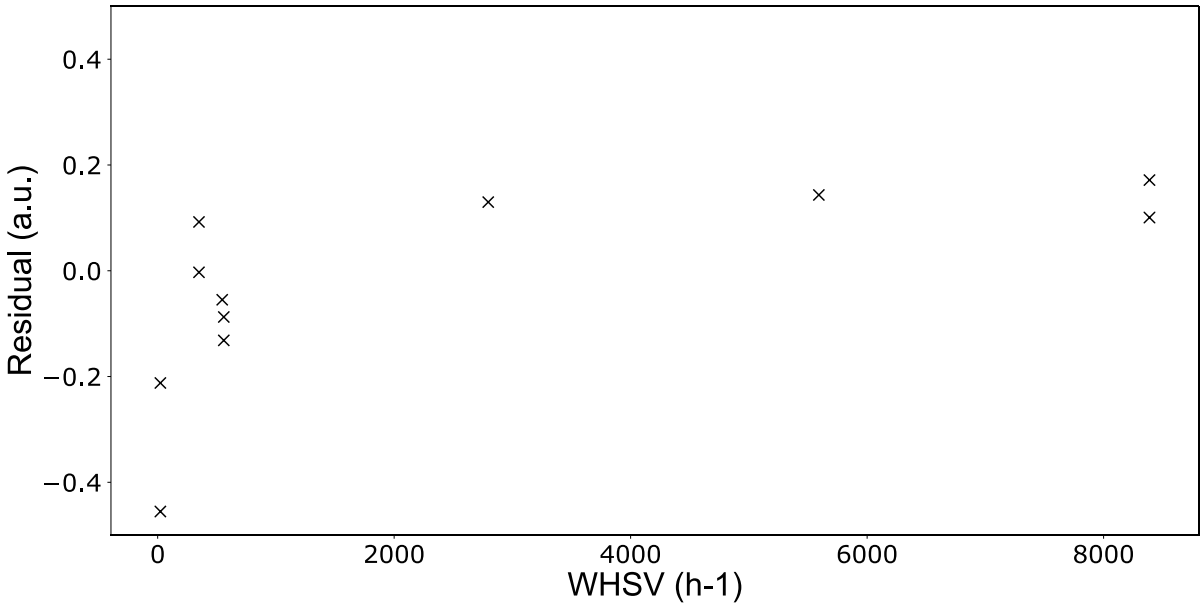

Figure 7.8: Residual trend with space velocity, full DoE.

A clear trend in residuals with WHSV indicates there is a phenomenon occurring which the modified Sestak-Berggren model is not accounting for. Changing WHSV would not impact the experimental results if intrinsic data were collected. As there is a clear impact based on the WHSV chosen, this implies non-kinetic phenomena within the experimental data.

7.4.3.4 Constant WHSV

In the experimental design used for the TGA experiments, it is possible to extract three experiments which are conducted at a constant WHSV of 555 h^{-1}. In these three experiments, only the temperature ramp rate varies, hence this trial mimics a traditional kinetic study. Temperature ramp rates of 1, 15 and 30 K min^{-1} were used. The results of the modified Sestak-Berggren parameter estimation are shown in Table 7.10.

Table 7.10: Parameter estimation results for the modified Sestak-Berggren equation, constant WHSV.

Parameter	Estimate	95% confidence interval
A_1 (s^{-1})	1.11×10^{14}	9.16×10^{12}
Ea_1 (kJ mol^{-1})	1.82×10^{2}	7.70×10^{-1}
n_1 (-)	3.72×10^{-1}	6.51×10^{-2}
m_1 (-)	5.31×10^{-2}	3.45×10^{-2}

In this case, all parameters have been estimated, and the statistical fit of the model is good; with an R^2 value of 0.998 and a MSE of 5.88%. The *n* and *m* parameters estimated indicate a 2-dimensional interface controlled reaction mechanism. Using this mechanism, the pre-exponential factor and activation energy were predicted to be $1.11 \times 10^{14} \pm 9.16 \times 10^{12}$ and 182.15 ± 0.8 kJ mol^{-1} respectively. The estimated activation energy falls within the range found in the literature (102-223 kJ mol^{-1}) [28].

This study at constant WHSV explains the variability of the energies estimated in the literature for kinetic of this reaction. It is possible for the modified Sestak-Berggren to obtain a statistically adequate fit and allow the estimation of a kinetic triplet, providing a constant WHSV is maintained, which is common practice in the literature [2]. The choice of different WHSVs may then explain the large range of apparent activation energies obtained in literature. As the WHSV impacts the results obtained, this implies non-kinetic phenomena within the data.

7.5 Conclusions

Although the modified Sestak-Berggren methodology has been successfully applied to some thermal analysis experiments as discussed in Chapters 4, 5 and 6, in others,

systematic trends in residuals with temperature ramp rates have been observed, and the plausibility of identified mechanisms and magnitudes of parameter estimates questioned. This critique can only be carried out when there is high confidence in the model of choice, as there now is with the modified Sestak-Berggren model. Other possible methods of modelling thermal analysis data, such as isoconversion models (which contain implicit irreversible kinetic models) would mask these effects. This emphasises the importance of model criticism; a high value of R^2 is not sufficient to call a model fit satisfactory.

The unlikely kinetic mechanism and lower than expected adsorption energy value obtained in the H-ZSM5 ammonia TPD case study has implied that there are effects present in the data which the irreversible, kinetically limited modified Sestak-Berggren model cannot capture. It appears that these effects could be associated with reversibility or transport phenomena. This was re-iterated with the zinc nitrate decomposition investigation, where the implausible mechanisms identified appeared influenced by transport phenomena. A design of experiments approach has been used to investigate the impact of WHSV on the decomposition of calcium carbonate. WHSV was shown to have an impact on the predictions of the modified Sestak-Berggren model; when varied WHSV was used, the model poorly described the data, and the Sestak-Berggren exponent parameters were indeterminate. If the data were kinetically limited, changing the WHSV would not impact the results obtained, hence this experimental design has highlighted that transport limitations may be present within these data.

These implausible mechanisms and issues with varying WHSV point not to a flaw in the modelling methodology *per se*, but to the assumptions made about the nature of

the experimental data. The causes of these non-kinetic phenomena will be investigated further in Chapter 8.

7.6 References

[1] R. L. Gibson, M. J. H. Simmons, E. Hugh Stitt, J. West, S. K. Wilkinson, and R. W. Gallen, 'Kinetic modelling of thermal processes using a modified Sestak-Berggren equation', *Chemical Engineering Journal*, vol. 408, 2021, doi: 10.1016/j.cej.2020.127318.

[2] M. E. Brown *et al.*, 'Computational aspects of kinetic analysis Part A: The ICTAC kinetics project-data, methods and results', *Thermochimica Acta*, p. 19, 2000.

[3] A. Burnham, 'Application of the Šesták-Berggren Equation to Organic and Inorganic Materials of Practical Interest', *Journal of Thermal Analysis and Calorimetry*, vol. 60, pp. 895–908, Jun. 2000, doi: 10.1023/A:1010163809501.

[4] A. K. Burnham, 'Computational aspects of kinetic analysis.: Part D: The ICTAC kinetics project — multi-thermal–history model-fitting methods and their relation to isoconversional methods', *Thermochimica Acta*, vol. 355, no. 1, pp. 165–170, Jul. 2000, doi: 10.1016/S0040-6031(00)00446-9.

[5] C. Dickinson and G. Heal, 'A review of the ICTAC kinetics project, 2000 Part 2 Non-isothermal results', *Thermochimica Acta*, vol. 494, pp. 15–25, Oct. 2009, doi: 10.1016/j.tca.2009.05.009.

[6] M. E. Brown, *Introduction to Thermal Analysis: Techniques and Applications*, 2nd ed. Springer Netherlands, 2001. doi: 10.1007/0-306-48404-8.

[7] A. Moropoulou, A. Bakolas, and E. Aggelakopoulou, 'The Effects of Limestone Characteristics and Calcination Temperature on the Reactivity of Quicklime',

Cement and Concrete Research, vol. 31, pp. 633–639, Apr. 2001, doi: 10.1016/S0008-8846(00)00490-7.

[8] N. F. Mohamed Yusof, H. Osman, and R. Rahman, 'Thermogravimetric Analysis of Different Calcination Temperature of Lemon Grass Ash', *Applied Mechanics and Materials*, 2015. https://www.scientific.net/AMM.695.232 (accessed Jan. 12, 2021).

[9] Z. N. Kayani, F. Saleemi, and I. Batool, 'Effect of calcination temperature on the properties of ZnO nanoparticles', *Appl. Phys. A*, vol. 119, no. 2, pp. 713–720, May 2015, doi: 10.1007/s00339-015-9019-1.

[10] W. Xie and W.-P. Pan, 'Thermal Characterization of Materials Using Evolved Gas Analysis', *Journal of Thermal Analysis and Calorimetry*, vol. 65, no. 3, pp. 669–685, Oct. 2004, doi: 10.1023/a:1011946707342.

[11] A. Khawam and D. R. Flanagan, 'Solid-State Kinetic Models: Basics and Mathematical Fundamentals', *The Journal of Physical Chemistry B*, vol. 110, no. 35, pp. 17315–17328, Sep. 2006, doi: 10.1021/jp062746a.

[12] D. H. Olson, G. T. Kokotailo, S. L. Lawton, and W. M. Meier, 'Crystal structure and structure-related properties of ZSM-5', *J. Phys. Chem.*, vol. 85, no. 15, pp. 2238–2243, Jul. 1981, doi: 10.1021/j150615a020.

[13] M. A. den Hollander, M. Wissink, M. Makkee, and J. A. Moulijn, 'Gasoline conversion: reactivity towards cracking with equilibrated FCC and ZSM-5 catalysts', *Applied Catalysis A: General*, vol. 223, no. 1, pp. 85–102, Jan. 2002, doi: 10.1016/S0926-860X(01)00745-1.

[14] D. J. Collins, R. J. Medina, and B. H. Davis, ‘Xylene isomerization by ZSM-5 zeolite catalyst’, *The Canadian Journal of Chemical Engineering*, vol. 61, no. 1, pp. 29–35, 1983, doi: https://doi.org/10.1002/cjce.5450610104.

[15] A. W. Peters, E. Bowes, and T. R. Stein, ‘Catalytic dewaxing of hydrocarbon oils’, US4229282A, Oct. 21, 1980 Accessed: Dec. 11, 2020. [Online]. Available: https://patents.google.com/patent/US4229282A/en

[16] I. Halikia, L. Zoumpoulakis, E. Christodoulou, and D. Prattis, ‘Kinetic study of the thermal decomposition of calcium carbonate by isothermal methods of analysis’, no. 2, p. 14, 2001.

[17] K. Suzuki, Y. Aoyagi, N. Katada, M. Choi, R. Ryoo, and M. Niwa, ‘Acidity and catalytic activity of mesoporous ZSM-5 in comparison with zeolite ZSM-5, Al-MCM-41 and silica–alumina’, *Catalysis Today*, vol. 132, no. 1–4, pp. 38–45, Mar. 2008, doi: 10.1016/j.cattod.2007.12.010.

[18] C. Lo and B. Trout, ‘Density-functional theory characterization of acid sites in chabazite’, *Journal of Catalysis*, vol. 227, no. 1, pp. 77–89, Oct. 2004, doi: 10.1016/j.jcat.2004.06.018.

[19] S. Sharma, B. Meyers, D. Chen, J. Miller, and J. Dumesic, ‘Characterization of catalyst acidity by microcalorimetry and temperature-programmed desorption’, *Applied Catalysis A: General*, vol. 102, no. 2, pp. 253–265, Aug. 1993, doi: 10.1016/0926-860X(93)80232-F.

[20] L. Rodríguez-González, F. Hermes, M. Bertmer, E. Rodríguez-Castellón, A. Jiménez-López, and U. Simon, ‘The acid properties of H-ZSM-5 as studied by NH3-TPD and 27Al-MAS-NMR spectroscopy’, *Applied Catalysis A: General*, vol. 328, no. 2, pp. 174–182, Sep. 2007, doi: 10.1016/j.apcata.2007.06.003.

[21] D. J. Parrillo, C. Lee, and R. J. Gorte, ‘Heats of adsorption for ammonia and pyridine in H-ZSM-5: evidence for identical Brprnsted-acid sites’, p. 8, 1994.

[22] H. G. Karge and V. Dondur, ‘Investigation of the distribution of acidity in zeolites by temperature-programmed desorption of probe molecules. I. Dealuminated mordenites’, p. 8.

[23] M. Niwa, N. Katada, M. Sawa, and Y. Murakami, ‘Temperature-Programmed Desorption of Ammonia with Readsorption Based on the Derived Theoretical Equation’, *The Journal of Physical Chemistry*, vol. 99, no. 21, pp. 8812–8816, May 1995, doi: 10.1021/j100021a056.

[24] W. E. Farneth and R. J. Gorte, ‘Methods for Characterizing Zeolite Acidity’, *Chemical Reviews*, vol. 95, no. 3, pp. 615–635, May 1995, doi: 10.1021/cr00035a007.

[25] K. P. Burnham and D. R. Anderson, ‘Multimodel Inference: Understanding AIC and BIC in Model Selection’, *Sociological Methods & Research*, vol. 33, no. 2, pp. 261–304, Nov. 2004, doi: 10.1177/0049124104268644.

[26] R. L. Gibson, M. J. H. Simmons, E. H. Stitt, L. Horsburgh, and R. W. Gallen, ‘Selection of formal baseline correction methods in thermal analysis’, Chem. Eng. Technol., 2021, doi: 10.1002/ceat.202100120.

[27] L. Lietti, I. Nova, S. Camurri, E. Tronconi, and P. Forzatti, ‘Dynamics of the SCR-DeNOx reaction by the transient-response method’, *AIChE Journal*, vol. 43, no. 10, pp. 2559–2570, Oct. 1997, doi: 10.1002/aic.690431017.

[28] M. Maciejewski, ‘Computational aspects of kinetic analysis. Part B: The ICTAC Kinetics Project - the decomposition kinetics of calcium carbonate revisited, or some tips on survival in the kinetic minefield’, *Thermochimica Acta*, p. 10, 2000.

8. Non-kinetic phenomena in thermal analysis data; Computational fluid dynamics reactor studies[5]

Summary

Computational fluid dynamics (CFD) has been used to develop a characterisation method for the transport phenomena occurring within thermal analysis reactors. This method allows the comparison of different equipment configurations to identify which are most suitable for obtaining intrinsic data. In this work, four equipment configurations are compared from two broad categories: pan-style and tubular reactors. In general, it was concluded that there are both heat and mass transport issues within pan-style and non-uniform diameter tubular reactor configurations and that these should be avoided, if extraction of kinetic parameters is the goal. Uniform diameter tubular reactors are suitable for kinetic experimentation, but checks should be made using the dimensionless analysis discussed in this work.

[5] This chapter has been published, in part: R. L. Gibson, M. J. H. Simmons, E. H. Stitt, L. Liu, and R. W. Gallen, 'Non-kinetic phenomena in thermal analysis data; Computational fluid dynamics reactor studies', *Chem. Eng. J.*, vol. 426, p. 130774, Dec. 2021, doi: 10.1016/j.cej.2021.130774.

8.1. Introduction

Within the thermal analysis literature, experimental conditions are often referred to as factors which can influence the kinetic analysis of reactions. These conditions, sample mass, pressure, gas flow rate or temperature ramp rate [1], [2], all impact the heat and mass transfer occurring within the thermal analysis reactor and sample. Understanding their impact on the internal and external transport phenomena is key to obtaining intrinsic data, hence enabling kinetic analysis.

The terminology of kinetic analysis has a broad interpretation, from complex mathematical modelling which extracts kinetic parameters, to qualitative evaluation such as judging 'by-eye' whether a peak has shifted in temperature. Often thermal analysis results are analysed simply: by looking at peak position/shape, onset temperature and peak temperature. Frequently these are only roughly estimated. Even simple qualitative 'by-eye' kinetic analysis will be flawed if transport limitations are present within the experimental data, thus understanding these phenomena is key for thermal analysis.

Chapter 7 presented three thermal analysis case studies, all modelled using the modified Sestak-Berggren equation, presented in Chapter 4 [3] (shown in Equation 8.1, a duplicate of Equation 4.1).

$$\frac{d\alpha}{dt} = \sum_{i=1}^{n_{events}} F_{v,i} \cdot A_i \cdot \exp\left(\frac{Ea_i}{R.T_{b,i}}\left(1 - \frac{T_{b,i}}{T}\right)\right) \cdot (1-\alpha_i)^{n_i} \alpha_i^{m_i}, \qquad \text{Eq.(8.1)}$$

Whilst confidence in the model has been established with *in silico* and experimental case studies, shown in Chapters 4, 5 and 6 [3], for some datasets residual trends with temperature ramp rate were present and nonsensical kinetic mechanisms were

estimated. These poor fits and anomalous predicted mechanisms imply possible heat and/or mass transport effects were present within the data. Although the Sestak-Berggren method gives some indication that behaviour which is not due to the intrinsic kinetics is present, it cannot currently identify or quantify it. It is worth noting that this is an improvement on isoconversion modelling, where deviations from kinetically limited behaviour may be difficult or impossible to detect, as discussed in Chapter 3.

In this chapter, suspected transport limitations present during thermal analysis experiments and their influence on the experimental data are investigated using Computational Fluid Dynamics (CFD). CFD has been used previously to study transport phenomena within thermogravimetric analysis (TGA) reactors [4] – [7]. Comesaña et al. [5] reported using CFD to improve the lag between FTIR measurements and sample weight loss profiles using a top loaded TG-DSC unit. In the same model TG-DSC unit the indium phase change process was simulated [6]. Good agreement between model predicted and experimentally obtained TG curves was observed, with discrepancies noted between theoretical and observed DSC curves. Buczynski et al. [4] used CFD with coupled kinetics to model the decomposition of coal in a suspended TGA. Heat transfer appeared a focus of this work, and it was concluded that discrepancies between measured sample temperatures and CFD modelled temperatures created errors in activation energy prediction. Benedetti et al. [7] studied the external transport limitations in a horizontal TGA reactor [8] for the decomposition of calcium carbonate, they concluded that the external mass transport issues could have a big effect on the TGA profile obtained for the experiment.

The work presented in this chapter investigates the differences in transport phenomena (both heat and mass transport) between four equipment configurations.

This will include pan-style TGA reactors, and flow-through tubular reactors used for other temperature programmed experimentation. A method to characterise and compare these reactors will be discussed, and recommendations for kinetic experimentation made.

8.2. Modelling methodology

8.2.1. Meshing

As discussed in Chapter 2, thermal analysis equipment can be broadly classified as pan style or flow-through reactors. This study will investigate four pieces of thermal analysis equipment; the Netzsch “Jupiter” STA 449 F3 reactor (reactor A) and the TA Instruments Q500 reactor (reactor B) represent the pan-style reactors, whilst the Micromeritics 2920 reactor (reactor C) and TA Instruments Altamira reactor (reactor D) represent the through-flow class.

All dimensions of the units have been measured with a ruler/callipers, and the 3D drawings were generated using SolidWorks. Meshing has been carried out in snappyHexMesh (OpenFOAM Ltd). A full mesh independence study was carried out based on the maximum velocity and the pressure drop, for the pan style and tubular reactors respectively. The resulting number of cells used in the fluid domain for each unit are shown in Table 8.1.

Table 8.1: Cell numbers used for meshing.

	Reactor A	Reactor B	Reactor C	Reactor D
Cell size (mm)	0.5	0.2	0.28	0.2
Number of cells in fluid region	1,567,437	3,703,353	621,652	1,485,645

Each sample was added as porous zone in the fluid region. The properties of this porous zone are given in Table 8.6. For the pan-style reactors, a cone has been used to represent the pile of powder (the sample), whereas for the flow-through reactors, the sample is represented by a cylinder with a diameter equal to the inside diameter of the reactor tube. For all sample regions, the volume has been calculated based on the mass of calcium carbonate (a model material) selected for each unit (Table 8.2).

For the flow through equipment (reactors C and D) quartz wool is required to hold the sample in place. This quartz wool has been added as an additional region and is represented by a cylinder of equal diameter to the sample.

Surface mesh refinement was used on the sample pan surface, and the fine features within the reactor tubes, as follows:

- Inlet = $\frac{1}{2}$ size of block mesh.
- Outlet = $\frac{1}{2}$ size of block mesh.
- Internals = $\frac{1}{2}$ size of block mesh.
- Reactor Wall = standard block mesh size.
- Sample = $\frac{1}{4}$ size of block mesh.

Reactor B has internal details, such as the hanging pan, which are orders of magnitude smaller than the overall reactor diameter. To capture these features, additional refinement regions (cylinders) where used, which used a $\frac{1}{4}$ of the block mesh size.

Figures 8.1 shows an example image of the resulting mesh, for reactor B.

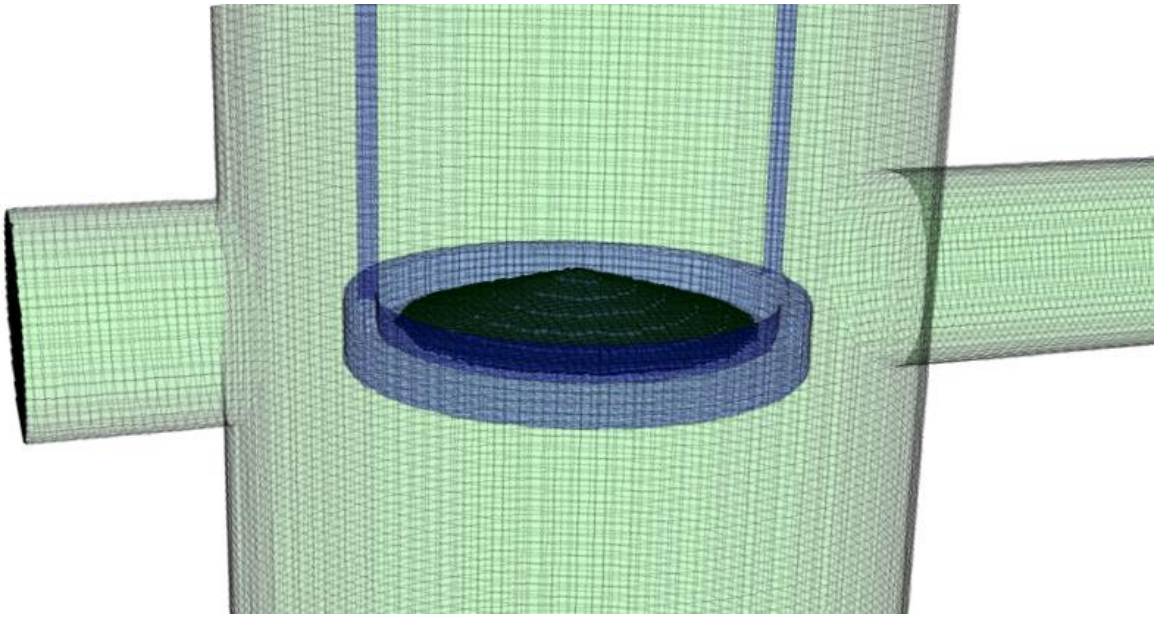

Figure 8.1: Example of mesh, reactor B.

8.2.2. CFD simulations

These simulations were solved in SmartFOAM© version 5.0.0, a user-friendly GUI based on OpenFOAM© version 4.2, using a finite volume methodology.

Figure 8.2 outlines the workflow for these simulations. The aim of these simulations is to investigate the mass and heat transport within the thermal analysis reactors, using simple simulations. To make the following results as general as possible, no endo/exothermic reaction terms have been applied.

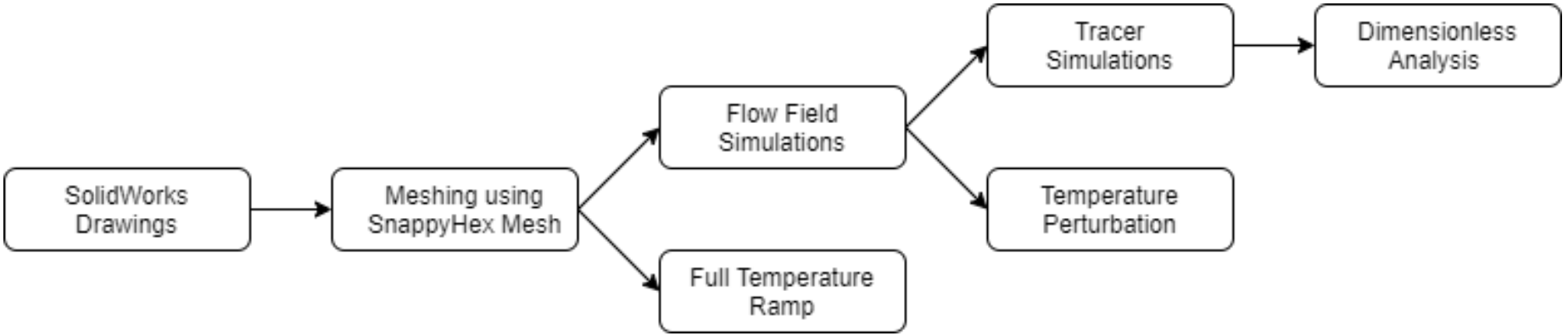

Figure 8.2: Workflow for CFD simulations

The conditions shown in Table 8.2 represent the sample mass and carrier gas flow rates used within the CFD simulations. These are based on standard operating methodology for the equipment studied, or plausible experimental conditions in thermal analysis.

Table 8.2: Sample mass and carrier gas flow rate conditions.

Reactor	Sample mass (mg)	Sample radius (m)	Sample height (m)	Carrier gas flow rate (mL min^{-1})
A	20	0.00225	0.0025	20
A	20	0.00225	0.0025	100
B	30	0.0043	0.001	110
C	250	0.005	0.01	20
C	250	0.005	0.01	50
D	100	0.002	0.005	40
D	100	0.002	0.005	100

In the following simulations, the mass of the sample is assumed constant, as the relatively small amounts of evolved gas would not impact the bulk flow properties studied in this work.

8.2.2.1. Flow simulations

Steady state incompressible flow fields were solved, using the simpleFoam solver, for all four geometries. The equipment is assumed to be operating at a constant temperature under atmospheric backpressure. These assumptions enable the simplification of the model. Gas properties have been assumed constant; as estimated

for a temperature in the middle of the ramp, in this case 793 K. Laminar flow was simulated based on Reynolds number calculations. For these calculations, the reactor internal diameter (d_i) and superficial gas velocity (u) were used. Values between 0.4 and 19.3 were obtained for the equipment discussed in this work. The gas was modelled as an incompressible fluid, as the relative pressure drop is sufficiently low that the change in density is negligible, and the problem is treated as isothermal. This approach enabled the rapid generation of representative flow fields for each of the equipment types in the middle of a ramped temperature experiment.

Equations 8.2 and 8.3 show the continuity and momentum equations respectively.

$$\nabla \cdot \boldsymbol{u} = 0 \qquad \text{Eq. (8.2)}$$

$$\rho(\boldsymbol{u} \cdot \nabla \boldsymbol{u}) = -\nabla \boldsymbol{P} + \nabla \boldsymbol{\tau} + \boldsymbol{S} \qquad \text{Eq. (8.3)}$$

In this case, as the gas was assumed to be Newtonian, the viscous stress tensor ($\nabla \boldsymbol{\tau}$) is equal to $\mu \nabla^2 \boldsymbol{u}$, where μ is the fluid viscosity. The source term, S, was set to zero, except in the sample porous region, where Darcy's law was used (Equation 8.4).

$$\boldsymbol{S} = -\frac{\mu}{K}\boldsymbol{u} \qquad \text{Eq. (8.4)}$$

The inlet boundary condition was set to a uniform velocity profile (normal to the boundary) of the selected flow rate for the simulation. A no-slip wall boundary condition was used for all solid surfaces. The outlet was set to a gauge pressure of 0.0 Pa. Initial conditions for the fluid zone were set to the velocity of the inlet(s), and a gauge pressure of 0.0 Pa.

Additional simulations at different temperatures (298 K and 1000 K) have been performed using the same method outlined in this section. The gas properties at these temperatures are given in Table 8.4.

8.2.2.2. Tracer simulations

The converged flow fields calculated in the previous simulations were fixed and do not require recalculation. A homogeneous species tracer (passive scalar) was introduced into the voids of the sample and released instantaneously. The tracer species were matched to the gas properties used for the bulk flow simulations. This simulation was transient, solved using the scalarTransportFoam solver, with the concentration of the tracer monitored for convergence.

In these simulations, the diffusion and convection of the tracer has been accounted for using Equation 8.5. The diffusion properties of the gas and tracer are given in Table 8.4.

$$\frac{\partial C}{\partial t} + \nabla \cdot (\boldsymbol{u}\, C_a) - D^{eff} \nabla \cdot (\nabla C_a) = 0 \qquad \text{Eq. (8.5)}$$

Monitors were placed on the surface of sample region to calculate the volume weighted average for the tracer, and the reactor outlet to calculate the mass weighted average for the tracer. The results from these monitors were used to calculate the residence time distributions for the sample and the reactor respectively, during post-processing.

8.2.2.3. Heat step simulation

In this heat step simulation, a small temperature difference between the sample and the reactor wall/inlet was imposed. An arbitrary difference of 5 K was selected, as it was calculated that the change in gas properties with this temperature increase would be negligible (< 1%), hence this simulation was treated as incompressible.

The tube wall and inlet had constant temperature (Dirichlet) boundary condition set to 798 K. The sample and continuum zones were given an initial temperature value of 793 K.

This was a transient simulation solving the energy Equation 8.6, while the flow field was assumed constant. All conditions were the same as the standard flow simulations with the addition of the temperature values. Temperature monitors were placed on the surface of the sample and the outlet. In this heat step case, $\frac{dP}{dt} = 0$ as isobaric conditions are assumed; however, this simplification is not applied during the heat ramp case (Section 8.2.2.4).

$$\frac{\partial(\rho h)}{\partial t} + \nabla(\rho \boldsymbol{u} h) = \nabla\left(\frac{k}{c_p}\nabla T\right) + \frac{dP}{dt} \qquad \text{Eq. (8.6)}$$

8.2.2.4. Heat ramp simulation

This simulation aimed to investigate heat transfer over a typical ramped temperature experiment. These experiments feature an initial room temperature (298 K) hold for 1000 s, followed by a steady ramp at a rate of 10 K min^{-1} to a final temperature of 1000 K, finishing with a final temperature hold for another 300 s. These parameters reflect a typical temperature programmed experiment. The initial hold helps establish flow in the reactor and any baseline signal. The final hold allows time for any ongoing reactions to reach completion and to establish any baseline drift.

The flow fields for a wall temperature boundary condition of 298 K were solved using the methodology discussed for the standard steady-state flow simulation, up to 1000 s. This simulates the initial isothermal temperature hold which is common for non-isothermal thermal analysis experiments. The compressible transient simulation was then started from 1000 s.

The properties of the gas change with temperature over this range (298 K to 1000 K) and can thus no longer be assumed constant. This simulation used the same boundary conditions as the standard flow simulations, except for the energy boundary condition for the wall. In this case, a temperature specification was used to incorporate a transient piecewise linear condition show in Table 8.3.

Table 8.3: Boundary conditions for heat ramp simulation.

Point	Time (s)	Temperature (K)
1	1000	298
2	5212	1000
3	5512	1000

This boundary condition simulates the common 10 K min^{-1} temperature ramp rate experiment used in thermal analysis experiments.

During this transient simulation Equations 8.1 - 8.3 and Equation 8.6 are solved. Monitors for the temperature were added to the inlet(s), outlet, and reactor wall. A volume averaged temperature was used for the sample. And a point monitor was added at the approximate location for a thermocouple.

8.2.2.5. Physical properties of the gas and sample

Table 8.4: Gas properties for constant temperature CFD simulations.

Temperature	Property	Value used	Units
298 K	Density [9]	1.204	kg m^{-3}
	Viscosity [10]	1.813×10^{-5}	kg m^{-1} s^{-1}
	Mass diffusivity	2.2×10^{-5}	m^2 s^{-1}
	Molar mass	28.97	g mol^{-1}
798 K	Density [9]	0.48	kg m^{-3}
	Viscosity [10]	3.46×10^{-5}	kg m^{-1} s^{-1}
	Mass diffusivity	1.0×10^{-4}	m^2 s^{-1}
	Molar mass	28.97	g mol^{-1}
	Specific heat capacity [11]	31.83	J kg^{-1}.K^{-1}
	Thermal conductivity [12]	0.05579	W m^{-1} K^{-1}
1000 K	Density [9]	0.2773	kg m^{-3}
	Viscosity [10]	4.788×10^{-5}	kg m^{-1} s^{-1}
	Mass diffusivity	2.14×10^{-4}	m^2 s^{-1}
	Molar mass	28.97	g mol^{-1}

The carrier gas used in these simulations was representative of air. The gas properties in Table 8.4 were used in the constant temperature simulations. For the heat ramp simulations, correlations are used to calculate the properties at each point in the temperature ramp. All correlations take the form of Equation 8.7 [13].

$$\Phi = \Phi_0(a_0 + a_1T + a_2T^2) \qquad \text{Eq. (8.7)}$$

Table 8.5 shows the parameters used for the temperature based variations. Density was set to an incompressible ideal gas (Equation 8.8).

$$\rho_g = \frac{Mr\,P}{RT} \qquad \text{Eq. (8.8)}$$

Table 8.5: Properties of gas with temperature based variations for CFD simulations.

Property	Φ_0	a_0	a_1	a_2	Units
Viscosity	1.84×10^{-8}	9.47×10^{2}	2.18×10^{0}	-5.44×10^{-4}	kg m^{-1} s^{-1}
Conductivity	5.58×10^{-2}	4.32×10^{-1}	1.25×10^{-3}	-3.58×10^{-7}	W m^{-1} K^{-1}
Specific heat	1.08×10^{3}	8.69×10^{-4}	-1.86×10^{-7}	-3.72×10^{-11}	J kg^{-1} K^{-1}

The properties of the solid sample and quartz wool support material are given in Table 8.6. The sample properties were based on calcium carbonate, to ensure values are realistic.

Table 8.6: Solid properties for CFD simulations.

Property	Sample [14] [15]	Quartz wool [16] [17]	Units
Density	2710	2200	kg m^{-3}
Specific heat capacity	837	720	J kg^{-1} K^{-1}
Thermal conductivity (dense material)	0.454543	1.4	W m^{-1} K^{-1}
Voidage	0.4	0.7	-
Viscous resistance ($1/K$)	4.05×10^{11}	1.17×10^{7}	-

8.3. Analysis of CFD results

From the outlet concentration profiles in the tracer simulations, described in Section 8.2.2.2, a residence time distribution (RTD) curve can be constructed. These tracer experiments simulate a ‘pulse’ experiment, so the E curve is represented by Equation 8.9 [18], which was solved using the trapezium rule.

$$E(t) = \frac{C_a(t)}{\int_0^\infty C_a(t)dt}$$ Eq. (8.9)

The mean residence time and variance for the reactor can be calculated using Equations 8.10-8.11 respectively [18]. These moments are extracted directly from the RTD curve [18].

$$t_m = \int_0^\infty tE(t)\, dt$$ Eq. (8.10)

$$\sigma^2 = \int_0^\infty (t - t_m)^2\, E(t)\, dt$$ Eq. (8.11)

From the concentration profile taken from the surface of the sample in the tracer simulations, described in Section 8.2.2.2, a residence time can be estimated. As the time for the tracer leaving the sample is fast, the residence time (t_{mp}) was taken to be the time for 99.5% of the tracer to leave the sample.

The number of continuous stirred tank reactors (CSTRs) in series can be used as an indication of the flow pattern occurring within the reactor. This model is also known as Tanks-in-Series (TIS) [19], shown in Equation 8.12. Whilst this model does have limitations [18], in this work it is used as an analytical tool, rather than a model of the RTD.

$$TIS = \frac{t_m^2}{\sigma^2}$$ Eq. (8.12)

An infinite TIS equates to plug flow. However, a value of 5 TIS is usually taken as an adequate approximation of plug flow [19]. Less than 1 TIS implies back mixing is occurring within the reactor. When attempting to extract kinetics, plug flow is desired, hence > 5 TIS.

The estimation of the kinetic rate is a simple approximation, using the typical time for a 10 K min^{-1} experiment. Calcium carbonate has been selected as the material of choice, as this would produce a single thermal event [1], [20]. In this case the kinetic reaction rate for calcium carbonate decomposition was taken to be 7.97×10^{-9}mol.s^{-1}. As values for the reaction rate given within the literature could be influenced by transport limitations, this rate has been estimated by assuming a standard value for the mass of the sample (10 mg), the average time for the 10 K min^{-1} decomposition reaction (1.2 h) and Equation 8.13. This simplification allows a comparison of a representative rate of reaction compared to the rate at which evolved gas moves inside the reactor, without solving a fully defined reaction model. In the real system, the rates will vary above and below the average rate, but the comparison will be order-of-magnitude correct.

$$r_k = \frac{(\frac{m_s}{Mr_{solid}})}{t_{av}} \qquad \text{Eq. (8.13)}$$

The amount of tracer present in the CFD simulation can be calculated from the total pore volume of the sample pile. For these simulations, the tracer properties are assumed to be the same as the carrier gas (air).

$$n_{tracer} = \frac{V_{bed} \cdot \varepsilon \cdot \rho_{air}}{Mr_{air}} \qquad \text{Eq. (8.14)}$$

From the residence time distribution, the mean residence time was calculated, this is used to calculate the reactor mass transfer rate in mol s^{-1}, Equation 8.15.

$$\dot{n_R} = \frac{n_{tracer}}{t_m} \qquad \text{Eq. (8.15)}$$

Similarly, the moles of tracer calculated in Equation 8.14 is used to calculate the sample mass transfer rate in mol s^{-1}.

$$\dot{n}_S = \frac{n_{tracer}}{t_{mp}}$$ Eq. (8.16)

Using these rates, variations of the dimensionless Damköhler numbers can be calculated. The Damköhler numbers are the ratio of reaction to transport timescales. Advective and diffusive mass transport are represented in Damköhler numbers I and II respectively [21]. The dimensionless numbers calculated in this work combine the advective and diffusive transport for each case. While these values are not strictly Damköhler numbers as normally defined [21], they illustrate similar properties, and are thus sufficiently analogous that they shall be referred to as Da(R) and Da(S) for the reactor and sample respectively.

Da(R) uses the reactor mass transport rate so shows the bulk transport, whilst Da(S) uses the sample mass transport rate, so shows the mass transport inside the porous sample pile.

$$Da(R) = \frac{r_k}{\dot{n}_R}$$ Eq. (8.17)

$$Da(S) = \frac{r_k}{\dot{n}_S}$$ Eq. (8.18)

These Damköhler numbers indicate if the system is mass transport limited; this is the case if Da > 1 [21].

If Da < 1 then the system is kinetically limited [22]. This means that the mass transport rate is faster than the reaction rate allowing the reaction to be monitored directly. For pure, or intrinsic kinetics a Da << 1 would be desired.

To resolve the relative impact of the advection and diffusion effects, the Bodenstein number (a mass transfer analogue of the Peclet number) can be used, as described in

Equation 8.19. This is defined as the ratio of the amount of substance introduced by advection to the amount introduced by diffusion [19].

$$Bo = Re \cdot Sc = \frac{d_p \cdot u \cdot \rho_{gas}}{\mu} \times \frac{\mu}{\rho_{gas} \cdot D^{eff}} \quad \text{Eq. (8.19)}$$

In this case, if Bo > 1 then the system is convection controlled. If Bo < 1 then the system is diffusion controlled [19]. This can be used in a similar way to the TIS model, to indicate whether conditions match plug flow behaviour. For the Bodenstein number a high value indicates plug flow, hence is required for kinetic studies.

8.3.1. Interpreting the analysis

Thermal analysis reactors are designed on the basis that they are dominated by bulk flow; hence the evolved gas leaving the reactor is representative of the gas evolved from the sample. This is the assumption which allows for kinetic analysis.

For a reactor to be considered as a point source (Equation 8.20), there either needs to be no possible reverse reaction or the removal of evolved gas must be considerably faster than the generation of evolved gas, such that any reverse reaction may be neglected. Many reactions studied by thermal analysis have reverse reactions, a good example of this is the decomposition of calcium carbonate. So, it is not desirable to restrict kinetic study to only unidirectional reactions.

$$\frac{dC_a}{dt} = r_a \quad \text{Eq. (8.20)}$$

A plug flow reactor (PFR) assumes there are thin ‘plugs’ of gas which have uniform composition (in the radial direction) flowing through the reactor. In this case, axial mixing (mixing between plugs) is negligible, this means that the gas exiting the reactor is representative of the gas evolved from the sample. Radial mixing by contrast is “fast”,

ensuring uniformity of the plug in the direction normal to flow. There is a geometry and flow specific offset between the time the gas is released, and the time the gas is detected. This is a simple offset which can be accounted for with suitable models, Equations 8.21 and 8.22 [18]. Note that most solid-state kinetic equations are in dimensionless form, so an appropriate scale factor would be needed to incorporate these into Equation 8.21.

$$\frac{dC_a}{dt} = -u\frac{dCa}{dz} - C_a\frac{du}{dz} + r_a(\alpha, C_a, T) \text{ in sample region} \qquad \text{Eq. (8.21)}$$

$$\frac{dC_a}{dt} = -u\frac{dC_a}{dz} - C_a\frac{du}{dz} \text{ elsewhere} \qquad \text{Eq. (8.22)}$$

Modifications would be required for the traditional thermokinetic models, to account for the inhomogeneity within the sample and the variation in residence time during the experiment. Similarly, if a reverse reaction is possible it must be accounted for in the thermokinetic model.

A CSTR assumes perfect back mixing within the reactor; the concentration is uniform and equal to the exit concentration, shown in Equation 8.23 [18]. This means that once evolved gas is released it is instantaneously mixed throughout the reactor.

$$\frac{dC_a}{dt} = u(C_a - C_{a,out}) + r_a \qquad \text{Eq. (8.23)}$$

For thermal analysis the amount of volatiles released at a specific temperature is the observed variable. Having the concentration uniformly mixed throughout the reactor would distort this. Although this flow pattern is amenable to analytical mathematical analysis, as the RTD for a temperature ramp rate experiment is dynamic, there is no guarantee that this ideal distribution will be present for the whole experiment. Most

likely at some point during the temperature ramp, the RTD will become non-ideal/complex. Hence, this flow profile is not desired for kinetic analysis.

In these dynamic experiments, mixing within the reactor is the same as mixing in time, which is the same as mixing across temperatures. This mixing can be simple (like a PFR, where there is a simple time lag) or complex (CSTR or other). Having a complex RTD means that it is no longer possible to simply fit kinetics, because there is no simple relationship between when a gas is measured and the temperature (or time) at which it was released. If the aim of the experiment is to perform kinetic analysis, a simple well understood flow pattern or residence time distribution is desired, such as a point source or PFR.

If a complex RTD is present for example $1 \leq TIS < 5$, this equipment may be suitable for kinetic studies however different conditions would be required. A higher flow rate may be possible, which could produce more PFR like behaviour. These conditions should be re-tested to confirm the new flow regime and considerations for pressure drop and sample retention should also be made before experiments are carried out.

Figure 8.3 shows the workflow when analysing the dimensionless numbers calculated in this work. This shows the scenarios in which kinetic analysis would be possible (even if traditional models may require some modification), and some scenarios which would not be desired for kinetic analysis.

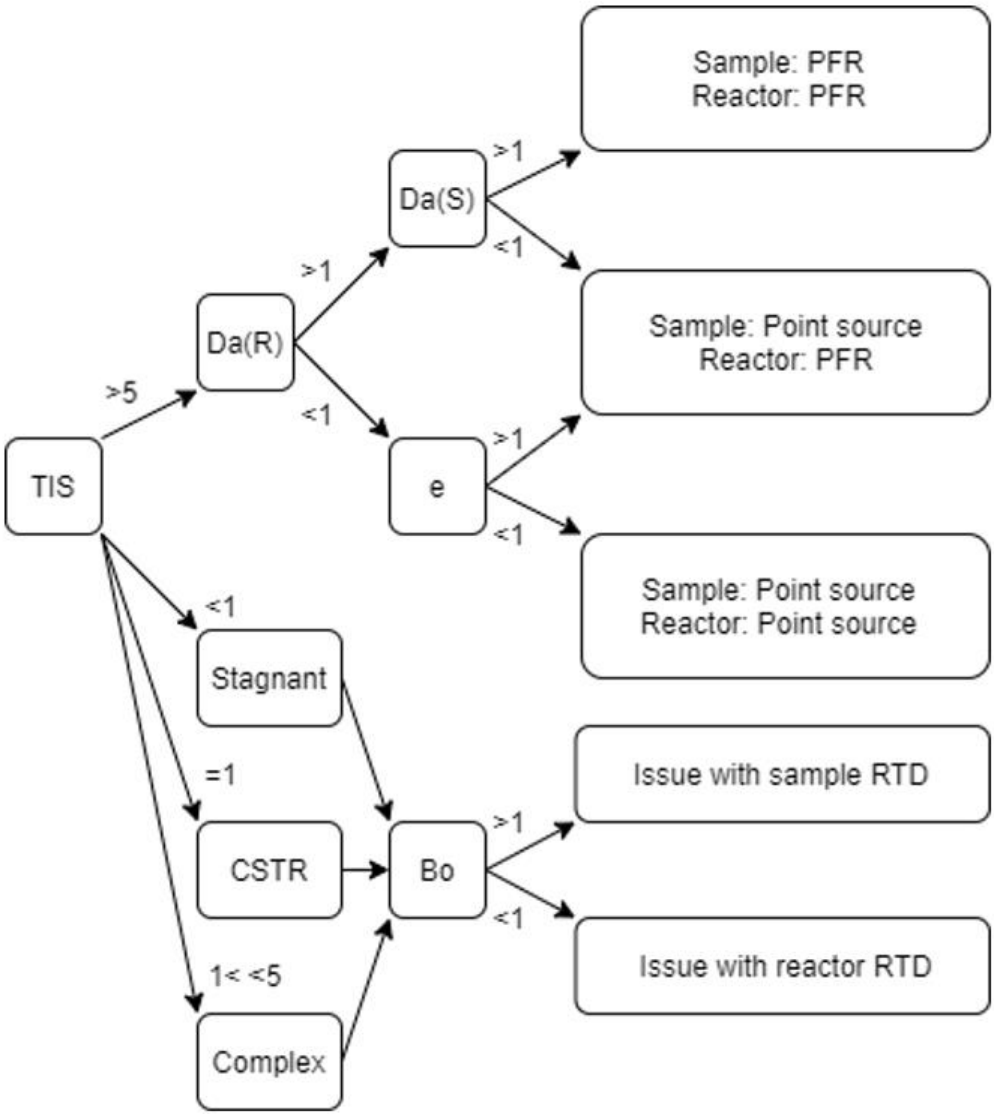

Figure 8.3: Interpreting dimensionless analysis.

The following scenarios are undesirable: stagnant zones/back mixing, CSTR, complex RTD (between CSTR and PFR). Each of these will be complex and changing throughout the temperature ramp experiment, making kinetic modelling infeasible. These scenarios arise in numerous ways, but the root cause is diffusion dominating the mass transport (which is evaluated using the Bodenstein number). Diagnosis of these scenarios using CFD may suggest alternate experimental protocols to improve the flow characteristics of the equipment.

Predictable well defined PFR or point source conditions are desirable for kinetic analysis. PFR behaviour is established using the TIS model and the Bodenstein numbers. Whether a reactor can be treated as a point source (the ideal case assumed by traditional thermokinetic models) will depend on the error tolerance for the temperature within the reactor (typically, of order ~0.5 K, depending on the temperature accuracy quoted by the reactor manufacturer), and the temperature ramp rate. This relationship is shown in Equation 8.24.

$$e = \frac{\beta . t_m}{\delta_T} \qquad \text{Eq. (8.24)}$$

Where β is the temperature ramp rate, t_m is the reactor mean residence time and δ_T is the error tolerance on the temperature.

If e < 1 then the reactor can be treated as a point source, as the temperature measured will match the temperature at which the gas evolved within error tolerances, as is intended for thermal analysis. However, if e > 1 this indicates the temperature discrepancy will be larger than the tolerable levels, hence the reactor must be treated as a PFR to account for this difference.

Once the reactor mass transport has been considered, and PFR behaviour established, the sample should also be considered. The gas phase within the sample can encounter two conditions: homogeneity and inhomogeneity. If the gas phase within the sample is homogeneous, this would result in a Da(S) << 1, meaning the reaction can be treated as a point source (providing the reactor is also point source). Physically, this means each part of the sample behaves identically.

If the sample has a Da(S) > 1, this implies gas phase inhomogeneity. In this case the sample can be treated as under PFR conditions, providing the reactor is either point

source or PFR. This would require modifications to traditional thermokinetic models (as these assume point source conditions).

8.4. Results and discussion

For simplicity, a single example of experimental conditions for each reactor configuration will be presented in this results section, with final dimensionless numbers presented for all conditions tested shown in Section 8.4.3.

8.4.1 Hanging-pan geometries

The tracer simulation results for reactors A and B are shown in Figure 8.4.

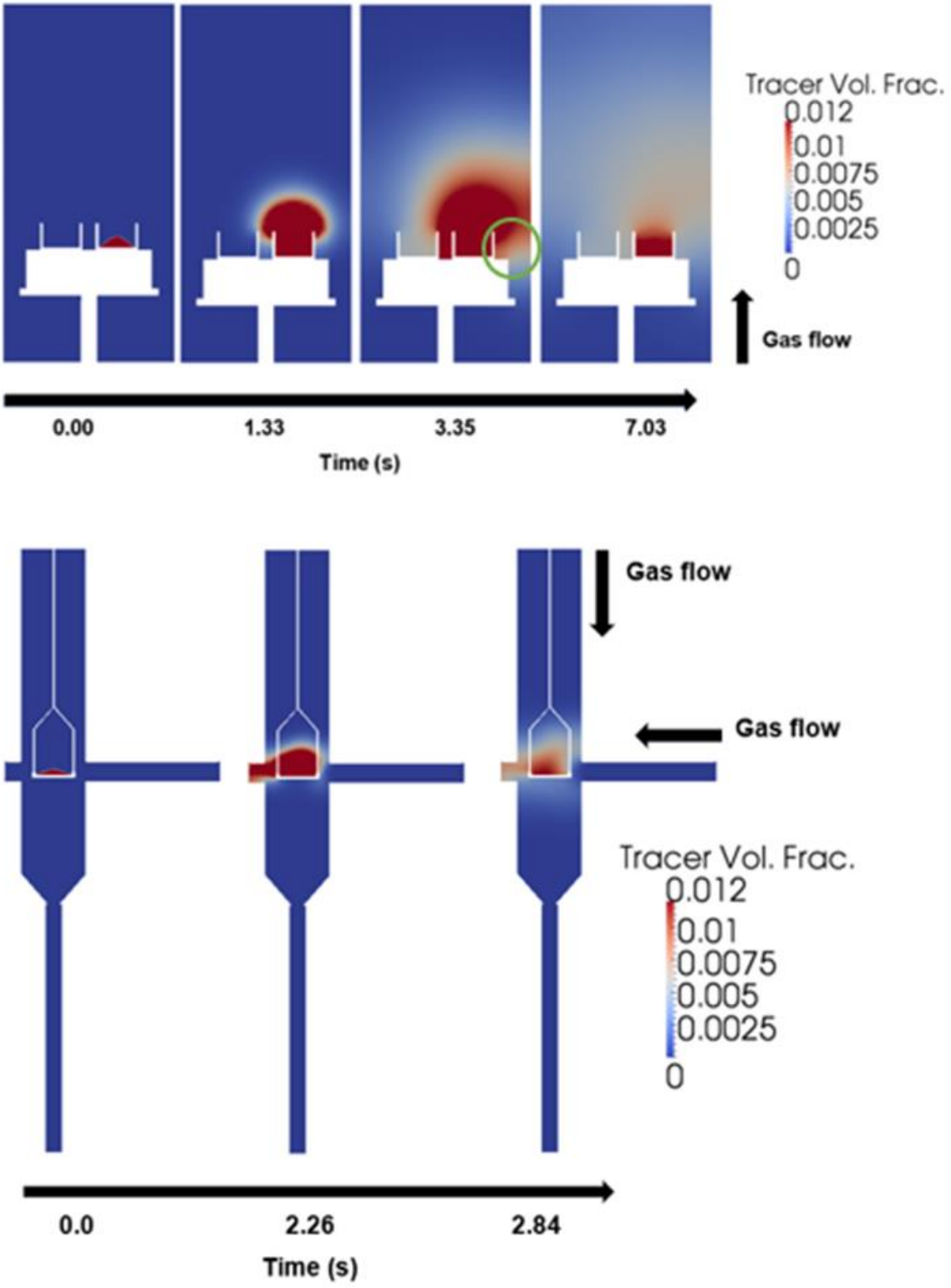

Figure 8.4: Tracer simulation results. Top: reactor A, 20 mL min^{-1}. Bottom: reactor B, 110 mL min^{-1}

In reactor A, the walls of the sample pan create a region of low bulk gas velocity, which inhibited the released tracer from mixing with the bulk gas. Back mixing was also observed around the sample pan, as tracer mixes with the bulk flow around the sample stand (3.35 seconds after tracer release). A significant fraction of the tracer remained within the sample pan 7 seconds after release.

Back mixing is also observed in reactor B; the tracer left the sample but travelled upwards and to the right, against the flow direction of gas. After 2.84 s, a significant portion of the gas remains in the sample pan with only small concentrations leaving the reactor.

These images indicate mass transport issues within the reactor, which were quantified using the reactor residence time distributions shown in Figure 8.5.

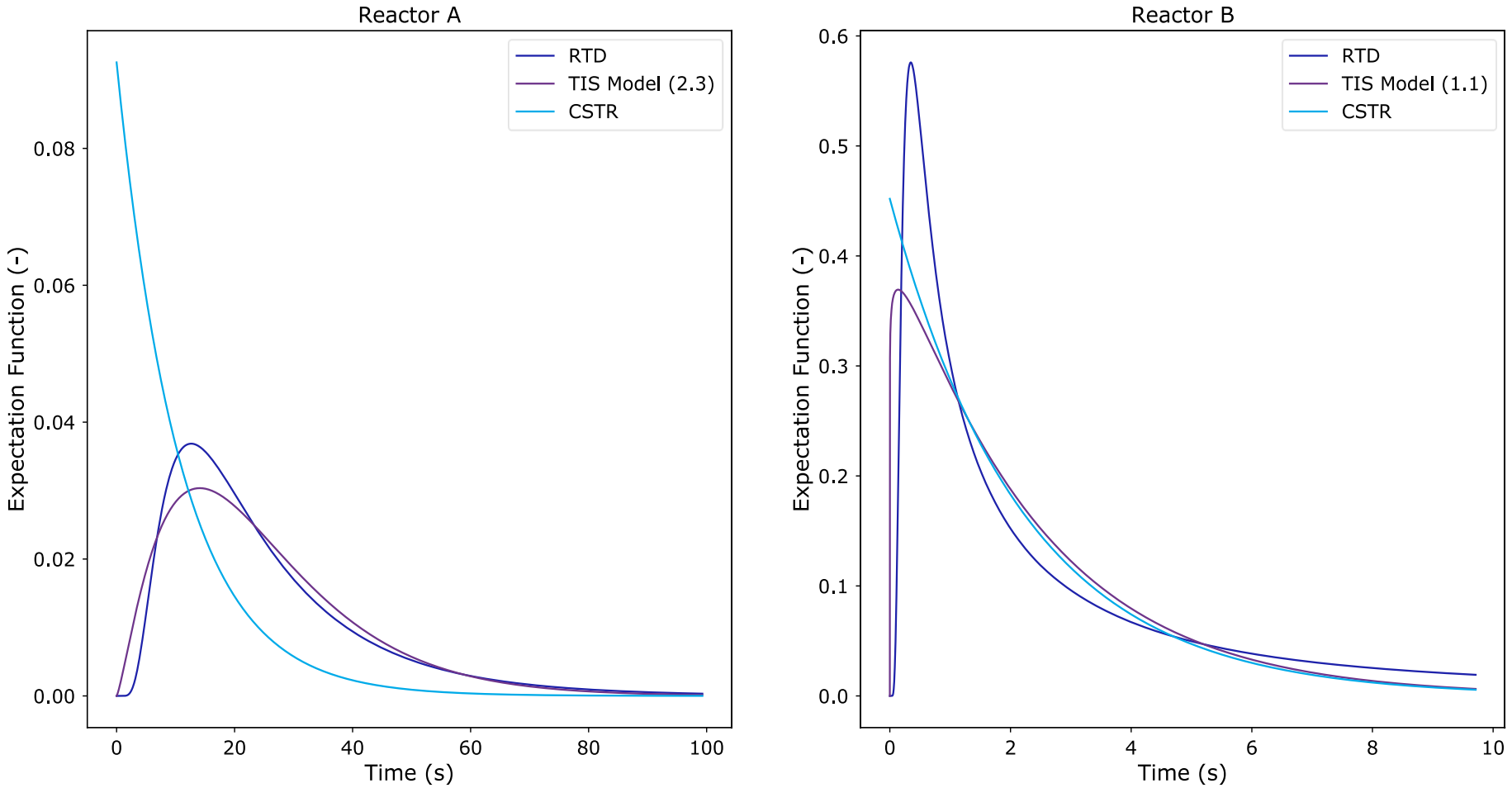

Figure 8.5: Residence time distributions. Left: reactor A, 20 mL min^{-1} Right: reactor B, 110 mL min^{-1}.

Both residence time distributions in Figure 8.5 show very skewed curves with long tails. For reactor A this was quantified with a mean residence time of 24.9 s and a variance of 269 s^2. This is equivalent to a TIS value of 2.3. From the dimensionless analysis, the following values were calculated: Da (R) = 4006, Da (S) = 6021, Bo = 0.6.

For reactor B, the mean residence time was 2.35 s and the variance 5.2 s^2, equivalent to a TIS value of 1.1. From dimensionless analysis the Damköhler numbers for the reactor and the sample were calculated to be 377 and 321 respectively. The Bodenstein number was calculated as 0.6.

Large Damköhler numbers and low Bodenstein numbers imply there are significant mass transport issues within these pan-style reactors, both in the bulk gas and sample. This is a clear case of a stagnant zone dominated by diffusion. Material is well-mixed within this zone but must diffuse into the gas jet to leave the reactor.

With the current experimental conditions and these reactor geometries, it would be unlikely that a kinetically limited condition could be reached. This means that this pan-style equipment should not be used for kinetic studies requiring removal of gaseous products.

8.4.1.1. Influence of temperature on residence time distribution

The simulations in Section 8.4.1 were completed for a mid-ramp temperature value of 793 K. In thermal analysis, large temperature variations within the reactor are expected. To investigate the impact of temperature on the residence time distribution for this reactor, additional flow and tracer simulations were carried out. The temperature for these were taken to be at the start (298 K) and the end of a

conventional temperature ramp (1000 K). The same inlet flow rate of 20 mL min^{-1} was used. Figure 8.6 shows the variation in the residence time distribution curves.

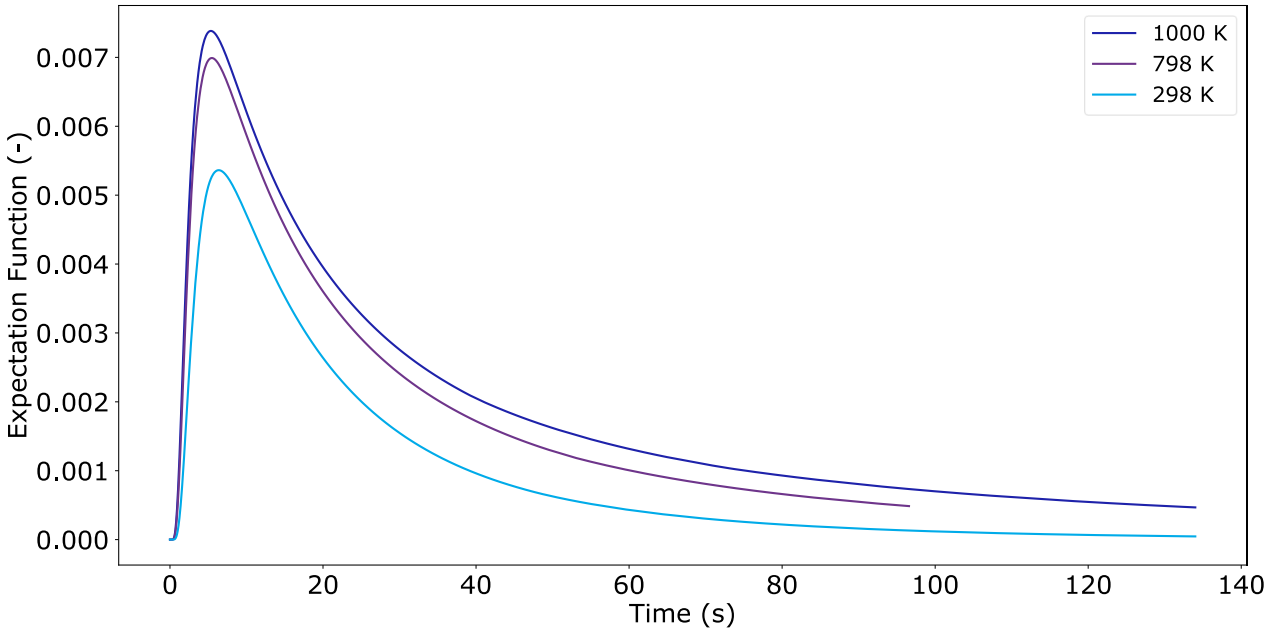

Figure 8.6: Influence of temperature on residence time distribution, reactor A, 20 mL min^{-1}.

The variation in these curves is expected because of the dependency of the gas density and other gas properties on temperature. The gas feed to the reactor is a constant standard volume, effectively a constant molar flow. As the gas warms, its density falls and so the actual volume flow of gas and actual velocities in the reactor increase. This leads to a small improvement in mixing and shorter mean residence times at higher temperature.

One implication of this is that because reactor RTD is a function of temperature and gas flow, building an RTD model to resolve the impact of the mass transport within the reactor would be complex, and ultimately not practicable.

8.4.1.2. Temperature step simulation

The objective of this simulation was to evaluate the time required following a thermal disturbance for the equipment to relax to the new temperature. Such thermal lag is common where the flowing heat capacity is insufficient relative to the stasis thermal mass of the equipment. In this case, no enthalpy of transformation (positive or negative) from the sample has been included, so this can be viewed as a least stressing scenario. With an endothermic reaction, the temperature lag in the sample would be worse than the example shown below. For an exothermic reaction, the temperature of the sample would no longer be related to the wall temperature hence it is possible to get falsification of the sample temperature and even runaway reactions.

Figure 8.7 shows the lag between the sample and the bulk gas temperature. This is caused by the static heat capacity of the sample and the limited rate of heat transfer from the bulk gas.

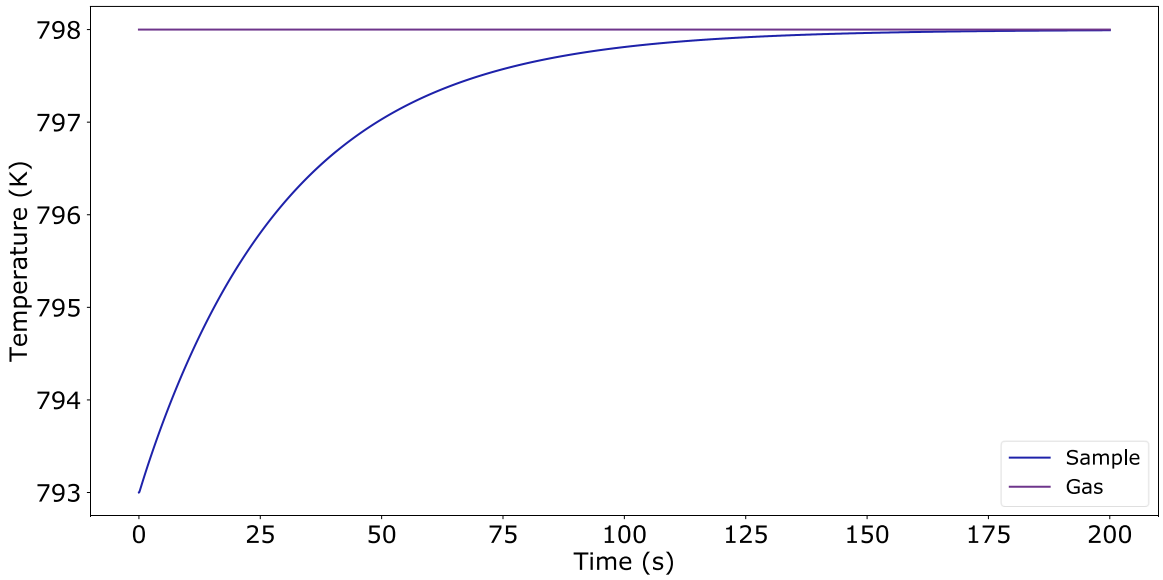

Figure 8.7: Temperature step experiment, reactor B, 110 mL min^{-1}.

Ideally a rapid convergence between gas and sample temperatures would be observed. However, the lag time for the sample to approach 0.5 K of the wall temperature for this simulation was calculated to be 70 s; this is 3.9 K min^{-1}, which is significant when compared to a typical temperature ramp rate of 10 K min^{-1}.

The thermal conductivity and heat capacity value of the solid and gas will impact the shape of the curve in Figure 8.7. However, as reasonable values (taken for calcium carbonate and air) have been used in this study, it is not expected that this lag issue would be eliminated when using most materials. In reality the size of the lag will depend on at least the heat capacity of the material under study, the rate and energetics of any reaction or phase change which occurs, and the efficiency of heat transfer, which will itself depend on gas flow and temperature. Most of these factors are either difficult to observe or are the object of study. This makes it exceptionally challenging to calibrate for or model.

8.4.1.3. Temperature ramp simulation

This simulation is the closest approximation to the linear temperature ramp rate experiments which are common in thermal analysis. As above, no enthalpy of transformation was assigned to the sample. This is the most computationally expensive of the simulations and was prompted by the observation that the relaxation time found in the heat step simulation is of a similar order to the imposed ramp rate in a typical experiment, making extrapolation challenging.

It was found that the gas temperature, as measured by the equipment thermocouple, is very close to the wall temperature throughout the ramp experiment. Figure 8.8 shows

the difference between the set wall temperature and the sample throughout the temperature ramp rate simulation.

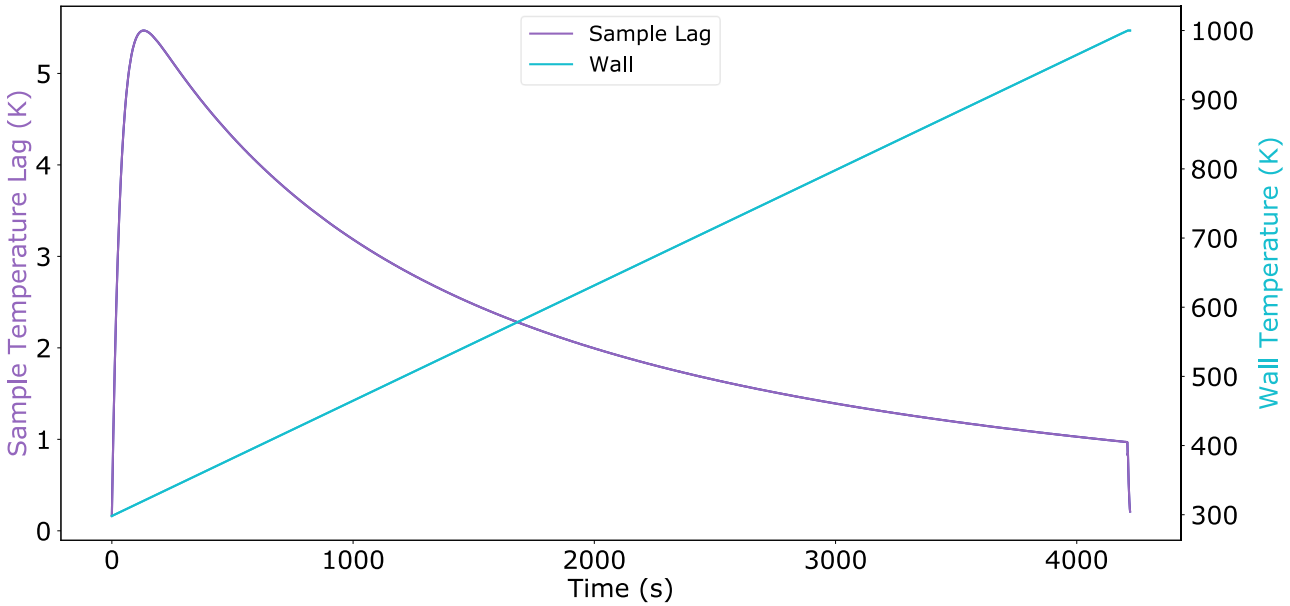

Figure 8.8: Temperature ramp simulation, reactor B, 110 mL min^{-1}.

Figure 8.8 shows that the difference between the sample and the set wall temperature is dynamic during the experiment. A maximum difference of ~5.5 K occurs early within the temperature ramp. The temperature ramp rate stops after 4221 s, and the difference quickly reduces to zero. The dynamic nature of this offset is likely due to the varying heat transfer coefficient of the bulk gas- this value increases with temperature, decreasing the offset between the sample and bulk gas.

This dynamic change in sample lag means that calibration is not sufficient to account for the temperature difference between the sample and the wall. Conventionally calibrations are carried out based on the onset temperature for known thermal events, as discussed in Chapter 2. This is carried out at multiple temperature ramp rates and compared to known values. This methodology would not be sufficient to account for

the changes shown in this simulation because the temperature lags within the simulation are material and quantity specific, as well as dynamic.

8.4.2. Flow-through geometries

The tracer simulation results for reactors C and D at 50 mL min^{-1} and 100 mL min^{-1} respectively, are shown in Figure 8.9.

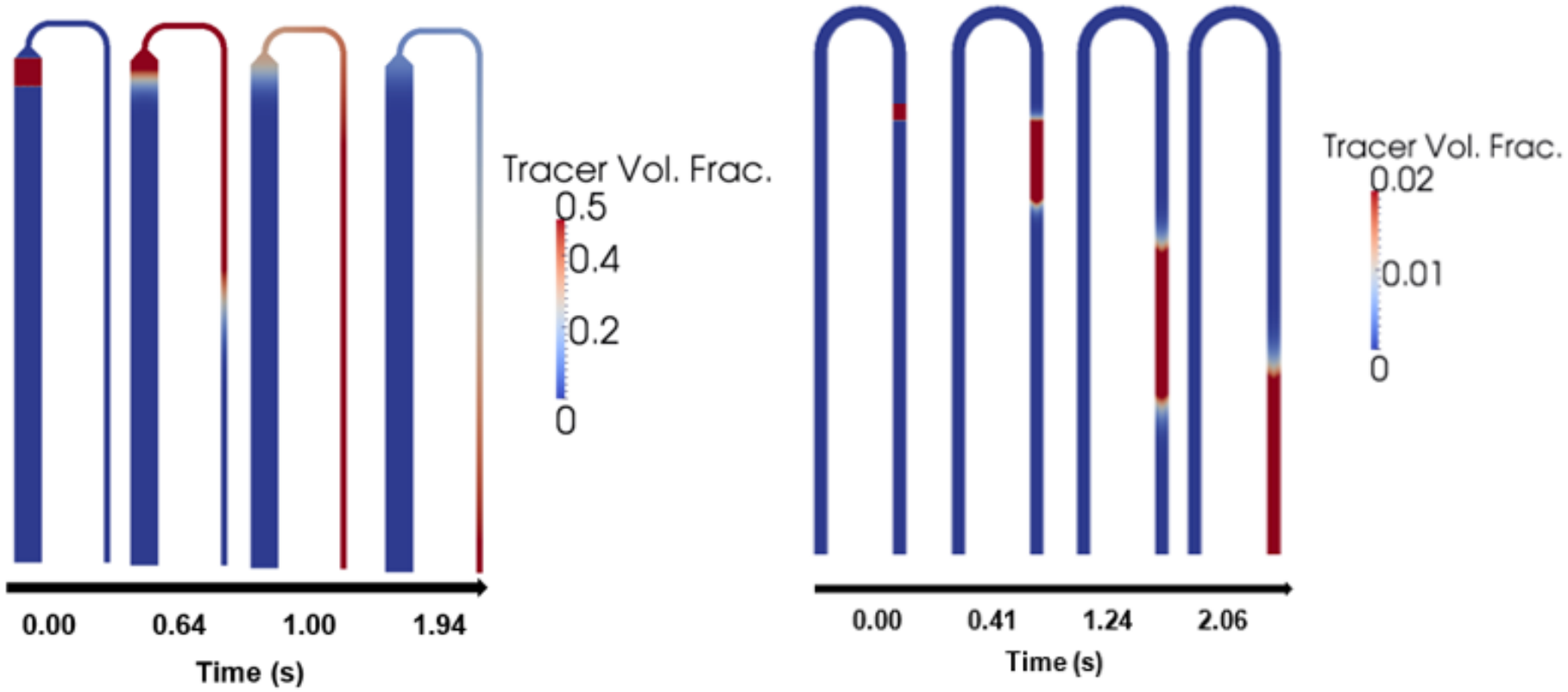

Figure 8.9: Tracer simulation results. Left: reactor C, 50 mL min^{-1}. Right: reactor D, 100 mL min^{-1}.

Figure 8.9 shows a front of tracer moving through the sample bed (0.64 seconds after tracer release) of reactor C. The constriction of the u-tube causes mixing, prior to the gas entering the thinner leg of the tube. The tube of uniform diameter (reactor D) shows very little axial mixing and the tracer quickly leaves the sample region. The residence time distributions for these reactors are shown in Figure 8.10.

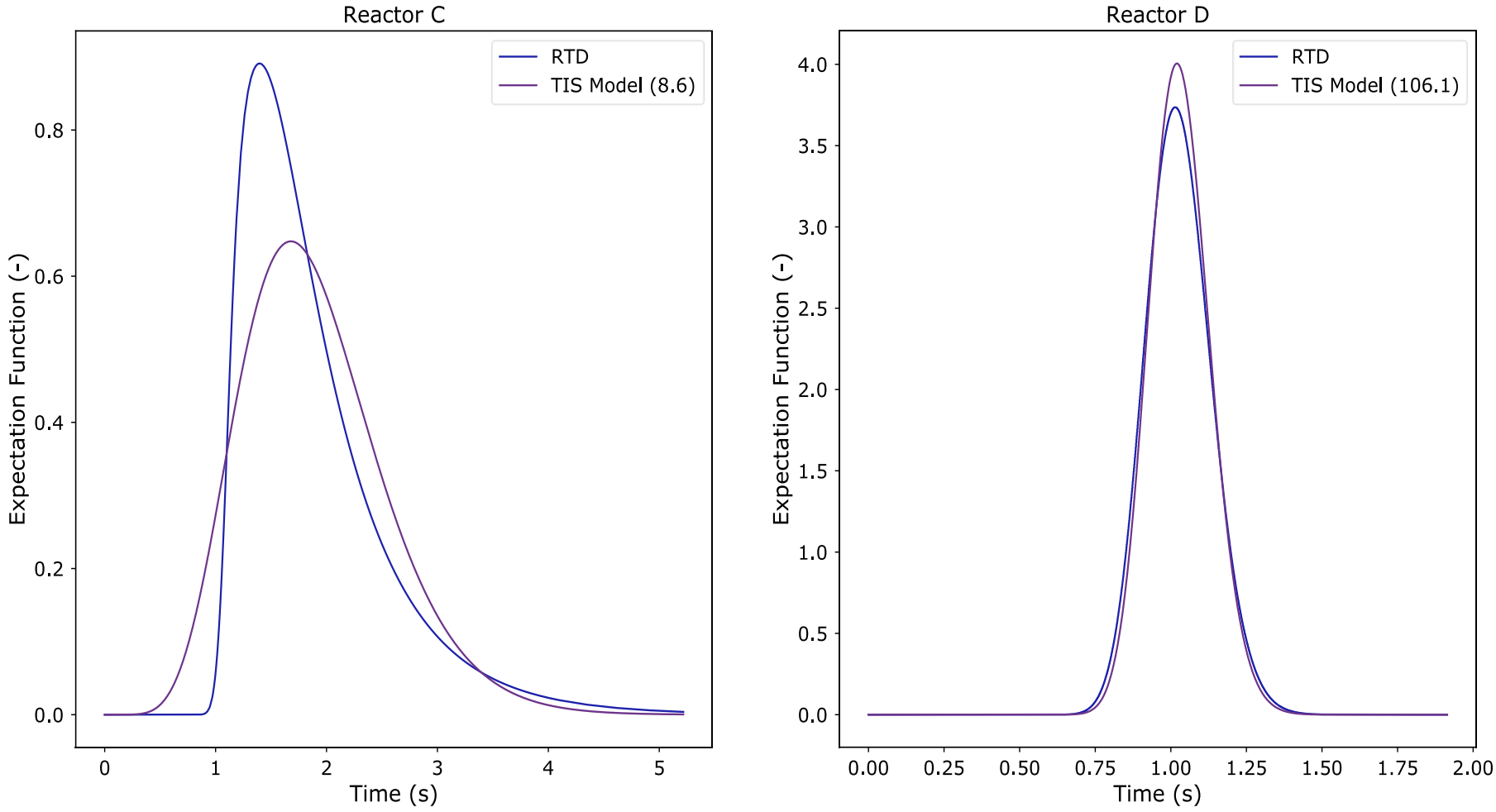

Figure 8.10: Residence time distribution. Left: reactor C, 50 mL min^{-1} Right: reactor D, 100 mL min^{-1}.

For reactor C, the mean residence time was calculated to be 1.9 s with a variance of 0.42 s^2. Although the TIS of 8.6 implies a good approximation of plug flow and the Bodenstein number is higher than 1 (at 4.12), the Da (R) and Da (S) values of 302 and 838 respectively, show that there are still mass transfer issues within this reactor. A higher value for Da (S) than Da (R) indicates that there is an issue with removing the tracer/produced gas from the sample region. In this equipment design, the sample is located just prior to a constriction of the tube. This constriction is causing the high Da (S) value as the gas released from the sample cannot leave the region in a timely manner.

The mean residence time calculated for reactor D was 1.03 s with a variance of 0.01 s^2. This curve could be represented by 106.1 CSTR reactors in series, giving a good approximation for plug flow. From dimensionless analysis the following values were calculated: Da(R) = 165, Da (S) = 15, Bo = 20.2. Again, both Damköhler numbers indicate mass transport is still an issue within this reactor, under these conditions, but that it could be plausible to adjust the space velocity used to achieve a kinetically limited regime within the sample. As the TIS model and Bodenstein number show a good approximation for plug flow, the mass transport in the bulk gas is most likely to manifest as a small time delay. This time delay would also result in a temperature offset (due to the convolved nature of time and temperature in thermal analysis experiments), which could be calculated. This means that this equipment configuration could be suitable for kinetic studies, depending on the conditions chosen. As a standard kinetic rate has been used here, experimentalists should check expected kinetic rates. For slower expected kinetic rates, this gas flow rate could be free from limitations. For

faster expected kinetic rates, a higher gas flow rate would be required to be free from bulk flow transport limitations.

8.4.2.1. Temperature step simulation

The heat step simulation for reactor D produced the graph shown in Figure 8.11. This shows an almost ideal curve, with the sample temperature increasing to match the specified wall temperature very quickly, in less than 0.05 seconds. This fast temperature change is likely due to the sample's contact with the reactor wall; this means that conductance will be the primary mode of heat transfer, rather than via convection (as is the case for the pan-style reactors).

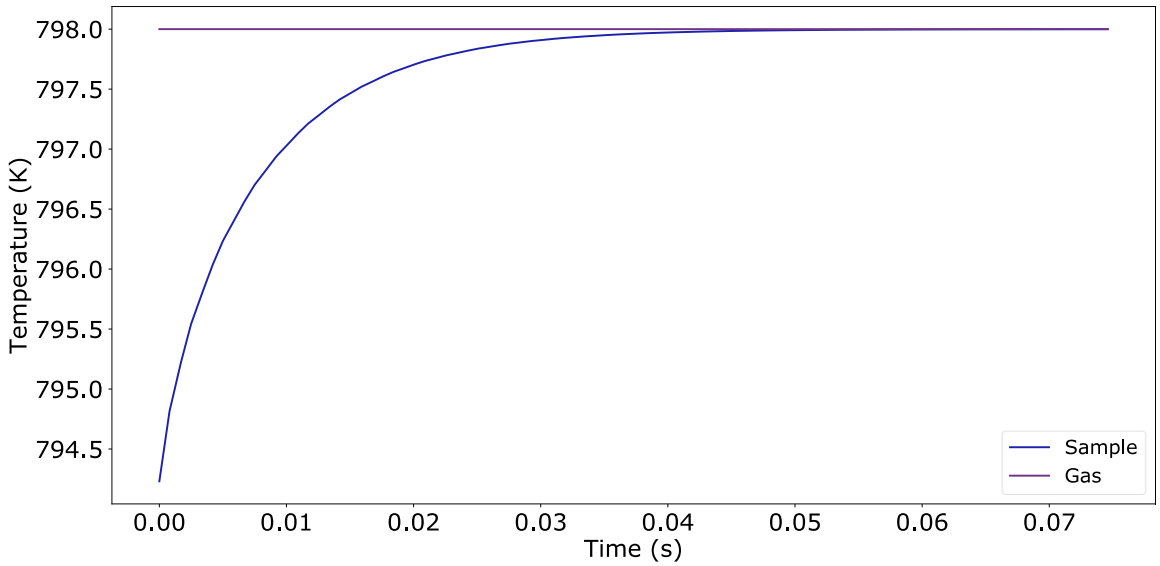

Figure 8.11: Temperature step simulation results, reactor D, 100 mL min^{-1}.

8.4.2.2. Temperature ramp simulation

Figure 8.12 shows the temperature lag between the sample and the carrier gas for a dynamic simulation representing a 10 K min^{-1} temperature ramp rate.

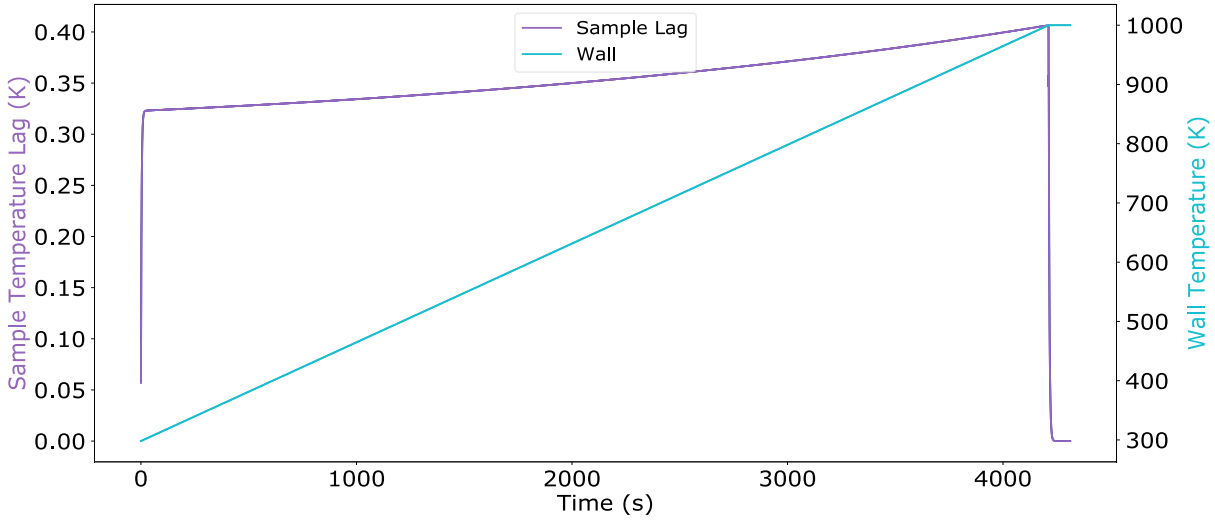

Figure 8.12: Temperature ramp simulation results, reactor D, 100 mL min^{-1}.

The lag between the sample and the wall temperature is very small for this simulation, again due to the improved heat transfer caused by the contact between the sample and the reactor wall. The magnitude of this lag is consistently less than 0.5 K, which is likely to be tolerable for this type of experiment.

8.4.3 Comparison of geometries

The results from the tracer simulations for all equipment configurations and carrier gas flow rates have been collated in Table 8.7.

Table 8.7: Comparison of dimensionless analysis results.

Equipment	Flow rate	Reactor Da(R)	Sample Da(S)	Bo	TIS
Reactor A	20mL min^{-1}	4006	6022	0.6	2.3
Reactor A	100mL min^{-1}	726	482	3.1	6.7
Reactor B	110mL min^{-1}	378	321	0.6	1.1
Reactor C	20mL min^{-1}	3139	9161	1.7	1.2
Reactor C	50mL min^{-1}	302	838	4.1	8.6
Reactor D	40mL min^{-1}	418	78	8.1	91
Reactor D	100mL min^{-1}	165	16	20.2	106.1

As a standard kinetic rate has been assumed for this dimensionless analysis (as shown in Section 8.3) it is advised that if kinetic interpretation is the goal of experimentation, then an estimate for the expected kinetic rate should be used to re-calculate these Damköhler numbers to determine the suitable equipment and conditions to carry out the experimentation.

8.5. Retrospective look at previous cases

Previous studies using uniform diameter tubular reactors have been successfully analysed using the kinetically limited Sestak-Berggren equation such as the temperature programmed reduction on an FT catalyst (Chapters 4 and 5) [3] and temperature programmed desorption of ammonia from SAPO-34 (Chapter 6). In these studies, plausible kinetic mechanisms were estimated along with sensible kinetic parameters such as activation energy for each thermal event.

Chapter 7 discussed a case study of a zinc nitrate catalyst precursor decomposition. This reaction was studied using a pan-style TGA coupled with MS. As a consequence, the TGA and MS data could be modelled separately using the modified Sestak-Berggren methodology [3], [22]. From the parameters estimated, it was possible to predict the extent of reaction for each methodology. For the TGA data set, this used the usual Sestak-Berggren method, however for the MS data the water and NOx signals were analysed separately. In order to construct the composite MS extent of reaction curve, the contribution term estimated for the water peak in the TGA data was used to weight the water and NOx MS data, allowing both to be plotted on the same axis. This extent of reaction curve for MS data could not have been constructed without the use of the Sestak-Berggren equation and the prediction of the curve contributions. The extent of reaction curves are shown in Figure 8.13.

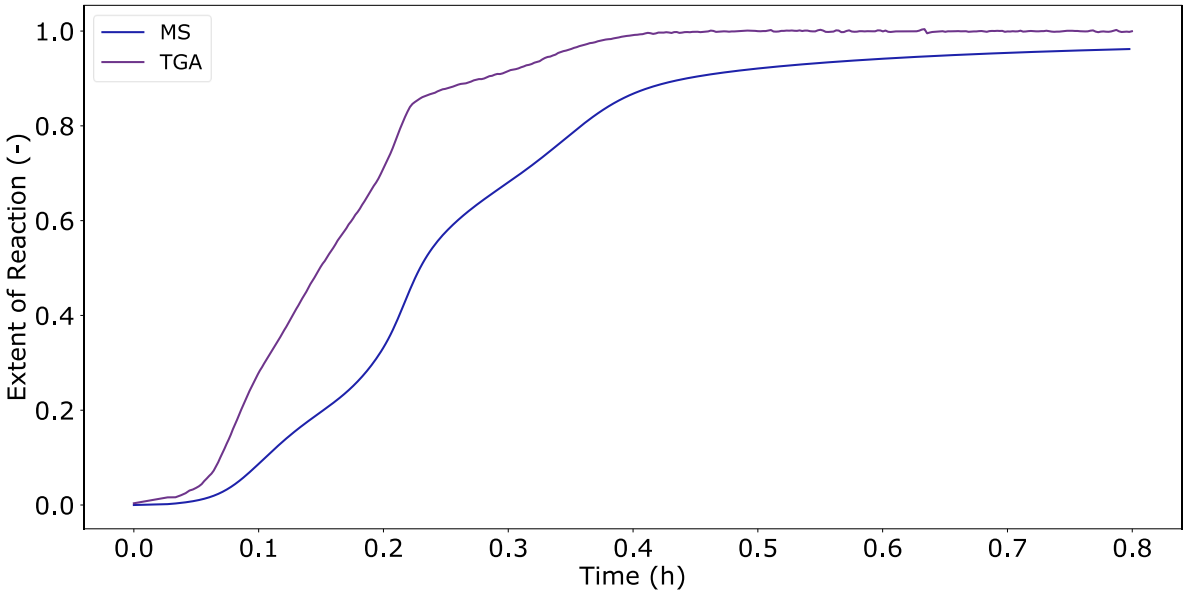

Figure 8.13: Comparison of thermogravimetric analysis extent of reaction and mass spectrometry extent of reaction constructed from Sestak-Berggren equation [3], reactor A, 20mL min^{-1}.

The TGA curve in Figure 8.13 shows the extent of reaction at the sample. However, this is affected by mass transport issues in the solid phase, so does not give a kinetically limited extent of reaction. As the signal has flatlined for a significant time, it can be assumed that all thermal events have gone to completion.

The calculated residence time between the sample pan and the reactor outlet for a gas flow rate of 20 mL min^{-1} is 1.3 min; this does not account for the capillary tube for the MS detection, or back mixing within the reactor. At an isoconversion point of 0.05, the delay time between the curves in Figure 8.13 is 1.68 min, reflecting the residence time distribution within the reactor. The change in MS curve shape, the delay in the start of the thermal events and the elongated nature of the events, reflects the bulk mass transport / back mixing occurring within this unit.

As the MS curve does not reach 1.0, at least one thermal event has not finished. This emphasises the need for an isothermal hold period at the end of these experiments, to allow all thermal events to reach completion. The possibility of unfinished thermal events should also be considered when baseline correcting such data. In the original study a baseline correction was applied to this data; this may not have been necessary and may have removed relevant data. This highlights the difficulties in trying to analyse transport limited data.

Figure 8.13 explains the difference in estimated parameter values from these datasets. They are describing the system at different points in space. The mass spectrometry data are convolved with the reactor RTD; this is reflected in the Da(R) value. From the Damköhler numbers, it is observed that neither the TGA nor the MS data are free from

transport effects, hence the nonsensical nature of the parameters estimated using the modified Sestak-Berggren model which assumes the data are kinetically limited.

However, the discrepancies in the ZSM-5 ammonia TPD case study discussed in Chapter 7 are not fully explained by this CFD study. As these TPD experiments were conducted in a tubular reactor, the bulk transport effects are small. This coupled with the lower than expected activation energy predicted implies another transport phenomenon may be occurring, such as internal diffusion issues or a reverse reaction. This would require further investigation and the development of kinetic models suitable for reversible reactions.

It is not clear from these results why the Sestak-Berggren modelling appeared successful for the SAPO-34 case, but not for the ZSM-5. It is possible that the effects of reversibility are impacted by strong diffusional resistances. It is also possible that the results of the SAPO-34 modelling are a coincidence. Further work is required to understand the impact of reversibility and internal diffusion on ammonia TPD profiles. The development of a criteria to demonstrate the absence of a reverse reaction and/or internal diffusion would be valuable.

8.6 Design of novel pan-style reactor

TGA experiments could be a vast opportunity for the extraction of scale independent kinetic parameters, providing intrinsic data can be obtained. The CFD study discussed earlier in this chapter has shown that obtaining intrinsic data from the current designs of pan-style reactors is difficult, hence a novel reactor design is required to allow TGA experiments to be carried out in a kinetically limited region.

A key finding from this CFD study was that to obtain intrinsic data, sufficient gas should flow through the sample. This minimises not only transport issues within the sample but also provides a better approach to plug flow for the carrier gas. The sketch in Figure 8.14 shows a proposed pan with a meshed bottom and top to retain the sample, which allows gas to pass through the sample.

As with existing hanging pan-style reactors, the reference and sample pans would be allowed to move freely to allow mass change to be measured. To force the carrier gas through the sample, a baffle with an annulus around each pan has been proposed. This would give a sufficient space velocity to prevent mass transport issues within the sample.

Preliminary design calculations related to a novel TGA reactor design concept have been completed, with full details supplied in Appendix B.

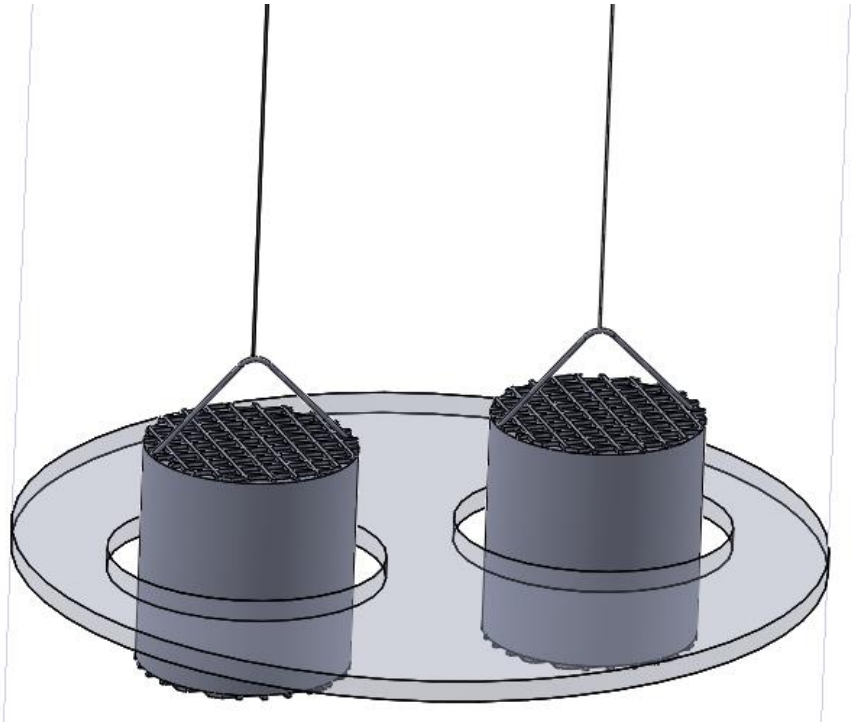

Figure 8.14: Sketch of novel TGA design concept.

In the following calculations, the weights of the reactor components have been converted to a scale-independent value of pressure drop to allow comparison, based on the area of each sample. Two theoretical cases have been considered, based on the results of the CFD study discussed above. First, ‘pan style 1’ was based on the sample diameter of 4 mm and a height of 5 mm (the same as reactor D), as this was shown to give the most favourable transport behaviour in the previous CFD study. Following the results for ‘pan style 1’, a second more extreme scenario, ‘pan style 2’ was investigated. ‘Pan style 2’ with a sample diameter of 30 mm and a height of 0.09 mm, represents a pan which would allow a single layer of sample particles. This scenario would not be feasible; however it shows the minimum possible pressure drop within the sample.

The pressure drop for ‘pan style 1 was taken from the previous CFD study on reactor D. A linear approximation based on the height of the sample was used to estimate the pressure drop for pan style 2.

Assumptions were made regarding the pan structure: the pan would be made of aluminium, the wall thickness would be 0.65 mm (based on the pans used in reactor B), and that mesh would be used to retain the powder sample on the top and bottom of the sample pan. These assumptions allowed an estimate to be made for the weight associated with the sample pan itself, converted to pressure drop for comparison.

For the sample, an initial mass of 100 mg has been assumed, with a mass loss of 45 %, based on calcium carbonate. The mass loss was translated into a pressure drop using the area of each sample.

Table 8.8 shows the values for the equivalent pressure drops for the flow through the packed bed, from the sample pan and the reduction in sample mass, for both proposed pan styles.

Table 8.8: Comparison of pressure drops, novel pan arrangements.

Contributor	Pan style 1	Pan style 2
	Pressure drop (Pa)	Pressure drop (Pa)
Flow through sample	4915	87.43
Sample pan	−130	−1.56
Initial sample	−44.4	−12.51
Change in sample mass	20	5.63

Table 8.8 shows the pressure drop associated with the flow of the carrier gas is much greater than the pressure drop associated with the weight, or weight change in the sample. This means detecting such small changes with a balance would be very unlikely. Retaining the sample within the sample pan may also be an issue, especially considering the meshed pan lid. Loss of sample from the pan would not only affect the measurement but could damage parts of the equipment downstream. These issues remain true for pan style 2, even with the reduced pressure drop, implying this issue cannot be solved by changing pan dimensions.

For the following calculations it has been assumed that the gas phase pressure drop is attributed to the annulus. Hence the pressure drop within the annulus is equal to the pressure drop in the sample/packed bed. This means that the full flow rate of gas is passing through the annulus and sample. For pan style 1, the required annulus size to ensure the specified pressure drop through the packed bed was calculated. First a feasible flow rate of 100 mL min^{-1} was used in the Darcy-Weisbach equation to calculate a combined annulus and sample pressure drop, given the target sample

pressure drop. From this, an annular width of $10\,\mu m$ can be inferred, which is not tenable for positioning of the sample pan consistently, or for manufacture. This small annular width would also cause turbulent flow through the annulus, which would cause the pan to move and is not consistent with the purpose of the equipment. Alternatively, a feasible annular width of 3 mm would require a flow rate of 1.69×10^6 mL min^{-1} which would be too high to give a meaningful EGA signal and equates to 99.9 % bypassing.

These calculations cover a wide range of conditions, of which none are suitable for conducting TGA experiments. It is unlikely that a balance would be sensitive enough to detect the small weight changes calculated, and the annular width required is unsuitable for experimentation of manufacture. Hence this proposed design was not feasible. Despite the flaws in the pan-style reactors studied using CFD, it appears these reactor designs may provide the best solution at the current time.

8.6.1 Alternative existing designs

There are several existing equipment designs which may be suitable for collecting intrinsic data. These include (but may not be limited to) a tapered oscillating microbalance (TEOM) and a DynTHERM unit from TA Instruments [23].

A TEOM measures inertial forces, rather than weight, and has often been used to measure the amount of a substance adsorbed onto a solid. The tapered glass element holds the sample and is attached to a cantilever beam. The natural frequency of oscillation of the glass element is monitored using a feedback amplifier. If the weight of the sample increases, the oscillating frequency decreases (and vice versa) [24]. A sketch of a TEOM is shown in Figure 8.15.

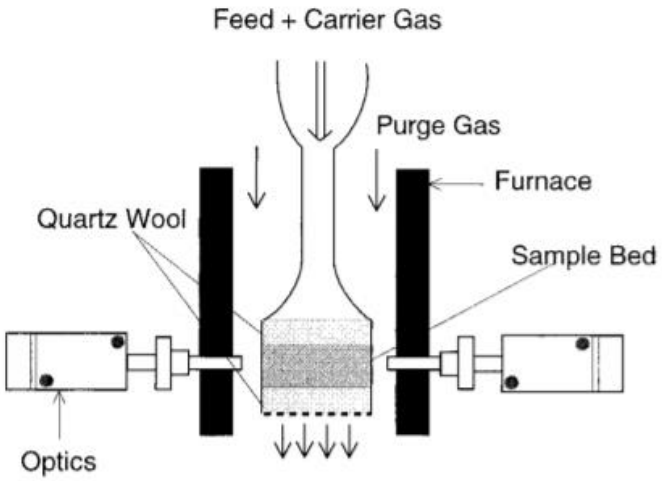

Figure 8.15: Sketch of TEOM [25].

Temperature programs, such as those needed for a TGA experiment are possible under isobaric conditions [25]. However, temperature ranges may be smaller when using the TEOM (up to around 973 K) and could limit thermal analysis experiments. This would require discussion with equipment manufacturers.

Initially the TEOM was designed to study the deactivation of catalysts by coke deposition [26], [27], but more recently this equipment has been used to investigate adsorption and diffusion in zeolites. Wang et al. [28] showed a TEOM could be used to monitor the oxidation and reduction of vanadium species. Chen et al. [29] showed examples of material characterisation of catalysts under reaction conditions. It may be possible to complete thermogravimetric analysis (TGA) on this type of instrument.

A DynTHERM unit has also been identified. Currently the DynTHERM is not primarily designed for thermal analysis of powders. The current design requires the gas to bypass the sample for a weight measurement to take place. Whilst this is acceptable for a coking reaction (which would stop when no gas flow is present), this would not be the case with a thermal transformation, which would continue. The weight

measurements for a coking reaction are also infrequent, whereas for thermal analysis ideally this would be continuous. These factors would mean that this equipment would require significant modifications to allow thermal analysis to be carried out.

To confirm intrinsic data could be achieved, from either the TEOM or the DynTHERM, a CFD study following the methodology outlined in Section 8.2 [30] would be required for these units.

8.7 Conclusions and recommendations

8.7.1 Pan-style reactors (reactors A and B)

Pan style equipment cannot be used for kinetic analysis, including comparing peak temperatures, onset temperatures or shapes of peaks. The only valid information which can be extracted from pan style thermal analysis equipment (most TGA units) is:

- A final residual mass (providing steady state has been observed for a sufficient period of time to be confident that no further reaction will occur).
- Species identification, when coupled with evolved gas analysis (EGA).
- A rough temperature range for a thermal event can be estimated.
- If thermal events are sufficiently separated, species and mass changes can be identified with a relevant event.

Due to the mass transport issues in these reactors, evolved gas is not removed sufficiently rapidly from the sample. For reversible reactions, this means that the reverse reaction could have a significant impact on the results obtained. It may be possible that irreversible reactions, when experiments are carried out at high carrier

gas flow rates, are free from bulk transport limitations however further study to confirm this is required.

These pan style arrangements cannot be used to compare different materials, as differing amounts of gas released, and the type of gas released will alter the residence time profiles shown in this chapter.

The pan style reactors show a significant temperature lag between the sample and the specified wall temperature. This lag is dynamic throughout a linear temperature ramp rate experiment, and worse at lower temperatures. Traditional calibration is insufficient to account for this temperature lag in the sample. As an accurate measurement for the temperature of the sample is required for kinetic experiments, it is not advised to use these pan-style reactors to extract intrinsic data.

Thermogravimetric analysis experimentation carried out on pan-style reactors could be heavily mass and heat transport limited and these experiments should be analysed carefully, to avoid kinetic parameters which appear dependent on temperature ramp rate [31]. Other reactor configurations are available for TGA and this methodology should be applied when selecting equipment. Novel designs for these thermal analysis reactors could also be considered.

8.7.2 Tubular reactors (reactors C and D)

Tubular reactors can be suitable for kinetic experiments, depending on the shape of the tube and carrier gas flow rates chosen. Specific care should be taken when using reactor tubes with constrictions after the sample bed, such as reactor C in this study, as these may not produce intrinsic data.

Tubular reactors with uniform diameters can produce intrinsic data, however the units considered in this work do not have the capability to carry out thermogravimetric analysis. Alternative tubular arrangements such as a tapered element oscillating microbalance (TEOM) could be viable alternatives for weight measurements [24]. It is advised that if carrying out kinetic studies, experimenters should either check the expected reaction rate from literature or generate a rough estimate after initial experiments.

Tubular reactors show a fast temperature change when perturbed and a minimal lag between the specified wall temperature and the sample temperature for a simulated linear temperature ramp. The contact between the sample and the walls of the reactor aids in conductance, resulting in good heat transfer. It is expected that these good heat transfer properties would be retained in any tubular arrangement where the sample is in contact with the reactor walls. This tendency for good heat transfer reinforces that these tubular reactor types would be the most suitable for kinetic experimentation.

8.7.3 Other learning

This dimensionless analysis has confirmed the uniform diameter tube style reactors operate in a plug flow regime, which means a reaction may not be treated as a point source. Currently models for solid-state reactions, including the modified Sestak-Berggren model, assume a point source. Strictly, these kinetic models would require adaptation for plug flow behaviour however there are some cases where the assumption of a point source may still be applicable, such as irreversible reactions studied under high carrier gas flow rates.

Trivial comparison of results between equipment types should be avoided. Comparison between reactors is only valid if it can be shown that the properties of the sample are measured, rather than the properties of the reactor. Each reactor type in this report has differing degrees of mass transport issues; these would need to be accounted for, which is not always trivial, prior to any comparisons being made. It is important to be aware of the transport limitations possible within the equipment chosen for a given experiment.

The following guidelines for the interpretation of thermal analysis data are recommended:

- For kinetic studies, uniform diameter tubular flow through reactors should be used.
- When performing kinetic analysis on any thermal analysis data, residual trends with temperature ramp rate should be analysed, as these can indicate the presence of heat/mass transport effects.
- Pan style or non-uniform tubular reactors should not be used for kinetic studies.
- Pan style or non-uniform tubular reactors should not be used to compare different materials.
- Thermal analysis results obtained using different equipment should not be directly or trivially compared. Comparison may be possible but requires careful analysis and a full understanding of the mass transport occurring within the reactors in question.

To validate these simulations, an instantaneous gas release would be required at a specific temperature. This means a decomposition reaction would need to be

extremely fast. In this case, a traditional reactor tracer experiment would not be suitable, as the tracer gas must be evolved from the sample location, rather than the inlet of the reactor. The author is not aware of any suitable reaction systems which could demonstrate the instantaneous release of gas from the sample which has been simulated with the CFD study. The inclusion of Section 8.5 aims to show the transport issues identified using these CFD simulations have been observed in experimental data.

An attempt was made to design a TGA pan style unit which could produce intrinsic data. It was concluded that the proposed designed was flawed. The balance was unlikely to detect the small mass changes in the sample compared to the force exerted by the carrier gas, and the annulus size required to achieve an appropriate pressure drop was too small to be practical. Although the current designs for these hanging pan style reactors are not ideal, they appear to be the best we can buy/commission presently with little evident opportunity for significant improvement. Alternative equipment such as a TEOM have been suggested, however a further CFD study would be required to confirm their ability to obtain intrinsic data.

8.8 References

[1] M. E. Brown *et al.*, ‘Computational aspects of kinetic analysis Part A: The ICTAC kinetics project-data, methods and results’, *Thermochim. Acta*, p. 19, 2000.

[2] I. Halikia, L. Zoumpoulakis, E. Christodoulou, and D. Prattis, ‘Kinetic study of the thermal decomposition of calcium carbonate by isothermal methods of analysis’, no. 2, p. 14, 2001.

[3] R. L. Gibson, M. J. H. Simmons, E. Hugh Stitt, J. West, S. K. Wilkinson, and R. W. Gallen, ‘Kinetic modelling of thermal processes using a modified Sestak-Berggren equation’, *Chem. Eng. J.*, vol. 408, 2021, doi: 10.1016/j.cej.2020.127318.

[4] R. Buczyński, G. Czerski, K. Zubek, R. Weber, and P. Grzywacz, ‘Evaluation of carbon dioxide gasification kinetics on the basis of non-isothermal measurements and CFD modelling of the thermogravimetric analyser’, *Fuel*, vol. 228, pp. 50–61, Sep. 2018, doi: 10.1016/j.fuel.2018.04.134.

[5] R. Comesaña, J. Porteiro, E. Granada, J. A. Vilán, M. A. Álvarez Feijoo, and P. Eguía, ‘CFD analysis of the modification of the furnace of a TG–FTIR facility to improve the correspondence between the emission and detection of gaseous species’, *Appl. Energy*, vol. 89, no. 1, pp. 262–272, Jan. 2012, doi: 10.1016/j.apenergy.2011.07.029.

[6] R. Comesaña, M. A. Gómez, M. A. Álvarez Feijoo, and P. Eguía, ‘CFD simulation of a TG–DSC furnace during the indium phase change process’, *Appl. Energy*, vol. 102, pp. 293–298, Feb. 2013, doi: 10.1016/j.apenergy.2012.07.019.

[7] A. Benedetti, M. Modesti, and M. Strumendo, ‘CFD Analysis of the CaO-CO2 Reaction in a Thermo-gravimetric Apparatus’, *Chem. Eng. Trans.*, vol. 43, May 2015, doi: 10.3303/CET1543174.

[8] M. E. Brown, *Introduction to Thermal Analysis: Techniques and Applications*. Springer Science & Business Media, 2001.

[9] ‘Air - Density, Specific Weight and Thermal Expansion Coefficient at Varying Temperature and Constant Pressures’. https://www.engineeringtoolbox.com/air-density-specific-weight-d_600.html (accessed May 18, 2020).

[10] ‘Air - Dynamic and Kinematic Viscosity’. https://www.engineeringtoolbox.com/air-absolute-kinematic-viscosity-d_601.html (accessed May 18, 2020).

[11] ‘Air - Specific Heat at Constant Pressure and Varying Temperature’. https://www.engineeringtoolbox.com/air-specific-heat-capacity-d_705.html (accessed May 18, 2020).

[12] ‘Air - Thermal Conductivity’. https://www.engineeringtoolbox.com/air-properties-viscosity-conductivity-heat-capacity-d_1509.html (accessed May 18, 2020).

[13] ‘A Guide to the NIST Chemistry WebBook’. https://webbook.nist.gov/chemistry/guide/ (accessed Apr. 21, 2021).

[14] ‘Materials Database - Thermal Properties’, *Thermtest Inc.* https://thermtest.com/materials-database (accessed May 18, 2020).

[15] B. A. Moreira, F. D. O. Arouca, and J. J. R. Damasceno, ‘Analysis of Relationships Between Permeability, Pressure on the Solids, and Porosity for Calcium Carbonate’, in *Sedimentation Engineering*, A. Amini, Ed. InTech, 2018. doi: 10.5772/intechopen.72913.

[16] A. Elements, ‘Fused Quartz Wool’, *American Elements*, 2020. https://www.americanelements.com/fused-quartz-wool-14808-60-7 (accessed Oct. 08, 2020).

[17] A. S. Iberall, ‘Permeability of glass wool and other highly porous media’, *J. Res. Natl. Bur. Stand.*, vol. 45, no. 5, p. 398, Nov. 1950, doi: 10.6028/jres.045.043.

[18] H. S. Fogler, *Elements of chemical reaction engineering*, Fifth edition. Boston: Prentice Hall, 2016.

[19] O. Levenspiel, *Chemical reaction engineering*, 3rd ed. New York: Wiley, 1999.

[20] M. Maciejewski, ‘Computational aspects of kinetic analysis. Part B: The ICTAC Kinetics Project - the decomposition kinetics of calcium carbonate revisited, or some tips on survival in the kinetic minefield’, *Thermochim. Acta*, p. 10, 2000.

[21] G. Damköhler, ‘Einflüsse der Strömung, Diffusion und des Wärmeüberganges auf die Leistung von Reaktionsöfen.: I. Allgemeine Gesichtspunkte für die Übertragung eines chemischen Prozesses aus dem Kleinen ins Große’, 1936. doi: 10.1002/BBPC.19360421203.

[22] J. Sestak and G. Berggren, ‘Study of the kinetics of the mechanism of solid-state reactions at increasing temperatures’, *Thermochim. Acta*, vol. 3, pp. 1–12, 1971.

[23] ‘DynTHERM – High Pressure TGA’, *TA Instruments*, 2020. https://www.tainstruments.com/dyntherm/ (accessed Aug. 10, 2020).

[24] R. J. Berger *et al.*, ‘Dynamic methods for catalytic kinetics’, *Appl. Catal. Gen.*, vol. 342, no. 1, pp. 3–28, Jun. 2008, doi: 10.1016/j.apcata.2008.03.020.

[25] W. Zhu, J. M. van de Graaf, L. J. P. van den Broeke, F. Kapteijn, and J. A. Moulijn, ‘TEOM: A Unique Technique for Measuring Adsorption Properties. Light Alkanes in Silicalite-1’, *Ind. Eng. Chem. Res.*, vol. 37, no. 5, pp. 1934–1942, May 1998, doi: 10.1021/ie970739q.

[26] D. Chen, A. Grønvold, H. P. Rebo, K. Moljord, and A. Holmen, ‘Catalyst deactivation studied by conventional and oscillating microbalance reactors’, *Appl. Catal. Gen.*, vol. 137, no. 1, pp. L1–L8, 1996, doi: 10.1016/0926-860X(96)00002-6.

[27] F. Hershkowitz, H. S. Kheshgi, and P. D. Madiara, ‘Activity and Deactivation in Catalytic Cracking Studied by Measurement of Adsorption During Reaction’, in

Fluid Catalytic Cracking III, vol. 571, 0 vols, American Chemical Society, 1994, pp. 178–192. doi: 10.1021/bk-1994-0571.ch015.

[28] D. Wang, H. H. Kung, and M. A. Barteau, 'Identification of vanadium species involved in sequential redox operation of VPO catalysts', *Appl. Catal. Gen.*, vol. 201, no. 2, pp. 203–213, Jul. 2000, doi: 10.1016/S0926-860X(00)00439-7.

[29] D. Chen, E. Bjorgum, K. O. Christensen, A. Holmen, and R. Lodeng, 'Characterization of Catalysts under Working Conditions with an Oscillating Microbalance Reactor', in *Advances in Catalysis*, vol. 51, B. C. Gates and H. Knözinger, Eds. Academic Press, 2007, pp. 351–382. doi: 10.1016/S0360-0564(06)51007-7.

[30] R. L. Gibson, M. J. H. Simmons, E. H. Stitt, L. Liu, and R. W. Gallen, 'Non-kinetic phenomena in thermal analysis data; Computational fluid dynamics reactor studies', *Chem. Eng. J.*, vol. 426, p. 130774, Dec. 2021, doi: 10.1016/j.cej.2021.130774.

[31] B. Janković, N. Manić, D. Stojiljković, and V. Jovanović, 'TSA-MS characterization and kinetic study of the pyrolysis process of various types of biomass based on the Gaussian multi-peak fitting and peak-to-peak approaches', *Fuel*, vol. 234, pp. 447–463, Dec. 2018, doi: 10.1016/j.fuel.2018.07.051.

9. Conclusions

Thermal processes are a common manufacturing step in many of the products supplied by JM. Gaining a fundamental understanding of these solid-state processes could allow for designed scale up and improvement of product formulations.

The introduction to this thesis outlined the benefits that a model-based approach to thermal processes could have on JM manufacturing. For example, use of thermal analysis to identify suitable temperatures, temperature ramp rates and processing times could minimise capital costs for new infrastructure, and reduce energy usage and operational costs. These small-scale experiments could give insight into potential safety hazards within a process, such as a release of flammable gas. Identifying these hazards and the conditions which they may arise, is key to a safe process scale-up.

To achieve these benefits, it is key to understand the fundamentals at a small-scale. This thesis has discussed the first steps taken to develop this knowledge via modelling of thermal analysis data and equipment.

Thermal analysis has been widely studied in the literature and there are many modelling methods available. However, these modelling methods are often employed without consideration of the underlying assumptions and model criticism is generally lacking in the literature. Chapter 3 discussed in detail the range of modelling techniques available, and for which scenarios these are applicable. This work aimed to develop a single modelling methodology that would apply to the broad range of experiments within the thermal analysis field. This modelling has been coupled with a high level of statistical rigor and consistent model criticism.

The modelling of thermal analysis data assumes that the data collected are kinetically limited, hence mass or heat transport effects are not present within the reactor. Quantifying the transport phenomena occurring within thermal analysis reactors is important to understand, as this impacts data analysis and the suitability of this data to provide information for process scale up. However, analysis of thermal analysis reactors is lacking in the literature. This thesis has outlined a methodology for quantifying the transport phenomena occurring within these reactors and allows for comparison of reactor configurations. This has led to recommendations for the collection of intrinsic data.

The introduction to this thesis outlined three objectives for this work and this final chapter will reflect on these and suggest possible future work in this area.

9.1. A unified approach for the kinetic modelling of thermal analysis experiments

A modified Sestak-Berggren modelling approach has been implemented and tested using *in silico* data, allowing the sensitivity and quality of fit to be explored systematically for the first time [1]. Further, in this *in silico* evaluation, the impact of "white noise" on the quality of fit was determined, indicating that additional temperature ramp rate experiments are required, over the standard recommendation of five temperature ramp rates.

The modified Sestak-Berggren modelling methodology has been outlined in Chapter 4, including *in silico* verification and experimental validation. Mathematical singularities within the existing Sestak-Berggren equation have been addressed using a Taylor series expansion around a specific point. This allowed the Sestak-Berggren model to

be applied over the full range for the extent of reaction (between 0 and 1). The modified Sestak-Berggren model was used for kinetic deconvolution of multiple overlapped thermal events simultaneously. The most statistically likely number of thermal events was identified using Akaike weights, which gives a rigorous statistical basis for event addition.

The modified Sestak-Berggren model indicates the most likely reaction mechanism for each thermal event, speeding up model discrimination. The identified reaction mechanism is then used to extract physically meaningful kinetic parameters. This unified approach allows for quantitative evaluation of thermal analysis experiments.

The methodology was also tested using an *in silico* dataset with added white noise. It was found that additional temperature ramp rate experiments may be required (over the standard five temperature ramp rates) to have confidence in the estimated parameter values. The amount of additional information required would depend on the level of noise in the data. It was concluded that for dataset which contained less than 5 % white noise, estimated using a moving average model, the standard five temperature ramp rate experiments would be sufficient for kinetic analysis.

9.2. Applied to a range of experiments and equipment

The applicability of the modified Sestak-Berggren modelling methodology to a wide range of thermal analysis experiments with a range of objectives has been demonstrated. Initial steps towards a suitable model for process scale up was demonstrated using a temperature programmed reduction (TPR) case study. The model was also used to extract kinetic information from ammonia temperature

programmed desorption (TPD), which provides an industrially relevant alternative characterisation method to expensive spectroscopic techniques.

Multiple experimental case studies have been treated with the modified Sestak-Berggren methodology, including TPR, TPD and temperature programmed decomposition (TPDecomp). These experiments have been carried out in a range of equipment, including the u-tube flow through and pan-style reactors and have a range of outputs: thermal conductivity detector, mass spectrometry and weight.

Both the TPR case study discussed in Chapters 4 and 5, and the TPD of ammonia on SAPO-34 in Chapter 6 demonstrated the success of the modified Sestak-Berggren methodology. In these case studies, kinetic deconvolution was completed using the Sestak-Berggren equation and suitable reaction mechanisms were identified for each thermal event. The thermal events were then modelled using the indicated reaction mechanisms to determine physically meaningful kinetic parameters. These examples show the validity and statistical rigour of this modelling methodology for a range of thermal analysis experiments.

Chapter 7 discussed two case studies for which implausible kinetic mechanisms were indicated by the modified Sestak-Berggren equation, and a case study which used design of experiments to investigate the impact of weight hourly space velocity (WHSV). These implausible mechanisms, along with systematic trends in residuals as a function of temperature ramp rate and the failure to estimate all parameters when using a range of WHSVs, implied effects within the data which were not captured by the irreversible, kinetically limited Sestak-Berggren equation. As confidence in the

modelling methodology had already been established, reversibility or transport phenomena were identified as possible sources of these non-kinetic effects.

9.3. Simultaneous regression of different temperature programs

Data gathered using linear temperature ramp rate experiments and constant rate thermal analysis (CRTA) have been regressed as a single dataset for the first time [2]. Although CRTA data may provide a better constraint for the model than the linear temperature ramp rate experiments, it was concluded that the use of CRTA coupled with linear temperature ramp rate experiments may provide an industrially relevant compromise by improving the separation of thermal events whilst minimising the experimental time and cost.

9.4. Characterisation of reactors using reaction engineering principles.

A high level of model criticism allowed for the identification of possible non-kinetic effects within certain datasets. This led to a new methodology using dimensionless groupings for the identification and comparison of transport phenomena occurring within thermal analysis reactors [3]. Pan-style reactors were shown to be heat and mass transport limited, while tubular reactors can extract intrinsic data.

Chapter 8 discussed the computational fluid dynamics (CFD) study of four different thermal analysis reactors. A methodology has been established for comparing these units and quantifying the transport phenomena occurring. This method uses residence time distributions gathered from the CFD modelling and dimensionless analysis,

specifically Damköhler numbers, to determine the dominant regime (either kinetic or transport limited).

Pan-style thermal analysis reactors were shown to have significant heat and mass transport limitations, within the sample and the bulk gas. This means data from these types of reactor should not be assumed to be kinetic or analysed as such, this includes the comparison of peak temperatures, onset temperatures or peak shapes.

Tubular reactors with uniform diameter were found to be capable of producing intrinsic data, however calculations to check the expected reaction rate (compared to that used in this study) should be made. Care should be taken if using tubular reactors with constrictions after the sample, as this could cause axial mixing. These tubular reactors showed a minimal temperature lag and benefit from the sample having direct contact with the reactor wall.

Although these tubular reactors with uniform diameter produce a PFR behaviour, these would likely not satisfy the point source assumption of the solid-state kinetic models discussed in this work. Modifications would be required to account for the PFR behaviour within the solid bed.

Some initial short calculations were completed to determine the feasibility of a new thermogravimetric analysis (TGA) unit. This unit aimed to minimise the bulk transport phenomena shown to be prevalent within pan style reactors. However, the results of the initial calculations showed that detecting small weight changes (as required in TGA) would not be possible. It was concluded that the current TGA / pan style reactor designs may be the best possible, despite the transport issues. It was suggested that

a tapered oscillating microbalance (TEOM) may provide an alternative source of intrinsic data.

9.5. Recommendations for industry practice

An output from this thesis is a list of key recommendations for obtaining and analysing thermal analysis data:

- Pan-style reactors should be assumed to be transport limited, unless demonstrated otherwise.
- Tubular reactors should be used to collect intrinsic data.
- Experimental conditions, including reactor choice, carrier gas flow rate and expected reaction rate should be evaluated using the dimensionless analysis outlined in this thesis to determine the expected dominating region.
    - Other suitable diagnostic methods demonstrated in this thesis would include:
        - Use of DoE to investigate the impact of weight hourly space velocity.
        - Model criticism; checks should be made for systematic trends in residuals as these imply non-kinetic behaviour.
- Non-kinetic behaviour will introduce bias and falsify the results of kinetic analysis, which includes interpretation of thermal analysis results by eye.
- Comparing different materials or results from different thermal analysis equipment should done with extreme caution. Full understanding of the transport phenomena occurring is required to make meaningful comparisons.

9.6. Future work

This thesis has highlighted the need for further investigations, which can be categorised as experimental, or modelling based.

9.6.1. Experimental

Having quantitative evolved gas analysis (EGA) as standard with all thermal analysis techniques could aid in mechanistic understanding of the processing occurring. This would not only give information about the composition of the gases produced but allow quantities to be used when deriving potential mechanisms, as discussed in Chapter 5.

The inadequacies of the current pan-style reactors, specifically the issues of long residence times and of diffusing evolved gases into the bulk flow, cannot be solved trivially through modelling. Obtaining intrinsic TGA data is an important requirement for industry, especially if this data is to be used as a basis of safety for process scale up. New reactor designs are required, or alternative set ups require investigation.

9.6.2. Modelling

A natural continuation of this work involves four main areas: the development of more solid-state models, incorporation of reactor-scale models, further scale up of thermal processes and use of models for inherently safe design.

Within this thesis, a methodology for independent overlapped thermal events has been developed. As discussed in Chapter 3, thermal events can also be competing or consecutive. Model development to capture competing and consecutive reactions would allow for more varied systems to be modelled accurately. Reversible reactions are another area for development as the modified Sestak-Berggren methodology outlined in this work accounts for irreversible reactions only. Many solid-state reactions

are reversible and suitable models to capture equilibrium limited reactions would also allow more systems to be described mathematically. Suitable models may already exist in the literature, such as those mentioned in Chapter 7, however these require further investigation with appropriate data.

For the tubular reactors discussed in Chapter 8, the approximate plug flow behaviour manifests as time lag between the sample and detector. The solid-state mechanisms, and Sestak-Berggren model discussed in this work assume point source behaviour of the sample and reactor. Reactor-scale models would be required to account for the lag issues identified in these tubular reactors.

Continued scale up of thermal processes based on small scale lab experiments coupled with modelling is still required. This could include analysis of calorimetry experiments, which are conducted on a slightly larger scale (grams compared to milligrams) than thermal analysis experimentation. Calorimetry is used to measure energy transfer during a chemical reaction and could be used to inform safety in the scale-up of thermal processes.

The modelling methods in this thesis could be applied to materials which pose safety issues during large-scale processing. For example, materials which produce an explosive atmosphere during calcination. Modelling of these processes could allow for the design of safe calcination procedures, such as stepwise isothermal temperature programs, to ensure flammable or explosive products are removed prior to their autoignition temperatures.

Generally, further work is required to improve the synergy between physical and statistical modelling techniques. This work has demonstrated that a combination of

both modelling types can provide insight above and beyond that obtained when these techniques are used in isolation.

9.7. References

[1] R. L. Gibson, M. J. H. Simmons, E. Hugh Stitt, J. West, S. K. Wilkinson, and R. W. Gallen, ‘Kinetic modelling of thermal processes using a modified Sestak-Berggren equation’, *Chem. Eng. J.*, vol. 408, 2021, doi: 10.1016/j.cej.2020.127318.

[2] R. L. Gibson, ‘Simultaneous kinetic modelling of data collected with different temperature programs’, *Paper in draft*.

[3] R. L. Gibson, M. J. H. Simmons, E. H. Stitt, L. Liu, and R. W. Gallen, ‘Non-kinetic phenomena in thermal analysis data; Computational fluid dynamics reactor studies’, *Chem. Eng. J.*, vol. 426, p. 130774, Dec. 2021, doi: 10.1016/j.cej.2021.130774.

A. Selection of formal baseline correction methods in thermal analysis unit

A.1 Introduction

Thermal analysis is an invaluable tool in materials research and development [1]. This class of experimentation can be used to extract information on mass changes and thermodynamics, kinetics, sintering and heat capacity, crystalline formations and oxygen content, amongst others [1]. In many of these thermal analysis experiments, baseline drifts are observed, and this must be accounted for prior to the extraction of kinetic information from the data. A rigorous and accurate methodology for baseline correction is required, as quantitative data analysis is being carried out more frequently with thermal analysis data [2]–[4], with the aim of extracting kinetic and mechanistic information.

A baseline is the signal produced when no detectable thermal events are occurring. These baselines are used to identify the start and end of the thermal events occurring during an experiment. To extract meaningful kinetic parameters from these thermal analysis experiments, the data must be treated with a baseline correction method [5], which is a function subtracted from the data. Some papers refer to the need for baseline correction, but do not identify the methods used to carry out this subtraction [6], [7]. Similarly, while the issues with extracting information from unstable baselines is referred to in Maciejewski [2], methods to overcome them are not addressed. Most of the literature which discusses thermal analysis does not refer to baseline correction. It may be that the data were deemed to be free from baseline drift (which can be the case), or that correction methods have been used but not stated. In some cases, the

figures presented in the literature appear to contain baseline drift, but this issue is not addressed [8], [9].

It is common to use computer software in the fitting of these baseline corrections [10]. These programs often require the experimenter to assign the initial and final baseline points, which can be subjective and based on experience. This work aims to remove the subjective nature of baseline correction and to show how the selection of a baseline correction method should be based on a statistical approach.

Many factors can cause the baseline to change during an experiment, and this change must be accounted for prior to extracting information from the data. For kinetic studies using TGA data, the first derivative is required. The baseline drift present in these data are recognised and mainly associated with buoyancy effects or changes in these effects [4]. The impact of these depends upon the experimental setup. For example, buoyancy effects may have a larger impact when using a vertical flow arrangement rather than a horizontal set up. The appearance of this baseline drift also depends on the instrument set up, as buoyancy can be observed as either a weight loss or weight gain depending on the instrument used. Baseline drifts within DSC measurements are well known, and it is recognised that the baseline originates from the temperature dependence of the heat capacities, reactants, intermediates, products and the amount by which these change throughout the process [4]. For TPR/TPD experiments there are several possible sources of baseline drift: pressure; an increase in pressure caused by a contraction/flow restriction, volume of gas; a leak in the system which would decrease the volume of gas passing the detector, water ingress; changes to the composition of the gas stream and hence the conductivity detected by the thermal conductivity detector (TCD). For mass spectrometry (MS), changes in baseline shown

in the data may be due to the presence of ambient gases in the supplied carrier gas, more than one species with a given mass-to-charge ratio or variation in vacuum within the equipment.

It is common, but not necessary [11], for peaks observed in thermal analysis experiments to be deconvoluted prior to kinetic modelling. Michael et al. [12] and Hemminger & Sarge [5] both recommend that this deconvolution be carried out prior to the baseline correction, such that each thermal event has its own baseline. Baselines based on the individual thermal event would not apply if the reasons for the baseline drift occur due to a process condition, such as a leak. This means that using this method of baseline correction would not account for these types of baseline drifts, though use of an overall baseline correction would. This study of baseline correction methods will be combined with the methodology reported in Chapter 4. [11], which does not require peak deconvolution, hence overall baselines are considered in this work.

The International Confederation for Thermal Analysis and Calorimetry (ICTAC) recommend that for kinetic analysis which requires multiple heating rate experiments, the same baseline correction method should be applied to all data sets [4]. Additionally, various baseline correction methods should be trialled, with the kinetic modelling completed and statistics for each method compared before a method is selected. This would, importantly, reveal the impact on the kinetic parameters estimated [4]. This work aims to show a methodology for comparing baseline correction methods, through the use of Akaike weights [13]. This statistical technique evaluates the amount of information lost through modelling and indicates which of the well-fitting models considered would be the most likely to describe the system.

Hemminger & Sarge [5] described the use of three groups of baseline correction methods; formal methods (these lack physical justification), methods based on physico-chemical assumptions and experimental methods. Although Hemminger & Sarge [5] study the baseline construction for DSC curves, these baseline categories can be extended to most thermal analysis experiments.

Experimental methods to establish a baseline are common within thermal analysis. For a TGA experiment, the buoyancy effects causing the baseline drift can be captured by carrying out a blank TGA run with an empty sample pan. The curve produced from this experiment would then be subtracted from the TGA curve when the sample is present [14]. This is the simplest form of obtaining a baseline experimentally. Other similar experiments can be run using inert samples [5]. Other more complex examples use simultaneous experimental techniques to identify suitable baselines for correction [5], [15].

Physico-chemical methods require physical reasoning. Niet et al. [16] use a step-change baseline correction for their TPD work, explained by the water used in the TPD adsorbing onto the stainless-steel walls of the reaction chamber. For DSC measurements it has been established that the tangential area-proportional baseline should be used to capture the heat capacity temperature dependencies [17]. Svoboda [18]–[20] has discussed this baseline correction technique in detail, including a comparison with interpolations commonly pre-programmed into commercial software.

It is advised that where possible and where a physical basis is present, either experimental or physico-chemical baseline correction methods should be attempted, for example the use of a tangential area-proportional baseline correction. However,

this work will focus on formal baseline correction techniques. These should only be considered in the absence of any physical or experimental reasoning for a baseline drift.

There are many possible options for the type of function to be constructed between two data points (initial and final baseline). Theoretical/nonphysical methods can range from a simple function such as straight lines to more complex ones such as sigmoidal curves [5]. It has been well established that models should use as few parameters as is practical whilst giving an accurate representation of the data [21], [22]. Over-parameterisation may lead to an improved closeness of fit (by capturing more of the variance in the measured data) and yet decrease quality of fit for a model (by introducing bias in the model) [22]. To avoid over-parameterisation, the only function which can be justified for connecting two points is a linear function, i.e. a straight line. In the absence of further data, other possible functions would be ill-constrained. This straight line can use either the time, temperature or extent of reaction as its independent variable. Other functions such as final point backwards (extrapolating from the final baseline back to the start time of the experiment), have no justification and should be avoided. Similarly, high order polynomials [23] and other curves should be avoided, as these have too many degrees of freedom. Along with these linear baseline correction methods, the absence of correction should also be considered.

In this work a method of selecting the most statistically likely formal baseline correction technique will be discussed and demonstrated with both *in silico* and experimental datasets. *In silico* data, representing a temperature programmed experiment, will be used to demonstrate the internal consistency of the baseline correction models, the impact of selecting an unsuitable correction method, and the use of Akaike weights to

select the most suitable correction method. The experimental case study, a zinc nitrate catalyst precursor decomposition, demonstrates the applicability of the proposed methodology using real data. The aim of this work is to remove the human or experiential element which is often present in baseline correction of thermal analysis data.

A.2 Modelling methods

The baseline correction methods are combined with the modified Sestak-Berggren modelling in Athena Visual Studio, as described in Chapter 4 and are estimated alongside the modified Sestak-Berggren model itself. The four baseline correction methods considered in this work take the forms shown in Equations (A.1-A.4).

No correction $$\varepsilon_{BL} = 0.0$$ Eq.(A.1)

Linear with time $$\varepsilon_{BL} = M.t + C$$ Eq.(A.2)

Linear with temperature $$\varepsilon_{BL} = M.T + C$$ Eq.(A.3)

Linear with extent of reaction $$\varepsilon_{BL} = M.(\sum F_{v,i}.\alpha_i) + C$$ Eq.(A.4)

The kinetic modelling used in this work is based on the modified Sestak-Berggren equation [11], Equation A.5. This methodology does not require *a priori* peak deconvolution. Non-linear least-squares regression has been used in Athena Visual Studio, with default tolerances [24], with the aim of minimising the residual on $\frac{d\alpha}{dt}$, the dimensionless signal. The model reported in Chapter 4 [11] is extended with the addition of the contribution from the unknown baseline.

$$\frac{d\alpha}{dt} = \sum_{i=1}^{n_{events}} F_{v,i} \cdot A_i \cdot \exp\left(\frac{Ea_i}{R.T_{b,i}}\left(1 - \frac{T_{b,i}}{T}\right)\right) \cdot (1-\alpha_i)^{n_i}\alpha_i^{m_i} + \varepsilon_{BL} \quad \text{Eq.(A.5)}$$

This form of the Sestak-Berggren equation can represent a range of solid-state reactions [25]–[27]. This methodology is also based on the assumption of independent thermal events. There may be cases which contain energetically similar sequential reactions or competing reactions [27], [28], for which this model would not be suitable.

This empirical kinetic model is used in this work to demonstrate the incorporation of the formal baseline into a regression, and the use of Akaike weights. The choice of kinetic model would not impact the baseline correction methodology described in this work; the modified Sestak-Berggren equation could be replaced with any other kinetic model.

Data are regressed with each of the four candidate formal baseline models. Akaike weights [13] which are based on the Akaike information criterion [29] can be used to discriminate candidate baseline correction methods. Equation A.6 shows a specific case of the corrected AIC, for least squares regression [30]. Equations A.7 and A.8 show the method for calculating the Akaike weights.

$$AICc = -\varphi \cdot log\left(\frac{RSS}{\varphi}\right) + 2\omega + \frac{2\omega(\omega+1)}{\varphi-\omega-1} \quad \text{Eq. (A.6)}$$

$$\Delta_j = AICc_j - AICc_{min} \quad \text{Eq. (A.7)}$$

$$w_j = \frac{exp\left(-\frac{\Delta_j}{2}\right)}{\sum_{s=1}^{S} exp\left(-\frac{\Delta_s}{2}\right)} \quad \text{Eq. (A.8)}$$

Where φ is the number of data points, ω is the number of estimable parameters (which is the number of explicit parameters in the model plus the variance of the error) and RSS represents the residual sum of squares.

This Akaike weights methodology incorporates the closeness of model fit (through the RSS value) and the number of estimated parameters in a model (ω - 1). This avoids the selection of over-parametrised models. Table A.1 shows a theoretical case of two models A and B, which have the same RSS value and number of datapoints but differ in the number of parameters estimated.

Table A.1: Comparison of Akaike weights for theoretical models.

Metric	Model A	Model B
Number of parameters	9	11
RSS	6.79×10^{-6}	6.79×10^{-6}
$\boldsymbol{\sigma}$	3910	3910
Akaike weight	0.88	0.12

Even though both models in Table A.1 would provide a good closeness of fit, reflected in the RSS value, Model A with the lower number of estimated parameters has a clear majority share of the Akaike weights. This emphasises the need to justify the addition of parameters to a model.

A.3 Experimental

A.3.1 *In silico* data generation

To verify the models added to the Athena Visual Studio script, an *in silico* study was carried out. The benefit to this kind of modelling study is that the internal consistency of a model can be confirmed, as the correct values for the parameter estimates are known prior to modelling. Four *in silico* datasets were produced; one for each baseline correction method.

For each dataset, five dimensionless temperature ramp rates are simulated (2, 4, 6, 8, 10 K min^{-1}) [11]. For the single peak system, the temperature ramp was between 315 K and 700 K, and for the multipeak system, between 315 K and 1273 K. A 15 min temperature hold was simulated at the end of the temperature ramp, to establish the end point for the baseline. Tables A.2 and A.3 show the kinetic parameters used to produce the 'no baseline added' data, for the single peak and multipeak datasets respectively. For the single peak case, the base temperature was 420 K. For the multipeak case, the base temperature values for the low and high temperature peaks were 420 K and 700 K respectively.

Table A.2: Kinetic parameters for *in silico* data generation, single peak dataset.

Parameter	Expected value
A_1 (s^{-1})	2.23×10^9
Ea_1 (kJ mol^{-1})	4.02×10^1
n_1(-)	1.00×10^0
m_1(-)	0.00×10^0
Fv_1 (-)	1.00×10^0

Table A.3: Kinetic parameters for *in silico* data generation, multipeak dataset.

Peak	Parameter	Expected value
Low temperature peak	A_1 (s^{-1})	2.23×10^{9}
	Ea_1 (kJ mol^{-1})	4.02×10^{1}
	n_1(-)	8.07×10^{-1}
	m_1(-)	5.15×10^{-1}
	Fv_1 (-)	6.00×10^{-1}
High temperature peak	A_2 (s^{-1})	1.01×10^{16}
	Ea_2 (kJ mol^{-1})	1.47×10^{2}
	n_2(-)	0.93×10^{-1}
	m_2(-)	-1.01×10^{0}
	Fv_2 (-)	4.00×10^{-1}

The parameters used to generate the *in silico* baselines are shown in Table A.4. These values were used for both the single and multipeak datasets.

Table A.4: Parameters used to generate simulated baselines.

Known baseline model	Parameter	
No baseline correction	Gradient	0.0000
	Intercept	0.0000
Linear with time	Gradient	0.2000
	Intercept	0.0000
Linear with temperature	Gradient	0.0008
	Intercept	-2.6624
Linear with extent of reaction	Gradient	0.3000
	Intercept	0.0000

Example curves with the simulated baselines added are shown in Figures A.1 and A.2 for single and multipeak cases respectively. Figures A.1 and A.2 demonstrate how similar these types of baselines can be, thus determining the correct baseline correction method by eye can be difficult. A rigorous statistical method should be applied when selecting a baseline correction technique.

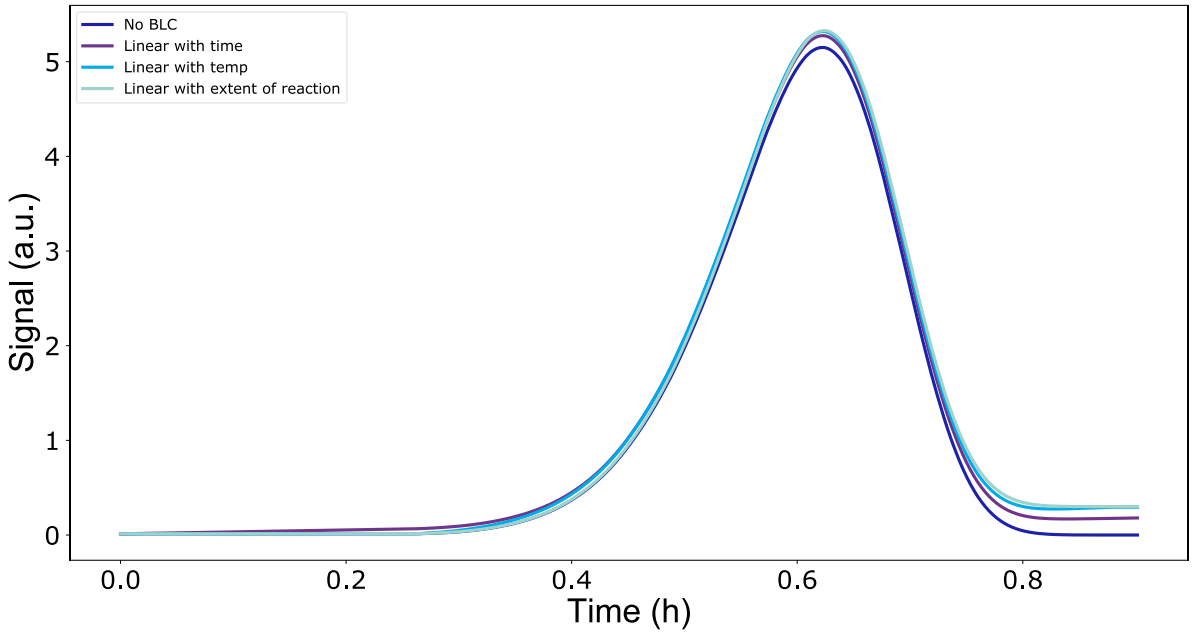

Figure A.1: Single peak 10 K min^{-1} *in silico* dataset with no baseline added, linear with time baseline added, linear with temperature baseline added and linear with extent of reaction baseline added.

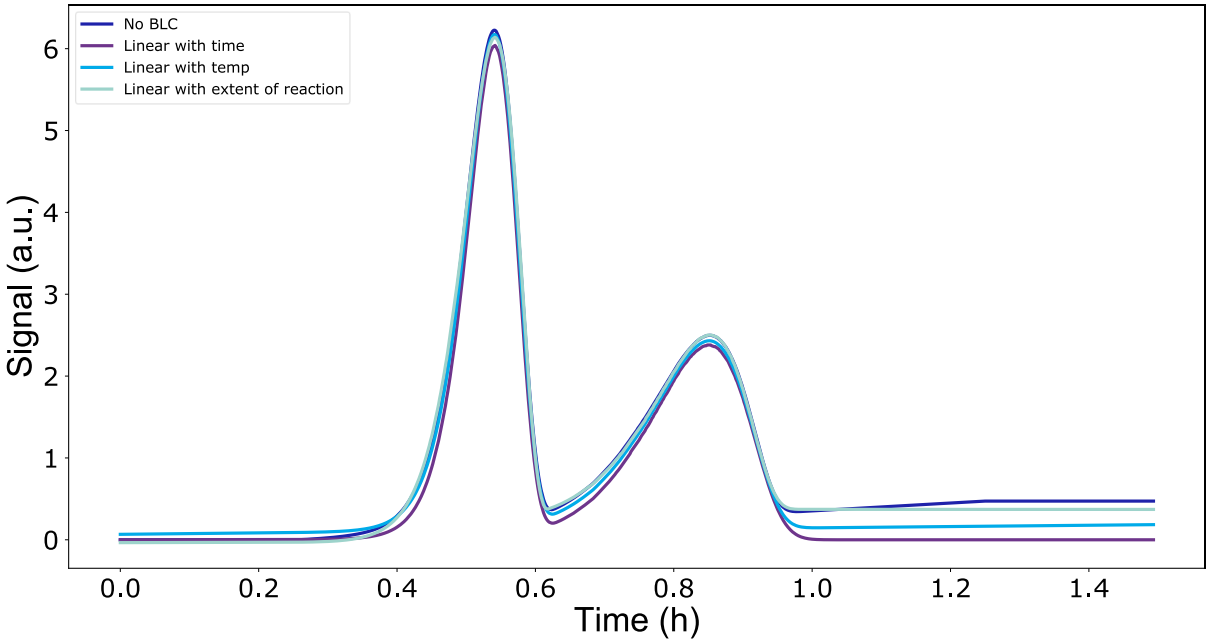

Figure A.2: Multiple peak 10K min^{-1} *in silico* dataset with no baseline added, linear with time baseline added, linear with temperature baseline added and linear with extent of reaction baseline added.

When baseline correcting thermal analysis data, only a single curve would be present (compared to the four shown in Figures A.1 and A.2). To reliably recognise the shape of an individual baseline by looking at a single curve is difficult, even with significant experience. Removing this experiential factor from baseline correction is one of the key aims of this work.

A.3.2 Mass spectrometry case study

Details of both the material and thermogravimetric analysis experiments are provided in Chapter 7.

A.4 Results and discussion

A.4.1 *In silico* case study

For the *in silico* datasets, the values for the baseline gradient and intercept are known prior to carrying out the modelling. The models can thus be checked for internal consistency and for a single global solution by comparing parameter estimation results to the input values. Table A.5 shows that for each dataset with an *in silico* baseline added (linear with time, temperature and extent of reaction) the correct input values are obtained through the parameter estimation regression for both single and multipeak cases. This means that the models for each baseline correction are internally consistent and achieve global minima values.

Table A.5:Parameter estimation results, baseline corrected *in silico* data.

Method for baseline addition	Correction method	Parameter	Input value	Single peak		Multiple peaks	
				Estimate	95% confidence interval	Estimate	95% confidence interval
Linear with time	Linear with time	M	2.0×10^{-1}	2.0×10^{-1}	4.1×10^{-6}	2.0×10^{-1}	2.3×10^{-6}
		C	0.0×10^{0}	1.6×10^{-6}	4.6×10^{-6}	3.0×10^{-6}	5.9×10^{-6}
Linear with temperature	Linear with temperature	M	8.0×10^{-4}	8.0×10^{-4}	2.1×10^{-8}	8.0×10^{-4}	5.5×10^{-8}
		C	-2.7×10^{-1}	-2.7×10^{-1}	1.0×10^{-5}	-2.7×10^{-1}	3.6×10^{-5}
Linear with extent of reaction	Linear with extent of reaction	M	3.0×10^{-1}	3.0×10^{-1}	3.5×10^{-5}	3.0×10^{-1}	2.5×10^{-5}
		C	0.0×10^{0}	2.9×10^{-4}	2.2×10^{-5}	2.8×10^{-4}	1.9×10^{-5}

A.4.1.1 Correction method discrimination

When faced with experimental data that shows a baseline drift, the source of this drift is not always clear, hence the best method of baseline correction may not be known. For each *in silico* dataset, all four correction methods have been regressed. Akaike weights has been used to compare the results from these four methods and establish which technique is the most statistically significant.

Tables A.6 and A.7 show, for a single peak and multiple peaks respectively, the comparison of fits using the four baseline correction methods on each of the four datasets. It should be noted that RSS and Akaike weight are only comparable within the same dataset.

Table A.6 emphasises that even when models achieve the same closeness of fit (reflected in the RSS value), the Akaike weights will select the model with fewest parameters. This should avoid overfitting.

Table A.6: Comparison of Akaike weights, baseline corrected *in silico* data, single peak.

Dataset	Metric	No baseline correction method	Linear with time method	Linear with temperature method	Linear with extent of reaction method
No drift added	RSS	$\mathbf{5.75 \times 10^{-7}}$	5.75×10^{-7}	5.75×10^{-7}	5.75×10^{-7}
	Akaike weight	0.70	0.10	0.10	0.10
Drift with time added	RSS	7.38×10^{0}	$\mathbf{8.35 \times 10^{-7}}$	1.41×10^{0}	1.08×10^{0}
	Akaike weight	0.0	1.0	0.0	0.0
Drift with temperature added	RSS	3.37×10^{0}	5.58×10^{-1}	$\mathbf{5.92 \times 10^{-7}}$	6.66×10^{-2}
	Akaike weight	0.0	0.0	1.0	0.0
Drift with extent of reaction added	RSS	4.21×10^{0}	2.01×10^{2}	5.56×10^{-1}	$\mathbf{2.15 \times 10^{-5}}$
	Akaike weight	0.0	0.0	0.0	1.0

Table A.7: Comparison of Akaike weights, baseline corrected *in silico* data, multiple peaks.

Dataset	Metric	No baseline correction method	Linear with time method	Linear with temperature method	Linear with extent of reaction method
No drift added	RSS	$\mathbf{1.22 \times 10^{-4}}$	1.25×10^{-4}	1.24×10^{-4}	1.25×10^{-4}
	Akaike weight	1.0	0.0	0.0	0.0
Drift with time added	RSS	4.39×10^{3}	$\mathbf{1.95 \times 10^{-4}}$	5.44×10^{2}	5.53×10^{2}
	Akaike weight	0.0	1.0	0.0	0.0
Drift with temperature added	RSS	1.27×10^{3}	1.38×10^{2}	$\mathbf{1.84 \times 10^{-3}}$	4.68×10^{1}
	Akaike weight	0.0	0.0	1.0	0.0
Drift with extent of reaction added	RSS	8.19×10^{2}	2.09×10^{1}	6.50×10^{1}	$\mathbf{1.44 \times 10^{-3}}$
	Akaike weight	0.0	0.0	0.0	1.0

The discrepancies between RSS values for the ‘no drift added’ case (Table A.7) are caused by the parameter tolerances for *M* and *C* in the linear baseline correction methods, as these parameters are attempting to converge to zero in this case.

The results of the Akaike weights comparison show that for each dataset, the correct method was identified as the most statistically probable (the largest Akaike weight), often giving a considerably better fit shown by the lowest values for RSS. This has been established for both single peak and multiple peak systems.

This methodology can thus be used to identify the most statistically likely baseline correction methodology, including whether a correction is required or not. This should be used for experimental data when the best baseline correction method is not known prior to modelling.

A.4.1.2 Impact of incorrect method

The accuracy of the rate determined through kinetic analysis can be negatively affected by the inaccuracy of the baseline determined [4]. Hemminger & Sarge [5] recommend a linear baseline correction with respect to time unless additional information is known. These authors found that when using an ‘incorrect’ baseline, the relative error of the enthalpy of melting could be as high as 3.2%, when compared to the exponential baseline correction function, which was taken as the ‘true’ function. This is outside the repeatability range of the instrument used and can greatly impact the kinetic information extracted from the data.

With the *in silico* data used in this study, the parameters for the kinetic modelling are also known, so the impact of correcting a baseline drift with the incorrect method can be determined. Table A.8 shows the percentage errors achieved when using the

incorrect baseline methods for each dataset. Table A.8 focuses on the activation energy parameter for simplicity, however similar results are obtained for all the parameters used in the modified Sestak-Berggren model.

Table A.8: Errors due to wrong baseline correction method.

Dataset			No baseline correction method	Linear with time method	Linear with temperature method	Linear with extent of reaction method
Single peak	Drift with time added	Ea_1	6.19%	-	2.46%	-3.09%
	Drift with temperature added	Ea_1	3.14%	0.39%	-	-3.84%
	Drift with extent of reaction added	Ea_1	**8.33%**	4.78%	Failed	-
Multiple peaks	Drift with time added	Ea_1	1.37%	-	0.82%	-3.76%
		Ea_2	5.55%	-	7.70%	-1.99%
	Drift with temperature added	Ea_1	0.68%	-0.03%	-	-2.57%
		Ea_2	4.37%	0.18%	-	-3.36%
	Drift with extent of reaction added	Ea_1	2.32%	2.00%	2.05%	-
		Ea_2	4.16%	4.04%	6.12%	-

Table A.8 shows that errors of up to 8.33% can be obtained when using the wrong baseline correction technique. This means selecting the wrong correction method could impact the kinetic parameters estimated severely. This reinforces the need to consider all four baseline correction methods and to have a rigorous method to select the most suitable

The use of this Akaike weights method would remove the experiential element which is currently associated with baseline correction in thermal analysis data. In some cases, such as the single peak linear with extent of reaction dataset, when different baseline correction methods are applied multiple could appear feasible, shown in Figure A.3.

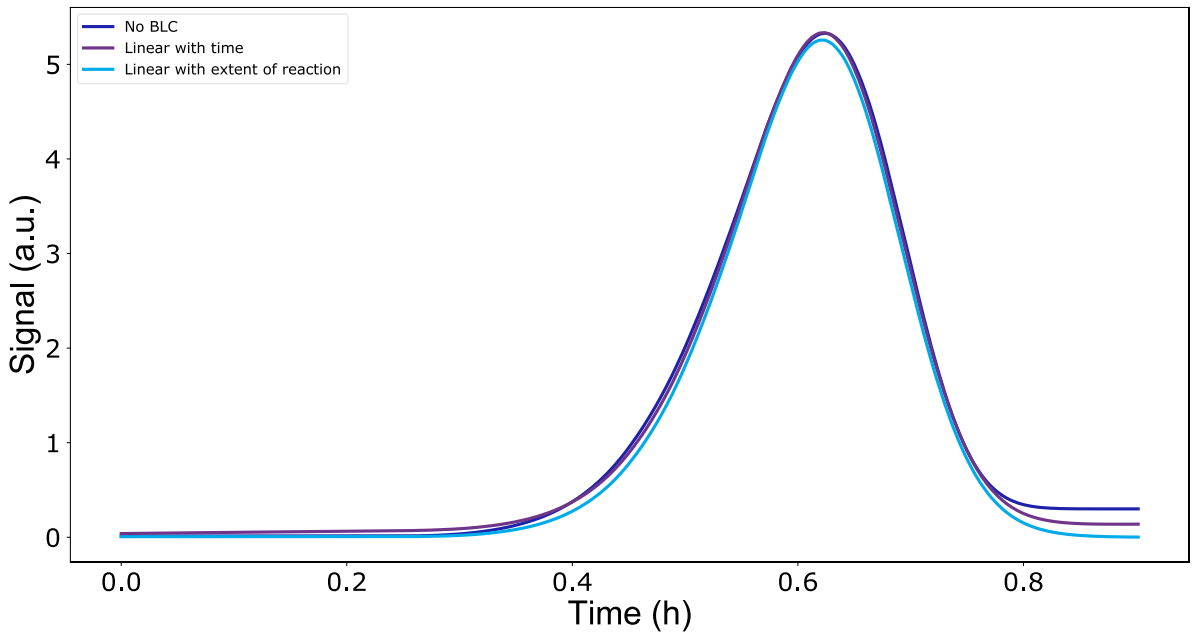

Figure A.3: Baseline correction of single peak, drift with extent of reaction dataset, 10 K min^{-1} examples.

Whilst in this case the no baseline correction may appear to be 'obviously' wrong, the linear with time baseline correction could be plausible for this system. If selected, this linear with time baseline correction would still result in an error of ~5 % on the activation

energy estimated. This Akaike weights method comparing multiple baseline correction options would allow even novice thermal analysis users to interpret data in a rigorous manner, accounting for the possibility of baseline drift. This comparison of baseline correction methods should be applied consistently to thermal analysis data, even in cases which appear ‘obvious’ to avoid bias fittings.

A.4.2 Mass-spectrometry study

The raw experimental data for m/z 30 are presented in Figure A.4.

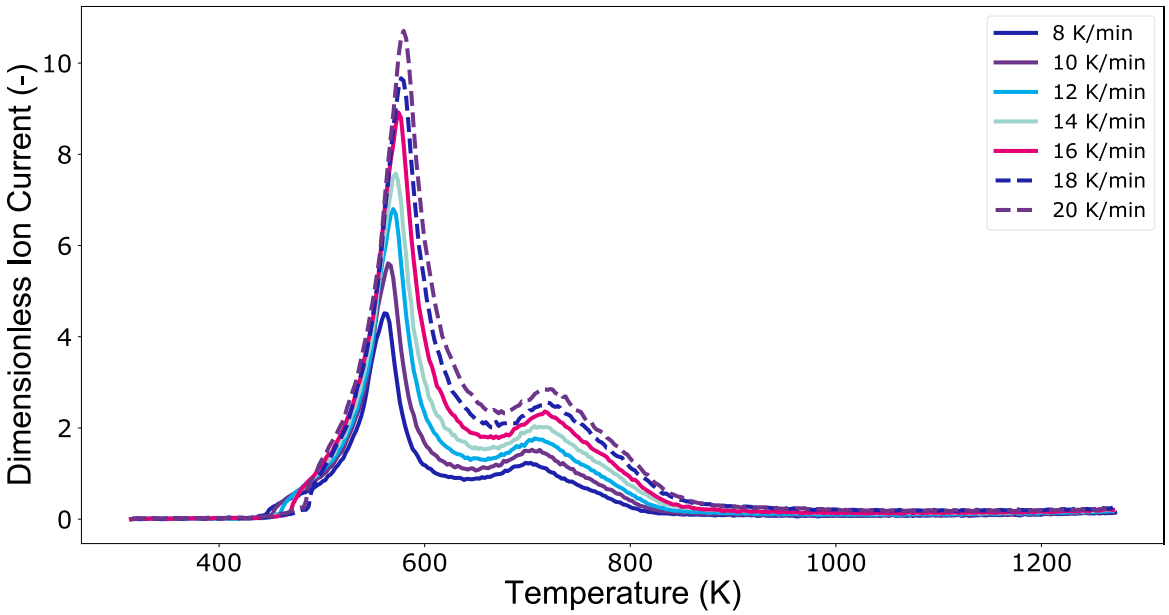

Figure A.4: Raw mass spectrometry data for m/z 30, $Zn(NO_3)_2/Al_2O_3$ decomposition.

The four baseline correction methods outlined above, were considered for this mass spectrometry data. Akaike weights were used to identify which method was the most statistically likely, shown in Table A.9.

Table A.9: Comparison of Akaike weights, m/z 30 data, $Zn(NO_3)_2/Al_2O_3$ decomposition.

Dataset	No baseline correction method	Linear with time method	Linear with temperature method	Linear with extent of reaction method
RSS	3.05×10^1	3.56×10^2	$\mathbf{2.44 \times 10^1}$	*Failed*
Akaike weight	0.0	0.0	1.0	

When the linear with extent of reaction baseline correction method was selected, not all kinetic parameters required were estimated. This means this model was poor and has been discounted from the Akaike weights comparison, as Akaike weights should only be used to discriminate good quality models [13].

For this data, the most appropriate baseline correction method was linear with temperature. This was used for all temperature ramp rate experiments (7 in total) and resulted in a good fit, with R^2 of 0.994 and an RSS of 24.40.

Table A.10 shows the baseline gradient and intercept estimated for this data, with Figure A.5 illustrating an example of the baseline and overall curve fit using the modified Sestak-Berggren equation [11].

Table A.10: Baseline correction parameter estimation results, m/z 30 data, $Zn(NO_3)_2/Al_2O_3$ decomposition.

Parameter	Estimate	95 % confidence interval
BL Gradient	0.04	9.49×10^{-3}
BL Intercept	0.02	7.57×10^{-3}

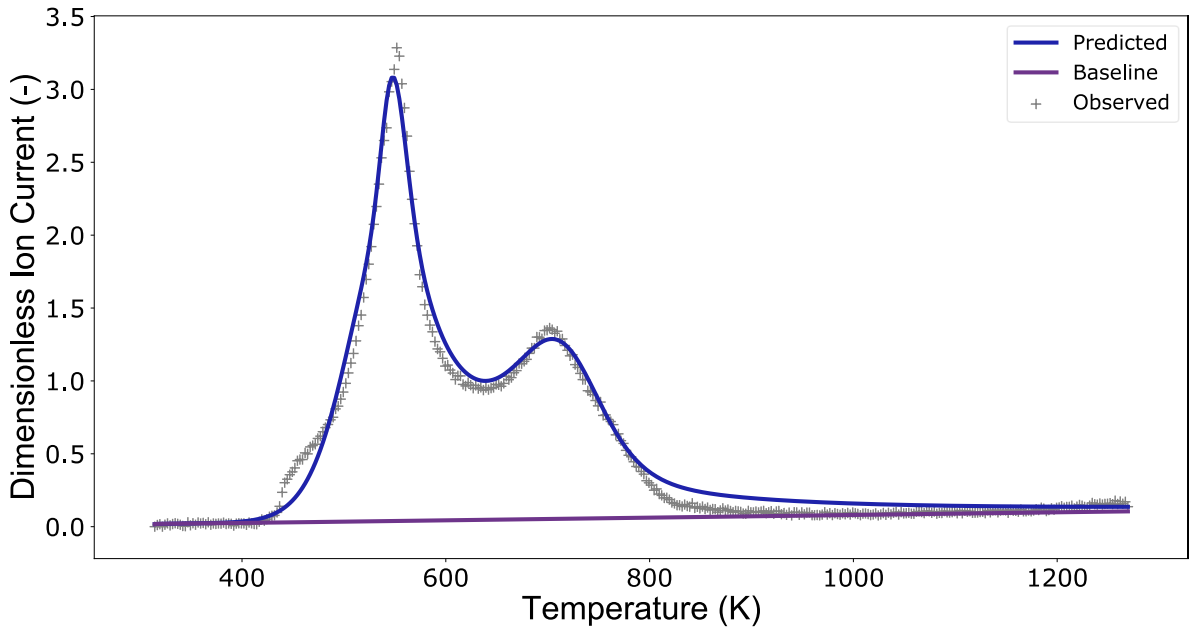

Figure A.5: Example of predicted baseline, 8 K min^{-1} experiment, m/z 30 data, $Zn(NO_3)_2/Al_2O_3$ decomposition.

This example shows that Akaike weights can be used to identify the most statistically likely formal baseline correction method for experimental thermal analysis data. This methodology should be applied to all modelling of thermal analysis data as this has a rigorous statistical basis for the correction method selection, which importantly, includes the possibility that no baseline correction is necessary.

A.5 Conclusions

This work has highlighted the importance of selecting a suitable baseline correction method for thermal analysis data. To remove the human/experiential factor which can

be associated with this pre-processing step, this work has recommended the use of a statistical basis for the choice of baseline correction, Akaike weights.

Formal baseline correction methods should only be used in the absence of a justifiable physiochemical or experimental baseline correction method. This work does not deconvolute thermal events or baseline drift prior to kinetic modelling, instead an overall baseline is accounted for.

This *in silico* case study showed that the choice of baseline correction can have a significant impact on the kinetic parameters estimated and that the correction method used may be selected using Akaike weights comparison of four formal baseline correction methods: no baseline correction, linear with time, linear with temperature and linear with extent of reaction. Once selected, the same baseline correction method should be applied across different temperature ramp rate experiments for a single dataset.

An experimental case study of mass spectrometry data showed the applicability of these baseline correction methods and Akaike weight comparison for a real system. The Akaike weights comparison indicated that a baseline which was linear with temperature was the most statistically likely. This baseline correction was applied to all temperature ramp rate experiments and resulted in a good fit for the experimental data once the modified Sestak-Berggren model had been applied.

This work has outlined a procedure to select the appropriate baseline correction method using Akaike weights, with formal baseline correction methods as examples. However, this selection technique is based on information theory, and could be applied to any baseline correction method, including those with a physical or experimental

basis. The modified Sestak-Berggren equation has been used to exemplify the coupling of the baseline correction methods with a kinetic model. This kinetic model could also be replaced with a model more suitable for a specific system.

A.6 References

[1] T. Ozawa, ‘Thermal analysis: review and prospect’, *Thermochim. Acta*, p. 8, 2000.

[2] M. Maciejewski, ‘Computational aspects of kinetic analysis. Part B: The ICTAC Kinetics Project: the decomposition kinetics of calcium carbonate revisited, or some tips on survival in the kinetic minefield’, *Thermochim. Acta*, p. 10, 2000.

[3] M. E. Brown et al.., ‘Computational aspects of kinetic analysis Part A: The ICTAC kinetics project-data, methods and results’, *Thermochim. Acta*, p. 19, 2000.

[4] S. Vyazovkin, ‘Computational aspects of kinetic analysis. Part C. The ICTAC Kinetics Project: the light at the end of the tunnel?’, *Thermochim. Acta,* p. 9, 2000.

[5] W. F. Hemminger and S. M. Sarge, ‘The baseline construction and its influence on the measurement of heat with differential scanning calorimeters’, *J. Therm. Anal*., vol. 37, no. 7, pp. 1455–1477, Jul. 1991, doi: 10.1007/BF01913481.

[6] R. Yahyaoui, P. E. S. Jimenez, L. A. P. Maqueda, K. Nahdi, and J. M. C. Luque, ‘Synthesis, characterization and combined kinetic analysis of thermal decomposition of hydrotalcite ($Mg_6Al_2(OH)_{16}CO_3{\cdot}4H_2O$)’, *Thermochim. Acta,* vol. 667, pp. 177–184, Sep. 2018, doi: 10.1016/j.tca.2018.07.025.

[7] S. Kouva, J. Kanervo, F. Schüßler, R. Olindo, J. A. Lercher, and O. Krause, ‘Sorption and diffusion parameters from vacuum-TPD of ammonia on H-ZSM-5’, *Chem. Eng. Sci*., vol. 89, pp. 40–48, Feb. 2013, doi: 10.1016/j.ces.2012.11.025.

[8] F. Arena, R. D. Chio, and G. Trunfio, ‘An experimental assessment of the ammonia temperature programmed desorption method for probing the surface acidic properties of heterogeneous catalysts’, *Appl. Catal. Gen*., vol. 503, pp. 227–236, Aug. 2015, doi: 10.1016/j.apcata.2015.05.035.

[9] J. Schittkowski, D. Buesen, K. Toelle, and M. Muhler, ‘The Temperature-Programmed Desorption of H2 from Cu/ZrO_2’, *Catal. Lett*., vol. 146, no. 5, pp. 1011–1017, May 2016, doi: 10.1007/s10562-016-1712-y.

[10] T. Hatakeyama and F. X. Quinn, Thermal analysis: fundamentals and applications to polymer science, 2nd ed. Chichester ; New York: Wiley, 1999.

[11] R. L. Gibson, M. J. H. Simmons, E. Hugh Stitt, J. West, S. K. Wilkinson, and R. W. Gallen, ‘Kinetic modelling of thermal processes using a modified Sestak-Berggren equation’, *Chem. Eng. J*., p. 127318, Oct. 2020, doi: 10.1016/j.cej.2020.127318.

[12] A. Michael, Y. N. Zhou, M. Yavuz, and M. I. Khan, ‘Deconvolution of overlapping peaks from differential scanning calorimetry analysis for multi-phase NiTi alloys’, *Thermochim. Acta*, vol. 665, pp. 53–59, Jul. 2018, doi: 10.1016/j.tca.2018.05.014.

[13] K. P. Burnham and D. R. Anderson, ‘Multimodel Inference: Understanding AIC and BIC in Model Selection’, *Sociol. Methods Res*., vol. 33, no. 2, pp. 261–304, Nov. 2004, doi: 10.1177/0049124104268644.

[14] S. Vyazovkin, A. K. Burnham, J. M. Criado, L. A. Pérez-Maqueda, C. Popescu, and N. Sbirrazzuoli, ‘ICTAC Kinetics Committee recommendations for performing kinetic computations on thermal analysis data’, *Thermochim. Acta*, vol. 520, no. 1–2, pp. 1–19, Jun. 2011, doi: 10.1016/j.tca.2011.03.034.

[15] R. Artiaga, S. Naya, A. García, F. Barbadillo, and L. García, ‘Subtracting the water effect from DSC curves by using simultaneous TGA data’, *Thermochim. Acta*, vol. 428, no. 1–2, pp. 137–139, Apr. 2005, doi: 10.1016/j.tca.2004.11.016.

[16] M. J. T. C. van der Niet, A. den Dunnen, L. B. F. Juurlink, and M. T. M. Koper, ‘A detailed TPD study of H2O and pre-adsorbed O on the stepped Pt(553) surface’, *Phys. Chem. Chem. Phys*., vol. 13, no. 4, pp. 1629–1638, Jan. 2011, doi: 10.1039/C0CP01162B.

[17] ‘J. Šesták: Thermophysical Properties of Solids - Their Measurements and Theoretical Thermal Analysis, aus der Reihe: Comprehensive Analytical Chemistry, ed. by G. Svehla. Subseries of Monographs on Thermal Analysis, ed. by W. W. Wendlandt: Vol. XII, Part D. Elsevier Science Publishers, Amsterdam and New York 1984. 440 Seiten, 122 Abbildungen, Ganzleinen US $ 115,50/Dfl. 300,-’, Berichte Bunsenges. Für Phys. Chem., vol. 89, no. 6, pp. 721–721, 1985, doi: https://doi.org/10.1002/bbpc.19850890630.

[18] R. Svoboda, ‘Importance of proper baseline identification for the subsequent kinetic analysis of derivative kinetic data: Part 3’, *J. Therm. Anal. Calorim*., vol. 136, no. 3, pp. 1307–1314, May 2019, doi: 10.1007/s10973-018-7738-1.

[19] R. Svoboda, ‘Importance of proper baseline identification for the subsequent kinetic analysis of derivative kinetic data: Part 2’, *J. Therm. Anal. Calorim*., vol. 131, no. 2, pp. 1889–1897, Feb. 2018, doi: 10.1007/s10973-017-6673-x.

[20] R. Svoboda and J. Málek, ‘Importance of proper baseline identification for the subsequent kinetic analysis of derivative kinetic data: Part 1’*, J. Therm. Anal. Calorim*., vol. 124, no. 3, pp. 1717–1725, Jun. 2016, doi: 10.1007/s10973-016-5297-x.

[21] G. E. P. Box, G. M. Jenkins, G. C. Reinsel, and G. M. Ljung, Time series analysis: forecasting and control, Fifth edition. Hoboken, New Jersey: John Wiley & Sons, Inc, 2016.

[22] K. P. Burnham and D. R. Anderson, Model Selection and Multimodel Inference: A Practical Information-Theoretic Approach, 2nd ed. New York: Springer-Verlag, 2002.

[23] T. Liu, I. Temprano, S. J. Jenkins, D. A. King, and S. M. Driver, ‘Nitrogen adsorption and desorption at iron pyrite FeS2{100} surfaces’, *Phys. Chem. Chem. Phys*., vol. 14, no. 32, p. 11491, 2012, doi: 10.1039/c2cp41549f.

[24] W. E. Stewart and M. Caracotsios, Computer-aided modelling of reactive systems. Hoboken, N.J: Wiley-Interscience : AIChE, 2008.

[25] J. Sestak and G. Berggren, ‘Study of the kinetics of the mechanism of solid-state reactions at increasing temperatures’, *Thermochim. Acta,* vol. 3, pp. 1–12, 1971.

[26] J. Šesták, ‘Šesták–Berggren equation: now questioned but formerly celebrated—what is right’, *J. Therm. Anal. Calorim*., vol. 127, no. 1, pp. 1117–1123, Jan. 2017, doi: 10.1007/s10973-015-4998-x.

[27] S. Vyazovkin et al.., ‘ICTAC Kinetics Committee recommendations for analysis of multi-step kinetics’, *Thermochim. Acta*, vol. 689, p. 178597, Jul. 2020, doi: 10.1016/j.tca.2020.178597.

[28] J. Málek and J. M. Criado, ‘Is the Šesták-Berggren equation a general expression of kinetic models?’, *Thermochim. Acta*, vol. 175, no. 2, pp. 305–309, Mar. 1991, doi: 10.1016/0040-6031(91)80076-U.

[29] J. Opfermann, ‘Kinetic Analysis Using Multivariate Non-linear Regression. I. Basic concepts’, *J. Therm. Anal. Calorim*., vol. 60, no. 2, pp. 641–658, May 2000, doi: 10.1023/A:1010167626551.

[30] H. Akaike, ‘Information theory and an extension of the maximum likelihood principle.’, B N Petrov F Caski EdsProceedings Second Int. Symp. Inf. Theory, pp. 267–281, 1973.

[31] C. M. HURVICH and C.-L. TSAI, ‘Regression and time series model selection in small samples’, Biometrika, vol. 76, no. 2, pp. 297–307, Jun. 1989, doi: 10.1093/biomet/76.2.297.

B. Design calculations for novel TGA unit

B.1 Design calculations

The first step in the design process should be some simple calculations to evaluate the efficacy of the proposed design.

The CFD study in Chapter 8 had identified conditions within a u-tube reactor to give suitable intrinsic data [1], hence this reactor case will be used as a design basis, details given in Table B.1.

Table B.1: Design parameters from previous CFD study.

Parameter	Value	Unit
Sample mass ($m_{sample1}$)	1.00×10^{-1}	g
Flow rate (Q)	1.67×10^{-6}	$m^3\ s^{-1}$
[6]**Pressure drop$_1$ (ΔP_1)**	4.92×10^{3}	Pa
Bed diameter$_1$ (d_{pan1})	4.00×10^{-3}	m
Bed height$_1$ (h_{bed1})	5.00×10^{-3}	m
Bed volume (V_{bed1})	6.28×10^{-8}	m^3

Additional parameter values used in these design calculations are given in Table B.2.

[6] This pressure drop is based on a mid-temperature ramp value. Due to changing temperature and gas density this would vary during a typical thermal analysis experiment.

Table B.2: Parameters used in novel TGA design calculations.

Parameter	Value	Unit
Sample mass (m_{sample})	1.00×10^{-1}	g
Pressure drop$_1$ (ΔP_1)	4.92×10^{3}	Pa
Sample diameter$_1$ ($d_{sample1}$)	4.00×10^{-3}	m
Bed height$_1$ (h_{bed1})	5.00×10^{-3}	m
Bed volume (V_{bed1})	6.28×10^{-8}	m^3
Density of pan (ρ)	2.71×10^{3}	$kg\ m^{-3}$
Wall thickness (w_T)	6.50×10^{-4}	m
Sample diameter$_2$ ($d_{sample2}$)	3.00×10^{-2}	m
Annulus length (L)	1.00×10^{-3}	m
Viscosity (μ)	3.46×10^{-4}	$kg\ m^{-1}.s^{-1}$
Flow rate (Q)	8.33×10^{-6}	$m^3\ s^{-1}$
Hydraulic diameter (Dh)	3.00×10^{-3}	m
Annulus size (A_{ann})	5.00×10^{-4}	m

B.2 Pan arrangement 1

To create a hanging pan reactor, a similar space velocity should be obtained. Initially, a sample pan with an equal sample volume was calculated.

It has been assumed that the sample pan would be made from aluminium.

A wall thickness for the sample pan has been assumed to be 6.50×10^{-4} m, based on the Q500 TGA design.

$$d_{pan1} = d_{sample1} + 2w_T = 5.30 \times 10^{-3} m \quad \text{Eq. (B.1)}$$

$$A_{pan1} = \pi . r_{pan1}^2 = 2.21 \times 10^{-5}\ m^2 \quad \text{Eq. (B.2)}$$

$$V_{wall1} = \left(A_{\text{pan1}} - A_{sample1}\right) \times h_{\text{bed1}} = 4.75 \times 10^{-8}\ m^3 \quad \text{Eq. (B.3)}$$

$$m_{wall1} = V_{\text{wall1}} \times \rho = 1.29 \times 10^{-4} kg \quad \text{Eq. (B.4)}$$

It was assumed that the mass of the retaining mesh on the top and bottom of the sample pan would be half the mass of the sample pan walls.

$$m_{pan1} = m_{\text{wall1}} + m_{\text{mesh1}} = 1.93 \times 10^{-4}\ kg \quad \text{Eq. (B.5)}$$

This equates to a force and pressure.

$$F_{pan1} = (m_{\text{pan1}} + m_{\text{sample1}}) \times g = 2.87 \times 10^{-3} N \quad \text{Eq. (B.6)}$$

$$\Delta P_{pan1} = \frac{F_{\text{pan1}}}{A_{sample1}} = 130\ Pa \quad \text{Eq. (B.7)}$$

With the estimated mass of the sample pan, it is possible to calculate the force measurement needed to detect the weight changes in the sample. Calcium carbonate was used as an example material, which has a residual mass of ~55 %.

$$\Delta F_{sample} = \Delta m_{sample1} \times g = 4.41 \times 10^{-4} N \quad \text{Eq. (B.8)}$$

This can be converted into a scale independent value using the area of the sample.

$$\Delta P_{sample} = \frac{\Delta F}{A_{sample1}} = 20\ Pa \quad \text{Eq. (B.9)}$$

B.3 Pan arrangement 2

To reduce the pressure drop within the sample, the dimensions of the sample pan can be changed. In this example, an extreme case has been taken, with a large diameter

sample pan of 3.00×10^{-2}m. An equal same volume was assumed, this allowed the depth of the bed to be calculated.

$$h_{\text{bed2}} = \frac{V_{\text{bed2}}}{\pi r^2_{\text{sample2}}} = 8.89 \times 10^{-5} m \quad \text{Eq. (B.10)}$$

This gives a similar order of magnitude to the particle size of the sample used in thermal analysis experiments, creating a single particle layer in the bottom of the pan. Hence, this is an extreme example.

Following the same procedure outlined above the mass of the proposed sample pan can be calculated, and from that a pressure exerted.

$$m_{pan2} = 2.26 \times 10^{-5} kg \quad \text{Eq. (B.11)}$$

$$\Delta P_{pan2} = \frac{(m_{\text{pan2}} + m_{\text{sample2}}) \times g}{A_{pan2}} = 1.56\ Pa \quad \text{Eq. (B.12)}$$

The loss of mass from the sample during the experiment will be the same as above, however due to the change in the pan area, the pressure will change.

$$\Delta P_{sample2} = \frac{\Delta m_{sample2} \times g}{A_{pan2}} = 5.63\ Pa \quad \text{Eq. (B.13)}$$

Finally, for this adapted pan arrangement the pressure drop through the sample can be estimated using a linear approximation.

$$\%\ h_{bed} = \frac{h_{bed_2}}{h_{\text{bed1}}} = 0.02\% \quad \text{Eq. (B.14)}$$

$$Flow\ \Delta P_2 = \%\ h_{bed} \times Flow\ \Delta P_1 = 87.34\ Pa \quad \text{Eq. (B.15)}$$

B.4 Pressure drop

The pressure drop through the annulus must be equal to the pressure drop through the packed bed (sample). The value for the pressure drop within the sample is known from previous CFD studies (Chapter 8). Hence either the annulus size or flow rate required to give an equivalent pressure drop can be calculated. This is based on the Darcy-Weisbach equation shown in Equation B.16 [2].

$$\frac{\Delta P}{L} = \frac{128}{\pi}\frac{\mu Q}{D_h^4} \qquad \text{Eq. (B.16)}$$

The following calculations were based on pan arrangement 1 above.

B.5 Annulus size

A calculation for the annulus size with an arbitrary, yet sensible, value for the carrier gas volumetric flow rate, was completed.

$$D_h = \left(\frac{\mu Q}{\frac{\pi}{128}\cdot\frac{\Delta P}{L}}\right)^{0.25} = 3.93 \times 10^{-4} m \qquad \text{Eq. (B.17)}$$

$$A_{eq} = \pi\left(\frac{D_h}{2}\right)^2 = 1.21 \times 10^{-7} m \qquad \text{Eq. (B.18)}$$

$$Ann.Size = \left(\frac{A_{eq}+A_S}{\pi}\right)^{0.5} - r_S = 9.64 \times 10^{-6}\, m \qquad \text{Eq. (B.19)}$$

This equates to;

$$Bypassing = \frac{Q_{ann}}{Q_{ann}+100\,\frac{ml}{min}} \times 100 = 83.3\% \qquad \text{Eq. (B.20)}$$

B.6 Flow rate

Another calculation was completed, assuming a feasible annulus size to calculate the carrier gas flow rate required for the pressure drop of 4.92×10^3 Pa [1].

$$A_{eq} = \left(r_{ann} + r_{sample}\right)^2 \pi - r_{sample}^2 \pi = 7.10 \times 10^{-6}\ m^2 \qquad \text{Eq. (B.21)}$$

$$D_h = 2.\left(\frac{A_{eq}}{\pi}\right)^{0.5} = 3.00 \times 10^{-3}\ m \qquad \text{Eq. (B.22)}$$

$$Q = \frac{\frac{\pi\ \Delta P}{128\ L}}{\mu}.D_h^4 = \ 2.82\ \times 10^{-2}\mathrm{m}^3 s^{-1} \qquad \text{Eq. (B.23)}$$

This equates to 99.9% by-passing.

B.7 References

[1] R. L. Gibson, M. J. H. Simmons, E. H. Stitt, L. Liu, and R. W. Gallen, 'Non-kinetic phenomena in thermal analysis data; Computational fluid dynamics reactor studies', *Chem. Eng. J.*, vol. 426, p. 130774, Dec. 2021, doi: 10.1016/j.cej.2021.130774.

[2] R. H. Perry and D. W. Green, Eds., *Perry's chemical engineers' handbook*, 8th ed. New York: McGraw-Hill, 2008.